UNIVERSIDADE ESTADUAL DE CAMPINAS (UNICAMP)
Faculdade de Engenharia Química

ISMAIL EŞ

SISTEMAS MICROFLUÍDICOS PARA A INCORPORAÇÃO DE SMALL INTERFERING RNA (SIRNA) EM LIPOSSOMAS CATIÔNICOS E TRANSFECÇÃO DE ESFERÓIDES TUMORAIS NO MICROCHIP

MICROFLUIDIC SYSTEMS FOR INCORPORATION OF SMALL INTERFERING RNA (SIRNA) IN CATIONIC LIPOSOMES AND ON-CHIP TRANSFECTION OF MULTICELLULAR TUMOR SPHEROIDS

CAMPINAS
2020

ISMAIL EŞ

MICROFLUIDIC SYSTEMS FOR INCORPORATION OF SMALL INTERFERING RNA (SIRNA) IN CATIONIC LIPOSOMES AND ON-CHIP TRANSFECTION OF MULTICELLULAR TUMOR SPHEROIDS

SISTEMAS MICROFLUÍDICOS PARA A INCORPORAÇÃO DE SMALL INTERFERING RNA (SIRNA) EM LIPOSSOMAS CATIÔNICOS E TRANSFECÇÃO DE ESFERÓIDES TUMORAIS NO MICROCHIP

Thesis presented to the School of Chemical Engineering of the University of Campinas in partial fulfillment of the requirements for the degree of Doctor in Chemical Engineering.

Tese apresentada à Faculdade de Engenharia Química da Universidade Estadual de Campinas como parte dos requisitos exigidos para a obtenção do título de Doutor em Engenharia Química.

Supervisor: Prof. Dr. Lucimara Gaziola de la Torre

ESTE TRABALHO CORRESPONDE À VERSÃO FINAL DA TESE DE DOUTORADO DEFENDIDA PELO ALUNO ISMAIL EŞ, E ORIENTADA PELA PROFª. DRª. LUCIMARA GAZIOLA DE LA TORRE

CAMPINAS
2020

Ficha catalográfica
Universidade Estadual de Campinas (UNICAMP)
Biblioteca da Área de Engenharia e Arquitetura
Rose Meire da Silva - CRB 8/5974

Es1m

Es, Ismail, 1985-
Microfluidic systems for incorporation of small interfering RNA (siRNA) in cationic liposomes and on-chip transfection of multicellular tumor spheroids / Ismail Es. – Campinas, SP : [s.n.], 2020.

Orientador: Lucimara Gaziola de la Torre.
Tese (doutorado) – Universidade Estadual de Campinas (UNICAMP), Faculdade de Engenharia Química.

1. Microfluídica. 2. Lipossomos. 3. RNA interferente pequeno. 4. Esferoides celulares. 5. Técnica de transferência de genes. I. Torre, Lucimara Gaziola de la, 1971-. II. Universidade Estadual de Campinas (UNICAMP). Faculdade de Engenharia Química. III. Título.

Informações Complementares

Título em outro idioma: Sistemas microfluídicos para a incorporação de small interfering RNA (siRNA) em lipossomas catiônicos e transfecção de esferóides tumorais no microchip
Palavras-chave em inglês:
Microfluidics
Liposomes
Small interfering RNA
Spheroids
Gene transfer techniques
Área de concentração: Engenharia Química
Titulação: Doutor em Engenharia Química
Banca examinadora:
Lucimara Gaziola de la Torre [Orientador]
Camila Foged
Tiago Albertini Balbino
Marco Cardoso Marques
Rosiane Lopes da Cunha
Data de defesa: 12-08-2020
Programa de Pós-Graduação: Engenharia Química

Identificação e informações acadêmicas do(a) aluno(a)
- ORCID do autor: https://orcid.org/0000-0002-7369-1039
- Currículo Lattes do autor: http://lattes.cnpq.br/5117822572648633

FOLHA DE APROVAÇÃO

Folha de Aprovação da Defesa de Tese de Doutorado defendida por Ismail Eş em 12 de agosto de 2020 pela banca examinadora constituída pelos doutores.

Profa. Dra. Lucimara Gaziola de La Torre
Presidente e Orientadora - FEQ / Unicamp
Videoconferência

Dra. Camila Foged
University of Copenhagen -Department of Pharmacy
Videoconferência

Dr. Tiago Albertini Balbino
Instituto Alberto Luiz Coimbra de Pós-graduação e Pesquisa de Engenharia
Videoconferência

Dr. Marco Cardoso Marques
University College London
Videoconferência

Profa. Dra. Rosiane Lopes da Cunha
FEA/UNICAMP
Videoconferência

A Ata da defesa com as respectivas assinaturas dos membros encontra-se no SIGA/Sistema de Fluxo de Dissertação/Tese e na Secretaria do Programa da Unidade

To my family,

Without whom none of this would have been achieved.

ACKNOWLEDGMENTS

Foremost, I would like to recognize the invaluable assistance that my supervisor, Prof. Dr. Lucimara Gaziola de la Torre, provided me during my Ph. D. I also wish to express my deepest gratitude to Prof. Dr. Nicolas Szita and Dr. Marco Marques for their assistance during my stay at University College London.

I also appreciate the following research institutes for their support and availability to conclude my experiments: School of Chemical Engineering, Institute of Biology, Center of Molecular Biology and Genetic Engineering of UNICAMP; Department of Biochemical Engineering, Division of Medicine, and the London Centre for Nanotechnology of University College London; Brazilian National Laboratory of Nanotechnology, The Microfabrication Laboratory and Brazilian Synchrotron Light Laboratory in the Brazilian Center for Research in Energy and Materials (CNPEM); and The Center for Information Technology "Renato Archer".

I gratefully acknowledge the São Paulo Research Foundation (FAPESP) (Process no: 2015/14468-0 and 2018/23895-7) for their financial support during my Ph.D. between 2015 and 2020. I also acknowledge the Department of Biochemical Engineering of University College London for partially supporting my experiments.

I wish to thank all the people whose assistance was very essential in the completion of this project: My dear colleagues from Nanobiotechnology Laboratory for Advanced Developments, the research group of Prof. Dr. Adriano Rodrigues Azzoni (USP), Prof. Dr. Nicolas Szita (UCL), Prof. Dr. Savio S. V. Vianna (UNICAMP), Prof. Dr. Marcelo Bispo de Jesus (UNICAMP), Prof. Dr. Maria Helena Santana (UNICAMP), Prof. Dr. Jorge Vicente Lopes da Silva (CTI-Renato Archer), Prof. Dr. Eneida de Paula (UNICAMP), Angelo Luiz Gobbi (CNPEM), and Dr Emad Moeendarbary (Mechanical Engineering/UCL).

I wish to acknowledge the emotional support and unconditional love of my family. They kept me going on and this work would not have been possible without their unconditional support.

“Above all, don't fear difficult moments.

The best comes from them.”

Rita Levi-Montalcini

ABSTRACT

Lipid-based nanotherapeutics are a promising solution to overcome the current limitations of conventional drug/gene delivery systems. Despite their vast potential, their clinical applications are still limited due to technical impediments in their efficient synthesis. The demand for the development of effective technological platforms for high-throughput production of these compounds is rapidly increasing. In this context, microfluidics emerged as a robust technological tool in the continuous synthesis of lipid-based vector systems for drug/gene delivery. This Ph. D. thesis aims the technological development of microfluidic systems to incorporate small interfering RNA (siRNA) into cationic liposomes (CLs) with stealth properties and on-chip transfection of multicellular spheroids with siRNA nanotherapeutics. In the first part, CLs were electrostatically complexed with siRNA using bulk mixing to better understand how siRNA interacts with liposomes. After our dynamic light scattering (DLS) analysis, the optimum molar charge ratio (R±) was found to be 3.27. This value was verified by employing siRNA accessibility assay and gel electrophoresis. The multilamellarity of the liposomes was confirmed using Cryo-electron microscopy. A significant knockdown of luciferase activity on HeLa cells was obtained with no cytotoxic effect. In the second part, conventional and stealth CLs were produced in a high-throughput microfluidic platform (chaotic advection-based) and physicochemical, structural, morphological and biological aspects of these lipid-based vector systems were evaluated. SAXS and Cryo-TEM analyses confirmed the unilamellarity of both CLs and *in vitro* transfection studies showed that they could deliver pDNA to the cancer cells. In this step, we achieved 70 times higher productivity in CL production compared to microfluidics hydrodynamic flow-focusing process. Moreover, we successfully eliminated the formation of micelle in the microchannels, which was inevitable in hydrodynamic flow-focusing devices. We also employed centrifugal vacuum concentrator as an alternative distillation process to remove the excess of ethanol in the final liposomal formulation, keeping the unilamellar structure of CLs. In the third part, a diffusion-based microfluidic platform was used to synthesize siRNA-containing lipid-based nanotherapeutics with stealth properties as one-step (phospholipids and PEG polymer with siRNA) and two-step (pre-formed stealth CLs with siRNA) approaches. One-step and two-step approaches led to the synthesis of lipid nanocarriers with different physico-chemical, structural, and morphological properties. SAXS analysis confirmed that the insertion of PEG into the formulation had a different impact on the structural properties. In the last part, static and dynamic microfluidic cell culture systems were developed to produce spheroids using GPF-expressing HEK-293 cells. The spheroids were transfected using siRNA on the selected microdevice (static system). Produced spheroids were morphologically characterized using advanced microscopy techniques and transfection levels were determined by evaluating GFP intensity. The transfection studies showed that static microfluidic platforms were not effective to test drug/gene formulations. Hence, new strategies are proposed to overcome the limitation of static microdevices. This dissertation provides original contributions of major significance in the field of microfluidics and its application in nanomedicine.

Keywords: microfluidics, liposomes, siRNA, gene delivery, spheroids

RESUMO

Veículos nanoterapêuticos baseados em lipídios são uma solução promissora para superar as limitações atuais dos sistemas convencionais de administração de medicamentos ou genes. Apesar de seu vasto potencial, suas aplicações clínicas ainda são limitadas devido a impedimentos técnicos em síntese eficiente. A demanda pelo desenvolvimento de plataformas tecnológicas eficazes para a produção com alta produtividade desses compostos está aumentando rapidamente. Nesse contexto, a microfluídica emerge como uma ferramenta tecnológica robusta na síntese contínua de sistemas vetoriais baseados em lipídios para entrega de medicamentos ou genes. Esta tese de doutorado visa o desenvolvimento tecnológico de sistemas microfluídicos para incorporar pequenos RNA interferentes (siRNA) em lipossomas catiônicos (CLs) com propriedades furtivas (Stealth) e avaliar a transfecção de agentes nanoterapêuticos de siRNA em esferóides multicelulares, utilizando microchip. Na primeira parte, os CLs foram eletrostaticamente complexados com siRNA explorando o efeito da razão molar de cargas para entender como o siRNA interage com os lipossomas. Após análise através de espalhamento de luz dinâmica (DLS), a razão molar de cargas (R ±) ideal foi de 3,27. Nesta condição foram realizados ensaios de acessibilidade ao siRNA e eletroforese em gel de agarose. A multilamelaridade dos lipossomas foi confirmada por microscopia Crioeletrônica. Um efeito "knockdown" significativo da atividade da luciferase nas células HeLa foi obtido sem observar efeito citotóxico nas célula. Na segunda parte, CLs convencionais e furtivos foram produzidos em uma plataforma microfluídica de alto rendimento (baseada em advecção caótica) e avaliados aspectos físico-químicos, estruturais, morfológicos e biológicos desses sistemas lipídicos. As análises raio X a baixo ângulo (SAXS) e Cryo-TEM confirmaram a unilamelaridade dos CLs e os estudos de transfecção in vitro mostraram que eles poderiam fornecer pDNA às células cancerígenas. O processo desenvolvido alcançou uma produtividade 70 vezes maior na produção de CL em comparação com o processo de focalização hidrodinâmica em microfluídica. Além disso, este processo evitou com sucesso a formação de micelas nos microcanais, o que era inevitável em dispositivos de foco de fluxo hidrodinâmico. Também foi empregada a técnica de concentração à vácuo centrífugo como processo alternativo de destilação para remover o excesso de etanol na formulação lipossômica final, mantendo a estrutura unilamelar dos CLs. Na terceira parte, uma plataforma microfluídica baseada em difusão foi usada para sintetizar sistemas lipídicos contendo siRNA com propriedades furtivas, avaliando duas estratégias de processo: uma etapa (fosfolipídios e polímero PEG com siRNA para autoagregação lipídica e complexação com material genético simultaneamente) e duas etapas (CLs furtivos pré-formadas para associação com siRNA). Abordagens de uma e duas etapas levaram à síntese de nanocarreadores lipídicos com diferentes propriedades físico-químicas, estruturais e morfológicas. A análise SAXS confirmou que a inserção do PEG na formulação teve um impacto diferente nas propriedades estruturais. Na última parte, foram desenvolvidos microchips para a formação e transfeção de esferoides de células HEK-293 que expressam GPF em condição estática e dinâmica . Os esferóides foram transfectados usando siRNA no microdispositivo de cultivo em sistema estático. Os esferóides produzidos foram caracterizados morfologicamente utilizando técnicas avançadas de microscopia e os níveis de transfecção foram determinados pela avaliação da intensidade da GFP. Os estudos de transfecção mostraram que plataformas microfluídicas estáticas não eram eficazes para testar formulações de fámacos ou genes. Portanto, novas estratégias são propostas para superar a limitação dos microdispositivos estáticos. Esta dissertação fornece contribuições originais de grande importância no campo da microfluídica e sua aplicação na nanomedicina.

Palavras-chave: microfluídica, lipossomas, siRNA, entrega de genes, esferóide

LIST OF FIGURES

CHAPTER 2

CHAPTER 3

CHAPTER 4

CHAPTER 5

CHAPTER 6

LIST OF TABLES

ABBREVIATIONS

DNA	Deoxyribonucleic acid
ADA	Adenosine deaminase
AML	
ASO	Antisense oligonucleotides
ATP	Adenosine triphosphate
CAM	Computer-aided manufacturing
CA-MD	Chaotic advection-based microfluidic device
CL	Cationic liposome
CNC	Computer Numerical Control
COP	Cyclic olefin (co)polymer
Cryo-EM	Cryo Electron Microscopy
D-MD	Diffusion-based Microfluidic device
DMEM	Dulbecco's Modified Eagle Medium
DOPE	1,2-Dioleoyl-sn-glycero-3-phosphoethanolamine
DOTAP	1,2-dioleoyl-3-trimethylammoniumpropyl chloride
DSPE-PEG(2000)	1,2-distearoyl-sn-glycero-3-phosphoethanolamine-N-[(polyethylene glycol)-2000]
dsRNA	Double-stranded RNA
ECM	Extracellular matrix
eGFP	Enhanced green fluorescent protein
EPC	Egg phosphatidylcholine
FBS	Fetal bovine serum
FDA	Food and Drug Administration
FRR	Flow Rate Ratio
GFP	Green fluorescent protein
GTAC	Gene Therapy Advisory Committee
GUV	Giant unilamellar vesicles
HEK-293	Human Embryonic Kidney 293 cells
HeLa	Human cervical cancer cells
hsiRNAs	Hydrophobically-modified small interfering RNAs
HT-29	Human colon adenocarcinoma cells
Kb	Kilo-base
LNP	Lipid nanoparticles
LPX	Lipoplex
MCF-7	Human breast cancer cells
MLV	Multilamellar vesicles
MPS	Mononuclear phagocyte system
MW	Molecular Weight
ODS	Oligodeoxyribonucleotide
PBS	Phosphate-buffered saline
PC	Polycarbonate
PC-3	Human prostate cancer cell line
PCR	Polymerase chain reaction
PdI	Polydispersity Index
PDMS	Polydimethylsiloxane
pDNA	Plasmid DNA

PEG	Poly-(ethylene glycol)
PI	Propidium iodide
PS	Polystyrene
$R_{\pm}$	Molar Charge Ratio
RAC	Recombinant DNA Advisory Committee
Re	Reynolds number
RLU	Relative light unit
RNA	Ribonucleic acid
RNAi	RNA interference
SAXs	Small Angle X-Ray Scattering
S-CL	Stealth cationic liposomes
SHM	staggered herringbone micromixer
shRNA	Short hairpin RNA
siRNA	Small interfering RNA
S-LNP	Stealth lipid nanoparticles
S-LPX	Stealth lipoplex
SSO	Splice switching oligonucleotides
STL	Stereolithography
TFR	Total Flow Rate
ULV	Unilamellar
UV	Ultraviolet
ζ-Potential	Zeta Potential

TABLE OF CONTENTS

CHAPTER 1. INTRODUCTION TO THE THESIS

1. A brief introduction

Genetic diseases have been a great concern in the public eye for centuries. A genetic disease is caused by a significant alteration in the DNA sequence (Friedmann & Roblin, 1972). As humanity discovers the secrets of the human genome, the links between these diseases and genetic components are eventually unlocked. Some diseases are a result of mutations inherited from the parents and some are caused by mutations in a single or a group of genes that occur along with the patient's life. The latter eventuates either randomly or due to some environmental exposure that damages the gene's instructions that control the way our cells function (Cavalli & Heard, 2019).

Cancer, as one of the most common genetic diseases, is responsible for millions of deaths worldwide every year. It is usually caused by environmental factors, whilst inherited genetic mutations cannot be ignored. Cancer cells are known to undergo more genetic changes compared to normal cells. As cancer progresses, additional mutations may come about and cancer cells may possess new characteristics that may complicate the treatment (Turajilic et al. 2019). Despite the progress achieved in medicine, there still exists critical issues in cancer therapy. These issues should be carefully addressed by putting a great deal of effort to find novel and effective therapeutic methods, employing a combination of multidisciplinary approaches.

Nanomedicine has been contributing to the development of efficient methods to correct or silence a faulty gene that leads to genetic disease (Guidolin & Zheng, 2019). A faulty gene can be replaced with a healthy one using plasmid DNA (pDNA) or the expression of defective proteins can be knocked-down using small interfering RNA, which is a key molecule in a post-transcriptional gene silencing process, RNA interference (RNAi) (Fire et al., 1998). However, the delivery of these genetic materials can be ensured only by using a carrier system. At this point, nanotechnology can be used to construct non-viral vectors to shuttle the genetic material inside the cell while protecting it from intra- and extracellular deleterious agents, resulting in more efficient gene delivery. Hence, novel non-viral vectors as promising nanotherapeutics should be efficiently developed.

Lipid-based vesicular vectors are efficient candidates for the controlled delivery of the genetic material as a promising solution to cancer therapy (Girimaldi et al. 2016). Unfortunately, high-throughput and continuous synthesis of these nanotherapeutics may be hindered due to the lack of a potent technological platform. Besides the synthesis of these nanotherapeutics, which revolutionize the history of medicine, the availability of platforms to test them is another critical point that must be addressed. For decades, preliminary screening tests of these nanotherapeutics have been carried out in 2D monolayer cell culture. In 2D monolayer cell culture systems, cell-cell communication does not reflect the interactions occurring within *in vivo* tissues, and hence these systems cannot truly mimic cell-drug interactions either and the success rate of drug testing drastically declines (Gupta et al. 2020). Thus, investigations are performed to develop 3D *in vitro* systems that better mimic the *in vivo* environment. In this context, spheroids, which are self-assembled aggregates of cells, emerged as an attractive opportunity for more effective nanotherapeutics screening. In spheroids, signal proteins, which are essential for intercellular communication, are overexpressed (Cui et al. 2017). This leads to a more realistic interaction between the cells and, consequently, enhances the meaning of the response of the cells for nanotherapeutics testing. The design of these promising nanotherapeutics and 3D platforms can be highly challenging; hence, engineering provides essential tools to enhance the manufacturing of these systems.

Among different engineering tools, microfluidic technologies have demonstrated unique opportunities for the synthesis of nanotherapeutics and the development of *in vitro* microenvironments by decreasing sample and reagent consumption, shortening the time of experiments, reducing human error and overall cost of bioprocesses (Colombo et al. 2018; Zhang et al. 2018). Currently, there is still a lot to exploit from microfluidic technology to explore its use in cancer therapy and more details will be given in the next chapters.

2. Aim and Research Strategies

The present thesis aims to manufacture microfluidic platforms to synthesize lipid-based nanotherapeutics for siRNA delivery and develop 3D cell culture systems for a more precise drug testing. By doing that, we aim to contribute to the field of nanobiotechnology and cancer research. To achieve this aim, the following research strategies were defined:

- **Electrostatics interaction between siRNA and cationic liposomes – Pysico-chemical and morphological characterization**: Evaluation of the interaction between siRNA and cationic liposomes composed of egg phosphatidylcholine (EPC), 1,2-dioleoyl-3-trimethylammonium-propane (DOTAP), and 1,2-dioleoyl-sn-glycero-3-phosphoethanolamine (DOPE) and its effect on physicochemical properties of the lipoplexes.

- **Synthesis of conventional and stealth cationic liposomes with increased productivity using a microfluidic device based on chaotic advection mixing**: Fabrication of chaotic advection-based microfluidic device to incorporate DSPE-PEG(2000) into conventional liposomes for passive targeting and comparison with the production of liposomes in microfluidics flow-focusing device.

- **Association between siRNA and conventional/stealth cationic liposome**s **using a diffusion-based microfluidic device**: Microfluidic synthesis of lipid nanoparticles (one-step approach) and lipoplexes (two-step approach) with stealth properties for siRNA delivery and their characterization as a comparative study.

- **Design of a microfluidic platform for the formation of spheroids and the delivery of siRNA into spheroids:** The design of a static and continuous-flow microfluidic cell culture system using stereolithography technique to form spheroids and the evaluation of in chip transfection of spheroids using siRNA.

3. Thesis organization

The thesis is divided into chapters to better follow the logical sequence of the investigations carried out to achieve the aforementioned aim and research strategies. The results were presented as original research papers that were already published (Chapters 3 and 4) and are in preparation (Chapters 5 and 6). The organization of the thesis in chapters is described as follows:

- ***Chapter 1 –*** *A brief introduction, aim and research strategies*

A brief introduction covering all of the technical aspects that are essential to conclude the thesis, as well as the aims and objectives of the thesis, is given.

❖ ***Chapter 2 –*** *Literature review*

In this chapter, the basic concepts used in this Ph. D. thesis will be given in more details as the state-of-the-art. The overall concept of gene therapy, the role of nucleic acids (particularly siRNA) in gene therapy application, lipid-based vesicular vectors as promising nanotherapeutics for the delivery of siRNA, and their functionalization to improve their therapeutic outcome will be introduced. Moreover, microfluidic technology will be explained as an approach for the synthesis of lipid-based nanotherapeutics and the development of biomimetic screening models to test these promising gene delivery systems. Finally, concluding remarks and future perspectives will be addressed.

❖ ***Chapter 3 -*** *Evaluation of siRNA and cationic liposome complexes as a model for in vitro siRNA delivery to cancer cells*

This chapter presents the data obtained from the complexation study between microfluidics-produced conventional cationic liposomes composed of EPC/DOTAP/DOPE lipids and siRNA as a model for *in vitro* gene delivery to HeLa cells. This study was published in Colloids and Surfaces A: Physicochemical and Engineering Aspects (*https://doi.org/10.1016/j.colsurfa.2018.06.073*). As it was the first investigation carried out using siRNA, this study was conducted using bulk mixing to better understand the complexation behavior of siRNA and liposomes before proceeding with microfluidic synthesis. In this study, liposomes and siRNA were mixed at different molar charge ratio, which is the ratio between the number of positive charges present in cationic phospholipids (in this study DOTAP) and negative charges in the phosphate backbone of siRNA. After our dynamic light scattering (DLS) analysis, the optimum molar charge ratio (R±) was found to be 3.27. This value was verified by employing siRNA accessibility assay and gel electrophoresis. The multilamellarity of the liposomes was confirmed using Cryo-electron microscopy. *In vitro* transfection efficiency of lipoplexes in HeLa cells was tested at three different siRNA concentrations (10, 25, and 35 nM). A significant knockdown of luciferase by siRNA lipoplexes was observed based on reduced luciferase activity of transfected HeLa cells. No cytotoxicity of lipoplexes was detected at the tested concentrations.

- ***Chapter 4*** *– High-throughput microfluidic synthesis of conventional and stealth liposomes*

Liposomes produced in the diffusion-based device was shown to have low productivity. Moreover, during stealth liposomes synthesis in such a platform, the agglomeration of micelle-like particles along with the channel is usually observed. This agglomeration is a great drawback for the industrial application of liposomes as it results in the presence of random particles (including micelles) with varying sizes in the final solution. This chapter presents the development of a microfluidic platform to overcome these limitations to manufacture conventional and stealth liposomes at very high productivity. This study was published in the Chemical Engineering Journal (https://doi.org/10.1016/j.cej.2019.122821) and the process of stealth cationic liposome production is submitted for a patent application (PCT/BR2019/050506). In this study, optimization steps to achieve the desired production and advance methods to characterize the produced liposomes are given. The conventional and stealth liposomes were found to be unilamellar and *in vitro* transfection studies showed that they could deliver pDNA to the cancer cells. The final liposomal solution was found to contain 50% ethanol and we employed a centrifugal vacuum concentrator to successfully remove ethanol to be suitable for biological applications.

- ***Chapter 5*** *– Diffusion-based microfluidic device to manufacture lipid-based vector system with stealth properties to improve therapeutic efficiency of siRNA on cancer cells*

There is an increasing trend in complexation studies in microfluidic systems. Complexation in microfluidic devices for the synthesis of lipid-based vector systems can be achieved by following two approaches. In the first approach, the genetic material in the aqueous solution is introduced into one inlet, while phospholipids dispersed in anhydrous ethanol are introduced from other inlets, hence, inducing the formation of lipid nanocarriers. Using this approach, it is possible to prompt the simultaneous incorporation of genetic material into these nanocarriers to form lipid nanoparticles (LNPs) in a single step. The second approach (two-step) involves the introduction of previously-produced liposomes

into the microfluidic channel together with genetic material to produce lipoplexes (LPXs). Considering both lipid-based nanotherapeutics, we hypothesized that LNPs and LPXs could present different phospholipid packing density and conformation and possess a unique mechanism of transfection as well as recognizably different physicochemical, morphological, and structural properties. In this chapter, the data obtained from characterization studies of two different lipid carrier systems for siRNA delivery will be introduced and the findings will be compared with the formulations in bulk mixing as shown in Chapter 3. It must be noted that conventional and stealth liposomes used in the complexation study to produce LPX (second approach) were synthesized in a chaotic advection-based device.

- ***Chapter 6*** – *Microfluidic platforms to deliver siRNA into spheroids as a biomimetic screening model of in vivo tumour microenvironments*

In this chapter, the development of static and continuous-flow microfluidic cell culture platforms that mimic *in vivo* conditions for a more precise drug testing will be introduced. The platforms are used to form spheroids and transfect them using lipid-based nanotherapeutics for the delivery of siRNA. The challenges that were encountered during the design of the microfluidic platforms, formation of spheroids, transfection studies, and the strategies followed to overcome these challenges will be given in detail. Finally, advanced microscopy techniques to morphologically characterize spheroids will be presented. Future perspectives to improve the precision of the biomimetic system will be also provided.

- ***Chapter 7*** – *Future perspective and conclusion*

In this chapter, all the obtained results will be interpreted to discuss how the project contributed to the scientific community to improve research in cancer treatment using lipid-based nanotherapeutics for the delivery of novel genetic machinery. Moreover, possible strategies to improve the efficiency of the microfluidic platform for further use in cancer research will be commented on.

- ANNEX I – Supplementary material of the research paper entitled "*High-throughput conventional and stealth cationic liposome synthesis using a chaotic advection-based*

microfluidic device combined with a centrifugal vacuum concentrator" and the results obtained from the synthesis of folate-functionalized liposomes.

❖ ANNEX II – Supplementary material of the manuscript entitled "*Static and dynamic microfluidic 3D cell culture to mimic in vivo siRNA penetration into solid tumor models.*"

References

1. Cavalli, G. and Heard, E., 2019. Advances in epigenetics link genetics to the environment and disease. Nature, 571(7766), pp.489-499.
2. Colombo, S., Beck-Broichsitter, M., Bøtker, J.P., Malmsten, M., Rantanen, J. and Bohr, A., 2018. Transforming nanomedicine manufacturing toward Quality by Design and microfluidics. Advanced drug delivery reviews, 128, pp.115-131.
3. Cui, X., Hartanto, Y. and Zhang, H., 2017. Advances in multicellular spheroids formation. Journal of The Royal Society Interface, 14(127), p.20160877.
4. Fire, A., Xu, S., Montgomery, M.K., Kostas, S.A., Driver, S.E. and Mello, C.C., 1998. Potent and specific genetic interference by double-stranded RNA in Caenorhabditis elegans. Nature, 391(6669), pp.806-811.
5. Friedmann, T. and Roblin, R., 1972. Gene therapy for human genetic disease?. Science, 175(4025), pp.949-955.
6. Grimaldi, N., Andrade, F., Segovia, N., Ferrer-Tasies, L., Sala, S., Veciana, J. and Ventosa, N., 2016. Lipid-based nanovesicles for nanomedicine. Chemical Society Reviews, 45(23), pp.6520-6545.
7. Guidolin, K. and Zheng, G., 2019. Nanomedicines Lost in Translation. ACS nano.
8. Gupta, P., Pérez-Mancera, P.A., Kocher, H., Nisbet, A., Schettino, G. and Velliou, E.G., 2020. A Novel Scaffold-Based Hybrid Multicellular Model for Pancreatic Ductal Adenocarcinoma—Toward a Better Mimicry of the *in vivo* Tumor Microenvironment. Frontiers in Bioengineering and Biotechnology, 8, p.290.
9. Turajlic, S., Sottoriva, A., Graham, T. and Swanton, C., 2019. Resolving genetic heterogeneity in cancer. Nature Reviews Genetics, 20(7), pp.404-416.
10. Zhang, H., Zhu, Y. and Shen, Y., 2018. Microfluidics for cancer nanomedicine: from fabrication to evaluation. Small, 14(28), p.1800360.

CHAPTER 2. MICROFLUIDICS TOWARDS THE SYNTHESIS OF LIPID-BASED NANOTHERAPEUTICS FOR GENE DELIVERY

1. Gene Therapy – Overall concepts

The investigation of genetic disorders and their treatment methods have been a great challenge to the scientific community for decades. Intense systematic investigations carried out in interdisciplinary fields of medicine for a better understanding of the molecular basis of these diseases led to the discovery of novel techniques. Eventually, in the 1970s, the nuclei of cells were transformed by using viral genome (Sambrook et al. 1968), as one of the groundbreaking advances achieved to pave the way to the clinical trials of gene therapy, which is a broad strategy for the treatment of genetic diseases by providing, blocking or editing (i.e. ZFNs, TALENs, and more recently CRISPR/Cas genome editing tools) individual genes or gene products (e.g. proteins) (Dai et al. 2016). Gene therapy is considered a treatment method with high sensibility regarding its ethical considerations. Approval of several protocols is strongly required by worldwide committees such as Gene Therapy Advisory Committee (GTAC), the Recombinant DNA Advisory Committee (RAC), Medicines Control Agency, and Food and Drug Administration (FDA). These ethical considerations exist due to the great risk that patients are being subjected to since the treatment might be without any benefits or even fatal. Therefore, the techniques should be improved to produce therapeutic agents that carry less risk and more granted benefits. In this case, the development of novel vector systems that meet these requirements becomes indispensable. In 1990, after the first clinical trial of gene therapy using a viral vector to treat adenosine deaminase (ADA) deficiency (Blaese et al. 1995), there were much concerns regarding the safety and efficiency of the use of viral vectors in gene therapy, therefore, particular attention was drawn to the non-viral materials as a potential group of vectors for gene/drug delivery to address most of the limitations of viral vectors.

2. Nucleic acids in gene therapy

Many nucleic acids have been employed for gene expression (Day & Tuite, 1998). This expression can be controlled at several levels through transcriptional and post-transcriptional mechanisms. One of the first methods studied for the introduction of exogenous genes into animal cells is the use of naked DNA (Wolff et al., 1990), which presents

advantages and disadvantages when compared to other gene delivery strategies (Luo & Saltzman, 2000). However, the use of naked DNA has been limited mainly due to immunization studies (Herweijer & Wolff, 2003). The most common form of DNA used for this purpose is plasmid DNA (pDNA), which is a circular, double-stranded molecule, physically separated from chromosomal DNA and ranges in size from a few thousand base pairs to more than 100 kilo-bases (kb) (Lodish et al., 2000).

In addition to pDNA, several synthetic and chemically modified nucleic acids called oligodeoxyribonucleotides (ODSs) have been investigated to block or restore the activity of defective genes. These ODSs in the nucleus can bind to pre-mRNA that is genetically defective and alter their processing pattern, allowing the production of novel functional proteins (Scholz & Wagner, 2012). After the use of ODSs, new oligonucleotides that correct the defective genes by specific binding began to be used. However, these double-stranded oligonucleotides, which are also a type of RNA, with more than 30 base pairs (bp), elicit immunological responses. Therefore, the use of short RNA molecules, called siRNA (small interfering RNA, silencer), has become a promising tool for post-transcriptional knock-down of defective genes (Tuschl, 2001). These molecules control the silencing process called RNA interference (RNAi).

3. Silencing process (RNA interference – RNAi) intermediated by small interfering RNA (siRNA)

RNA interference (RNAi), in many organisms, is a natural process of post-transcriptional silencing of specific genes and can be used as a technique to reduce the level of gene expression (Jain, 2008). Since the discovery of RNAi by Andrew Z. Fire and Craig C. Mello (Fire et al., 1998), who won the 2006 Nobel Prize for Medicine for this discovery, billions of dollars have been invested in gene silencing in humans for therapeutic purposes (Whitehead et al., 2009). The process of RNAi in the host genome is highly effective for gene silencing in various experimental organisms (Zhao et al. 2016).

siRNA is a double-stranded RNA (dsRNA) with a size ranging from 21-25 base pairs and has the biological function that rapidly degrades messenger RNA (mRNA), which has the complementary sequence (Herweijer & Wolff, 2003) (Figure 2.1). Studies in mammalian cell

culture have identified that siRNA causes a less immunogenic response, which makes the use of these molecules more advantageous (Elbashir et al., 2001) when compared to other nucleic acids. A study carried out on mice injected with the cationic liposome/siRNA complex demonstrated that some specific sequences of siRNA may activate the innate immune response that may bring benefit to cancer treatment (Sioud & Sorensen, 2003).

As a consequence, there has been a growing number of publications in the scientific literature related to the use of the siRNA as a promising tool in functional genomics to discover the complete mechanism of silencing. However, the use of siRNA in therapeutic applications for disease prevention and treatment requires knowledge of accessibility of the specific target sequences, as well as its delivery process into the target cell and its stability in both extracellular and intracellular medium (McManus & Sharp, 2002). After intense studies, two RNA-I drugs have been recently approved by FDA. The first RNAi drug approved by FDA was Alnylam's Onpattro used for the treatment of the polyneuropathy of hereditary transthyretin-mediated amyloidosis in adults. The second one was Alnylam's Givlaari (givorisan) for acute hepatic porphyria.

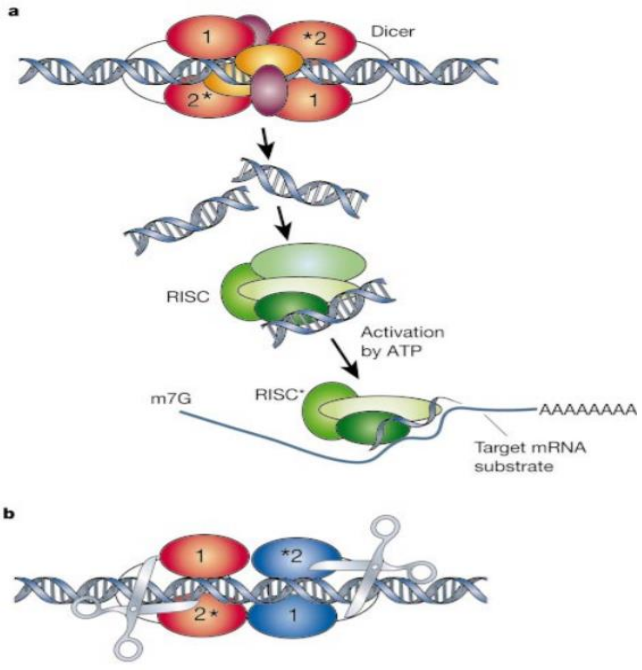

Figure 2. 1. The principal mechanism of RNA interference. RNAi is firstly activated by the Dicer enzyme (RNAse III family of enzymes, a dimeric enzyme, and each Dicer molecule has five domains), which transforms double-stranded RNA into 21-25 nucleotide small

interfering RNAs. The siRNAs are incorporated into a multicomponent nuclease, RISC (shown in green). RISC then uses the unwound siRNA as a guide to substrate selection (a). Representation of Dicer binding and cleaving dsRNA (b) (Adapted from Hannon, 2002).

The use of siRNA in almost all fields of biomedical research has shown great advantages: (i) siRNA is a potent and robust inhibitor, which can be activated by natural processes and (ii) RNAi allows the regulation of individual genes as a powerful tool and can generate therapeutic benefits by reversing the pathogenic effects caused by the over-expression of these genes. Not surprisingly, cancer-related researches have become the most exciting and dynamic area for the application of siRNA (Lu & Woodle, 2005).

siRNAs are much smaller than plasmid DNA (pDNA), so vascular extravasation and cellular uptake can be facilitated. siRNAs demonstrate their mechanism of action in the cytoplasm. In this way, delivery into the nucleus as a more time-consuming step is avoided, which is an additional barrier in case pDNA is used. Barriers for delivery to the cytoplasm, in addition to lysosomes, include the extracellular matrix and cell membrane. It is still unclear how long the effect of the silencing process lasts after a single dose of siRNA. The high selectivity of siRNA to target sequences in the genome brings advantages to gene therapy. Despite the greater facility of siRNA uptake by cells (compared to pDNA), it is essential to increase their stability in the bloodstream or extracellular matrix and eliminate nonspecific interactions with the immune system to improve efficiency in gene therapy (Herweijer & Wolff, 2007).

As mentioned above, the efficacy of the gene expression depends on several extra and intracellular barriers (Degors et al. 2019). The therapeutic effect of naked DNA only occurs if the nucleic acid reaches the nucleus of the cells, which is considered a great challenge. In the case of siRNA, the target delivery is the cytosol. This challenge can be overcome by using nucleic acid delivery systems such as viral or non-viral vectors. The use of viral vectors to introduce into animal cells has been extensively studied (Li & Samulski, 2020) to explore the ability of these systems to deliver material into cells. The most frequently used viral vectors are retroviruses, adenoviruses, herpes virus, etc. (Manikandan et al. 2019). Although virus transfer into target cells is highly efficient, viral vectors generally

require more laborious procedures for preparation and purification. As a disadvantage, gene transfer with a virus can result in recombination that produces a harmful infectious form, which can induce an immune response and cause side effects (Terova et al. 2018). Due to increasing concerns about the toxicity and immunogenicity of viral vector delivery systems, the use of other strategies such as non-viral vectors has become desirable and advantageous (Bordet et al. 2019).

In this circumstance, gene transfer for the treatment of human diseases can be exploited using non-viral vectors, in which genetic materials can be administered efficiently, safely, and repeatedly. Thus, the use of synthetic colloidal systems for gene delivery has become essential to comply with all the requirements. Almost all DNA delivery systems developed up to now - from calcium phosphate to artificial lipids - involve two components: the transfection reagent and the genetic material to be delivered. They still have low efficiency when compared to viral vectors, but present lower health risk (Nyamay'Antu et al. 2019). Therefore, the discovery of new techniques that improve the efficiency of gene delivery for gene therapy is crucial.

4. Lipid-based vesicular vector system

The cells are highly organized units of life and maintain their integrity due to the efficient compartmentalization of the cell membrane that allows essential biochemical functions to take place (Honigmann and Pralle, 2016). The complex structure and principal role of cell membranes have promoted the development of novel vesicular structures using natural or synthetic molecules to mimic the cell membrane functions (Figure 2.2). However, this immense complexity of the cell structure, which is the product of billions of years of evolution, has always been an obstacle for mimicking; hence, simplified and controllable models have been introduced to carry out these functions (Rideau et al. 2018). These models are based on the membrane-building blocks, the phospholipids, and they are also used for the design of lipid vesicles based-vectors.

Lipid-based vesicular vectors are mostly composed of phospholipid molecules and due to the poor solubility characteristics in aqueous solution, they tend to self-assemble into bilayers in excess of water. However, such formation highly depends on the type of lipids,

which should be mixed at a certain ratio to form liposomes. During the aggregation process, thermodynamic and energetic stabilities of the bilayer show significant alterations. During the lipids hydration process, bilayer sheets are formed, and the energy instability can be associated with its edge, where the hydrophobic tails are in exposure to water and are proportional to the perimeter of the bilayer sheet. As their natural behavior, the phospholipids tend to minimize this energy by closing in a bilayer patch, forming the vesicles. When the edge energy exceeds the bending energy, the smallest size of a vesicle is achieved (Huang et al. 2017). One must notice that there is also the energy required to close the disc into vesicles and this energy is also associated with the elastic energy which is required to bend the disc (Zook and Vreeland, 2010). Depending on several factors (i.e. phospholipid concentration, amount of water, etc.), this process can lead to the formation of either unilamellar (ULV) or multilamellar vesicles (MLV). Consequently, the encapsulating volume of vesicles varies depending on this formation. Approximate volume of small unilamellar liposome varies between 10-15 and 10-13 μL whereas this volume for large unilamellar vesicles can be between 10-13 and 10-9 μL and for the giant unilamellar vesicles (GUV) as big as 10-3 μL (Rideau et al. 2018). Hence, understanding the mechanics that underlie vesicle formation is of extreme importance since it will help to optimize the surface engineering of these vesicles as well as the amount of drug/gene to be incorporated. Moreover, incorporation of some molecules (i.e. bile salts, amine groups, acrylate tail, etc.) into the bilayer of these vesicles gives them additional characteristics and these molecules will be addressed along with the text in terms of chemical structure to better understand their attachment mechanism.

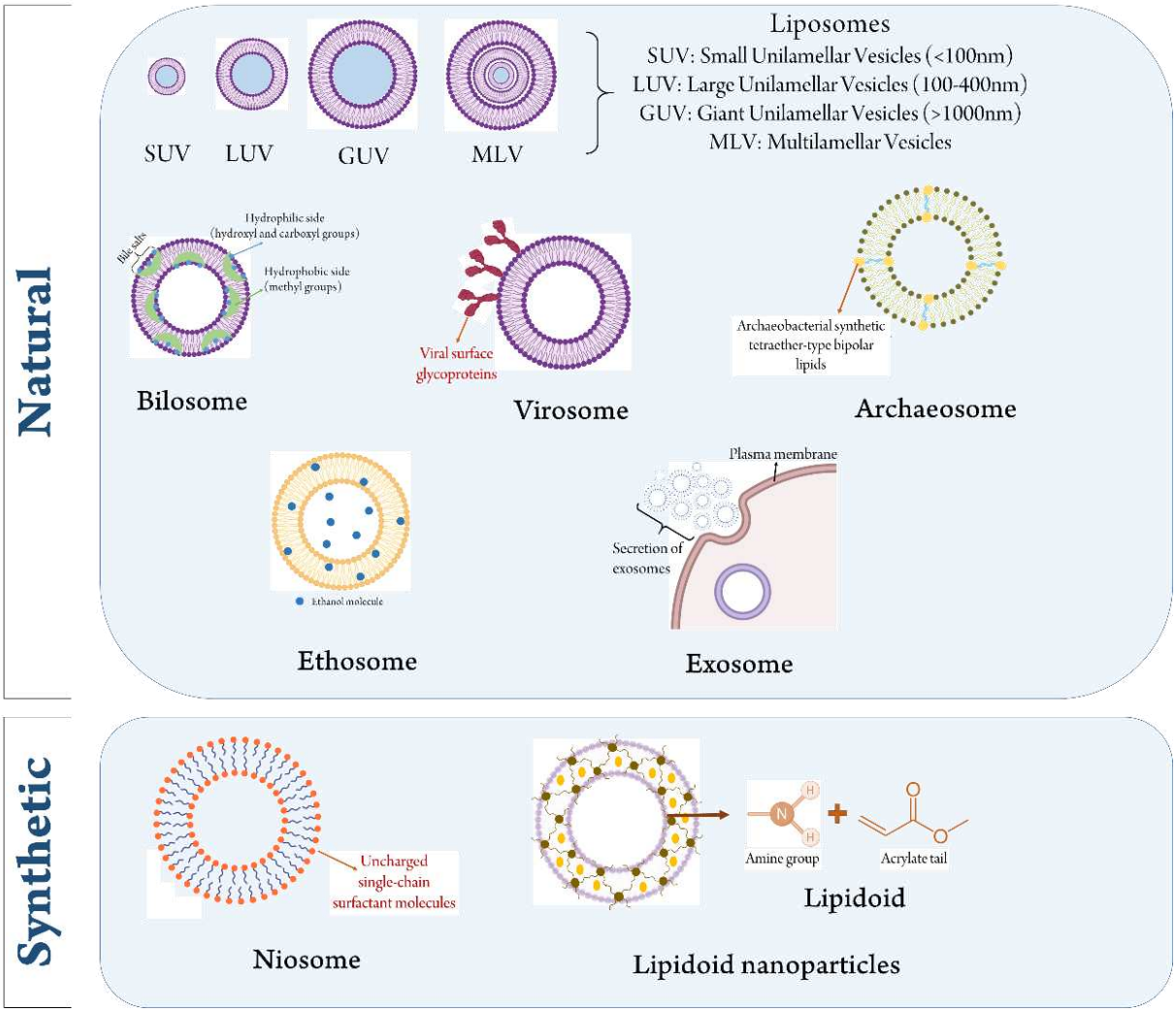

Figure 2. 2. Non-functionalized natural and synthetic vesicular vector systems used for gene delivery.

4.1. Liposomes

Several synthetic vesicles have been formulated for gene delivery applications. Liposomes are one of the first groups of the colloidal system designed to mimic the cell membrane. Liposomes are spherical lipid assemblies consisting of polar hydrophilic head groups and non-polar hydrophobic tail to form one or more phospholipid bilayers. This promising vesicular vector was first discovered by Alec D. Bangham in 1965 as swollen phospholipid systems (Bangham et al. 1965) and since then, liposomes have been widely used in several drug and gene delivery formulations as a non-viral vector (Khadke et al. 2019; Marwah et al. 2019).

The most promising and widely-used lipid-based vector system is liposomes. The size of these vectors ranges from a few nanometers to several micrometers (Bozzuto and Molinari, 2015) (Figure 2.2). The vesicular aggregation offers advantages since in most cases it mimics the cell membrane, interacting easier with cells. They are supramolecular colloidal systems consisting of one or more amphiphilic lipids, whereas the most used are the phospholipids. These vesicular systems tend to self-assemble into spherical bilayers when amphiphilic molecules with a hydrophilic head and a hydrophobic chain at opposing ends are exposed to an aqueous solution (Gregoriadis and Perrie, 2010). They have the capacity to entrap or incorporate different solute molecules such as genetic material consisting of hydrophilic nitrogen bases or chemotherapeutic drugs, which can possess either hydrophilic or hydrophobic nature. Due to the chemically-active substituents or moieties present within vesicular vector systems and their high affinity to several chemical groups, engineering with specific chemical ligands (i.e. aptamers, peptides or antibodies, etc.) steps forward as an important and rapid strategy to enhance their therapeutic efficiency and consequently, increase their success rate when used in clinical trials.

4.2. Functionalization of lipid-based vesicular vector systems

The synthesis of vesicle systems allows the incorporation of drugs and genetic material for drug delivery. In the case of genetic material, vesicles can be designed to have a cationic characteristic to properly retain the nucleic acid into the structure. The net positive charge of the non-viral vector is the driving force to the cells that have an anionic characteristic. However, this characteristic is not enough for proper and efficient *in vivo* gene delivery due to the lack of specificity. An alternative to overcome this drawback is the functionalization of vesicular carriers. It is highly required in order to enhance the target-specific delivery to achieve a desired therapeutic outcome. Functionalization is mostly carried out by the incorporation of specific ligands into the inner or outer surface of vectors. Several factors (i.e. target cell type, chemical properties of both ligand and vector as well as the affinity between both, etc.) should be precisely taken into account in order to select proper ligand to synthesize and incorporate into vectors. In this topic, the most common ligands, which have been used to functionalize these promising vector systems, and their expected therapeutic outcome will be discussed.

2.1.1. PEG-functionalized liposomes for passive targeting

Non-functionalized vesicular vector systems are most likely to suffer from non-specific electrostatic interaction with cell/tissues or proteins present in the bloodstream (He et al. 2010). This non-specific interaction will lead to random uptake of the vector-gene complex by non-target cells, causing an immune response, consequently, decreasing the half-life of the gene carrier system (Ditto et al. 2009). Hence, lipid-based vectors should be functionalized with specific molecules to provide long-circulating characteristics by preventing their uptake (stealth effect) by mononuclear phagocyte system (MPS); a process called opsonization (Immordino et al. 2009). The most commonly-used molecule known to give stealth characteristics to the vesicular vectors by its inclusion is an uncharged, hydrophilic polymer "poly-(ethylene glycol)" (PEG) (Zhang et al. 2012). Surface PEG coating provides a steric hindrance to the vector by occupying its surface and mask the surface charge since PEG presents almost neutral zeta potential (Semple et al. 1989). Moreover, due to the hydrophilic characteristics of the PEG molecule, the surface becomes robustly hydrated and this creates a hydrophilic barrier on the surface of the vector system (Bergström et al. 1992). Consequently, this barrier slows down or sterically prevents protein adsorption (Figure 2.3), increasing the success rate of drug/gene delivery.

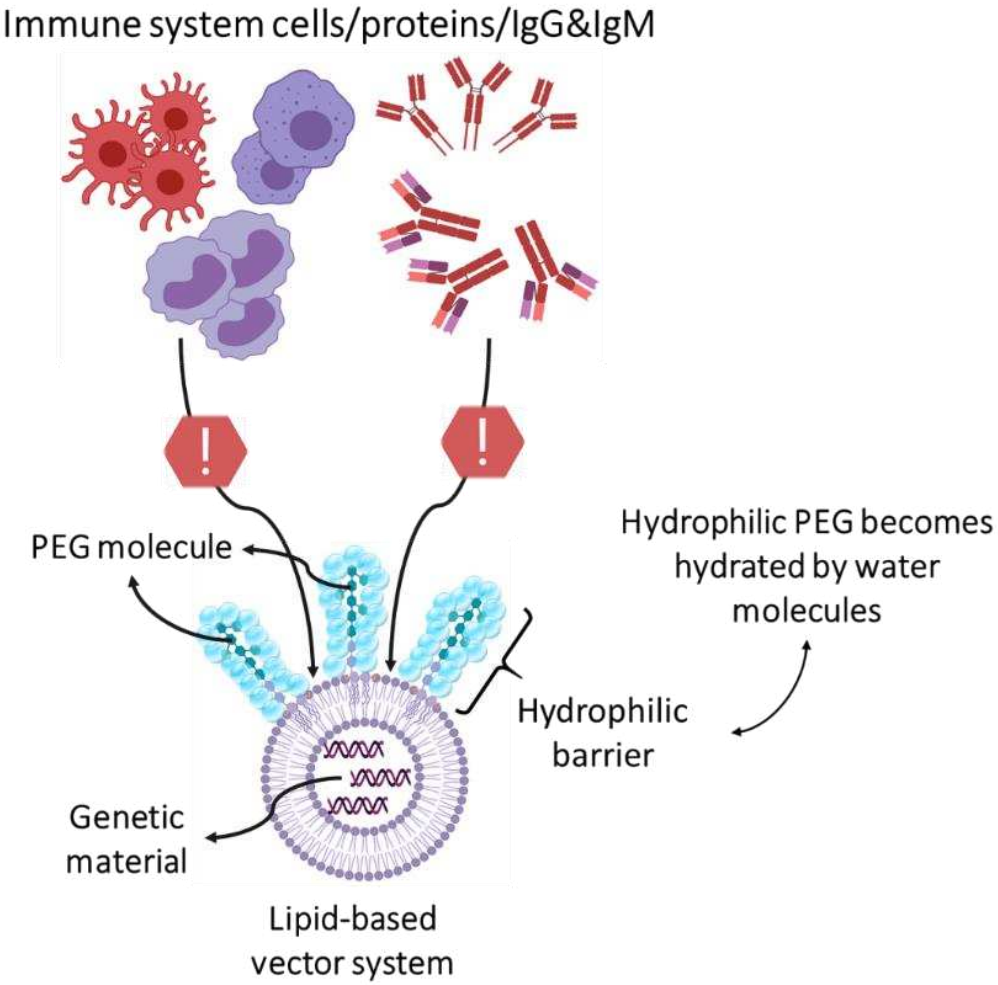

Figure 2. 3. The steric hindrance effect of PEG on the lipid-based vector, protecting against immune system cells or plasma proteins to increase circulation time in the blood. PEG chain length and quantity are the main factors that influence the reduction of protein adsorption (Eş et al. 2020, in preparation).

Around the early 1970s, Frank F. Davis and his team discovered PEG and PEGylation processes. Shortly after, the first promising use of PEG in gene/drug delivery was shown as a part of this work in a patent application (US patent code: US4179337A). Polypeptides were coupled to PEG at varying molecular weight (MW ranging between 500 and 20.000 Daltons) to protect polypeptides from activity loss and eliminate their immunogenicity when injected into the mammalian circulatory system (Abuchowski et al. 1977). Afterward, several investigations have shown that the circulation half-life of vector system strongly depends on the particle size and surface charge of the carrier, quantity of PEG molecules to coat surface of the vector, and, most importantly, MW (chain length) of PEG (Zhang et al. 2012). However,

the relation between MW and protein adsorption remains unclear. But, it was hypothesized that PEG's chain folding and water binding capacity explains why there is a critical MW range, below which PEGylated vectors present fewer stealth characteristics (Bergström et al. 1992). In other words, surfaces with PEG at MW varying between 300 and 1000 couldn't resist the protein adsorption; but, as the MW increases, it binds the secondary water within the coil and acts like a water-filled balloon, consequently, repels the proteins that are trying to bond to the surface (Hoffman, 2017). These characteristics are essential to optimize during the design of further vesicular vector system prior to the clinical applications.

For a successful gene delivery to treat genetic diseases such as cancer, the issue related to the use of PEG "PEG dilemma" must be addressed. Although PEG has promising applications in gene delivery, surprisingly, several studies reported the existence of antibodies (anti-PEG) that could recognize PEGylated products and results in both immunogenic and antigenic reactions in the body, consequently, limit the therapeutic efficiency. PEGylation, depending on the molecular weight and total content in the formulation, may strongly inhibit cellular uptake and endosomal escape (Hatakeyama et al. 2011). Moreover, PEG carries functional hydroxyl groups (-OH) as electron donors, which interact with hydrophobic compounds (or lipid bilayer of vector system) through hydrogen bonds, consequently, it destabilizes the lipid bilayer (Cao et al. 2012). Therefore, new alternatives have been considered to replace with PEG to be employed in gene delivery. Recently, zwitterions, which are polyelectrolytes that contain both positively and negatively-charged groups (the surface charge is internally balanced), are considered efficient candidates in creating different non-viral vector systems with stealth properties. PEG insertion usually contributes to the delivery systems with passive targeting properties since it is strictly associated with the circulation time of the vector system, thus, PEG is mostly used in combination with other molecules that generate active targeting.

5. Microfluidic technology

Microfluidics is a multidisciplinary field that operates devices in a micrometric scale and works with small amounts of fluids. The fluid-dynamic characteristics imposed in these systems allow laminar flow, where diffusion is the predominant process, allowing the control of chemical reagents, cells, lipids, nucleic acids in space and time (Whitesides, 2006; Baek et

al., 2011). Microfluidics uses technologies that involve the flow of single or complex fluids, mono- or multiphase, that circulate in artificial microsystems designed by using a specific material. Microfluidics has great advantages over conventional systems such as the use of lower reagent volume, use of low-cost material, advanced experimental control, reduced reaction time, minimization of mass and heat transfer effects, low energy consumption, real-time data acquisition, easy automation, and high throughput reactions and processes (Halldorsson et al., 2015).

A widely used material for the construction of microfluidic devices is polydimethylsiloxane (PDMS), which is an elastomer (Lee et al., 2013). PDMS elastomers such as Slygard 184® can be found commercially and widely used in soft lithography for microfluidic applications (Lovchik & Wolf, 2011). PDMS is commonly used for cell culture because of its low cytotoxicity, its easy use, permeation capacity of gases like O_2 and CO_2, and optical transparency (Kamei, 2013).

Since the initial phase of microfluidics (the 1990s), biological sciences and chemistry have become the main fields of application (Manz et al., 1990) and then the biotechnological processes have gained great importance as a field of application and are exclusively linked to microfluidics. One of the main applications of microfluidics is that it allows a single-cell analysis. Microfluidic techniques have great potential to improve these conventional techniques (flow cytometry and automated microscopy) in the analysis of individual cells (Gomez, 2008). Microfluidics also has many advantages for PCR (polymerase chain reaction), such as decreased manufacturing costs, decreased DNA amplification time, and reduced consumption of reagents and PCR samples (Kumar, 2010). Recently, microfluidic technologies have been widely used to form spheroids/organoid models as an effective biomimetic screening model that mimics *in vivo* microenvironments. The testing of new drug/gene formulations can be highly precise and increase the success rate of drug approval. The materials used to construct such devices possess excellent optical transparency so the visualization under the microscopy can be carried out easily.

Thus, microfluidics emerges as a potential to significantly change the way modern biology is conducted (Beebe et al., 2002), allowing the development of new tools/devices that contribute substantially in the medical and biological areas (Hansen & Quake, 2003; Yager et

al., 2006; Whitesides, 2006). The micrometric devices designed to perform specific tasks have demonstrated superiority over their macroscale analogs and in many cases, it allows applications that would not be feasible on the macroscale (Cui et al. 2019). Obtaining nanoparticles and liposomes in microfluidic systems has also been explored in recent years, representing a new area of research.

5.1. Microfabrication techniques

Currently, several microfabrication techniques and methods are available and highly accessible for the microfluidics community due to the increasing research efforts and interest in this field (Guckenberger et al. 2015). Such techniques and methods significantly profit the rapid advancement and expansion of microfluidic platforms in a variety of fields for both academic and industrial purposes. The design criteria of the microfluidic platforms, in which nanotherapeutics are synthesized and multicellular tumor spheroids are formed and analyzed, must be well studied.

Before proceeding with widely-used microfabrication techniques, it is important to explain the molding process in microfabrication techniques. Hence, understanding the basic concept of negative and positive molds in molding & casting processes is crucial. Negative mold, so-called master mold, is the mold, in which a liquid polymeric solution (i.e. PDMS) is poured inside to cast them. A positive mold is an exact replica of the desired objects. The basic concept of molding and casting is shown in Figure 2.4**.**

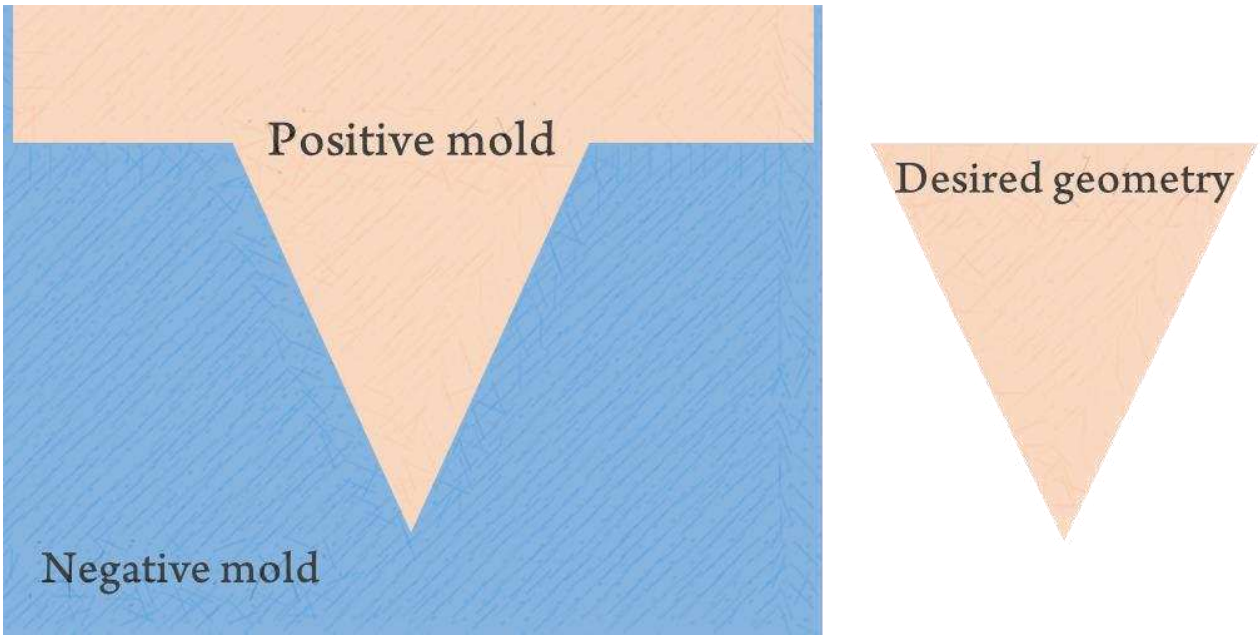

Figure 2. 4. Schematic representation of negative mold (master mold), positive mold, and desired geometry.

2.1.2. Photolithography

Photolithography is an optical process to transfer patterns from a mask onto a substrate using visible ultraviolet (UV) lights as a radiation source (Ma et al. 2010). Photolithographic fabrication steps involve wafer cleaning, barrier layer formation, photoresist application, soft baking, mask alignment, exposure to UV light followed by hard-baking (Sivasankar, 2008). First, the wafers are chemically cleaned to remove any small particles from the surface. Afterward, silicon dioxide (SiO_2) is deposited on the wafer's surface to form a SiO2 layer. The photoresist material is then poured on the surface of the wafer and the surface is coated with photoresist using high-speed centrifugal whirling process. This step is known as spin coating and performed to form a very thin and uniform layer on the surface of the wafer. In the soft-baking step, all of the solvents are removed from the photoresist coating. This step is very crucial as the photoresist coating becomes photosensitive only after the soft-baking process. After soft-baking, the mask is aligned with the wafer to transfer the desired pattern onto the surface of the wafer and then photoresist material is exposed to high-intensity UV light. After the UV light exposure, the process is finished with hard-baking. This process is highly required to harden the photoresist and enhance the adhesion of the photoresist to the wafer surface.

The photolithography process has been employed as a major technique for the microfabrication of microfluidic devices designed for different purposes. This process is usually carried out in costly photolithographic facilities (usually in a clean room) with a specialized lighting system to be able to work with UV-sensitive materials such as SU-8. Although photolithographic facilities require high capital and maintenance costs, this technique usually results in a more precise pattern construction compared to other techniques, which will be introduced in this chapter.

2.1.3. Soft lithography

Soft lithography has become a prominent technique for fabricating structures from the micrometer to the nanometer scale. It encompasses the fabrication of the elastomeric molds to create very precise features with geometry defined by the negative mold. The technique involves casting a liquid elastomer precursor against a topographically-patterned mold that is fabricated with photolithography or other microfabrication technique. The soft lithography technique is mostly inexpensive and very simple to employ. Due to recent advances in material science, several polymers have emerged, but poly(dimethyl-siloxane) (PDMS) is still the most widely used silicon-based organic polymer. PDMS has several advantages over other polymers such as high flexibility, durability, good biocompatibility and chemical inertia, low surface energy, which allows reversible bonding, and most importantly, gas permeability, hydrophobicity, and optically transparency make it extremely attractive to develop lab-on-a-chip systems, biosurfaces, microreactors, sensors, and microelectromechanical systems (MEMS).

2.1.4. Micromilling: A method for prototyping of microfluidic devices

Computer numerical control (CNC) is a system, in which software controls a machine tool, and has been widely used in the manufacturing of microfluidic devices. Micro-milling is an effective microfabrication method that creates patterns/features at microscale through cutting tools that remove material. This technique requires a complex programming system. In this software, it is essential to optimize feed and speed parameters such as spindle and surface speed, plunge feed-rate, and feed per revolution. And the movement of the milling tool should be set carefully. Although microfluidic devices fabricated with this technique have been employed for different applications (mainly cell culturing, imaging, and drug

testing), the method is underused due to the limitations such as high start-up cost, lack of availability of cutting tools with small resolution and polymers, the requirement for large lab space and technical skills (Guckenberger et al. 2015). Moreover, micromilling tools cannot precisely cut arbitrary shapes. Despite these drawbacks, the technique seems highly potential for automated microfluidic device fabrication. It allows the fabrication of 3D design with multi-height structures. The materials (e.g. PMMA) can be easily milled into a microdevice in a very short time, reducing overall turn-around time from design to prototype.

2.1.5. Laser ablation

Laser ablation is a process of removing atoms from a solid material using intense, continuous, or pulsed laser beams with high fluency and short-wavelength (Shaegh et al. 2018). There are several commercially-available laser engravers. Laser ablation, as a rapid prototyping method, is highly effective in microfluidic technology to fabricate whole-thermoplastic chips. Thermoplastic materials possess excellent physical and chemical properties such as inherent robustness to mechanical deformation and resistance to temperature and chemicals. Hence, a variety of thermoplastic materials such as poly(methyl methacrylate) (PMMA), polycarbonate (PC), polystyrene (PS), or cyclic olefin (co)polymer (COP) have been used in microfluidics to fabricate advanced microchips. Since they are highly resistant to high temperatures, they are easily used in thermal-bonding processes to create microfluidic devices. Comparing to the micro-milling technique, laser engraver is easier and faster to operate. More importantly, the design can be drawn in 2D in one of the CAD software (Autodesk AutoCAD or Adobe Illustrator) and upload to the PC, of which laser engraver is connected. The laser engraver has different laser configurations. The time of the laser as well as the intensity vary depending on the thickness and type of the polymer.

2.1.6. Stereolithography: 3D printing of highly-precise molds

The techniques that have been shown so far based on the removal of material from polymers. However, STL is an additive manufacturing technology, commonly known as vat photopolymerization or resin 3D printing (Miri et al. 2018). In principle, a light source inside a 3D printer works similar to a laser or a projector to cure liquid resin material into a hardened plastic. Resins are light-reactive thermoset materials and when they are exposed

to a light source with specific wavelengths, the short molecular chains in their chemical structure join together and consequently polymerize both monomers and oligomers into rigid structures. Different from the other two techniques, the CAD design of the software does not require complex CNC programming, and the design is drawn in 3D geometry using SolidWorks or Autodesk Inventor. The drawings must be saved as ".STL" format in order to be recognized by the 3D printer.

One of the most important criteria in such a fabrication technique is the proper selection of resin material, which will be used for mold production. Several resin materials such as standard, engineering, dental, and ceramic resins are commercially-available for high-resolution rapid prototyping. Each resin has different characteristics such as rigidity, light transmission, biocompatibility, and temperature resistance. After 3D printing negative molds, the resin is not completely formed with desired properties. Hence, an additional post-curing process of the resin-based molds should be carried out. The post-curing process involves both solvent and UV-light treatments. These parameters should be also investigated for a successful curing process of negative mold and post-curing conditions vary depending on the resin material.

5.2. Microfluidic approaches for lipid-based nanotherapeutics synthesis for gene delivery

Since the reveal of favorable functions of liposome as promising non-viral carriers, many studies have been conducted to expose its new utilities in gene delivery. Conventional liposomes production has been well-established as a bulk system in terms of energetics, kinetics, and characterization. The production can be performed simply by mixing two or more phases (liquid-liquid or liquid-solid), provoking self-assembly of spherical membranes (Patil and Jadhav, 2014). However, this kind of production is highly laborious. Recently, conventional methods for liposome production and complexation studies with genetic materials have been dismissed, and these techniques have been substituted with new technology platforms, in particular with microfluidics-based liposome generation platforms (Dimov et al. 2017).

Recent advances in microfluidics have created new perspectives for the field of gene delivery and gene therapy. The environment within microfluidic systems allows precise control and optimization of various processes, since typical microchannel sizes vary in the range of 10 to 100 μm, and flow rates are between 10 and 1000 nl/s. This leads to one of the most important applications of microfluidics, which is the synthesis, formation, and self-aggregation of nanoparticles and liposomes. In general, microfluidic technology allows the development of processes that allow the generation of nanoparticles with reproducible physicochemical properties in terms of size and polydispersity (Joanicot & Ajdari, 2005). Many nanoparticles, such as quantum dots, metallic colloidal particles, and, liposomes were formed using microfluidics (Jahn et al., 2008). The formation of liposomes in microfluidic systems is a derivation from the classical ethanol injection method. Basically, the lipids are dispersed in ethanol (organic phase) which is compressed hydrodynamically by two aqueous streams. As the flow occurs, the diffusion of ethanol to water occurs (and vice versa), and consequently the solubility of the lipids decreases. Thus, lipids initiate the auto-aggregation process, leading to the formation of phospholipids bilayer fragments and later in liposomes (Balbino et al., 2013).

The formation of liposomes in microfluidic systems is a derivation from the classical ethanol injection method. Briefly, the lipids are dispersed in ethanol (organic phase) which is compressed hydrodynamically by two aqueous streams. As the flow occurs, the diffusion of ethanol to water occurs (and vice versa), and consequently the solubility of the lipids decreases. Thus, lipids initiate the auto-aggregation process, leading to the formation of phospholipids bilayer fragments and later in liposomes (Figure 2.5) (Balbino et al., 2013). The size of the liposomes was controlled by adjusting the flow rate and with this technique, it was possible to obtain liposomes with desirable polydispersity and the diameter ranging from 100 to 300 nm.

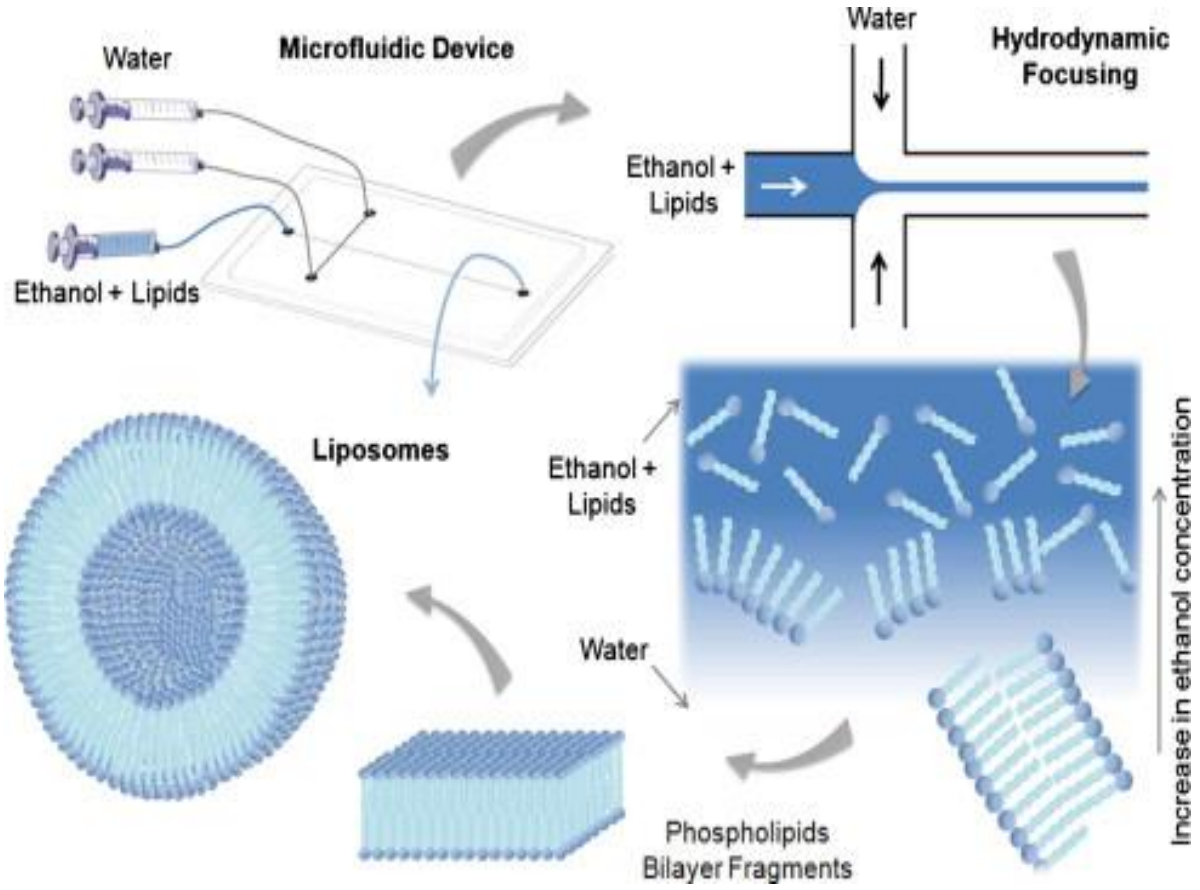

Figure 2. 5. Schematic diagram representing the formation of liposomes in a microfluidic device through the hydrodynamic focusing technique (Adapted from Balbino et al., 2013).

Previously, our research group evaluated the continuous production of pDNA/CL complexes using microfluidic devices as illustrated in Figure 2.6 (Balbino et al., 2013). In this work, two different microfluidic devices were used (simple hydrodynamic focusing (HF), Figure 2.6A, and HF followed by barriers to increase the degree of mixing, Figure 2.6B). Considering the conventional bulk complexation method as a reference, the two types of devices were capable of producing CLs/pDNA complex with size (130-150 nm) and controlled polydispersity index (0.2-0.3) and transfect HeLa cells *in vitro*. The conventional device reached the same level of transfection with bulk method; however, the device developed with barriers had a lower level of transfection, suggesting that the DNA/LCs association was altered by the mixing pattern.

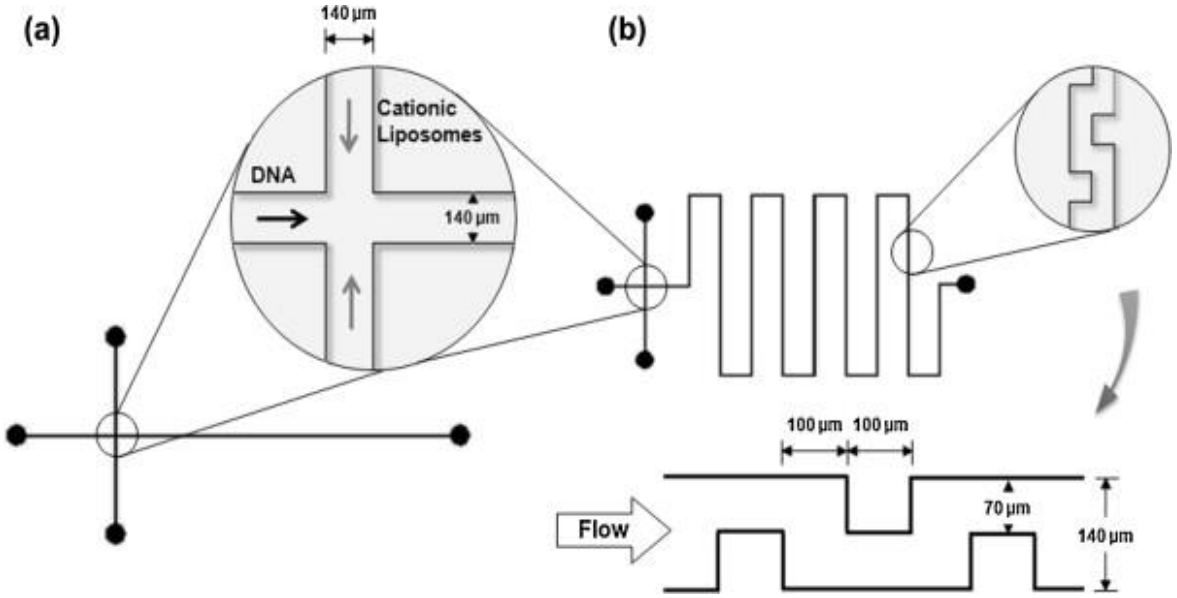

Figure 2. 6. Schematic diagram of the microfluidic device based on hydrodynamic flow focusing (A); the device with barriers in the microchannels (B). The microchannels are 140 µm wide and 100 µm deep (Adapted from Balbino et al., 2013).

In turbulence flow, the turbulence eddies have ability to carry the mass across the flow. However, in case of laminar flow, the mass has to diffuse across the flow. Therefore, in the case of turbulence, the mass gets carried as well as diffusing, resulting in a greater mass transfer coefficient. In microfluidic devices, an efficient mixing is usually difficult to achieve due to the predominance of laminar flow. The absence of turbulence flow significantly reduces mass transfer, hence new microfluidic devices should be designed to mimic turbulence flow. Chaotic advection is an effective mixing type where a particle is advected in a velocity field with a chaotic trajectory (Aref, 2002; Xie and Xu, 2017). Chaotic advection mixing can be achieved by introducing barriers, restrictions, or other geometrical structures to generate transverse components of flow, promoting stretching and folding of fluid volumes inside the device. This way, it is possible to achieve the desired mixing with decreased channel length.

Studies involving the complexation between cationic lipids and RNA in microfluidic systems using chaotic advection mixing started in the early 2010s. Belliveau et al. (2012) performed the direct complexation in microfluidic devices from the mixing of an aqueous stream containing siRNA with another alcoholic stream containing the lipids (ethanol phase). The microfluidic device so-called Staggered Herringbone Micromixer (SHM) had small

mixing units at its base to aid the mixing and complexation process. In this system, lipid nanoparticles with size ranging from 60-90 nm were formed (Figure 2.7). In this case, the term lipid nanoparticle is used instead of lipoplex, since there is no previous lipid aggregation into liposomes.

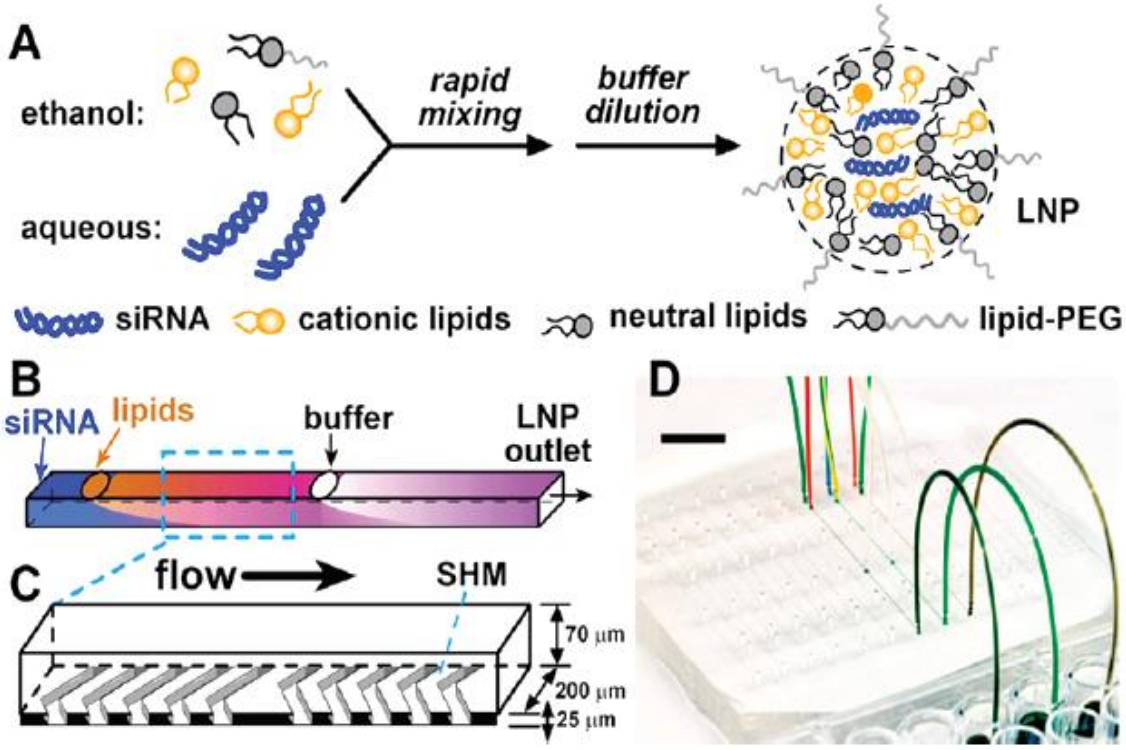

Figure 2. 7. Illustrative figure of the strategy of the formation of lipid particles containing siRNA. In this case, the lipids were dispersed in ethanol and this stream is mixed with the second aqueous phase stream containing siRNA in herringbone-like sub-channels. A second step allowed the addition of buffer, performing a dilution. The device contains depressions in the base to facilitate mixing (Adapted from Belliveau *et al*., 2012).

Similarly, Leung et al. (2012) prepared cationic lipid nanoparticles in microfluidic systems using a cationic lipid, phospholipid, cholesterol, and PEG incorporating siRNA. In this study, the authors identified that the interior of the nanoparticles contains the siRNA complexed with the cationic lipid and that the interior also contains phospholipid and cholesterol in a nanostructured form. In another similar study, the cationic lipid/siRNA complex introduced into mouse hepatocytes (20-100 nm) presented gene silencing with 50% efficiency (Belliveau et al., 2012). The microfluidic technique in each study allowed high

efficiency of siRNA incorporation and the produced nanoparticles presented the ideal size for gene therapy.

Following the same strategy of direct complexation of RNA with lipids in alcoholic phase, in one of the more recent studies, Yang et al., 2014 used the lipid nanoparticles that contain siRNA LOR-1284, which is an agent used to overcome the drug resistance in the case of Acute Myeloid Leukemia (AML) and could manage to reduce the tumor in the body. The microfluidic technique used was highly efficient and the nanoparticles produced had the most uniform structure, with excellent polydispersity index and high drug loading efficiency (Yang et al., 2014).

In the cases mentioned above, the use of microfluidic techniques to perform complexation between lipids and RNA is performed in a single step, without the previous formation of liposomes. In fact, the strategy used to effect the complexation (with the previous formation of liposomes or not) may interfere with the release capacity of RNA into the cell cytoplasm, but this aspect has not yet been intensively investigated in the scientific literature.

The number of studies on the complexation of liposomes and genetic material has been steadily increasing. The novelty of these studies is attributed mostly to chemical modifications on liposome structure, type of genetic material, and, above all, the design of microfluidic devices and fluid dynamics that determine the efficiency of nanotherapeutics synthesis. The lack of optimization of microfluidic systems mostly causes needless waste of drug or genetic material. Considering the high cost of these specific materials with promising pharmaceutical importance (e.g. siRNA with the specific target), this significant material loss might increase overall production cost. Therefore, the optimization of these systems in terms of engineering aspects like fluid dynamics is crucial to produce a more precise gene delivery vector system.

5.3. Microfluidic approaches for 3D cell culture: Tumour-on-a-chip platforms

Microfluidics amplifies the possibilities of cellular studies in dynamic conditions, allowing studies of mechanisms of responses, chemotaxis, and cytotoxicity since it can mimic the cellular microenvironment. Also, it allows the development of new techniques of isolation

and culture of microbial and animal cells (Weibel et al., 2007). These devices can also evaluate the kinetics of the reactions in real-time through sensor systems, reducing the test time (Zhang et al., 2007). Therefore, microfluidics is a promising tool and if it is coupled with biophotonic techniques, great advances in the field of biology, medicine, and engineering will be possible.

In the human body, virtually every cell is surrounded by an extracellular matrix (ECM) that continuously promotes direct physical contact with other cells. However, to date, most studies associated with gene delivery have been performed on two-dimensional (2D) cell cultures; in these 2D cultures, the cells grow on a polystyrene material treated to be compatible with cell cultures. Although this approach has delivered well-controlled and homogeneous culture environments, as well as ease of microscopic analysis, it is in most cases insufficient to mimic the natural microenvironment that cells encounter *in vivo* (Bersini et al. 2014). Alternatively, in three-dimensional (3D) cell culture methods, cells are immobilized within a 3D polymeric scaffold as spheroids (cell aggregates). In this way, it is possible to prevent the loss of phenotype of the cells (which can be significant in 2D culture settings), and enhance the cell-cell interaction typical of *in vivo* situations, creating thus a more biologically relevant microenvironment that mimics the natural cell environment much better.

Spheroids are exceptionally suited to investigate the fundamental mechanisms of all kinds of cellular responses. Spheroids can be formed by conventional techniques such as liquid overlay and hanging drop technique, or just by centrifugation (Fennema et al. 2013). However, conventional monolayer and 2D culture methods do not provide high-throughput 3D tissue screening. In this context, a microfluidic approach becomes more promising for spheroid culture, since it facilitates the investigation of complex phenomena in combination with controllable biochemical microenvironments, coupled with high-resolution real-time imaging. Moreover, microfluidic 3D cell cultures allow a high degree of control over the flow through a controllable and integrated pumping system, potentially enabling comprehensive analysis from a single cell to the tissue level, and can be designed as a completely automated microchip (Mehling and Tay, 2013).

Spheroids have different zones and pathophysiologic gradients similar to *in vivo* tissues (Figure 2.8). The outer zone is proliferating zone where the cells are exposed to surroundings and grow rapidly. Quiescent zone or so-called hypoxic zone is the zone where there is a certain level of decrease in oxygen and nutrient concentration and the cells start to secrete growth factors that may lead to angiogenesis (Barisam et al. 2018). In the necrotic zone, most of the cells face a serious lack of oxygen and nutrients and undergo death. Spheroids may vary in size and depending on the size of the spheroid, the size of these zones also varies. The concentration of nutrients, oxygen, and ATP decreases whereas the amount of waste, CO2, and lactase concentration increase from proliferating zone to the necrotic zone. The size of spheroid can vary depending on the techniques used to form spheroids and culture time. Several investigations have reported the size of spheroid between 400 and 600 μm (Zanoni et al. 2016).

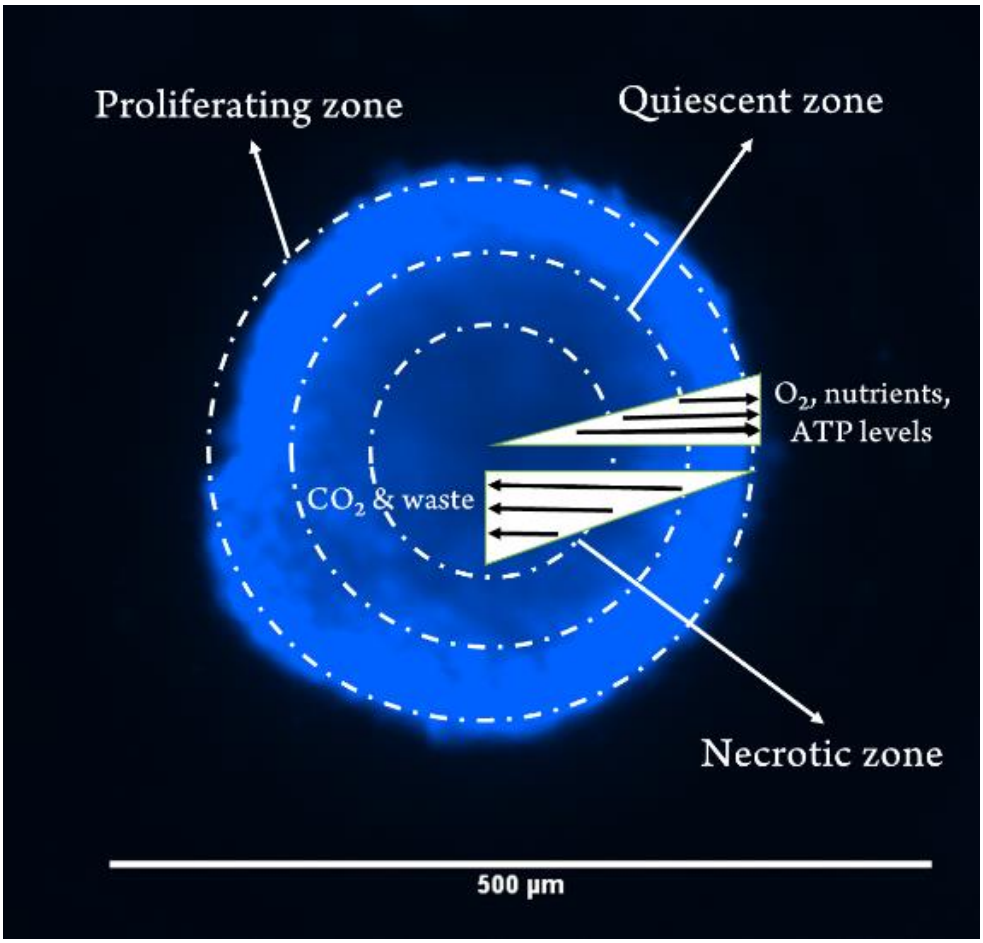

Figure 2. 8. A spheroid with proliferating, quiescent, and necrotic zones is shown. The spheroid was stained with Hoechst dye and visualized under DAPI filter in fluorescent microscopy. The size of spheroid is approximately 375 µm.

When studying *in vitro* transfection, stimuli generated by the flow of fluids are normally ignored and transfection assays are performed under static conditions. However, both in the theory (Decuzzi and Ferrari, 2008) and in practice (Farokhzad et al., 2005), it was demonstrated that mechanical stimuli generated by the fluid flow in the microfluidic environment are an important factor for the internalization of particles by the cells (Shin et al., 2009). In the case of traditional transfection performed in wells, there is only the process of diffusive transport of the lipoplexes through the cells. However, the transfection in microfluidic systems, a convective contribution to the process is also added, which increases the rate of lipoplexes collision on cell surfaces, and consequently, results in a better-controlled transfection (Harris and Giorgio, 2005).

6. Concluding remarks

New trends in the delivery of genetic materials into mammalian cells for gene therapy have been emphasized so far. Technology platforms such as microfluidics, which was addressed before, have been put into use as an advantageous tool to provide rapid production of colloidal systems with desired properties. Microfluidics also ensures to find the optimal interplay of bio-physicochemical parameters of these systems such as their size, charge, surface composition, etc. Since these parameters are strictly related to molecular targeting, immune evasion and controlled drug release (Valencia et al. 2013), the complexation of genetic material with specific carrier systems on a microfluidic platform became an important issue to achieve practical approach of gene therapy. Many viral and non-viral gene carrier systems have been tested and commercialized. Nevertheless, due to the high toxicity level of viral systems, their use is mostly restricted. At this point, the use of liposomes as a non-viral vector system, whose advantages and disadvantages have been pointed out before, meet the requirements of an appropriate gene carrier system. Additionally, the incorporation of genetic materials such as oligonucleotides, pDNA, RNA (i.e. siRNA) into these carrier systems mostly by electrostatic interactions paves the way for the production of indispensable therapeutic agents. Microfluidic processes have been gaining more attention and gathering more availability for the production of liposomal complexes in adequate quantity and efficiency to help the improvement of these therapeutic agents that might be used with confidence in animals and humans. The researches in microfluidics will intensify even more due to the global market share, which is estimated to be worth billions of dollars.

References

1. Abuchowski, A., McCoy, J.R., Palczuk, N.C., van Es, T. and Davis, F.F., 1977. Effect of covalent attachment of polyethylene glycol on immunogenicity and circulating life of bovine liver catalase. Journal of Biological Chemistry, 252(11), pp.3582-3586.
2. Aref, H., 2002. The development of chaotic advection. Physics of Fluids, 14(4), pp.1315-1325.

3. Baek, J., Allen, P.M., Bawendi, M.G. and Jensen, K.F., 2011. Investigation of indium phosphide nanocrystal synthesis using a high-temperature and high-pressure continuous flow microreactor. Angewandte Chemie International Edition, 50(3), pp.627-630.
4. Balbino, T.A., Aoki, N.T., Gasperini, A.A., Oliveira, C.L., Azzoni, A.R., Cavalcanti, L.P. and Lucimara, G., 2013. Continuous flow production of cationic liposomes at high lipid concentration in microfluidic devices for gene delivery applications. Chemical engineering journal, 226, pp.423-433.
5. Balbino, T.A., Azzoni, A.R. and de La Torre, L.G., 2013. Microfluidic devices for continuous production of pDNA/cationic liposome complexes for gene delivery and vaccine therapy. Colloids and Surfaces B: Biointerfaces, 111, pp.203-210.
6. Bangham, A.D., Standish, M.M. and Watkins, J.C., 1965. The accumulation of steroids and streptolysin S on the permeability of phospholipid structures to cations. J Mol Biol, 13, pp.238-53.
7. Barisam, M., Saidi, M.S., Kashaninejad, N. and Nguyen, N.T., 2018. Prediction of necrotic core and hypoxic zone of multicellular spheroids in a microbioreactor with a u-shaped barrier. Micromachines, 9(3), p.94.
8. Beebe, D.J., Mensing, G.A. and Walker, G.M., 2002. Physics and applications of microfluidics in biology. Annual review of biomedical engineering, 4(1), pp.261-286.
9. Belliveau, N.M., Huft, J., Lin, P.J., Chen, S., Leung, A.K., Leaver, T.J., Wild, A.W., Lee, J.B., Taylor, R.J., Tam, Y.K. and Hansen, C.L., 2012. Microfluidic synthesis of highly potent limit-size lipid nanoparticles for *in vivo* delivery of siRNA. Molecular Therapy-Nucleic Acids, 1, p.e37.
10. Bergstrom, S., 1992. The HBV model-its structure and applications.
11. Bersini, S., Jeon, J.S., Dubini, G., Arrigoni, C., Chung, S., Charest, J.L., Moretti, M. and Kamm, R.D., 2014. A microfluidic 3D *in vitro* model for specificity of breast cancer metastasis to bone. Biomaterials, 35(8), pp.2454-2461.
12. Bertrand, N., Wu, J., Xu, X., Kamaly, N. and Farokhzad, O.C., 2014. Cancer nanotechnology: the impact of passive and active targeting in the era of modern cancer biology. Advanced drug delivery reviews, 66, pp.2-25.

13. Blaese, R.M., Culver, K.W., Miller, A.D., Carter, C.S., Fleisher, T., Clerici, M., Shearer, G., Chang, L., Chiang, Y., Tolstoshev, P. and Greenblatt, J.J., 1995. T lymphocyte-directed gene therapy for ADA− SCID: initial trial results after 4 years. Science, 270(5235), pp.475-480.
14. Bordet, T. and Behar-Cohen, F., 2019. Ocular gene therapies in clinical practice: Viral vectors and nonviral alternatives. Drug discovery today.
15. Bozzuto, G. and Molinari, A., 2015. Liposomes as nanomedical devices. International journal of nanomedicine, 10, p.975.
16. Braxton, S.M., Incyte Corp, 1998. Cysteine-pegylated proteins. U.S. Patent 5,766,897.
17. Cao, Z., Zhang, L. and Jiang, S., 2012. Superhydrophilic zwitterionic polymers stabilize liposomes. Langmuir, 28(31), pp.11625-11632.
18. Cui, P. and Wang, S., 2019. Application of microfluidic chip technology in pharmaceutical analysis: A review. Journal of Pharmaceutical Analysis, 9(4), pp.238-247.
19. Dai, W.J., Zhu, L.Y., Yan, Z.Y., Xu, Y., Wang, Q.L. and Lu, X.J., 2016. CRISPR-Cas9 for *in vivo* gene therapy: promise and hurdles. Molecular Therapy-Nucleic Acids, 5, p.e349.
20. Day, D.A. and Tuite, M.F., 1998. Post-transcriptional gene regulatory mechanisms in eukaryotes: an overview. The Journal of endocrinology, 157(3), pp.361-371.
21. Decuzzi, P. and Ferrari, M., 2008. Design maps for nanoparticles targeting the diseased microvasculature. Biomaterials, 29(3), pp.377-384.
22. Degors, I.M., Wang, C., Rehman, Z.U. and Zuhorn, I.S., 2019. Carriers break barriers in drug delivery: endocytosis and endosomal escape of gene delivery vectors. Accounts of chemical research, 52(7), pp.1750-1760.
23. Dimov, N., Kastner, E., Hussain, M., Perrie, Y. and Szita, N., 2017. Formation and purification of tailored liposomes for drug delivery using a module-based micro continuous-flow system. Scientific reports, 7(1), pp.1-13.
24. Ditto, A.J., Shah, P.N. and Yun, Y.H., 2009. Non-viral gene delivery using nanoparticles. Expert opinion on drug delivery, 6(11), pp.1149-1160.
25. Elbashir, S.M., Harborth, J., Lendeckel, W., Yalcin, A., Weber, K. and Tuschl, T., 2001. Duplexes of 21-nucleotide RNAs mediate RNA interference in cultured mammalian cells. nature, 411(6836), pp.494-498.

26. Farokhzad, O.C., Khademhosseini, A., Jon, S., Hermmann, A., Cheng, J., Chin, C., Kiselyuk, A., Teply, B., Eng, G. and Langer, R., 2005. Microfluidic system for studying the interaction of nanoparticles and microparticles with cells. Analytical chemistry, 77(17), pp.5453-5459.

27. Fennema, E., Rivron, N., Rouwkema, J., van Blitterswijk, C. and de Boer, J., 2013. Spheroid culture as a tool for creating 3D complex tissues. Trends in biotechnology, 31(2), pp.108-115.

28. Fernández, M., Javaid, F. and Chudasama, V., 2018. Advances in targeting the folate receptor in the treatment/imaging of cancers. Chemical science, 9(4), pp.790-810.

29. Fire, A., Xu, S., Montgomery, M.K., Kostas, S.A., Driver, S.E. and Mello, C.C., 1998. Potent and specific genetic interference by double-stranded RNA in Caenorhabditis elegans. Nature, 391(6669), pp.806-811.

30. Gomez, F.A. ed., 2008. Biological applications of microfluidics. John Wiley & Sons.

31. Gregoriadis, G. and Perrie, Y., 2010. Liposomes in Nanomedicine. Wiley.

32. Guckenberger, D.J., de Groot, T.E., Wan, A.M., Beebe, D.J. and Young, E.W., 2015. Micromilling: a method for ultra-rapid prototyping of plastic microfluidic devices. Lab on a Chip, 15(11), pp.2364-2378.

33. Halldorsson, S., Lucumi, E., Gómez-Sjöberg, R. and Fleming, R.M., 2015. Advantages and challenges of microfluidic cell culture in polydimethylsiloxane devices. Biosensors and Bioelectronics, 63, pp.218-231.

34. Hannon, G.J., 2002. RNA interference. Nature, 418(6894), pp.244-251.

35. Hansen, C. and Quake, S.R., 2003. Microfluidics in structural biology: smaller, faster… better. Current opinion in structural biology, 13(5), pp.538-544.

36. Harris, S.S. and Giorgio, T.D., 2005. Convective flow increases lipoplex delivery rate to *in vitro* cellular monolayers. Gene therapy, 12(6), pp.512-520.

37. Hatakeyama, H., Akita, H. and Harashima, H., 2011. A multifunctional envelope type nano device (MEND) for gene delivery to tumours based on the EPR effect: a strategy for overcoming the PEG dilemma. Advanced drug delivery reviews, 63(3), pp.152-160.

38. He, Z.Y., Zheng, X., Wu, X.H., Song, X.R., He, G., Wu, W.F., Yu, S., Mao, S.J. and Wei, Y.Q., 2010. Development of glycyrrhetinic acid-modified stealth cationic liposomes for gene delivery. International journal of pharmaceutics, 397(1-2), pp.147-154.

39. Herweijer, H. and Wolff, J.A., 2003. Progress and prospects: naked DNA gene transfer and therapy. Gene therapy, 10(6), pp.453-458.

40. Hoffman, A. (2017). Acta Biomaterialia Gold Medal lecture: "PEG and PEGylation, Then and Now—A Historical Commentary and Review", Acta Biomaterialia Medal plenary session, Society For Biomaterials (SFB) Annual Meeting & Exposition, Minneapolis, USA.

41. Honigmann, A. and Pralle, A., 2016. Compartmentalization of the cell membrane. Journal of molecular biology, 428(24), pp.4739-4748.

42. Huang, C., Quinn, D., Sadovsky, Y., Suresh, S. and Hsia, K.J., 2017. Formation and size distribution of self-assembled vesicles. Proceedings of the National Academy of Sciences, 114(11), pp.2910-2915.

43. Immordino, M.L., Dosio, F. and Cattel, L., 2006. Stealth liposomes: review of the basic science, rationale, and clinical applications, existing and potential. International journal of nanomedicine, 1(3), p.297.

44. Jahn, A., Reiner, J.E., Vreeland, W.N., DeVoe, D.L., Locascio, L.E. and Gaitan, M., 2008. Preparation of nanoparticles by continuous-flow microfluidics. Journal of Nanoparticle Research, 10(6), pp.925-934.

45. Joanicot, M. and Ajdari, A., 2005. Droplet control for microfluidics. *Science*, *309*(5736), pp.887-888.

46. Kamei, K.I., 2013. Cutting-edge microfabricated biomedical tools for human pluripotent stem cell research. Journal of laboratory automation, 18(6), pp.469-481.

47. Khadke, S., Roces, C.B., Cameron, A., Devitt, A. and Perrie, Y., 2019. Formulation and manufacturing of lymphatic targeting liposomes using microfluidics. Journal of Controlled Release, 307, pp.211-220.

48. Lee, J., Kim, J., Kim, H., Bae, Y.M., Lee, K.H. and Cho, H.J., 2013. Effect of thermal treatment on the chemical resistance of polydimethylsiloxane for microfluidic devices. Journal of Micromechanics and Microengineering, 23(3), p.035007.

49. Leung, A.K., Hafez, I.M., Baoukina, S., Belliveau, N.M., Zhigaltsev, I.V., Afshinmanesh, E., Tieleman, D.P., Hansen, C.L., Hope, M.J. and Cullis, P.R., 2012. Lipid nanoparticles containing siRNA synthesized by microfluidic mixing exhibit an electron-dense nanostructured core. The Journal of Physical Chemistry C, 116(34), pp.18440-18450.

50. Li, C. and Samulski, R.J., 2020. Engineering adeno-associated virus vectors for gene therapy. Nature Reviews Genetics, pp.1-18.

51. Lodish, H., Baltimore, D., Berk, A., Zipursky, S.L., Matsudaira, P. and Darnell, J., 1995. Molecular cell biology (Vol. 3). New York: Scientific American Books.

52. Lovchik, R.D., Wolf, H. and Delamarche, E., 2011. High-grade optical polydimethylsiloxane for microfluidic applications. Biomedical microdevices, 13(6), pp.1027-1032.

53. Lu, P. Y., Woodle, M. C. In: Fire, A., Nirenberg, M., (Ed.), 2005. RNA interference technology: From basic science to drug development. Cambridge University Press, p. 303-305, 2005.

54. Luo, D. and Saltzman, W.M., 2000. Synthetic DNA delivery systems. Nature biotechnology, 18(1), pp.33-37.

55. Ma, J., Jiang, L., Pan, X., Ma, H., Lin, B. and Qin, J., 2010. A simple photolithography method for microfluidic device fabrication using sunlight as UV source. Microfluidics and nanofluidics, 9(6), pp.1247-1252.

56. Manikandan, C., Kaushik, A. and Sen, D., 2019. Viral vector: potential therapeutic for glioblastoma multiforme. Cancer Gene Therapy, pp.1-10.

57. Manz, A., Graber, N. and Widmer, H.Á., 1990. Miniaturized total chemical analysis systems: a novel concept for chemical sensing. Sensors and actuators B: Chemical, 1(1-6), pp.244-248.

58. Marwah, M., Perrie, Y., Badhan, R.K.S. and Lowry, D., 2019. Intracellular uptake of EGCG-loaded deformable controlled release liposomes for skin cancer. Journal of liposome research, pp.1-14.

59. McManus, M.T. and Sharp, P.A., 2002. Gene silencing in mammals by small interfering RNAs. Nature reviews genetics, 3(10), pp.737-747.

60. Mehling, M. and Tay, S., 2014. Microfluidic cell culture. Current opinion in Biotechnology, 25, pp.95-102.

61. Miri, A.K., Nieto, D., Iglesias, L., Goodarzi Hosseinabadi, H., Maharjan, S., Ruiz-Esparza, G.U., Khoshakhlagh, P., Manbachi, A., Dokmeci, M.R., Chen, S. and Shin, S.R., 2018. Microfluidics-enabled multimaterial maskless stereolithographic bioprinting. Advanced Materials, 30(27), p.1800242.

62. Nyamay'Antu, A., Dumont, M., Kedinger, V. and Erbacher, P., 2019. Non-viral vector mediated gene delivery: the outsider to watch out for in gene therapy. Cell Gene Ther Insights, 5, pp.51-57.

63. Patil, Y.P. and Jadhav, S., 2014. Novel methods for liposome preparation. Chemistry and physics of lipids, 177, pp.8-18.

64. Rideau, E., Dimova, R., Schwille, P., Wurm, F.R. and Landfester, K., 2018. Liposomes and polymersomes: a comparative review towards cell mimicking. Chemical Society Reviews, 47(23), pp.8572-8610.

65. Sambrook, J., Westphal, H., Srinivasan, P.R. and Dulbecco, R., 1968. The integrated state of viral DNA in SV40-transformed cells. Proceedings of the National Academy of Sciences of the United States of America, 60(4), p.1288.

66. Scholz, C. and Wagner, E., 2012. Therapeutic plasmid DNA versus siRNA delivery: common and different tasks for synthetic carriers. Journal of controlled release, 161(2), pp.554-565.

67. Semple, S.C., Chonn, A. and Cullis, P.R., 1998. Interactions of liposomes and lipid-based carrier systems with blood proteins: Relation to clearance behaviour *in vivo*. Advanced drug delivery reviews, 32(1-2), pp.3-17.

68. Shaegh, S.A.M., Pourmand, A., Nabavinia, M., Avci, H., Tamayol, A., Mostafalu, P., Ghavifekr, H.B., Aghdam, E.N., Dokmeci, M.R., Khademhosseini, A. and Zhang, Y.S., 2018. Rapid prototyping of whole-thermoplastic microfluidics with built-in microvalves using laser ablation and thermal fusion bonding. Sensors and Actuators B: Chemical, 255, pp.100-109.

69. Shin, H.S., Kim, H.J., Sim, S.J. and Jeon, N.L., 2009. Shear stress effect on transfection of neurons cultured in microfluidic devices. Journal of nanoscience and nanotechnology, 9(12), pp.7330-7335.

70. Sioud, M. and Sørensen, D.R., 2003. Cationic liposome-mediated delivery of siRNAs in adult mice. Biochemical and biophysical research communications, 312(4), pp.1220-1225.

71. Sivasankar, B., 2008. Engineering chemistry (pp. 145-150). New Delhi: Tata McGraw-Hill.

72. Terova, O., Soltys, S., Hermans, P., De Rooij, J. and Detmers, F., 2018. Overcoming downstream purification challenges for viral vector manufacturing: enabling advancement of gene therapies in the clinic. Cell. Gen. Ther. Ins, 4(2), pp.101-111.

73. Tuschl, T., 2001. RNA interference and small interfering RNAs. Chembiochem, 2(4), pp.239-245.

74. Valencia, P.M., Pridgen, E.M., Rhee, M., Langer, R., Farokhzad, O.C. and Karnik, R., 2013. Microfluidic platform for combinatorial synthesis and optimization of targeted nanoparticles for cancer therapy. ACS nano, 7(12), pp.10671-10680.

75. Weibel, D.B., DiLuzio, W.R. and Whitesides, G.M., 2007. Microfabrication meets microbiology. Nature Reviews Microbiology, 5(3), pp.209-218.

76. Whitehead, K.A., Langer, R. and Anderson, D.G., 2009. Knocking down barriers: advances in siRNA delivery. Nature reviews Drug discovery, 8(2), pp.129-138.

77. Whitesides, G.M., 2006. The origins and the future of microfluidics. Nature, 442(7101), pp.368-373.

78. Wolff, J.A., Malone, R.W., Williams, P., Chong, W., Acsadi, G., Jani, A. and Felgner, P.L., 1990. Direct gene transfer into mouse muscle *in vivo*. Science, 247(4949), pp.1465-1468.

79. Yager, P., Edwards, T., Fu, E., Helton, K., Nelson, K., Tam, M.R. and Weigl, B.H., 2006. Microfluidic diagnostic technologies for global public health. Nature, 442(7101), pp.412-418.

80. Yang, D.K. and Wu, S.T., 2014. Fundamentals of liquid crystal devices. John Wiley & Sons.

81. Xie, T. and Xu, C., 2017. Numerical and experimental investigations of chaotic mixing behavior in an oscillating feedback micromixer. Chemical engineering science, 171, pp.303-317.

82. Zanoni, M., Piccinini, F., Arienti, C., Zamagni, A., Santi, S., Polico, R., Bevilacqua, A. and Tesei, A., 2016. 3D tumor spheroid models for *in vitro* therapeutic screening: a systematic approach to enhance the biological relevance of data obtained. Scientific reports, 6(1), pp.1-11.

83. Zhang, C., Xing, D. and Li, Y., 2007. Micropumps, microvalves, and micromixers within PCR microfluidic chips: Advances and trends. Biotechnology advances, 25(5), pp.483-514.

84. Zhang, Y., Satterlee, A. and Huang, L., 2012. *In vivo* gene delivery by nonviral vectors: overcoming hurdles?. Molecular therapy, 20(7), pp.1298-1304.

85. Zhao, Y., Wang, W., Guo, S., Wang, Y., Miao, L., Xiong, Y. and Huang, L., 2016. PolyMetformin combines carrier and anticancer activities for *in vivo* siRNA delivery. Nature communications, 7(1), pp.1-9.

86. Zook, J.M. and Vreeland, W.N., 2010. Effects of temperature, acyl chain length, and flow-rate ratio on liposome formation and size in a microfluidic hydrodynamic focusing device. Soft Matter, 6(6), pp.1352-1360.

CHAPTER 3. EVALUATION OF SIRNA AND CATIONIC LIPOSOMES COMPLEXES AS A MODEL FOR *IN VITRO* SIRNA DELIVERY TO CANCER CELLS

Evaluation of siRNA and cationic liposomes complexes as a model for *in vitro* siRNA delivery to cancer cells

Ismail Eş[1†], Meryem Tyrrasch Ok[2a†], Ximena Puentes[3], Marcelo Augusto Szymanski de Toledo[4], Marianna Teixeira de Pinho Favaro[4], Leide Passos Cavalcanti[1], Alexandre Cassago[3], Rodrigo Villares Portugal[3], Adriano Rodrigues Azzoni[5], Lucimara Gaziola de la Torre[1*]

[1]Department of Material and Bioprocess Engineering, School of Chemical Engineering, University of Campinas (UNICAMP), Campinas, São Paulo, Brazil

[2]Department of Biological Engineering, Massachusetts Institute of Technology, Cambridge, Massachusetts, United States of America

[3]Brazillian National Center for Research in Energy and Materials, CNPEM

[4]Laboratory of Genetics and Molecular Analysis, Molecular Biology and Genetic Engineering Center, University of Campinas, Campinas, São Paulo, Brazil

[5]Chemical Engineering Department, Polytechnic School, University of São Paulo, São Paulo, SP, Brazil

[a]Current Address: University of North Carolina School of Medicine, Chapel Hill, North Carolina, United States of America

This study was published in ***Colloids and Surfaces A: Physicochemical and Engineering Aspects:***

Eş, I., Ok, M.T., Puentes-Martinez, X.E., de Toledo, M.A.S., de Pinho Favaro, M.T., Cavalcanti, L.P., Cassago, A., Portugal, R.V., Azzoni, A.R. and de la Torre, L.G., 2018. Evaluation of siRNA and cationic liposomes complexes as a model for in vitro siRNA delivery to cancer cells. Colloids and Surfaces A: Physicochemical and Engineering Aspects, 555, pp.280-289.

ABSTRACT

Controlled release of genetic material such as small interfering RNA (siRNA) using lipid-based non-viral vectors has gained substantial importance in gene therapy applications. Therefore, the interaction between siRNA and these vectors must be well understood. This study aims to investigate the effect of different molar charge ratios ($R_{+/-}$) between positive charges from microfluidics-produced cationic liposomes (CL) (egg phosphatidylcholine, 1,2-dioleoyl-3-trimethylammonium-propane and 1,2-dioleoyl-sn-glycero-3-phosphoethanolamine) and negative charges from siRNA and on physico-chemical and morphological properties of the lipoplexes (CL/siRNA) as well as their *in vitro* luciferase silencing effect in HeLa cells. $R_{+/-}$ 3.27 was found to be the optimum point for complexation. This finding was confirmed by gel retardation and siRNA accessibility assays. According to Cryo-TEM analysis, the lipoplexefs had multi-lamellarity. *In vitro* transfection efficiency of lipoplexes in HeLa cells was tested at three different siRNA concentrations (10, 25, and 35 nM). Significant knockdown of luciferase by siRNA lipoplexes was observed based on reduced luciferase activity of transfected HeLa cells. Our findings were comparable with the silencing effect of siRNA complexed with Lipofectamine®. No cytotoxicity of lipoplexes was detected at the tested concentrations. This study was essential for further complexation studies which will be performed using microfluidic systems to formulate next-generation lipid-based controlled release systems.

Keywords: siRNA, Cationic liposomes, microfluidics, molar charge ratio, gene delivery

1. Introduction

Over the past decades, several comprehensive studies have led to the discovery of efficient treatment or prevention methods against genetic diseases. For this purpose, gene therapy, which is the introduction of suitable genetic material into cells to correct abnormal genes, appeared as a critical approach (Gin et al. 2013). However, the success of gene therapy relies on safe and competent delivery of genetic material into target cells, which, in most cases, is challenging to achieve. Thus far, several genetic materials such as plasmid DNA (pDNA) (Park et al. 2016), anti-sense oligodeoxynucleotides (AS-ODNs) (Cao et al. 2017), and microRNAs (Wang et al. 2015) have been employed for gene therapy. Furthermore, since the discovery of RNA interference (RNAi) as one of the major breakthroughs in medicine (Fire et al. 1998), much attention has been given to small interfering RNA (siRNA), which is a double-stranded RNA molecule that is 21-23 nucleotides long and shows a silencing effect on genes via RNAi (Whitehead et al. 2009). Therefore, the delivery of siRNA into cells in order to silence them shows great potential for gene therapy.

Numerous viral and non-viral vectors have been employed in clinical trials of gene therapy. Nevertheless, ~70% of these trials were performed with viral vectors such as retroviral (Touzot et al. 2015), lentiviral (Hacein-Bey et al. 2015), adeno-associated viral (Nathwani et al. 2014), and adenoviral vectors (Schooley et al. 2010). Despite all of the advanced studies performed with viral vectors, they present many limitations such as immunogenicity, toxicity, low gene loading, complexity of vector design, and even carcinogenesis (Mingozzi and High, 2011; Yin et al. 2014). The use of non-viral vectors exhibits great potential to overcome these limitations, particularly given safety considerations. At this point, cationic liposomes (CLs), spherical assemblies of lipids that consist of polar head groups and hydrophobic tails, are important candidates for siRNA delivery due to electrostatic interactions (Safinya et al. 2014) and similarities with the cell membrane.

Besides the study of liposomes' composition and potential as therapeutics, novel production methods have also been explored. Several techniques have been employed in order to produce liposomes such as reversed phase evaporation (Chen et al. 2014), thin-film hydration (Ghanbarzadeh et al. 2013), and the solvent injection technique (Jaafar-Maalej et

al. 2010). However, conventional methods usually result in uncontrollable and heterogeneous liposome production, which usually complicates *in vivo* use (Yin et al. 2014). Hence, advanced methods have been developed for more suitable liposome production. At this point, microfluidics, which is the engineering of fluids at micron scales, appears as an emerging technology (Sackmann et al. 2014). Compared to conventional methods, microfluidics exhibits economic and technical advantages such as low reagent use, low-cost design, high control, reduced reaction time, minimization of the effect of mass and heat transfer, low energy consumption, real time data acquisition, and easy automation (Halldorsson et al. 2015). Different investigations have been previously performed to evaluate the complexation efficiency between CLs and DNA (Coumo et al. 2012). Recently, our research group demonstrated the efficient microfluidic complexation of CLs using egg phosphatidylcholine (EPC), 1,2-dioleoyl-3-trimethylammonium-propane (DOTAP) and 1,2-dioleoyl-sn-glycero-3-phosphoethanolamine (DOPE) lipids with pDNA. The study revealed the viability of this system for efficient pDNA delivery (Balbino et al. 2013a; Balbino et al. 2013b). Moreover, there are other successful Hence, the evaluation of this carrier system for siRNA delivery is also essential for studies in gene therapy.

The electrostatic interaction between siRNA and CLs determines the physico-chemical properties of lipoplexes (siRNA/CL), and is directly related to *in vitro* and *in vivo* applications. Living organisms consist of several biological and chemical barriers that complicate the efficient delivery of genetic materials to the treatment site (Pozzi et al. 2014). Therefore, physico-chemical characterization of lipoplexes is critical in order to increase success rates of *in vivo* siRNA delivery. In this context, one of the important parameters to evaluate is the molar charge ratio ($R_{+/-}$) between siRNA and CLs as well as its effect on physico-chemical parameters. However, variable lipid composition or surface modifications of CLs that produce target-specific lipoplexes could alter the $R_{+/-}$ value. Hence, this value should be supported with additional tests such as gel retardation, fluorescence assays, or morphological analyses using Cryo-TEM.

Although there are several important studies investigating physico-chemical properties of liposomes complexed with oligonucleotides, pDNA, and polynucleotides (de la Torre et al. 2009; Anderson and Chiu, 2000), it is known that lipid composition can interfere

in the final lipoplex aggregation (Elbashir et al. 2001). In this context, there is no systematic study reported in the literature that evaluates the lipoplexes of siRNA and CLs using EPC/DOTAP/DOPE phospholipids .Therefore, new investigations are necessary to obtain this critical in-formation. In the present study, siRNA molecules were complexed using a conventional bulk mixing technique with CLs that were produced via a hydrodynamic flow-focusing microfluidic device. Structural stability between the lipid composition of EPC/DOTAP/DOPE and DNA was previously studied (Toledo et al. 2012). In the present study, the same lipid composition was evaluated for cationic liposome production and the capacity to form lipoplexes with siRNA at different molar charge ratios. Finally, the lipoplexes formed at the optimum molar charge ratio were tested to determine *in vitro* transfection efficiency, targeted gene silencing, and cytotoxicity in human epithelial carcinoma (HeLa) cells.

2. Materials and methods

2.2. Materials

The lipids egg phosphatidylcholine (EPC), 1,2-dioleoyl-sn-glycero-3-phosphoethanolamine (DOPE), and 1,2-dioleoyl-3-trimethylammonium-propane (DOTAP) were purchased from Lipoid (Ludwigshafen, Germany) and used with no further purification. Ethanol used to dissolve lipids was obtained from Labsynth (São Paulo, Brazil). The Sylgard® 184 Silicone Elastomer Kit for fabrication of microfluidic devices was purchased from Dow Corning (Auburn, MI, United States). Deionized water was obtained from Samtec Biotechnology (São Paulo, Brazil).

2.3. Microfluidic device fabrication

Fabrication of Polydimethylsiloxane (PDMS)/glass microfluidic devices was carried out according to the method previously described (Anderson et al. 2000). Prior to microfabrication, microfluidic devices were geometrically designed and projected using AutoCAD software. After photolithography, the mask layouts were photo-plotted with 8000 dpi resolution, and the UV exposures were made in a MJB-3 UV300 contact mask aligner (Karl-Suss, Garching, Germany). The Sylgard® 184 Silicone Elastomer Kit was used as material precursor of PDMS layers. PDMS channels and glass were irreversibly sealed by O_2

plasma surface activation sealing techniques (Plasma Technology PLAB SE80 plasma cleaner, Wrington, England). All channels had a rectangular cross section with a depth of 100 μm and a width of 140 μm (Balbino et al. 2013a).

2.4. Cationic liposome production

CL production was performed using a hydrodynamic flow-focusing microfluidic device according to Balbino et al. 2013. EPC, DOTAP, and DOPE at a molar ratio of 2:1:1 were dispersed in anhydrous ethanol at a lipid concentration of 25 mM. Prior to CL production, the lipid solution was sonicated for 15 min at 35 ^{o}C (Ultrasonic Cleaner 8890, Cole-Parmer). The lipid solution and deionized water were loaded into a 1 mL and two 2.5 mL glass syringes (Hamilton, NV, USA), respectively. Syringe pumps (PHD Ultra, Harvard Apparatus) were used to maintain constant infusion rates of each solution into 3-inlet microchannels. Lipid solution dispersed in ethanol was introduced into systems through the center inlet while deionized water was introduced through 2 side inlet channels. A flow rate ratio (FRR) of 10 and an average fluid flow velocity of 143 mm/s were set for CL production.

2.5. Luciferase-specific dsRNA preparation

Single-stranded RNA (ssRNA) sequences targeting the luciferase GL3 gene, (5'-CUUACGCUGAGUACUUCGATT-3' and 3'-TTGAAUGCGACUCAUGAAGCU-5'), which was previously published (Anderson and Chiu, 2000), were synthesized (Sigma-Aldrich, Germany) and solubilized in UltraPure DEPC-treated water to a final concentration of 1 mM. The RNA single strands were annealed to a final concentration of 40 μM double-stranded RNA (dsRNA) in annealing buffer (100 mM potassium acetate, 30 mM HEPES-KOH, 2 mM magnesium acetate; pH 7.4, DEPC-treated) using a single cycle treatment of 90 ºC for 1 min followed by 60 min at 37 ºC in a PTC-200 Peltier Thermal Cycler (MJ Research, Canada).

2.6. Preparation of CL/siRNA complexes

CL/siRNA complexes were produced with the conventional bulk mixing method. The bulk complexation was performed in an ice bath using different CL/siRNA molar charge ratios in order to optimize the ratio for *in vitro* transfection in HeLa cells. Basically, siRNA was added into a CL solution in an ice bath, vortexed for 30 s, and stored at 4 ^{o}C for further analysis. The theoretical molar charge ratio ($R_{+/-}$) between CL and siRNA was calculated by

dividing the number of DOTAP lipid (positive charge) used to produce CL by the number of phosphates in the backbone of siRNA (negative charge). In this study, the siRNA molecule we designed consists of 21 base pairs (bp) with a total molecular weight of 13,860 g/mol.

2.7. Physicochemical characterization

2.7.1. Hydrodynamic diameter, polydispersity index (PdI), and Zeta potential

Intensity-weighted mean hydrodynamic size (Z-average) and polydispersity of cationic liposomes and lipoplexes were measured using dynamic light scattering (Zetasizer NanoZS, Malvern). The backscattering configuration was set, and detection was performed at a scattering angle of 173°. The He/Ne laser emission and power source to analyze lipid particles were 633 nm and 4.0 mW, respectively. All samples were diluted to 0.206 mM before measurement.

Zeta potential was determined using Laser Doppler Anemometry by measuring the magnitude of the electrostatic attraction between CL and siRNA in order to determine stability of particles. The measurement was performed in triplicate in water at 25 °C (Zetasizer NanoZS, Malvern).

2.7.2. Morphology

The morphology of bulk-produced lipoplexes and microfluidic-produced CLs was analyzed with Cryo-Transmission Electron Microscopy (Cryo-TEM). An automated vitrification system (Vitrobot Mark IV, FEI, The Netherlands) was used for grid preparation. Grids were exposed to glow discharge treatment (easiGlow discharge system, Pelco) with 15 mA current during 25 s to increase hydrophilicity. Samples were prepared in a controlled temperature (22 °C) and humidity (100%) in order to avoid evaporation of specimens. 3 μL of sample was dropped on a carbon-coated cooper grid of 300 mesh (Ted Pella) with a blot time of 3 s. Later on, samples were evaluated with Jeol JEM-2100 operating at 200 kV with a defocus range of -2 to -4 μm. Images were obtained using a F-416 CMOS camera (TVIPS, Germany). Data acquisition was performed in the Electron Microscopy Laboratory of the Brazilian National Laboratory of Nanotechnology.

2.7.3. Gel retardation assay

A gel retardation assay was performed in order to evaluate the ability of siRNA and CLs to form complexes. Hence, lipoplexes at different molar charge ratios (0.44, 1.29, 3.27, and 10.0) were prepared and run on agarose gel (1%) containing ethidium bromide (EtBr) at a constant voltage of 50 V for 1 h in TBE (Tris/Borate/EDTA) electrophoresis buffer (10X). The mass of siRNA to run on agarose gel was fixed at 0.1 μg. The gel was visualized using a ChemiDoc™ XRS+ System with Image Lab™ Software (Bio-Rad, CA, USA).

2.8. siRNA accessibility assay

The siRNA accessibility was evaluated using ethidium bromide (EtBr) as a fluorescence probe. The saturated concentration of EtBr was determined to be 6.75 mM by fixing the molar charge ratio ($R_{+/-}$) and mass of siRNA at 3.27 and 0.2 μg, respectively, and varying the concentration of EtBr, adding 100 μL EtBr to the same volume of lipoplexes. Then, a working solution was similarly prepared by adding 100 μL of 6.75 mM EtBr to lipoplexes while varying $R_{+/-}$. The absolute fluorescence intensity was measured using a plate fluorometer (Infinite M200 Pro, TECAN) using excitation and emission wavelengths of 526 and 605 nm, respectively. The fluorescence was expressed as the relative fluorescence intensity using siRNA at varying $R_{+/-}$.

2.9. Plasmid DNA vector

For *in vitro* siRNA delivery assays, a plasmid vector coding for GL3 luciferase (pVAX1-LUC) under the control of the CMV (cytomegalovirus) promoter (Toledo et al. 2012) was used. The plasmid DNA was purified by using a PureLink HiPure Plasmid Filter Maxiprep Kit (Invitrogen, Thermo Fisher Scientific), and its concentration was determined by reading the absorbance at 260 nm.

2.10. *In vitro* luciferase activity silencing assay

HeLa cells were grown in F-12 (Ham) nutrient mixture (Gibco, UK) containing 10% (v/v) fetal bovine serum (Gibco, UK) in 75 cm^2 culture flasks and incubated in a 5% CO_2 humidified environment at 37 °C. Once cells reached a confluence of 70-90% they were trypsinized and seeded in 24-well culture plates (5×10^4 cells per well). Cells were further

incubated at 37 °C in a 5% CO_2 humidified environment until they reached a confluence of 70% and were transfected with pVAX1-LUC plasmid (1 μg/well) using Lipofectamine® 2000 (Invitrogen) as the transfection reagent following manufacturer instructions. Cells were incubated for an additional 5 hours at 37 °C in a 5% CO_2 humidified environment. Afterwards, the growth medium was replaced by F-12 (Ham) nutrient mixture not supplemented with fetal bovine serum. Then, cells were transfected with 35 nM luciferase targeting dsRNA using Lipofectamine® 2000 as the control transfecting reagent (following manufacturer instructions) and with 10, 25, and 35 nM luciferase targeting dsRNA using the studied cationic liposome as the transfecting reagent. As negative controls, cells were treated with the same concentration of Lipofectamine® 2000 and cationic liposome in each case but without the dsRNA. Cells were further incubated for an additional 6 hours at 37 °C in a 5% CO_2 humidified environment, and the growth medium was then replaced by 10% FBS supplemented F-12 medium. After 24 hours of transfection, cells were collected and analyzed for luciferase activity using the luciferase Assay System (Promega, USA), following manufacturer's instructions. Luminescence intensity was normalized by total protein concentration which was determined by using Micro BCA in each sample via a Micro BCA Protein Assay Kit (Thermo Scientific, USA). All assays were performed in triplicate.

2.11. Cell viability assay

In order to analyze the effects of the lipoplexes studied in this work on cell viability, we performed a cell viability assay using Cell Proliferation Reagent WST-1 (Roche Applied Science, USA). Shortly, HeLa cells were seeded on a 96-well plate (1×10^4 cells per well), and after they reached 70% confluence they were transfected as described previously for an *in vitro* luciferase silencing assay. After 6 hours of dsRNA transfection, the growth medium was replaced by 10% FBS-supplemented F-12 growth medium, and 10 uL of WST-1 reagent was added in each well. Cells were further incubated at 37 °C in a 5% CO_2 humidified environment for 4 hours, and afterwards absorbance was read after 60 s agitation at 440 nm using a Spectramax 384 Plus UV/VIS Microplate Reader (Molecular Devices, USA). All assays were performed in hexaplicates.

2.12. Statistical analysis

All of the data obtained were expressed as the mean of triplicates with standard deviation (SD). Tukey's test was used to make a single-step multiple comparison of values obtained for different molar charge ratios between siRNA and CLs.

3. Results and Discussion

In our previous studies, the production of cationic liposomes (CLs) using an EPC/DOTAP/DOPE lipid formulation was investigated in order to evaluate the capacity of CLs as a vector system for plasmid DNA delivery (Balbino et al. 2013a; Balbino et al. 2013b; Balbino et al. 2012). In the present work, the complexation between EPC/DOTAP/DOPE-based liposomes with siRNA is characterized. We evaluated the physico-chemical properties of lipoplexes as a function of the molar charge ratio ($R_{+/-}$) and subsequently studied the *in vitro* silencing as well as cytotoxic effect of the lipoplex composition on HeLa cells.

3.1. Effect of molar charge ratio on physico-chemical properties of lipoplexes

First, we determined physico-chemical properties of the CLs produced via a microfluidic platform in order to complex them with siRNA. The microfluidics-produced CLs presented an average size of 164.0 ± 13.3 nm, zeta potential of 49.1 ± 1.8 mV, and polydispersity index of 0.117 ± 0.016. These results were in accordance with other similar studies (Carugo et al. 2016). In order to investigate the effect of the molar charge ratio ($R_{+/-}$) on physico-chemical properties of lipoplexes, siRNA was complexed with CLs using the bulk mixing method to generate lipoplexes (siRNA/CL). The effect of different $R_{+/-}$ on average diameter, zeta potential, and polydispersity index (PdI) is presented in Figure 3.1.

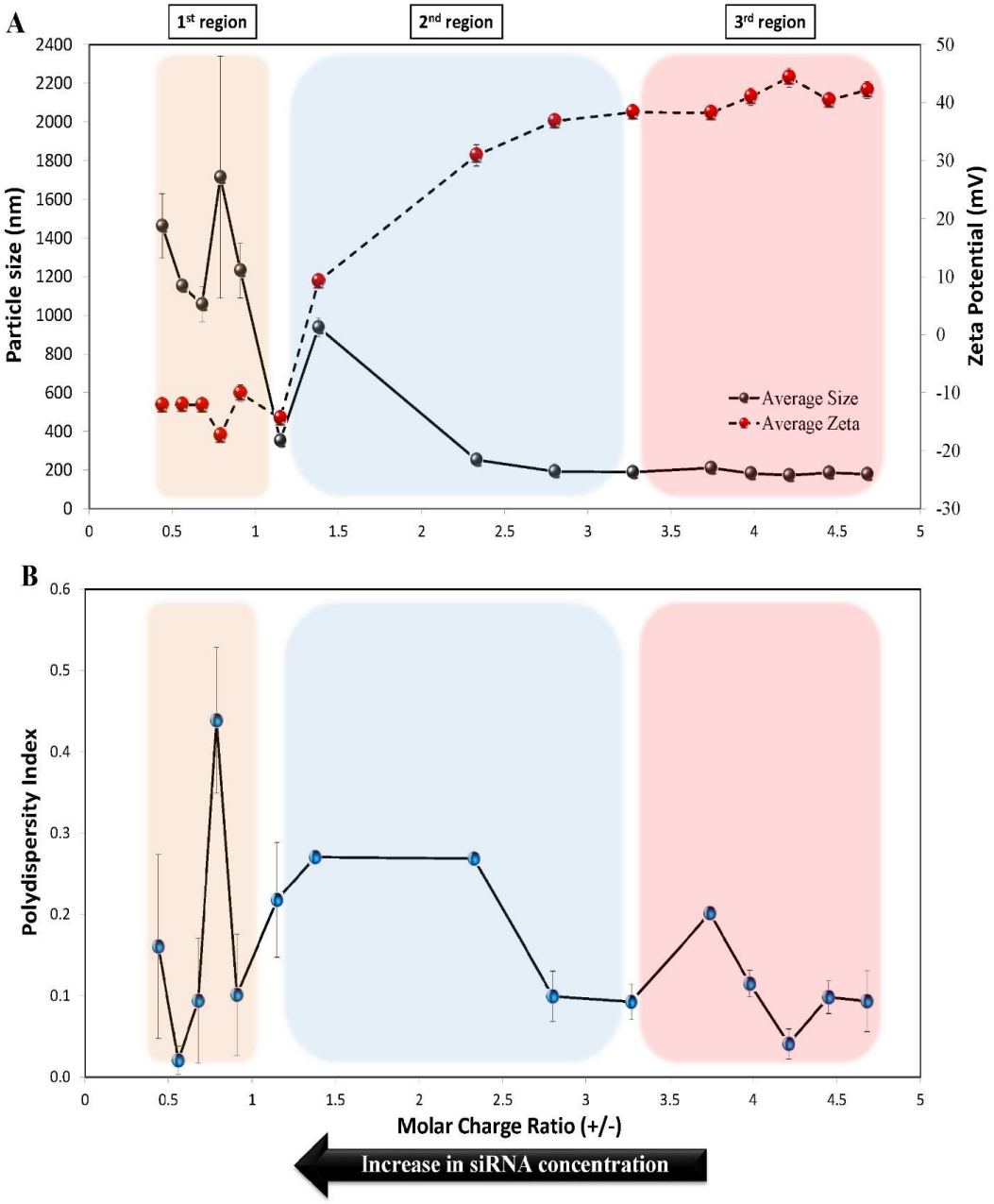

Figure 3. 1. Intensity-weighted mean hydrodynamic diameter and zeta potential (A) and Polydispersity (B) profiles of siRNA/CL complexes at different molar charge ratios (R+/-). The solid and dashed lines visually demonstrate the trend of the variations. The error b ars represent the standard deviation of independent triplicates. The microfluidics-produced empty CLs presented an average size of 164.0 ± 13.3 nm, zeta potential of 49.1 ± 1.8 mV, and polydispersity index of 0.117 ± 0.016.

It is possible to observe in Figure 3.1 that the size of the lipoplexes tends to decrease as the molar charge ratio ($R_{+/-}$) increases (while the amount of siRNA decreases). There is a

decrease in size from approx. 1400 nm to approx. 350 nm with $R_{+/-}$ ranging from 0.44 to 1.15 (Region 1, Figure 3.1A). While $R_{+/-}$ ranging from 1.15 to 2.33 presented slight fluctuations in terms of mean particle diameter (Region 2, Figure 3.1A), at $R_{+/-}$ higher than 2.33 the average particle size was stabilized at 200 nm. In region 3, with $R_{+/-}$ higher than 3.5, the average diameter was mostly smaller than 200 nm.

The alteration in zeta potential values was also observed at varying $R_{+/-}$ ranges and was indicated by the three different regions (Figure 3.1A). For the lipoplexes with $R_{+/-}$ ranging from 0.44 to 1.15, the average zeta potential was around -12.1 mV (Region 1). For $R_{+/-}$ values ranging from 1.15 to 3.27 (Region 2, Figure 3.1A), there is a drastic increase in zeta potential values, reaching almost +40 mV, indicating the region of iso-neutrality is between region 1 and 2, where $R_{+/-}$ is close to 1. However, in this region, the average size of lipoplexes did not show a steady profile and was partially maintained at high values. Between $R_{+/-}$ 2.33 and 3.27, zeta potential increased from +30.9 to approx. +40 mV and started to show constant values after 3.27. Likewise, the average size dropped drastically from ~900 nm (transition point) at the start of Region 2 to ~200 nm (Region 3, Figure 3.1A). This point ($R_{+/-}$ = 3.27) can be considered as the critical concentration for the change in size and zeta potential as a function of $R_{+/-}$ values (i.e., smaller amounts of RNA after this point did not alter the physico-chemical characteristics of lipoplexes).

Figure 3.1B presents the PdI profile as a function of $R_{+/-}$. In order to better compare PdI variation with the average diameter and zeta potential, we also displayed the data in three regions. In the first region ($R_{+/-}$ up to 1.15), as the average diameter maintained high values (1400 nm), the PdI significantly varied, reaching a maximum value of 0.4. The PdI in Region 2 decreased from 0.3 to 0.1 and presented smaller standard deviations than those of the first region. The lowest values of PdI (between 0.1 and 0.2) were obtained after $R_{+/-}$ 3.27 as shown in Region 3, where RNA is also at the lowest level.

Compared to “empty” CLs, complexation increased the average size (189.1 nm) and decreased zeta potential (38.3 mV) at $R_{+/-}$ 3.27 as was expected due to the negative charge effect of siRNA on CLs. Based on PdI results of “empty” CLs and those complexed with siRNA, there was only one point ($R_{+/-}$ 0.79) where PdI achieved the maximum value (0.439) and was

considered too high for *in vitro* and *in vivo* applications (Buñuales et al. 2011). At $R_{+/-}$ 3.27, PdI was the closest to 0.1 and was considered acceptable for *in vivo* applications (Figure 3.1B, Region 3).

When we compare the trends on average diameter, zeta potential, and PdI obtained for siRNA lipoplexes with those obtained with pDNA in the same CL composition (Balbino et al. 2012), we observe some similarities and differences. In terms of average diameter, in the case of pDNA:CLs, $R_{+/-}$ values lower than 1 (Balbino et al. 2012) generated small nanoaggregates (below 100 nm), which is different from siRNA:CLs (Figure 3.1A) with larger aggregates (1400 nm). This is due to the fact that siRNA strictly differs from plasmids in terms of size. pDNAs employed in gene therapy mostly have a length of several kilo base pairs, and their flexible molecular structure allows the formation of smaller particles (DNA condensation) when complexed with cationic agents such as liposomes. However, siRNA is considerably shorter (~21 bp) than pDNA and behaves as rigid rods. In addition, because of its molecular structure, no condensation occurs. When siRNA interacts with CLs, it is most likely to produce large complexes as observed in our study (Gary et al. 2007). This situation could be attributed to the effect of the smaller size of siRNA, which probably allows its incorporation into the lipid membranes to occur more rapidly than that of pDNA and results in the merging of small unilamellar vesicles that consequently form large multilamellar liposome vesicles.

In both cases, pDNA:CLs and siRNA:CLs presented the lowest average diameter at $R_{+/-}$ higher than 3. Moreover, PdI values showed similar behavior as average diameters, where siRNA:CLs complexes had high polydispersity at $R_{+/-}$ lower than 1. In addition, zeta potential profiles of pDNA:CLs and siRNA:CLs were similar.

There have been very few published data in the literature related to the effect of $R_{+/-}$ on physico-chemical properties of lipoplexes involving the use of siRNA. Zhang et al. (2010) investigated this effect on physico-chemical properties of lipoplexes formed by using DC-Chol/DOPE liposomes with pDNA and siRNA, separately. For siRNA, they observed a decrease in the size of lipoplexes as the weight ratio (weight ratio between liposome and siRNA) started to increase from the neutralization point (where the zeta potential is zero),

which was approximately 5. Until the neutralization point, large lipoplexes appeared. They concluded that this could be due to the formation of double-bilayers as the aggregates of CL and siRNA were getting larger. After this point, the size kept decreasing and was maintained at approx. ~ 200 nm only after a weight ratio of 20. These findings were in accordance with our results. In our study, until the neutralization point, which was found to be $R_{+/-}$ 1.29, the average size of lipoplexes was high, and from this point on they started to decrease in size. In the case of liposomes and pDNA, similar behavior was observed (Zhang et al. 2010). Particle size increased until the point of neutralization, which was obtained at the weight ratio of ~3. After this point, the size started to decrease until the weight ratio reached a value of 5, after which the size was more stable. Interestingly, the particle size was strongly influenced by the proportion of DC-Chol and DOPE. Moreover, it must be noted that the analysis in their study was performed based on weight ratio; however, in our study, molar charge ratio was taken into consideration. Nevertheless, both studies were comparable since molar charge ratio and weight ratio are associated.

Ramezani et al. 2009 also performed a similar study that complexed pDNA with liposomes formed using DOTAP:DOPE:DPPE (1,2-Dipalmitoyl-sn-glycero-3-phosphoethanolamine) at different ratios between 0.5 and 6.0 (Ramezani et al. 2009). However, they did not report whether they used charge ratios or weight ratios. At a ratio of 0.5, the zeta potential was found to be -4.1 mV. Increasing the ratio to 3 and then 6 resulted in a zeta potential of 15.8 and 23.8 mV, respectively. In the same range, the mean size did not change significantly (85.6-104.2 nm). Rodríguez-Pulido et al. 2008 also evaluated the change in zeta potential at different molar charge ratios between DC-Chol/DOPE and calf-thymus-DNA [34]. In this study, the iso-neutralitiy point was 4, and after the value of 5 there was no change in zeta potential. The behavior observed in these studies was in accordance with our results shown in Figure 3.1.

It is known that the particle size of lipoplexes strongly influences the internalization of non-viral vector systems, and a particle size between 100-200 nm is generally adequate for *in vitro* gene delivery studies (Buñuales et al. 2011). However, the size of lipoplexes varies depending on the interaction between carrier system and genetic material. This interaction

is mostly associated with differences in charge density, which directly influences zeta potential. The value of zeta potential is an important parameter for cellular uptake.

Several lipid-based siRNA delivery systems with varying zeta potential have been tested *in vitro* in order to analyze silencing effect. In most of the vector systems with a negative zeta potential, the silencing efficiency was poor (Ortega et al. 2008). On the other hand, for zeta potential values over +25, the silencing efficiency was mostly between 70-90% (Spagnou et al. 2004; Ásgeirsdóttir et al. 2010; Li et al. 2010). However, it must be noted that these zeta potential values were obtained using different lipid compositions, which have a great influence on zeta potential and present varying silencing effects.

3.2. Gel retardation assay analysis

In order to validate the previous findings, we carried out a gel retardation assay (Figure 3.2). Naked siRNA was used as a control and can be observed on agarose gel as a single band. The migration of siRNA was still observable after complexation with CL at $R_{+/-}$ 0.44 and 1.29. This is attributed to the excess siRNA that is not electrostatically linked to CL. This behavior can be associated with zeta potential since for both $R_{+/-}$ values, the zeta potential did not reach the maximum value, confirming that there exists a fraction of free RNA in the system. Starting from $R_{+/-}$ 3.27, a clear siRNA band was no longer observable. However, at this $R_{+/-}$ we observed a smear and also slightly visible siRNA band (Figure 3.2), suggesting that, in this condition, RNA partially interacts with the CLs with a fraction remaining unbound. Moreover, we should take into account that the gel retardation assay was carried out with a total run time of 75 min. In the previous assay with the same conditions, the total run time was 45 min and there was no observable band or smear at 3.27 (data not shown). This behavior suggests that the run time and consequent increase in buffer temperature can destabilize the electrostatic interactions between RNA and CLs. The same smear was also observed at $R_{+/-}$ 10, but there was no siRNA band in this lane. It can be clearly stated that for $R_{+/-}$ higher than 3.27, there was no free siRNA since all RNA interacted with CLs to forms lipoplexes. The extended run time (~30 min) of the gel retardation assay could explain the additional drag of siRNA on agarose gel over time. This behavior is in accordance with Figure 3.1, where we observed that for $R_{+/-}$ higher than 3.27 there is no significant

variation in size and zeta potential. This indicates that the amount of RNA did not influence liposome physico-chemical properties and that virtually all of the RNA was incorporated into the liposomes.

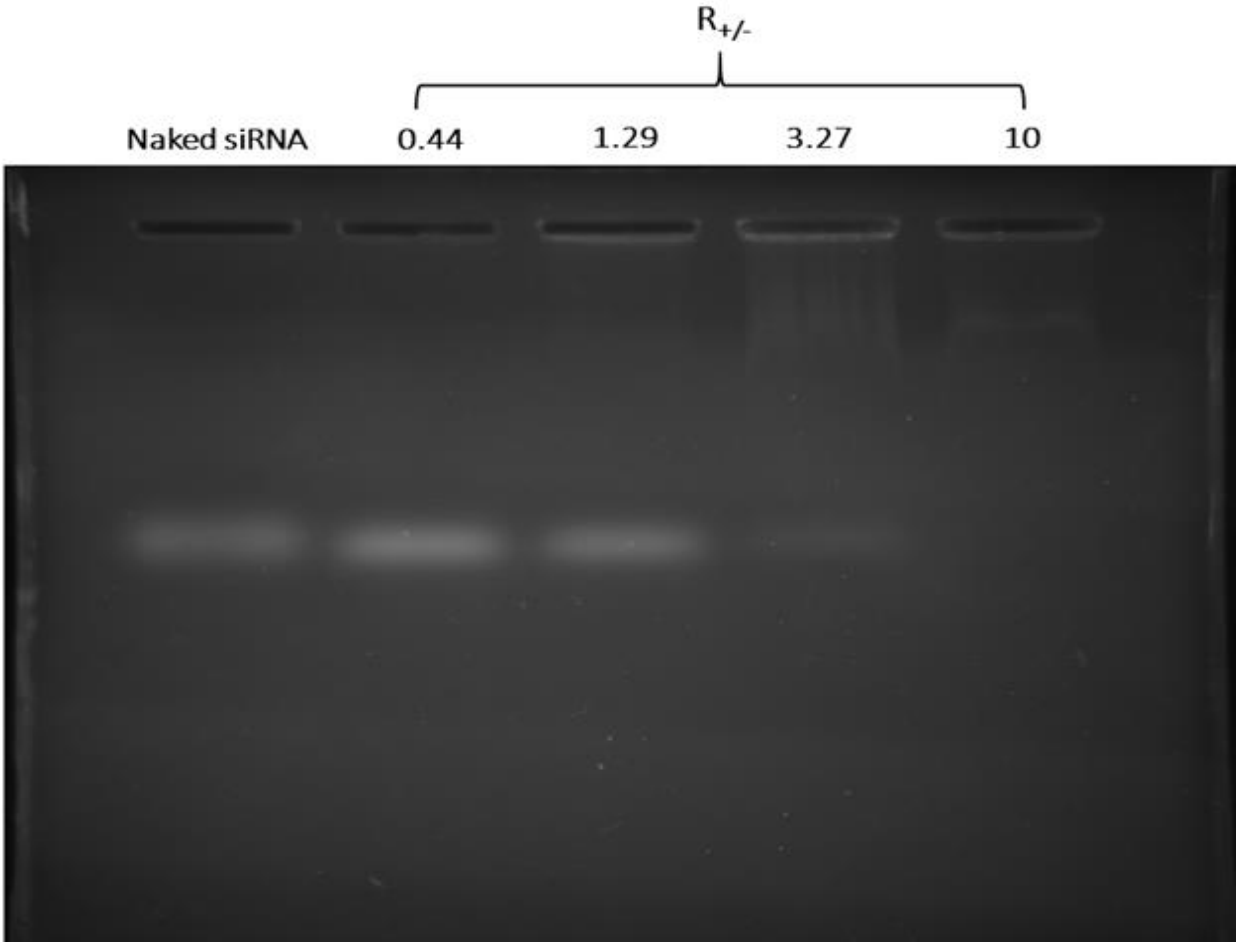

Figure 3. 2. Gel retardation assay at 5 different molar charge ratios: 1st lane: free siRNA as control; 2nd lane: R+/-=0.44; 3rd lane: R+/-=1.29 (Isoelectric point or transition point of zeta potential); 4th Lane: R+/-=3.27; 5th Lane: R+/-=10.0.

3.3. Morphological analysis

The morphological analysis was performed using Cryo-TEM and presented in Figure 3.3. The images obtained were of lipoplexes at $R_{+/-}$ of 2.33 (Figure 3.1, Region 2), 3.27 (critical molar proportion between CL and siRNA, Figure 3.1), and 4.21 (Figure 3.1, Region 3). It was observed that in most of the images (both regions, as indicated in Figure 3.1), there was high similarity in terms of multi-lamellarity of lipoplexes. After our image processing, the estimated thickness between each lamella of lipoplex was found to be around 5.7 nm, in

accordance with the previous study involving complexation with pDNA (Balbino et al. 2013a). Chang et al. 2011 used palmitoleyl MTO lipids to incorporate the siRNA (Chang et al. 2011). They measured the thickness between each membrane before and after addition of siRNA. According to the images obtained by Cryo-TEM and analysis of Fast-Fourier transform patterns, the liposome-like structure had a thickness of 3.7 nm, and this thickness increased to 6.66 nm after complexation of liposomes with siRNA. This difference indicates that the addition of nucleic acid increases the thickness between each membrane of multilamellar liposomes. These results were in accordance with the bilayer thickness we observed on Cryo-TEM (Figure 3.3).

In a previous study, liposomes with the same composition used in this current work were complexed with pDNA. Lipoplexes were generated for which the number of double bilayers prevailed (at R=3 for DNA) in structures where DNA was linked to two vesicles (Balbino et al. 2012). The same liposome composition, when complexed with hyaluronic acid, also presented a double bilayer structure (depending on the amount of hyaluronic acid) (Gasperini et al. 2015). The presence of EPC could also play an important role in defining the final structure of the lipoplexes as was previously reported in the literature using other lipid formulations (DOPE-DOTAP and DOPC-DOTAP) (Koltover, 2012). When we complexed liposomes of the same EPC/DOTAP/DOPE composition with siRNA, multi-layer structures were generated as in many different cases of DNA and RNA complexes with CL. In this case, the differences in DNA and RNA size most likely influenced the generation of multi-layer structures.

Apparently, these Large Multilamellar Vesicles (LMLVs) occur when CLs are complexed with nucleic acid molecules containing a small number of nucleotides such as oligodeoxynucleotides (ODNs), pDNA, or siRNA. This type of morphological study was previously observed (Weisman et al. 2004). They performed comparative Cryo-TEM analyses of “empty” liposomes (DOTAP/Chol, 4:1) and liposomes complexed with ODNs, separately. The authors showed that liposomes containing DOTAP and cholesterol were mostly unilamellar or oligolamellar; however, when incorporated with ODNs, multilamellar liposomes were observed. Similar structures were obtained by Kuntsche et al. (2011) using DOTAP/Chol at a ratio of 1:1 complexed with ODNs. Likewise, Jeffs et al. 2005 evaluated the

effect of different techniques to form lipoplexes consisting of liposomes (DOPE, DODAC, and PEG-CerC$_{20}$) and pDNA. Cryo-TEM analysis showed that lipoplexes presented mostly bilamellar structures, whereas the addition of pDNA resulted in the formation of a mixed population of uni-, bi-, and oligolamellar structures. Our results were comparable with those of these two studies. In our study, after complexation of CLs (EPC, DOTAP and DOPE) with siRNA, we obtained a population which predominantly consists of multilamellar nanostructures. The samples subjected to Cryo-TEM imaging were specific from the three main regions of interest: the critical concentration (R=3.27), higher, and lower amounts of RNA (R=2.33 and 4.21, respectively).

Typical multilayered structures of liposomes (DOTAP/NaChol) complexed with siRNA were also observable in previously obtained Cryo-TEM images (Geusens et al. 2009), while empty liposomes generally appeared as unilamellar vesicles. When complexed with siRNA, strong aggregation of the complexes occurred. However, highly concentrated lipoplex samples (100-times more than the transfection concentration) were used in order to acquire images in Cryo-TEM, whereas these aggregations were not visible when a normal transfection concentration was used. Similar onion-like structures were previously observed after the complexation of siRNA with CLs, which were formulated separately using BGTC, DOST, DOSK, DOSP, and DOSN lipids (Desigaux et al. 2007).

These results clearly show that addition of molecules like pDNA, siRNA, or ODN strongly alters the morphology of the lipid-based vector system. This could be attributed to the electrostatic interaction between CLs and genetic material. This type of morphological structure was not observed on Cryo-TEM after complexation of liposomes with important drug formulations, such as an iodinated or non-iodinated amino-benzyl derivate of daunorubicin or doxorubicin (Kuntsche et al. 2011), due to the lack of electrostatic interaction. However, in the case of genetic material, the electrostatic binding of genetic material to the cationic lipids results in nucleic acid condensation and consequent formation of the diverse morphology of liposomes.

It must be emphasized that factors such as lipid composition and type and concentration of genetic material vigorously influence the number of lamellae inserted into

formulated lipoplexes. Besides the number of these lamellae, these critical factors are also shown to alter the thickness between each membrane of multilamellar liposomes (Angelov et al. 2011).

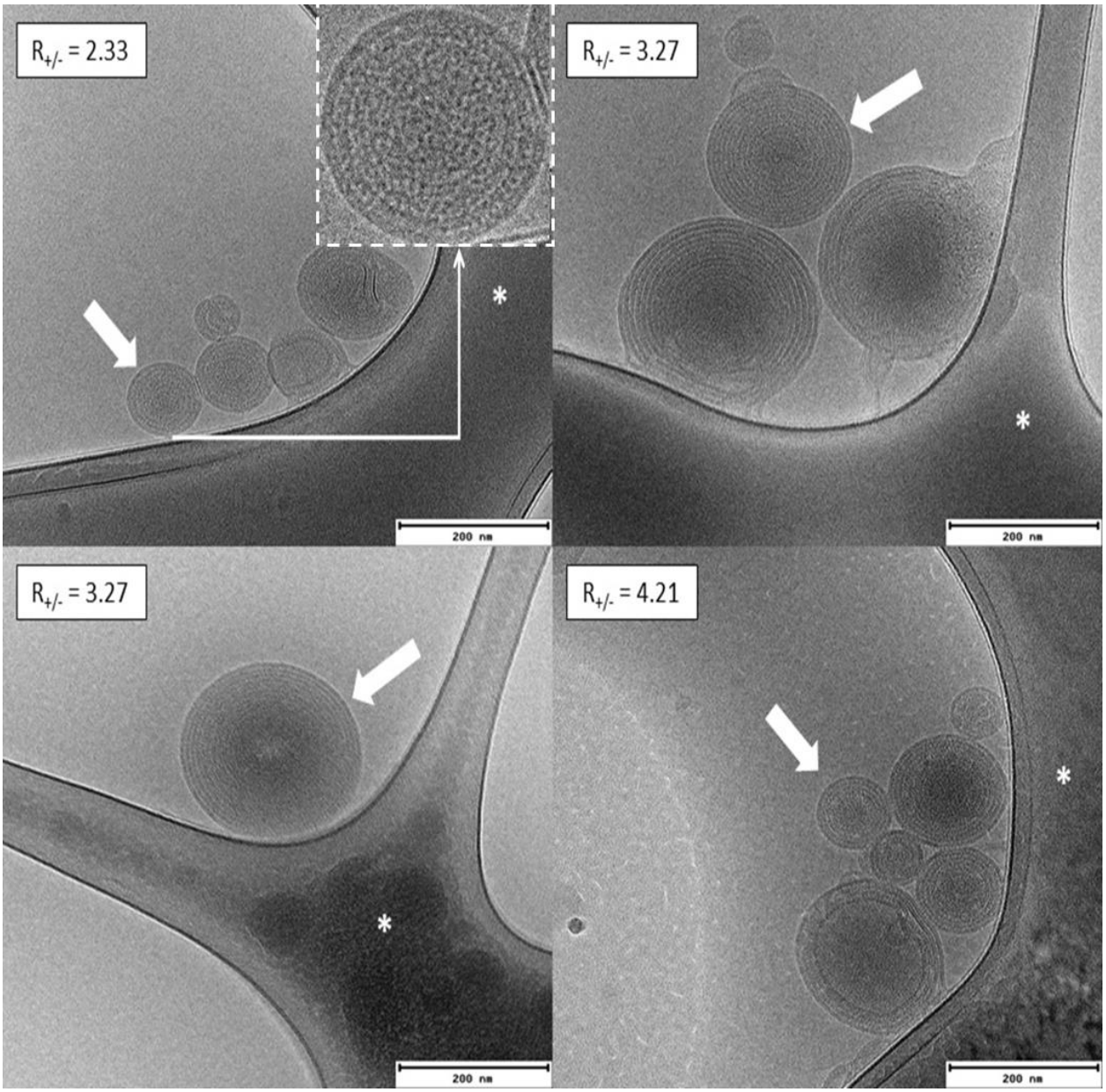

Figure 3. 3. Cryo-TEM images of lipoplexes at molar charge ratios of 2.33, 3.27, and 4.21. The scale bars represent 200 nm. Arrows indicate the multilamellar lipoplexes. Asterisks show the areas of supporting carbon film.

3.4. siRNA accessibility

We employed a fluorescence assay using ethidium bromide (EtBr) as a fluorescent probe in order to assess siRNA anchorage to the liposome at molar charge ratios varying from 1.38 to 3.74.

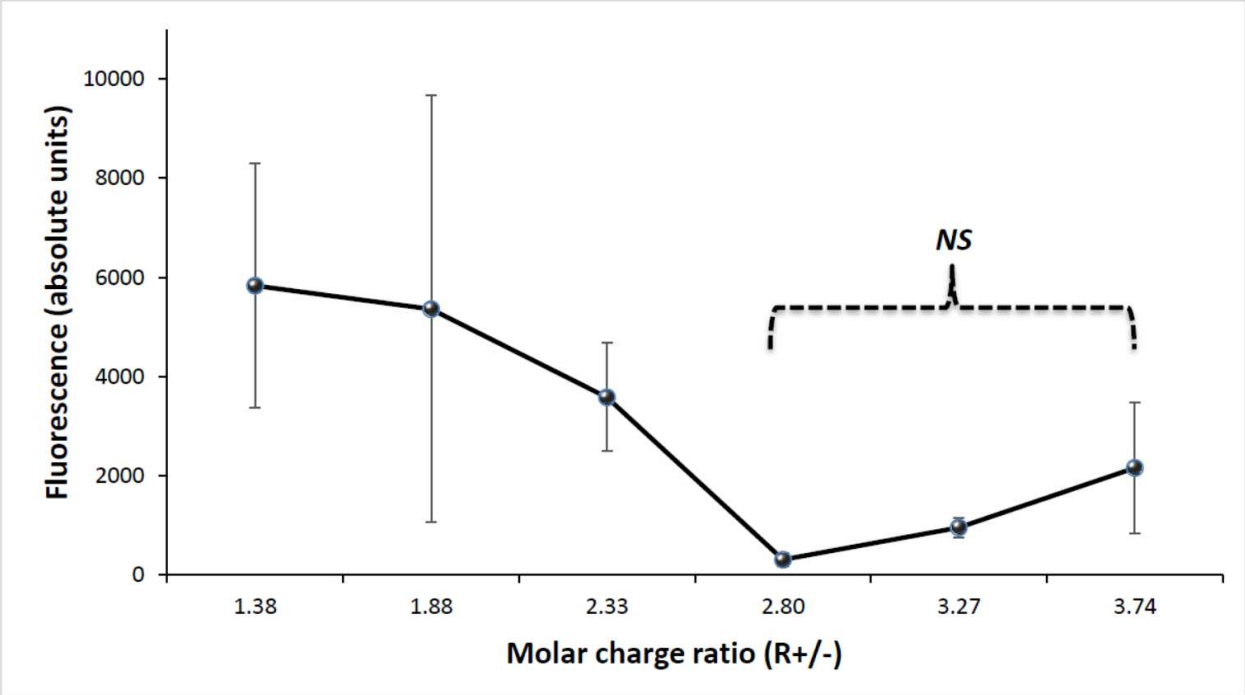

Figure 3. 4. Fluorescence profile as a function of molar charge ratio (R+/-) using ethidium bromide (EtBr) as a probe for EPC/DOTAP/DOPE-siRNA complexes. The complexations were carried out at room temperature in water. The absolute fluorescence of siRNA/CL complexe s was measured in triplicate for varying $R_{+/-}$. The error bars represent the standard deviation of independent triplicates. No significant difference between the groups at $R_{+/-}$ 2.80, 3.27, and 3.74 was found after Tukey´s test and t-test were applied ($p<0.05$). "NS" means not significant for given $R_{+/-}$ values.

Fluorescent probes have been employed to specifically investigate the effect of di- and multivalent anions, including those of pDNA or siRNA, on cationic liposome complexation. EtBr is highly specific to base pairs of free siRNA due to its anionic charge; consequently, the fluorescence will decrease as the number of electrostatic bonds between siRNA and CLs increases, which confirms the decrease in the number of free siRNA (non-incorporated with CLs). According to Figure 3.4, the fluorescence value decreased for each reading when $R_{+/-}$ increased from 1.38 to 2.80. This could be because the concentration of

free siRNA was decreasing due to more electrostatic binding with CLs. The bigger standard deviations between $R_{+/-}$ 1.38 and 2.33 could also indicate that the lipoplexes were still close to the point of iso-neutralitiy. This strongly demonstrates the point where the maximum association between siRNA and CLs was achieved and where the concentration of siRNA was lowest to be able to interact with EtBr. Above the $R_{+/-}$ value of 3.27, there is an excess of lipids and no significant alterations in fluorescence, which was also confirmed by statistical analysis. Moreover, the absolute units obtained at $R_{+/-}$ 2.80 and 3.27 exhibited low values of standard deviation, which denotes that $R_{+/-}$ 2.80 is the point at which zeta potential and size become constant as $R_{+/-}$ increases. At $R_{+/-}$ higher than 2.80, the fluorescence stopped decreasing since lipoplexes had an excess of lipids and all siRNA was interacting with CLs (as observed in Figure 3.2). Although essentially all RNA was incorporated into lipoplex at $R_{+/-}$ values above this point, the residual fluorescence indicated that there is a certain portion of RNA not electrostatically linked to cationic lipids. This situation can be attributed to multi-lamellarity caused by the interaction between CL and siRNA as obtained with Cryo-TEM images (Figure 3.3). It must be stated that there was no significant difference between the groups at $R_{+/-}$ 2.80, 3.27, and 3.74. This result was expected since there were no significant changes in zeta potential after $R_{+/-}$ 2.80.

Bedi et al. (2011) investigated the delivery of siRNA into breast cancer cells using liposomes (EPC:CHOL:DOTAP:PEG2k-PE) as non-viral vectors (Bedi et al. 2011). PicoGreen was used as a fluorescent probe, and the intensity of fluorescence was proportional to the number of free siRNA. In that study, the siRNA molecules were shielded by liposomes and could not react with the probe to emit fluorescence. We found similar results in our studies since fluorescence intensity radically decreased until a certain point of molar charge ratio ($R_{+/-}$ 2.80) and after this point showed a steady profile. Besides its use for *in vitro* studies, the siRNA accessibility assay is also critical to evaluate *in vivo* efficiency of lipoplexes. However, due to the different physical and chemical conditions of biological systems compared to *in vitro* conditions, fluorescence emitted by siRNA can be shielded by other factors which complicate the evaluation of vector system efficiency. Therefore, it is highly important to prepare lipoplexes with greater initial stability to increase their life span.

3.5. *In vitro* transfection of HeLa cells and siRNA-mediated knockdown

We evaluated the effect of lipoplexes (siRNA-EPC/DOTAP/DOPE liposomes) on the capability of silencing luciferase in HeLa cells. In this case, we selected lipoplexes with a molar charge ratio ($R_{+/-}$) of 3.27. This $R_{+/-}$ was selected since it was the minimal value (with maximal amount of RNA) where maximum zeta potential (~40 mV), minimal size (~200 nm), and low polydispersity index were achieved (Figure 3.1). In this condition, most of the RNA is anchored in the liposome structure (Figure 3.2 and 4). In order to evaluate the effect of siRNA concentration on gene silencing, we investigated three siRNA concentrations (35, 25, and 10 nM), keeping $R_{+/-}$ constant in all three cases. Commercial Lipofectamine® was also used to evaluate and compare transfection efficiency with CLs and lipoplexes as it is regarded as the gold standard of efficient delivery. In this case, we used siRNA at a concentration of 35 nM. 24 hours post-transfection, the luciferase activity (RLU/mg of total protein) of cells transfected with lipoplexes and Lipofectamine® was significantly ($p>0.05$) lower than that of cells transfected with liposomes alone (Figure 3.5). Luciferase activity for 10 and 25 nM of siRNA were 2.81×10^{10} and 2.45×10^{10} RLU/mg, respectively. The significant decrease in luciferase activity for siRNA of 10 nM (8.05×10^{7} RLU/mg) and 25 nM (6.34×10^{8} RLU/mg) in the lipid complexes suggested a successful siRNA-mediated knockdown of GL3. However, increasing the ratio from 10 to 25 nM of siRNA did not provoke a proportional increase in luciferase knockdown, which could indicate that the higher efficiency of the proposed delivery system allows the use of a lower amount of siRNA, potentially representing a more cost-effective therapy. Nevertheless, as we increased siRNA concentration from 25 nM to 35 nM, luciferase activity was significantly ($p>0.05$) inhibited (from 24.5×10^{9} to 2.64×10^{9}). In this case, since we fixed $R_{+/-}$ at 3.27, the increase in siRNA concentration implies an increase of lipid content and number of vesicles. At this concentration, we assume that 35 nM of siRNA probably altered the metabolism of HeLa cells because of the higher concentration of CLs when compared to the other two cases (10 and 25 nM of siRNA). We concluded that 10 nM of siRNA would be sufficient for efficient gene silencing. As a comparison, the luciferase activity obtained with Lipofectamine® alone was 2.62×10^{10} RLU/mg, which was not significantly different from that of empty CLs used for transfection of 10 and 25 nM of siRNA. We observe that siRNA (10 nM and 25 nM) incorporated with microfluidic-produced CLs exhibited an efficient gene knockdown of GL3. Our findings suggest that these lipoplexes can

be used to deliver siRNA *in vitro* and knock down the luciferase gene expression, being an alternative to commercial Lipofectamine®, which has a similar performance to CLs complexed with 10 nM of siRNA.

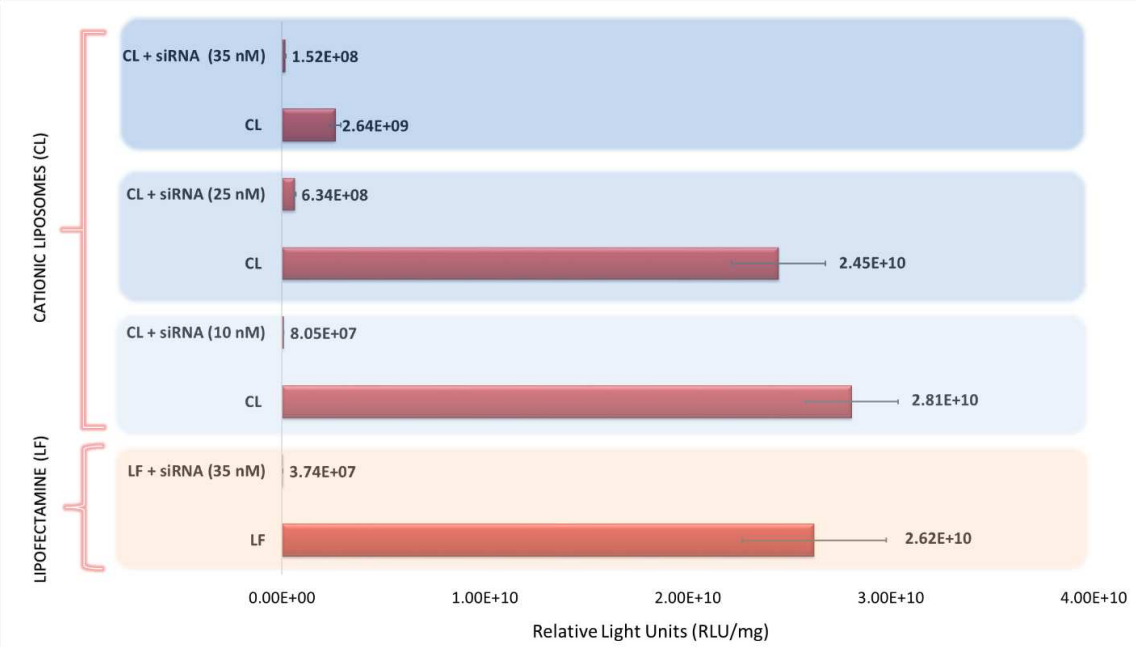

Figure 3. 5. Luciferase activity (RLU/mg protein) and its siRNA-mediated knockdown. LF refers to Lipofectamine®, which was used as the control group. "CL (10 nM)" refers to cationic liposomes without siRNA but at the same liposome concentration as in the lipoplexes with a final siRNA concentration of 10 nM ($R_{+/-}$ is fixed at 3.27) and so forth. After t-test ($p<0.05$), no significant difference was found between the group "LF" separately comparing with "CL (10 nM)" and "CL (25 nM)" or "LF + siRNA" compared with "CL + siRNA (10 nM)" and "CL + siRNA (35 nM)". The difference between "CL + siRNA (10 nM)" and "CL + siRNA (35 nM)" was ignorable. Luciferase activity for "CL (35 nM)" was significantly different compared to that of other groups without siRNA. The error bars represent the standard deviation of independent triplicates.

3.6. Cytotoxicity analysis

Low cytotoxicity is an essential attribute to allow delivery vectors to be considered for *in vivo* applications. It is well known that liposome-based gene carrier systems present lower cytotoxicity compared to other viral and non-viral systems. However, since varying lipid compositions may affect this parameter, we assessed the cytotoxicity of microfluidic-produced CL, lipoplexes, and Lipofectamine® (for reference). HeLa cells alone were established as the control group, and their viability was defined as 100%. The data obtained

for CL alone with increasing concentrations of siRNA did not show any significant difference in terms of cytotoxicity (Figure 3.6), and even in higher concentrations no dose-dependent effect was observed.

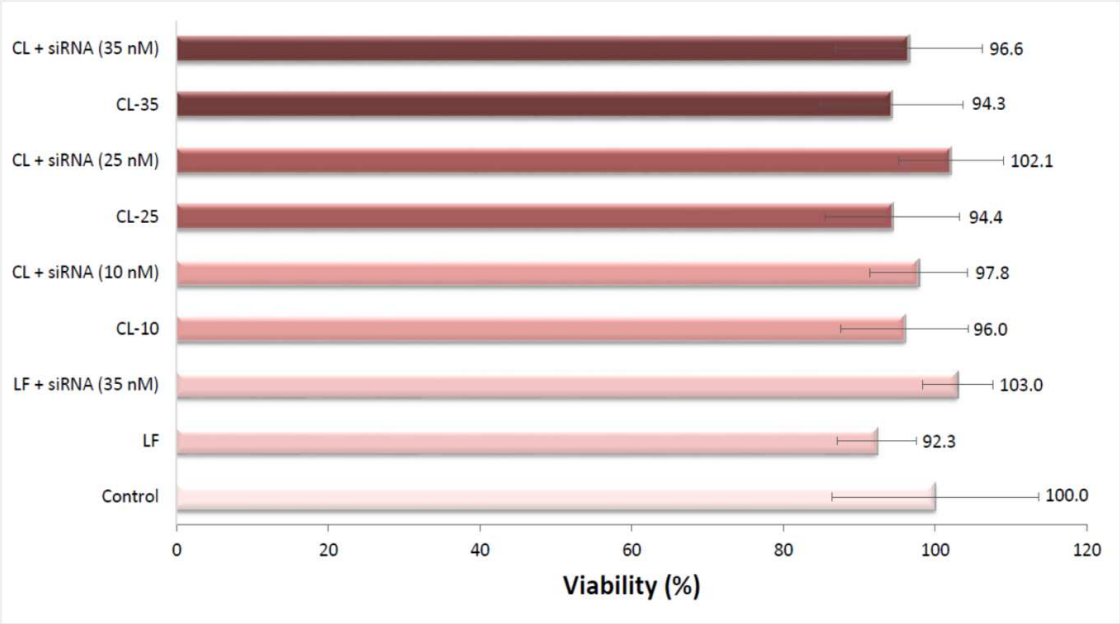

Figure 3. 6. Cytotoxicity analysis of lipoplexes and liposomes in HeLa cells. Cytotoxicity was quantified as a percentage of the control cell viability (HeLa cells only). "CL-10," "CL-25," and "CL-35" refer to cationic liposomes at the same concentration as in the lipoplexes with final siRNA concentrations of 10, 25, and 35 nM, respectively. No significant difference was found between each group of lipoplexes (CL + siRNA) and CL. The error bars represent the standard deviation of independent triplicates. There is not significant difference between control group and cell viability in the presence of LF alone or with siRNA as well as CL alone or with siRNA at varied concentration. The viability of cells with LF + siRNA (35 nM) and CL + siRNA (25 nM) presented slightly higher viability than control group, but, no statistical difference was determined.

4. Conclusion

We have studied the physico-chemical properties of siRNA lipoplexes built with different molar charge ratios between siRNA and microfluidics-produced cationic liposomes composed of EPC/DOTAP/DOPE lipids. The zeta potential profile of lipoplexes obtained in this study, representing the constant change in surface charge of the lipoplexes from negative to positive values, was found to be similar to that of previous studies performed with pDNA. The lipoplexes formulated with siRNA showed an average size of ~200 nm at molar charge ratios below 3.27 and presented predominantly LMLVs at higher RNA concentrations, which

could also be observed by Cryo-TEM. Lipoplexes, which were produced at $R_{+/-}$ 3.27 using the lowest tested concentration of siRNA (10 nM), showed excellent *in vitro* transfection efficiency and siRNA-mediated knockdown of luciferase genes in HeLa cells, comparable to Lipofectamine® efficiencies. Additionally, cytotoxicity studies revealed that lipoplexes exhibited negligible effect on cell viability. Evaluation of physico-chemical properties of lipoplexes formulated with siRNA and CLs as a function of molar charge ratio was essential in order to perform efficient *in vivo* transfection of cells and knockdown of genes. This study holds great value in order to formulate further lipid-based controlled release systems to perform efficient delivery of siRNA.

Author information

† I. Eş and M. T. Ok contributed equally in this work.

Acknowledgments

I. Eş gratefully acknowledges the financial support of the São Paulo Research Foundation (FAPESP) (Grant # 2015/14468-0). M. T. Ok acknowledges the financial support of the MIT International Science and Technology Initiatives Program (MISTI-Brazil). The authors also thank the Microfabrication Laboratory of Brazilian National Nanotechnology Laboratory (LNNano) at The Brazilian Center for Research in Energy and Materials (CNPEM).

Conflict of interest

Authors declare that they have no conflict of interest.

References

1. Abina, S.H.B., Gaspar, H.B., Blondeau, J., Caccavelli, L., Charrier, S., Buckland, K., Picard, C., Six, E., Himoudi, N., Gilmour, K. and McNicol, A.M., 2015. Outcomes following gene therapy in patients with severe Wiskott-Aldrich syndrome. Jama, 313(15), pp.1550-1563.
2. Angelov, B., Angelova, A., Filippov, S.K., Karlsson, G., Terrill, N., Lesieur, S. and Štěpánek, P., 2011. Topology and internal structure of PEGylated lipid nanocarriers for neuronal transfection: synchrotron radiation SAXS and cryo-TEM studies. Soft Matter, 7(20), pp.9714-9720.

3. Ásgeirsdóttir, S.A., Talman, E.G., de Graaf, I.A., Kamps, J.A., Satchell, S.C., Mathieson, P.W., Ruiters, M.H. and Molema, G., 2010. Targeted transfection increases siRNA uptake and gene silencing of primary endothelial cells *in vitro*—a quantitative study. Journal of controlled release, 141(2), pp.241-251.
4. Balbino, T.A., Aoki, N.T., Gasperini, A.A., Oliveira, C.L., Azzoni, A.R., Cavalcanti, L.P. and Lucimara, G., 2013. Continuous flow production of cationic liposomes at high lipid concentration in microfluidic devices for gene delivery applications. Chemical engineering journal, 226, pp.423-433.
5. Balbino, T.A., Azzoni, A.R. and de La Torre, L.G., 2013. Microfluidic devices for continuous production of pDNA/cationic liposome complexes for gene delivery and vaccine therapy. Colloids and Surfaces B: Biointerfaces, 111, pp.203-210.
6. Balbino, T.A., Gasperini, A.A., Oliveira, C.L., Azzoni, A.R., Cavalcanti, L.P. and de La Torre, L.G., 2012. Correlation of the physicochemical and structural properties of pDNA/cationic liposome complexes with their *in vitro* transfection. Langmuir, 28(31), pp.11535-11545.
7. Bedi, D., Musacchio, T., Fagbohun, O.A., Gillespie, J.W., Deinnocentes, P., Bird, R.C., Bookbinder, L., Torchilin, V.P. and Petrenko, V.A., 2011. Delivery of siRNA into breast cancer cells via phage fusion protein-targeted liposomes. Nanomedicine: Nanotechnology, Biology and Medicine, 7(3), pp.315-323.
8. Buñuales, M., Düzgüneş, N., Zalba, S., Garrido, M.J. and Tros de ILarduya, C., 2011. Efficient gene delivery by EGF-lipoplexes *in vitro* and *in vivo*. Nanomedicine, 6(1), pp.89-98.
9. Cao, F., Ju, X., Chen, D., Jiang, L., Zhu, X., Qing, S., Fang, F., Shen, Y., Jia, Z. and Zhang, H., 2017. Phosphorothioate-modified antisense oligonucleotides against human telomerase reverse transcriptase sensitize cancer cells to radiotherapy. Molecular medicine reports, 16(2), pp.2089-2094.
10. Carugo, D., Bottaro, E., Owen, J., Stride, E. and Nastruzzi, C., 2016. Liposome production by microfluidics: potential and limiting factors. Scientific reports, 6, p.25876.

11. Chang, R.S., Suh, M.S., Kim, S., Shim, G., Lee, S., Han, S.S., Lee, K.E., Jeon, H., Choi, H.G., Choi, Y. and Kim, C.W., 2011. Cationic drug-derived nanoparticles for multifunctional delivery of anticancer siRNA. Biomaterials, 32(36), pp.9785-9795.

12. Chen, G., Li, D., Jin, Y., Zhang, W., Teng, L., Bunt, C. and Wen, J., 2014. Deformable liposomes by reverse-phase evaporation method for an enhanced skin delivery of (+)-catechin. Drug development and industrial pharmacy, 40(2), pp.260-265.

13. Cuomo, F., Ceglie, A. and Lopez, F., 2012. Specific interactions between nucleolipid doped liposomes and DNA allow a more efficient polynucleotide condensation. Journal of colloid and interface science, 365(1), pp.184-190.

14. de la Torre, L.G., Rosada, R.S., Trombone, A.P.F., Frantz, F.G., Coelho-Castelo, A.A., Silva, C.L. and Santana, M.H.A., 2009. The synergy between structural stability and DNA-binding controls the antibody production in EPC/DOTAP/DOPE liposomes and DOTAP/DOPE lipoplexes. Colloids and surfaces B: Biointerfaces, 73(2), pp.175-184.

15. Desigaux, L., Sainlos, M., Lambert, O., Chevre, R., Letrou-Bonneval, E., Vigneron, J.P., Lehn, P., Lehn, J.M. and Pitard, B., 2007. Self-assembled lamellar complexes of siRNA with lipidic aminoglycoside derivatives promote efficient siRNA delivery and interference. Proceedings of the National Academy of Sciences, 104(42), pp.16534-16539.

16. Elbashir, S.M., Harborth, J., Lendeckel, W., Yalcin, A., Weber, K. and Tuschl, T., 2001. Duplexes of 21-nucleotide RNAs mediate RNA interference in cultured mammalian cells. nature, 411(6836), pp.494-498.

17. Ferrari, M.E., Rusalov, D., Enas, J. and Wheeler, C.J., 2001. Trends in lipoplex physical properties dependent on cationic lipid structure, vehicle and complexation procedure do not correlate with biological activity. Nucleic acids research, 29(7), pp.1539-1548.

18. Fire, A., Xu, S., Montgomery, M.K., Kostas, S.A., Driver, S.E. and Mello, C.C., 1998. Potent and specific genetic interference by double-stranded RNA in Caenorhabditis elegans. nature, 391(6669), pp.806-811.

19. Foged, C., Nielsen, H.M. and Frokjaer, S., 2007. Liposomes for phospholipase A2 triggered siRNA release: preparation and *in vitro* test. International journal of pharmaceutics, 331(2), pp.160-166.

20. Gary, D.J., Puri, N. and Won, Y.Y., 2007. Polymer-based siRNA delivery: perspectives on the fundamental and phenomenological distinctions from polymer-based DNA delivery. Journal of Controlled Release, 121(1-2), pp.64-73.

21. Gasperini, A.A., Puentes-Martinez, X.E., Balbino, T.A., de Paula Rigoletto, T., de Sá Cavalcanti Corrêa, G., Cassago, A., Portugal, R.V., de La Torre, L.G. and Cavalcanti, L.P., 2015. Association between cationic liposomes and low molecular weight hyaluronic acid. Langmuir, 31(11), pp.3308-3317.

22. Geusens, B., Lambert, J., De Smedt, S.C., Buyens, K., Sanders, N.N. and Van Gele, M., 2009. Ultradeformable cationic liposomes for delivery of small interfering RNA (siRNA) into human primary melanocytes. Journal of controlled release, 133(3), pp.214-220.

23. Ghanbarzadeh, S., Valizadeh, H. and Zakeri-Milani, P., 2013. Application of response surface methodology in development of sirolimus liposomes prepared by thin film hydration technique. BioImpacts: BI, 3(2), p.75.

24. Ginn, S.L., Alexander, I.E., Edelstein, M.L., Abedi, M.R. and Wixon, J., 2013. Gene therapy clinical trials worldwide to 2012–an update. The journal of gene medicine, 15(2), pp.65-77.

25. Halldorsson, S., Lucumi, E., Gómez-Sjöberg, R. and Fleming, R.M., 2015. Advantages and challenges of microfluidic cell culture in polydimethylsiloxane devices. Biosensors and Bioelectronics, 63, pp.218-231.

26. Jaafar-Maalej, C., Diab, R., Andrieu, V., Elaissari, A. and Fessi, H., 2010. Ethanol injection method for hydrophilic and lipophilic drug-loaded liposome preparation. Journal of liposome research, 20(3), pp.228-243.

27. Jeffs, L.B., Palmer, L.R., Ambegia, E.G., Giesbrecht, C., Ewanick, S. and MacLachlan, I., 2005. A scalable, extrusion-free method for efficient liposomal encapsulation of plasmid DNA. Pharmaceutical research, 22(3), pp.362-372.

28. Koltover, I., Salditt, T., Rädler, J.O. and Safinya, C.R., 1998. An inverted hexagonal phase of cationic liposome-DNA complexes related to DNA release and delivery. Science, 281(5373), pp.78-81.

29. Kuntsche, J., Horst, J.C. and Bunjes, H., 2011. Cryogenic transmission electron microscopy (cryo-TEM) for studying the morphology of colloidal drug delivery systems. International journal of pharmaceutics, 417(1-2), pp.120-137.

30. Li, J., Chen, Y.C., Tseng, Y.C., Mozumdar, S. and Huang, L., 2010. Biodegradable calcium phosphate nanoparticle with lipid coating for systemic siRNA delivery. Journal of controlled release, 142(3), pp.416-421.

31. McDonald, J.C., Duffy, D.C., Anderson, J.R., Chiu, D.T., Wu, H., Schueller, O.J. and Whitesides, G.M., 2000. Fabrication of microfluidic systems in poly (dimethylsiloxane). ELECTROPHORESIS: An International Journal, 21(1), pp.27-40.

32. Mingozzi, F. and High, K.A., 2011. Therapeutic *in vivo* gene transfer for genetic disease using AAV: progress and challenges. Nature reviews genetics, 12(5), pp.341-355.

33. Nathwani, A.C., Reiss, U.M., Tuddenham, E.G., Rosales, C., Chowdary, P., McIntosh, J., Della Peruta, M., Lheriteau, E., Patel, N., Raj, D. and Riddell, A., 2014. Long-term safety and efficacy of factor IX gene therapy in hemophilia B. New England Journal of Medicine, 371(21), pp.1994-2004.

34. Park, J.S., Yi, S.W., Kim, H.J. and Park, K.H., 2016. Receptor-mediated gene delivery into human mesenchymal stem cells using hyaluronic acid-shielded polyethylenimine/pDNA nanogels. Carbohydrate polymers, 136, pp.791-802.

35. Pozzi, D., Colapicchioni, V., Caracciolo, G., Piovesana, S., Capriotti, A.L., Palchetti, S., De Grossi, S., Riccioli, A., Amenitsch, H. and Laganà, A., 2014. Effect of polyethyleneglycol (PEG) chain length on the bio–nano-interactions between PEGylated lipid nanoparticles and biological fluids: from nanostructure to uptake in cancer cells. Nanoscale, 6(5), pp.2782-2792.

36. Ramezani, M., Khoshhamdam, M., Dehshahri, A. and Malaekeh-Nikouei, B., 2009. The influence of size, lipid composition and bilayer fluidity of cationic liposomes on the transfection efficiency of nanolipoplexes. Colloids and Surfaces B: Biointerfaces, 72(1), pp.1-5.

37. Rodríguez-Pulido, A., Ortega, F., Llorca, O., Aicart, E. and Junquera, E., 2008. A physicochemical characterization of the interaction between DC-Chol/DOPE cationic liposomes and DNA. The Journal of Physical Chemistry B, 112(39), pp.12555-12565.

38. Sackmann, E.K., Fulton, A.L. and Beebe, D.J., 2014. The present and future role of microfluidics in biomedical research. Nature, 507(7491), pp.181-189.

39. Safinya, C.R., Ewert, K.K., Majzoub, R.N. and Leal, C., 2014. Cationic liposome–nucleic acid complexes for gene delivery and gene silencing. New Journal of Chemistry, 38(11), pp.5164-5172.

40. Schooley, R.T., Spritzler, J., Wang, H., Lederman, M.M., Havlir, D., Kuritzkes, D.R., Pollard, R., Battaglia, C., Robertson, M., Mehrotra, D. and Casimiro, D., 2010. AIDS clinical trials group 5197: a placebo-controlled trial of immunization of HIV-1-infected persons with a replication-deficient adenovirus type 5 vaccine expressing the HIV-1 core protein. The Journal of infectious diseases, 202(5), pp.705-716.

41. Spagnou, S., Miller, A.D. and Keller, M., 2004. Lipidic carriers of siRNA: differences in the formulation, cellular uptake, and delivery with plasmid DNA. Biochemistry, 43(42), pp.13348-13356.

42. Toledo, M.A., Janissen, R., Favaro, M.T., Cotta, M.A., Monteiro, G.A., Prazeres, D.M.F., Souza, A.P. and Azzoni, A.R., 2012. Development of a recombinant fusion protein based on the dynein light chain LC8 for non-viral gene delivery. Journal of controlled release, 159(2), pp.222-231.

43. Touzot, F., Moshous, D., Creidy, R., Neven, B., Frange, P., Cros, G., Caccavelli, L., Blondeau, J., Magnani, A., Luby, J.M. and Ternaux, B., 2015. Faster T-cell development following gene therapy compared with haploidentical HSCT in the treatment of SCID-X1. Blood, The Journal of the American Society of Hematology, 125(23), pp.3563-3569.

44. Wang, H., Jiang, Y., Peng, H., Chen, Y., Zhu, P. and Huang, Y., 2015. Recent progress in microRNA delivery for cancer therapy by non-viral synthetic vectors. Advanced drug delivery reviews, 81, pp.142-160.

45. Weisman, S., Hirsch-Lerner, D., Barenholz, Y. and Talmon, Y., 2004. Nanostructure of cationic lipid-oligonucleotide complexes. Biophysical journal, 87(1), pp.609-614.

46. Whitehead, K.A., Langer, R. and Anderson, D.G., 2009. Knocking down barriers: advances in siRNA delivery. Nature reviews Drug discovery, 8(2), pp.129-138.

47. Yin, H., Kanasty, R.L., Eltoukhy, A.A., Vegas, A.J., Dorkin, J.R. and Anderson, D.G., 2014. Non-viral vectors for gene-based therapy. Nature Reviews Genetics, 15(8), pp.541-555.

48. Zhang, Y., Li, H., Sun, J., Gao, J., Liu, W., Li, B., Guo, Y. and Chen, J., 2010. DC-Chol/DOPE cationic liposomes: a comparative study of the influence factors on plasmid pDNA and siRNA gene delivery. International journal of pharmaceutics, 390(2), pp.198-207.

CHAPTER 4. HIGH-THROUGHPUT MICROFLUIDIC SYNTHESIS OF CATIONIC LIPOSOMES

High-throughput conventional and stealth cationic liposome synthesis using a chaotic advection-based microfluidic device combined with a centrifugal vacuum concentrator

Ismail Eş[1], Leonardo Jose Montebugnoli[1], Maria Fernanda P. Filippi[1], Antonio A. Malfatti-Gasperini[2], Allan Radaic[3], Marcelo Bispo de Jesus[3], Lucimara Gaziola de la Torre[1*]

[1] Department of Material and Bioprocess Engineering, School of Chemical Engineering, University of Campinas (UNICAMP), Campinas, São Paulo, Brazil

[2] Brazilian Synchrotron Light Laboratory (LNLS), Brazilian Center for Research in Energy and Materials (CNPEM), Zip Code 13083-970, Campinas, São Paulo, Brazil

[3]Department of Biochemistry and Tissue Biology, Institute of Biology, University of Campinas (UNICAMP), Campinas, São Paulo, 13083-862, Brazil

**Corresponding author:*
Lucimara Gaziola de la Torre
E-mail address: latorre@feq.unicamp.br
Telephone: + 55 19 35210397

The process employed in this study was submitted as the patent application (PCT/BR2019/050506) and is still in process. This study was published in ***the Chemical Engineering Journal***:

"Eş, I., Montebugnoli, L.J., Filippi, M.F.P., Malfatti-Gasperini, A.A., Radaic, A., de Jesus, M.B. and de la Torre, L.G., 2020. High-throughput conventional and stealth cationic liposome synthesis using a chaotic advection-based microfluidic device combined with a centrifugal vacuum concentrator. Chemical Engineering Journal, 382, p.122821."

ABSTRACT

Microfluidics is an emerging technology that allows efficient mixing of fluids on the nanoliter scale and has recently been employed for the production of lipid-based systems. In this study, we investigated the manufacturing of conventional (EPC/DOTAP/DOPE) and stealth (EPC/DOTAP/DOPE/DSPE-PEG(2000)) cationic liposomes (CLs) in a high-throughput chaotic advection-based microfluidic device (CA-MD) using water and ethanol. We assessed the effects of total flow rate (TFR), flow rate ratio (FRR), and flow configuration on CL formation. We compared the results with properties of CLs produced on a diffusion-based microfluidic device (D-MD). FRR (aqueous/solvent ratio) values were found to have a strong correlation with vesicle formation and values close to 1 led to the production of conventional and stealth CLs with diameter and polydispersity indices close to 200 nm and 0.2, respectively. Both liposomes are unilamellar, and stealth CL production could minimize micelle formation and operate at high flow velocities without altering characteristics of CLs. These findings were supported with dynamic light scattering (DLS), cryo-transmission electron microscopy (Cryo-EM), and synchrotron small angle X-ray scattering (SAXS) techniques. The high solvent content in liposomes after microfluidic synthesis (FRR = 1) was reduced by employing centrifugal vacuum concentrators (CVC) at low pressure and 43 °C as an alternative distillation process for successful ethanol removal without changing the structural properties of these nanoaggregates. Finally, both CLs were able to transfect pDNA into PC-3 cancer cells. The CA-MD coupled to a CVC technique produced conventional and stealth CLs with high productivity, which makes it readily applicable for industrial production.

Key-words*: Stealth liposomes, cationic liposomes, microfluidics, chaotic advection, distillation, centrifugal vacuum concentrators*

1. Introduction

Genetic diseases have been a great mystery to the scientific community for centuries. Due to recent technological advancements, several treatment methods started to come forward along with a comprehensive understanding of the molecular basis of genetic diseases. As a promising technique, nucleic acids delivery has been employed to manipulate gene expression and was used as a proof-of-concept for correcting these genetic disorders (Dowaidar et al. 2017). The delivery of nucleic acids in their naked form is unsatisfactory due to many factors. Since the composition of both nucleic acids and the targeted cell membrane contain highly polyanionic groups, a repulsive electrostatic force reduces cell permeability for the genetic material. In addition, nucleic acids are easily removed from the body by the immune system. More recently, new studies have focused on more efficient delivery techniques, such as viruses, which turned out to be favorable vectors for delivering naked genes (Pluvinage et al. 2017). Despite their advantages, the idea of using a lethal pathogen and the results obtained in clinical trials put forward several safety issues concerning this delivery method (Naldini et al. 2016). Hence, new investigations focused on the use of non-viral vectors for gene delivery.

In this context, nanotechnology emerged as a promising field of science for the engineering of novel non-viral vectors, which present great potential to overcome limitations such as limited loading capacity of viral vectors, their complex design, and safety issues (Villate-beitia et al. 2017). Among numerous non-viral vectors, cationic liposomes (CLs) are supramolecular colloidal structures formed by phospholipids that are self-assembled into a spherical bilayer in aqueous solution. These vectors represent a controlled release agent of great importance for delivering genetic material inside specific cells (Eş et al. 2018; Heuts et al. 2018) while sheltering it from intra- and extra-cellular degradative agents, resulting in efficient gene delivery (Majzoub et al. 2016). The use of cationic lipids ensures a positive charge to the structure surface, which electrostatically interacts with nucleic acids and forms complexes (Sternberg et al. 1994). Moreover, due to their molecular structure, they can be precisely engineered and made functional by the incorporation of different molecules with great pharmaceutical importance such as polyethylene glycol (PEG) in order to produce stealth liposomes.

Remarkable progress in stealth liposome manufacturing was made with the insertion of the modified lipid-PEG molecule into conventional liposomes. The effects of PEG in the liposome include the reduction of vesicle size, the stabilization of particles, and an enhancement of the lipid layer self-assembly due to the formation of a steric barrier. Most importantly, PEG provides an enhanced permeability and retention effect (EPR) because it confers an inert characteristic to the particle and increases circulation time through the body by providing steric hindrance (Nag and Awasthi, 2013; Kesharwani et al. 2012; Mui et al. 2013; Milla et al. 2012). These properties make stealth liposomes great candidates for delivery systems and therefore, further investigations are necessary to increase their efficient manufacturing with a high productivity (Hood et al. 2013). These stealth liposomes can be chemically engineered for specific targeting and more efficient manufacturing methods are being investigated (Mineart et al. 2018). The conventional manufacturing of liposomes at a laboratory scale has been previously studied and is well-established (Bangham et al. 1965; Patil and Jadhay, 2014). However, new preparation techniques are highly recommended to improve physicochemical, structural, morphological and biological properties of liposomes. Recently, novel techniques have been employed to produce liposomes, such as double solvent displacement (Sala et al. 2017), supercritical fluid processing (Tsai and Rizvi, 2016), electrospray processing (Collier et al. 2017), and microfluidics (Carugo et al. 2016).

In comparison to other techniques, microfluidics plays a special role since it pioneers numerous nanobiotechnological applications by bringing out the concept of lab-on-a-chip. Microfluidics is a pivotal tool that allows engineering of fluids at the microscale by simply altering geometrical patterns of microdevices, providing economic and technical advantages over other techniques regarding reaction times, energy consumption, automation, data acquisition, and, most importantly, mass and heat transfer (Halldorsson et al. 2015). In addition, there is an improvement in the physicochemical properties of vectors caused by microfluidic techniques over bulk techniques (Carugo et al. 2016). Despite these advantages, the mixing process through microchannels may present poor results due to the predominance of laminar flow, which is represented by a low Reynolds number (Balbino et al. 2013). Hence, improving mixing in microchannels is an important aspect of concern in

microfluidics since the absence of turbulence reduces mass transfer phenomena. In this case, it is crucial to fabricate novel microfluidic devices with improved microchannel systems that provide chaotic advection mixing. Chaotic advection can be observed in a system where a particle is advected in a velocity field that has a chaotic trajectory (Aref, 2002). In microfluidic devices, different designs can be used to promote chaotic advection. Barriers, restrictions or other strategies can be designed to generate transverse components of flow, promoting stretching and folding of fluid volumes along the channel. This type of flow is capable of reducing the required channel length for proper mixing. Considering this principle, chaotic advection-based microfluidic devices (CA-MDs) emerged as a potential solution to the mentioned limitations. Among these devices, the staggered herringbone micromixer (SHM) has recently appeared as an excellent micromixer for the formulation of efficient lipid-based delivery systems (Kastner et al. 2014).

The production of conventional CLs in a diffusion-based microfluidic device (D-MD) employing a hydrodynamic flow-focusing technique by maintaining controlled laminar flow along the channel was previously investigated (Hood et al. 2013; Kastner et al. 2014) using different lipid compositions. In this system, the mechanism of liposome formation based on a flow-focusing microfluidic device (diffusion-based microfluidic device, D-MD) depends on ethanol (or other solvent miscible in water) and water diffusion along the flow. In this case, the lipids are dispersed in ethanol have their solubility decreased as the mixture with water gradually occurs. Then, bilayer fragments start aggregating and vesicles start forming. The flow-focusing microfluidic approach allows precise control of the concentration gradient, influencing liposome aggregation and resulting in a low polydispersity and reproducible sizes (Balbino et al. 2013; Mcdonald et al. 2000).

Besides conventional CLs, two studies (Hood et al. 2013; Jahn et al. 2007) demonstrated the microfluidic production of stealth CLs using DMPC/cholesterol/DCP/PEG5000-PE in a similar D-MD, but their productivity was insufficient for industrial application. The high-throughput production of liposomes (Phospholipon®90G lipids and purified phosphatidylcholine from soybean lecithin) was demonstrated using a 3D-printed diffusion-based microfluidic device which could be operated at higher flow rates (1, 3, and 6 mL/min). Unfortunately, in this study, the authors

focused on the fabrication of a microfluidic device and not on the characterization of the produced liposomes (Kastner et al. 2014) or on the production of stealth liposomes. Recently, a study described the production of conventional CLs using 1,2-dioleoyl-3-trimethylammonium-propane (DOTAP) and 1,2-dioleoyl-sn-glycero-3-phosphoethanolamine (DOPE) in a CA-MD with an increased productivity (Kastner et al. 2014). However, to the best of our knowledge, there are no systematic studies exploring the chaotic advection microfluidic mixing phenomenon on stealth CL production and its effect on the physicochemical, morphological, and structural characteristics of these liposomes.

In this context, the present study investigated the effect of a chaotic advection mixture in the synthesis of stealth and cationic liposomes. We studied the influence of important parameters such as the flow rate ratio (FRR), total flow rate (TFR), flow configuration, and number of inlet channels on the physicochemical properties (size, polydispersity index, and ζ-potential), as well as on the structural (SAXS) and morphological (Cryo-TEM) characteristics of CLs in comparison to D-MD-produced CLs. Moreover, since each tested flow configuration resulted in different final phospholipid and ethanol concentrations, the effect of these concentrations on the given characteristics was also evaluated. Most interestingly, we performed solvent a removal process using centrifugal vacuum concentrators (CVC) at low pressure and room temperature as an alternative distillation process, eliminating the time-consuming dialysis process without interfering on the produced CL properties. Finally, we assessed the conventional and stealth CLs' abilities to transfect cancer cells (PC-3 cells) as a possible pharmaceutical application. This study aids better understanding of the important aspects of the production of these important lipid-based colloidal systems while preventing the formation of micelles at a large scale for industrial applications.

2. Materials and Methods

2.1. Materials

1,2-dioleoyl-sn-glycero-3-phosphoethanolamine (DOPE), 1,2-dioleoyl-3-trimethylammonium-propane (DOTAP) and egg phosphatidylcholine (EPC) were purchased from Lipoid (Ludwigshafen, Germany) and used as phospholipids to form cationic liposomes (CL) with no further purification. 1,2-distearoyl-sn-glycero-3-phosphoethanolamine-N-

[amino(polyethylene glycol)-2000] (DSPE-PEG(2000)) was used to produce stealth CLs and purchased from Avanti Polar Lipids, Inc. (Alabama, USA). Ethanol was obtained from Labsynth (São Paulo, Brazil) and used after the dehydration process to disperse phospholipids. The Sylgard® 184 Silicone Elastomer Kit for the fabrication of microfluidic devices was purchased from Dow Corning (Auburn, MI, United States). Deionized water was obtained from Samtec Biotechnology (São Paulo, Brazil).

2.2. Microfluidic device fabrication

CA-MDs with two and three inlets were micro-fabricated according to the method previously described by McDonald et al. (2000) (Mcdonald et al. 2000) using Sylgard® 184 Silicone Elastomer Kit as a material precursor of polydimethylsiloxane (PDMS) with a mixing ratio of 10:1 between PDMS and the curing agent. The device was designed based on its commercial version used in previous studies, with slight modifications (Kastner et al. 2014). Geometrical design of the main channel (two and three inlets) (Figure 4.1A) and herringbone-like units (Figure 4.1B) of the microdevice was separately performed in AutoCAD software. After photolithography, the mask layouts were exposed to photo-plotting with an 8000 dpi resolution, and the UV exposures used MJB-3 UV300 contact mask aligner (Karl-Suss, Garching, Germany). Y-channel and herringbone units as the two PDMS layers were irreversibly sealed by O_2 plasma surface activation sealing techniques (Plasma Technology PLAB SE80 plasma cleaner, Wrington, England). Before sealing two PDMS layers, the surface of the layer containing the main channel was maintained in a KOH solution for 10 seconds to increase sealing efficiency and then washed with ethanol. In addition, the whole microdevice was covered with an additional PDMS layer to strengthen its mechanical properties. Both CA-MDs with two and three inlets consisted of 40 herringbone-like sub-units; the number of herringbone-like sub-units was based on a previous study that evaluated mixing in a CA-MD (Hood and DeVoe, 2015; Tóth et al. 2015). A similar method was used for the microfabrication of a D-MD. PDMS channels and glass were irreversibly sealed by oxidizing the surfaces with an oxygen plasma cleaner (Plasma Technology PLAB SE80 plasma cleaner, Wrington, England). All channels of the D-MD had a rectangular cross-section 100 μm high and 140 μm wide. The microchannel cross-section dimensions of the CA-MD were set to 80 μm (height) × 200 μm (width). The grooves are patterned at a 45° angle

to the x-axis and in an asymmetrical fashion dividing the microchannel at 1/3 and 2/3 of the total width, as previously shown by Stroock et al. 2002. The width and height of the grooves were 35 and 50 µm, respectively.

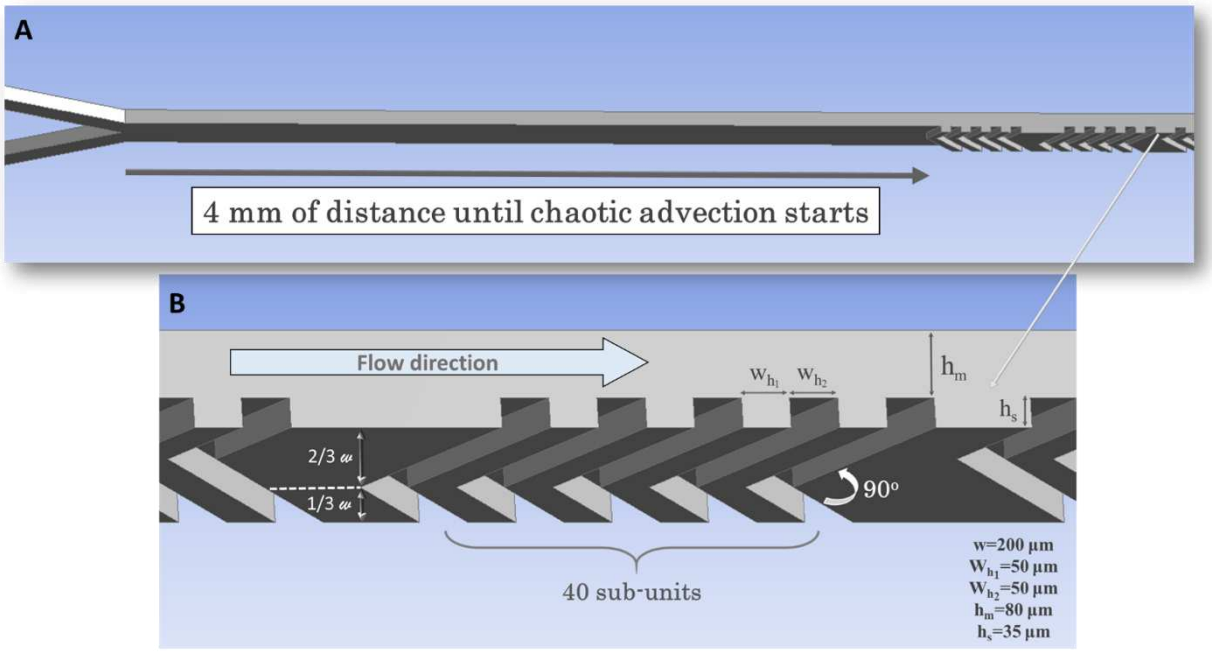

Figure 4. 1. Geometric design values of chaotic advection-based microfluidic device with 2-inlets (A) and herringbone-like structures (B). The geometry was drawn using ANSYS design modeler (DM).

2.3. Cationic Liposome formation in a microfluidic system

Conventional and stealth CL production was performed using D-MD (as control) and CA-MDs with two and three inlets. EPC, DOTAP, and DOPE at a molar ratio of 50-25-25 (%) were dispersed in anhydrous ethanol at a lipid concentration of 25 mM. For stealth CL production, the molar ratio of EPC, DOTAP, DOPE and DSPE-PEG(2000) was 50-25-24-1 (%). Prior to production, the lipid solution was sonicated for 15 min at 35 °C (Ultrasonic Cleaner 8890, Cole-Parmer). The lipid solution and deionized water were loaded into glass syringes with varying volumes (Hamilton, NV, USA). Syringe pumps (PHD Ultra, Harvard Apparatus) were used to maintain constant infusion rates of each solution into D-MD and CA-MD. CL production on D-MD was tested only at FRR = 10 (Figure 4.2A), with a total flow rate of 120.12 µL/min (Reynolds number of 13.98). Different flow configurations and their effects on CL formation were evaluated for the CA-MD with three inlets. The tested configurations

were as follows: (1) phospholipid solution through a central inlet and aqueous solutions through two lateral inlets at a flow rate ratio of 10; (2) phospholipid solution through a central inlet and aqueous solutions through two lateral inlets at flow rate ratio of 1 (Figure 4.2B). For the CA-MD with two inlets (Figure 4.2C), lipid and aqueous solutions were introduced through the two inlets at the same flow rate. The TFRs varied between 100 and 1500 µL/min for each flow configuration using CA-MDs with both two and three inlets. The Reynolds numbers for 100 and 1500 µL/min were 9.6 and 144.5, respectively; this ensures that all flows are in a laminar regime. It must be noted that the Re number for CA-MD was calculated using the rectangular cross-section of the microchannel without considering the area taken by the grooves. In this study, FRR is defined as the ratio between lateral flows and central flow, while TFR is the total flow volume (µL) introduced in the inlet channels of the microfluidic device per minute. During each run, samples were collected at three different times.

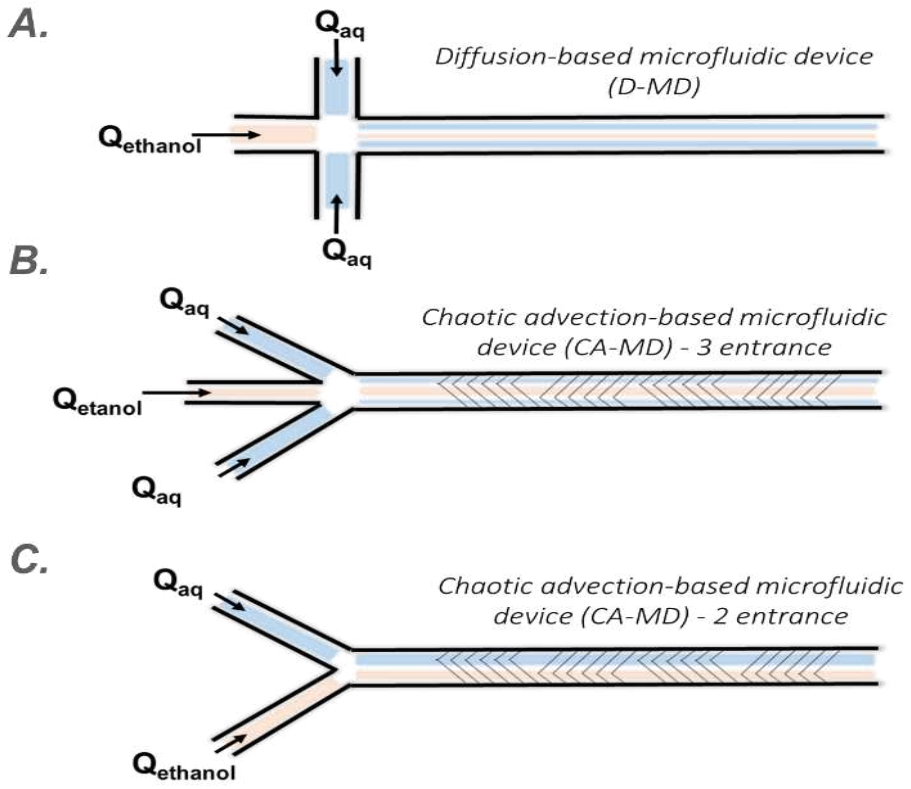

Figure 4. 2. Flow configurations of the tested microfluidic devices. (A) Diffusion-based microfluidic device; (B) Chaotic advection-based microfluidic device with three inlets; (C) Chaotic advection-based microfluidic device with two inlets. The microfluidic devices shown

in ***B*** were used for CL formation at varying flow rate ratios (between 1 and 10), while the D-MD in ***A*** was only evaluated using FRR = 10. TFR was set to 120.12 µL/min in the D-MD, whereas it varied between 100 - 1500 µL/min in the other devices. Q_{aq} and Q_{etanol} indicate the flows of aqueous solution and phospholipids dispersed in ethanol, respectively. Arrows show the flow direction.

2.4. Removal of ethanol from the liposome solution

The total ethanol concentration in the final liposome solution was found to be 50% for the CA-MD with two inlets and three inlets at FRR = 1. However, this value was below 10% for the D-MD and the CA-MD with three inlets at FRR = 10. Savant DNA 110 SpeedVac Concentrator (Marshall Scientific, New Hampshire) was used to remove ethanol from the final solution at medium drying rate. This configuration maintains the concentrator chamber at approximately 43 °C and the equipment can provide a maximal vacuum of <10 Torr, while centrifugation helps in avoiding foaming and bumping of samples and samples are concentrated by evaporation.

2.5. Physicochemical characterization

The average hydrodynamic diameter and polydispersity index (PdI) of cationic liposomes were measured using Dynamic Light Scattering (ZetasizerNanoZS, Malvern). The backscattering configuration was set with a detection angle of 173°. The He/Ne laser emission and power source used to analyze lipid particles were of 633 nm and 4.0 mW, respectively. The results obtained with DLS were also presented as intensity, volume-weighted particle size, and Z-average. Zeta potential was determined using Laser Doppler Anemometry as a measurement of electrophoretic mobility/velocity of particles, based on Henry's equation. The analyses were performed in triplicates in water at 25 °C (Zetasizer NanoZS, Malvern). All samples were diluted to a phospholipid concentration of ~0.3 mM for size measurement and 0.1 mM for Zeta potential measurement.

2.6. Structural characterization using Synchrotron SAXS

Structural analysis was performed for conventional and stealth CLs after microfluidic synthesis (containing 50% v/v ethanol) and after CVC processing (ethanol completely removed). Structural information on the produced CLs, such as the fractions of uni- and multilamellar vesicles and bilayer sizes, were obtained with the small angle X-ray

scattering (SAXS) technique. The experiments were performed at the SAXS1 beamline at the Brazilian Synchrotron Light Laboratory (LNLS) using a beam energy of 8.3 keV (λ = 0.149 nm^{-1}) and a sample-to-detector distance of 880 mm. The measured intensity is displayed as a function of the reciprocal space momentum transfer modulus $Q = 4\pi\sin(\theta)/\lambda$, where 2θ is the scattering angle and λ is the radiation wavelength. The typical range of Q values was from 0.20 nm^{-1} to 5.0 nm^{-1}.

The analyses were performed using models described in previous studies (Balbino et al. 2012; Balbino et al. 2013; Tóth et al. 2015). We assumed that the system was composed of two phases: a fraction of single bilayer vesicles and a fraction of multilayered vesicles. Therefore, the scattering intensity $I(q)$ can be written as follows:

$$I(Q) = P(Q)\, S_{eff}(Q) \quad (1)$$

where $P(Q)$ is the bilayer form factor and $S_{eff}(Q) = f_{sb} + f_m S_{MCT}(Q)$ is the effective structure factor. f_{sb} is the fraction of single bilayers, $f_m = (1 - f_{sb})$ is the fraction of multilayered vesicles and $S_{MCT}(Q)$ is the Modified Caillé structure factor (Trevisan et al. 2011).

2.7. Morphological analysis

The morphology of CLs was analyzed by Cryo-Transmission Electron Microscopy (Cryo-TEM). An automated vitrification system (Vitrobot Mark IV, FEI, Netherlands) was used for grid preparation. Grids were exposed to glow discharge treatment (easiGlow Discharge System, Pelco) with a 15 mA current during 25 s to increase hydrophilicity. Samples were prepared at controlled temperature (22 °C) and humidity (100%) to avoid specimen evaporation. Three µL of each sample was dropped on a carbon-coated copper grid of 300 mesh (Ted Pella) with a blot time of 3 s. Thereafter, samples were evaluated with Jeol JEM-2100 operating at 200 kV with a defocus range of -2 to -4 µm. Images were obtained using an F-416 CMOS camera (TVIPS, Germany). Data acquisition was performed in the Electron Microscopy Laboratory of the Brazilian Nanotechnology National Laboratory (LNNano, CNPEM, Brazil). Ethanol was removed from the liposome samples using CVC processing as it can significantly interfere with the imaging quality; afterwards, we added sterile water to maintain liposome concentrations between 10 and 15 mM prior to Cryo-TEM analysis. This procedure is in accordance with the CVC process developed in this study.

2.8. Cell culture and transfection studies on PC-3 cells

PC-3 human caucasian prostate adenocarcinoma cells were cultured in RPMI medium (with 10% FBS and 1% penicillin and streptomycin) under a humid atmosphere at 37 °C and 5% CO_2. Cells were divided using trypsin/PBS every 2 or 3 days.

The 4.7 kbp plasmid pEGFP-N1 (BD Biosciences Clontech, Palo Alto, USA) was amplified in *Escherichia coli* and purified using PureLink™ HiPure Plasmid pDNA Purification Kit-Maxiprep K2100-07 (Invitrogen, Carlsbad, CA, United States) following the manufacturer's instructions. pDNA quality and quantity were spectrophotometrically measured by Cytation 5 (BioTek, USA).

The transfection assay was performed in PC-3 cells by seeding 10^5 cells/well in a 12-well plate and allowing them to adhere overnight. On the next day, 4.6 µL of either conventional or stealth CL liposomes were diluted to 25µL/well water, while 1.6 µg of the plasmid was added to another 25 µL/well of water. The liposomes were added to the DNA-containing media and incubated at RT for 20 min, thus, forming the lipoplexes. Then, the cells were washed once with PBS and incubated with 400 µL of antibiotic- and FBS-free media containing either of conventional or stealth CL lipoplexes for 4 h. After 4 h, the transfection media were replaced with complete RPMI medium, and cells were kept in the incubator for 24 h. Finally, cells were washed with PBS, trypsinized and, GFP fluorescence was read on a FACScalibur cytometer (BD, USA). Then the obtained data were analyzed by FlowJo software to estimate the transfection efficiency and GFP fluorescence intensity.

For the comparison study between D-MD and CA-MD techniques, the same protocol was used, only changing the total volume of sample/well. In this case, 40 µL solution was produced by diluting 4.6 µL of CA-MD liposomes or 26.2 µL of D-MD liposomes in water. Liposomes were added to 40 µL of DNA solution in water containing 1.6 µg of the plasmid. Samples were then incubated for 20 minutes prior to cell treatment.

2.9. Statistical analysis

All of the obtained data was expressed as the mean of triplicates with standard deviation (SD). Tukey's test was used to make a single-step multiple comparison of values obtained for different flow rates. Student's *t*-test was used to confirm the statistical difference

between the physicochemical properties of both conventional and stealth CLs before and after CVC processing. A significance level of 0.05 was used in this study.

3. Results and Discussion

In this study, we investigated the synthesis of both conventional (EPC/DOTAP/DOPE) and stealth CLs (EPC/DOTAP/DOPE/DSPE-PEG(2000)) using a diffusion-based microfluidic device (D-MD), and the effects of a chaotic advection-based microfluidic device (CA-MD). The efficiency of both microfluidic devices concerning CL production was compared.

3.1. Synthesis of conventional and stealth CLs in a diffusion-based bicrofluidic device

CL production on a D-MD using DOPE/DOTAP/EPC phospholipids has been previously demonstrated by our group (Balbino et al. 2013). In this procedure, we applied the previously optimized process parameters, where TFR and fluid flow velocity were 120.12 μL/min and 143 mm/s, respectively, with a FRR of 10. The initial lipid concentration in the ethanolic dispersion was set to 25 mM, whereas the final lipid concentration was found to be 2.27 mM. We obtained CLs with an average diameter of 146.8 ± 4.9 nm, PdI of 0.12 ± 0.04 and a ζ potential of 55.5 ± 2.1 mV, confirming the high reproducibility of this procedure. Moreover, previous studies have demonstrated that conventional CLs produced by this system were unilamellar and capable of transfecting human epithelial carcinoma (HeLa) and human prostate cancer cells (PC-3) using plasmid DNA (pDNA) (Balbino et al. 2012; Balbino et al. 2013; Balbino et al. 2016; Balbino et al. 2017) and small interfering RNA (siRNA) (Eş et al. 2018).

We tested the D-MD in stealth CL production, using the same process configuration of conventional CL production and adding DSPE-PEG(2000) (1% of total lipid molar quantity) to the lipid/ethanol dispersion in the central stream (Figure 4.2A). Nevertheless, we observed intense particle agglomeration along the central microchannel (Figure 4.3A), which could significantly alter final lipid concentration and CL composition. As this behavior

was not found in conventional CL production, a possible hypothesis is that diffusion between ethanol and the aqueous phase induced DSPE-PEG(2000) molecules to stick to each other and spontaneously form irregular particle aggregates or clusters (Figure 4.3A). Despite the formation of aggregates along the channel, we could still produce nanoaggregates, and their physicochemical properties are shown in Figure 4.3B. However, when observing the characterization via Dynamic Light Scattering (DLS) (Figure 4.3C), the intensity-weighted size distribution revealed the presence of populations with different sizes (approximately 30 nm, 125 nm and a third one with a larger size). As the intensity–weighted size distribution is sensitive to the presence of different populations (scattered light is proportional to the diameter raised by the 6th power) (Balbino te al. 2017; Egelhaaf et al. 1996), we observed the relevance of different populations in the volume-weighted size distribution. In this distribution, the most relevant population was the one with 30 nm, characterizing the formation of micelle-like particles possibly caused by PEG molecules (Figure **4.**3C) (Egelhaaf et al. 1996).

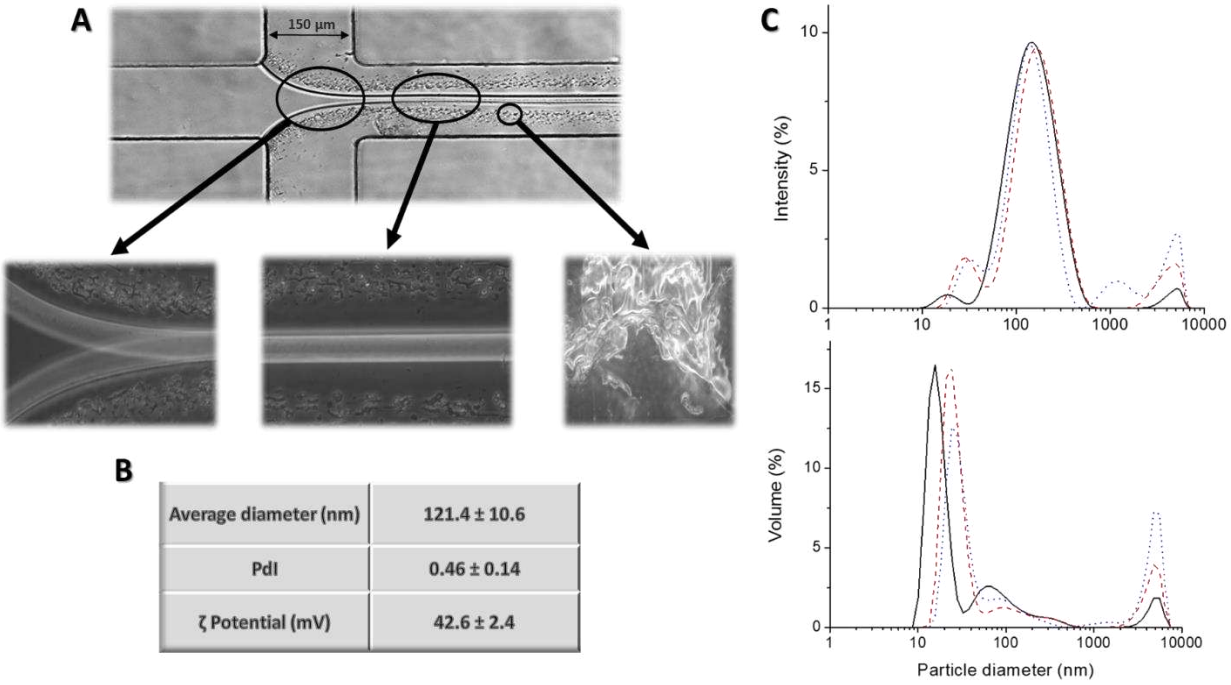

Figure 4. 3. Particle agglomeration possibly caused by the presence of DSPE-PEG(2000) along the central channel during stealth-CL production in the D-MD (A); Physicochemical properties of stealth-CLs produced on the same microfluidic device (B); Intensity and volume-weighted size distribution of stealth-CLs characterized by DLS (*C*). The central (10.92 µL/min) and lateral flows (54.6 µL/min each inlet) are PEG-included phospholipids

dispersed in ethanol and aqueous solution, respectively. The lines in each size distribution represent the profile of three independent replicates.

A critical issue associated with stealth CL production is the uncontrollable formation of micelles (Hu et al. 2012), as PEG polymer can be used to form micelle particles for drug delivery applications (Danafar et al. 2016). In aqueous solution, during the diffusion process of PEG and other phospholipids, micelle formation (10^{-3}–10^{-6} s) occurs more rapidly than the phospholipid bilayer formation (10^{-1}–10^{-3} s) (Fendler, 1994). In these circumstances, the diffusion processes employed in microfluidic systems for stealth CL production are not efficient due to possible micelle formation and consequent accumulation of aggregates along the channel, resulting in unfavorable physicochemical properties. Hood et al. 2013 demonstrated the synthesis of stealth CLs in a D-MD using a DMPC/cholesterol/DCP/PEG5000-PE phospholipid-PEG conjugate. These authors produced stealth liposomes in buffer solution, probably minimizing the effect of particle aggregation and micelle formation.

A crucial design parameter for stealth CL manufacturing is how to incorporate the maximum amount of PEG into the phospholipid bilayer (lamellar phase) before PEG is converted into micelles (micellar phase). Several factors play roles in the phase transition (from lamellar to micellar phase) of phospholipid-PEG conjugates. It was demonstrated that the main reason behind this phase transition is the polymorphic property of phospholipids, through which amphiphilic molecules form lipid aggregates under different water/organic solvent content, temperature, and pH conditions (Hristova et al. 1995). Another critical factor that may lead to micelle formation is the chain length of PEG/phospholipid conjugates, which is associated to PEG molecular weight (MW) (Bedu-addo, 1995). It was previously shown that increasing PEG concentration for incorporation on the bilayer surface can result in micellar phase, which is energetically more favorable than the bilayer phase (Hristova and Needham, 1995). In the present study, we used PEG (MW = 2000), but the diffusion-based microfluidic system was incapable of producing micelle-free liposomes with a EPC/DOTAP/DOPE/DSPE-PEG(2000) conjugate. As a possible solution to produce stealth CLs in a D-MD with no micelle formation, PEG with a lower MW could be employed. Nevertheless, we proposed a microfluidic solution by altering mixing strategies to eliminate

micelle formation. In this context, we tested the CA-MD for conventional and stealth CL manufacturing.

3.2. Synthesis of conventional and stealth CLs in a chaotic advection-based microfluidic device

Since micelle formation and particle agglomeration along the microchannel in stealth CL production is a drawback for biological applications, and manufacturing CLs on a diffusion-based microfluidic platform mostly requires an extended processing time (only 5-10 mL per hour), we investigated the effect of chaotic advection on CL synthesis (*Figure* 4*.2B, 4.2C, and* 4*.2E)*. In this context, we constructed CA-MDs with two and three inlets based on the well-reported "Staggered Herringbone Micromixer" (Belliveau et al. 2012) to investigate the synthesis of conventional and stealth CLs.

The mixing process in non-turbulent flows can be significantly improved by altering complex particle behavior using chaotic advection, which is a crucial concept generated from the non-linear dynamics of flow (Aref, 2002; Stroock et al. 2002). In the present study, the initial idea was to compare only the effects of mixing (diffusion or chaotic advection), while maintaining FRR and final lipid concentration (2.27 mM) constant, as well as the amount of organic solvent (<10%). Therefore, we applied the same FRR (10) that was used for the D-MD to the CA-MD with three inlets (Supplementary material 4.1A) while varying TFR from 100 to 1500 μL/min.

At a FRR of 10, the D-MD was suitable for synthesis of conventional CL. Interestingly, at the same FRR, even though there was no evidence of aggregation in the CA-MD (three inlets) at FRR = 10 (Figure 4.2B), the physicochemical properties of conventional CLs were worsened (Supplementary material 4.1B). DLS detected a strong peak (close to the 10 nm region), possibly indicating disorganized aggregation as a consequence of chaotic advection. In this case, conventional CLs produced in the CA-MD (TFR = 120.12 μL/min; FRR = 10) provided particle sizes close to ~110 nm, while PdI was over 0.5 and ζ-potential was significantly smaller (~44 mV) than the D-MD-produced CLs. In the production of stealth CLs on the CA-MD (three inlets), no aggregation along the channel was observed; however, according to DLS characterization, their physicochemical properties were similar to

conventional CLs (results not shown). For both conventional and stealth CLs, the physicochemical properties presented large standard deviations and aggregates with sizes close to 10 nm (Supplementary material 4.1C). The DLS results indicate the formation of disorganized structures that are not related to the expected conventional CL formation, compromising biological applications.

As previously discussed, diffusion is predominant in D-MDs and strongly depends on flow velocity, which is the reason why a low TFR is used to increase residence time in the microchannels and allow the formation of a proper concentration gradient. In contrast, since mixing occurs by chaotic advection in CA-MDs, we hypothesized that this microfluidic device could function more efficiently at higher flow rates. Therefore, we tested different TFRs (up to 1500 μL/min) to find out whether the results could be attributed to flow velocity at a constant FRR of 10. However, DLS results showed no significant change between the tested TFRs (Supplementary material 4.2). We also produced stealth CLs using the same conditions, but results were similar to the ones we obtained with conventional CLs (data not shown).

To investigate the mixing effects of the CA-MD (3-inlets) on the physicochemical properties of both conventional and stealth CLs, we made alterations to the system's FRR. This rate was decreased from 10 to 1 and the flow configuration was maintained (Figure 4.2B), resulting in promising results concerning diameter, PdI and ζ-potential. We firstly tested the same TFR employed in the D-MD (120.12 μL/min) to confirm whether the FRR had a significant effect on those properties. DLS results for both conventional and stealth CLs were significantly improved. At this TFR, average diameter, PdI, and ζ-potential of conventional CLs were 200 ± 14 nm, 0.120 ± 0.008, and 61.3 ± 2.7 mV, respectively. Comparing to D-MD-produced conventional CLs (FRR = 10), CA-MD-produced CLs were approximately 50 nm larger in size and had a 6 mV higher ζ-potential, while PdI showed no significant difference. In comparison to the properties of CA-MD-produced conventional CLs obtained at FRR = 10, average diameters and ζ-potentials of conventional CLs at FRR = 1 significantly increased (from ~110 nm to ~200 nm and ~44 mV to 61 mV, respectively). The most promising improvement was observed in PdI. It could be possible to produce liposomes with PdI as small as 0.03 in certain TFRs, which makes these CLs suitable for injection in the human body (Karnik et al. 2008; Harashima et al. 1994; Woodle, 1995).

Regarding stealth-CLs, average diameter, PdI, and ζ-potential were 168 ± 1 nm, 0.08 ± 0.03, and 57.0 ± 1.8 mV, respectively. The intensity and volume-weighted diameter distributions of conventional and stealth CLs (Figure 4.4) indicated a typical population of liposomes without smaller peaks that could correspond to micelles. Moreover, the total surface charge of stealth CLs was relatively smaller than the surface charge of conventional CLs produced at the same FRR and TFR. This behavior suggests the proper formation of liposomes, and in the case of stealth CLs, the insertion of the DSPE-PEG(2000) conjugate into the bilayer structure of liposomes, since no micelle formation was observed in the particle size distribution (Figure 4.4). Another interesting change was observed in the average diameter. Stealth CLs were approximately 30 nm smaller than the conventional ones, which can be caused by the DSPE-PEG(2000) insertion. We then varied TFRs between 120.12 and 1250 μL/min, but we did not observe any significant changes in physicochemical properties of both conventional and stealth CLs (Supplementary material 4.3).

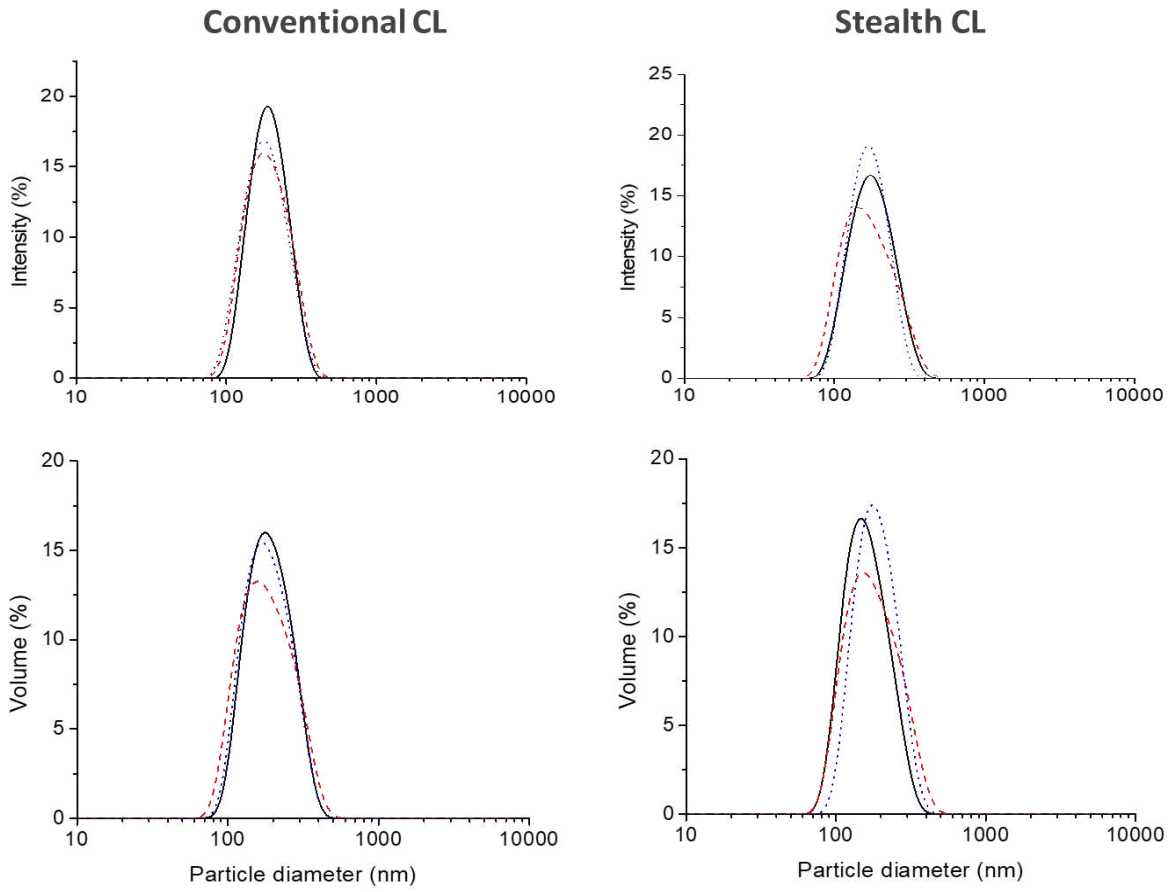

Figure 4. 4. Intensity and volume-weighted particle size of conventional and stealth-CLs produced on the CA-MD with three inlets at FRR = 1 and TFR = 500 µL/min. The lines in each size distribution represent the profile of three independent replicates.

The microfluidic device was designed with a 4 mm-long linear entrance (Figure 4.1) before the mixing patterns start in the CA-MD, where diffusion occurs. In order to investigate the influence of mixing in this region, we compared the theoretical mixing time with the residence time in this segment. Assuming a flow rate of 500 µL/min, residence time of the particles was found to be 7.68 ms. According to Karnik et al. (2008), the time scale of mixing (τ_{mix}) in a rectangular microchannel can be estimated by Equation 1.

$$\tau_{mix} \sim \frac{w_f^2}{4D} \approx \frac{w_0^2}{9D(1+\frac{1}{R})^2} \quad (1)$$

where w_0 is the width of the channel (200 μm), D is the diffusion coefficient of the solvent (usually 10^{-9} m^2/s) and R is the inverse of FRR (R = 1/FRR). For an FRR of 10, τ_{mix} has a value of 36.73 ms and for FRR = 1, τ_{mix} is 8.53 s. In this case, the theoretical mixing time is 4.78 (FRR = 10) and 1,110 (FRR = 1) times higher than the residence time in the first 4 mm of the main channel. In both cases, the theoretical mixing time is superior to the residence time, indicating that the initial linear segment of 4 mm is not sufficient to mix all fluids; thus, we can conclude that chaotic advection is the main factor that influences liposome formation.

Besides significant improvements in the physicochemical properties of conventional and stealth CLs produced at FRR = 1, final lipid concentration in CLs was also increased. Using the D-MD and the CA-MD with three inlets at FRR = 10, final lipid concentration was 2.27 mM; meanwhile, at FRR = 1, this concentration was increased to 12.5 mM. Since final lipid concentration is proportional to the amount of lipid production and the CA-MD can operate at a TFR of 1500 μL/min without any changes in the physicochemical properties of both CLs, the output at FRR = 1 can increase productivity (g mL^{-1} min^{-1}) around 70 times (5.5 times due to the concentration increase "12.5/2.27", and 12.5 times due to the TFR increase, 1500/120) when compared to the D-MD. Nevertheless, although this decrease in FRR from 10 to 1 resulted in a higher final lipid concentration, it also leads to a significant increment in the total amount of organic solvent (ethanol) in the final solution (from 9.09 to 50%), which represents a concern for biological applications of this non-viral vector system. It must be emphasized that all the samples were diluted in water for DLS analysis, achieving equivalent ethanol concentration values to the ones of D-MD-produced CLs, since an increase in ethanol concentration could alter average liposome diameters.

In our investigation with the D-MD, we hypothesized that FRR could significantly influence stealth CL formation since an FRR of 10 resulted in unfavorable physicochemical properties and precipitation along the channel. Therefore, we decreased the FRR from 10 to 1 to confirm whether FRR could improve CL production in the D-MD. After DLS analysis, we observed that micelle-like particles (smaller than 50 nm) did not appear in the size distribution profiles (data not shown). The average diameter, PdI, and ζ-potential of stealth CLs were around 230 nm, 0.21, and ∼54 mV, respectively. Moreover, the intensity and volume-weighted size distribution confirmed the presence of peaks over 5000 nm, which

could indicate inappropriate formation of particles. Consequently, we concluded that the CA-MD at a FRR of 1 was more effective and productive in stealth CL manufacturing when compared to the D-MD at a FRR of 1, and continued our investigations using the CA-MD.

In general, nanoparticle formation is driven by nanoprecipitation, which occurs at the contact between the solvent and aqueous phase streams. Regarding liposomes, their formation is mainly produced by a polarity alteration due to the geometrical design of the channel and to grooves in the CA-MD. Moreover, surface area of the interface between solvent and aqueous phases significantly increases as the fluids are folded over each other, resulting in chaotic mixing. Polarity through the microchannel can be modified in favor of liposome formation by manipulating TFR as well as FRR, the latter being directly associated to the ratio between aqueous phase and solvent. The polarity increase rate and its effect on liposome formation have been previously demonstrated (Bally et al. 2012; Zhigaltsev et al. 2012). In addition, we previously showed that both conventional and stealth CLs were bigger at FRR = 1 (~170 nm) in comparison to FRR = 10 (~120 nm). At FRR = 10, final ethanol concentration (from 50% to 9.09%) and lipid concentration decreased, resulting in a reduction of liposome size. When FRR = 1 was used, lipid concentration was higher, favoring the formation of larger bilayer fragments (Balbino et al. 2013) and as consequence, there was a slight increase in liposome size. The ethanol content also increased, but DLS measurements required dilution in water, minimizing the ethanol effect on liposome size.

As it was previously shown, the final lipid concentration of CLs produced on the CA-MD (3-inlets) at FRR = 10 and FRR = 1 were 2.27 and 12.5 mM, respectively. The increase in phospholipid concentration in the microfluidic system is another critical factor that may influence proper liposome formation at FRR = 1. For the diffusion-based microfluidic production (D-MD), this increase can potentially spoil diffusion effectiveness since it might interfere in the formation of several bilayer fragments and consequently form bigger and polydisperse lipid vesicles. In contrast, the increase in phospholipid concentration did not negatively affect liposome formation in chaotic advection-based microfluidic production. Once the chaotic advection mixing started, the high ethanol percentage could control the bilayer fragment formation through polarity changes, favoring the formation of liposomes with suitable characteristics. However, ethanol concentration should be maintained close to

50% v/v since an excessive amount of solvent can be incorporated to the vesicles' bilayer and rupture them.

We adapted the same process conditions to the CA-MD with two inlets (Figure 4.2C) by maintaining the solvent–to-aqueous ratio at 1:1 (FRR = 1) and testing TFRs from 100 to 1250 μL/min. This would simplify the process, the equipment required for operation (syringe pumps, syringes and tubes) would be reduced while maintaining the same properties. DLS analysis showed similar results to those obtained using the CA-MD with three inlets at FRR = 1. For all the tested TFRs, conventional CLs presented average diameter, PdI and, ζ-potential of 163 ± 13 nm, 0.13 ± 0.03, and 62 ± 1 mM, respectively, whereas stealth CLs had average diameter, PdI and, ζ-potential of 153 ± 5 nm, 0.11 ± 0.01, and 60 ± 2 mV. After t-test analysis, as expected, there was no statistical difference between conventional and stealth CLs produced on the CA-MD (three inlets) at FRR 1 and on the CA-MD (two inlets). Although ζ-potential was slightly smaller in stealth CLs, the difference could not be supported statistically. In addition, we did not observe any peaks that might belong to micelle-like structures, suggesting proper liposome formation. Both intensity and volume-weighted particle diameter were similar to the CLs obtained with the CA-MD with three inlets at FRR = 1 (***data not shown***). Although the production of conventional CLs on a CA-MD was previously demonstrated by Kastner et al. 2015; the produced liposomes were only characterized by DLS and no data associated with intensity, volume, or number-weighted size distribution was presented. The conventional CLs presented an average size, PdI, and ζ-potential of approximately 180 nm, 0.2, and 60 mV, respectively, at a solvent/aqueous flow rate ratio of 1. Differently from our study, they used a DOTAP/DOPE phospholipid formulation. According to a previous study (Koltover, 2012), the DOTAP/DOPE formulation does not allow proper lipid bilayer formation since it may result in the coexistence of both lamellar (L_α) and inverted hexagonal phases (H_{II}), which can cause liposome instability. The presence of both L_α and H_{II} is relevant for pharmaceutical applications since it leads to differentiated interaction in the cells, consequently creating a considerable variation. In the same study (Koltover, 2012), the inclusion of EPC (50 mol%) resulted in the exclusive formation of lipid bilayers, characterizing the formation of liposomes. Therefore, although Kastner et al., 2015 state that liposomes are formed, no structural evidence supports this

formation. The present study shows that it is possible to produce CLs without the presence of an inverse hexagonal phase (H_{II}). Moreover, we compared these results with production in a D-MD and stealth CLs were also produced.

In most cases, DSPE-PEG(2000) significantly decreases the surface charge of liposomes due to the stealth action (Fröhlich, 2012). However, this decrease also depends on the quantity of PEG that is incorporated to the CL surface, as well as on the phospholipid formulation and method used for incorporation of PEG into liposomes. We conducted our experiments with 1% PEG. To better understand the effect of PEG polymer incorporated to CLs, we repeated all the experiments with 5% PEG polymer. First, we ran the experiment using the CA-MD (3-inlets) at FRR = 10 and obtained similar results to the ones obtained with 1% PEG for conventional and stealth CLs. DLS results showed different peaks below 10 nm, possibly belonging to micelle-like structures. As we decreased FRR from 10 to 1 on the CA-MD with three inlets, DLS results once again were significantly improved. Average size, PdI and ζ-potential of stealth CLs (5% PEG) were 145.1 ± 1.5 nm, 0.11 ± 0.01, and 61.0 ± 1.8 mV, respectively. Statistical analysis showed no significant difference between stealth CLs produced on the same system with 1% PEG. However, when we used the CA-MD with two inlets, stealth CLs presented an average size of 144 ± 3 nm, PdI of 0.12 ± 0.01 and ζ-potential of 51.4 ± 4.4 mV. Compared to the CA-MD (3-inlets) at FRR = 1, size and PdI did not change, but ζ-potential significantly decreased with the addition of 5% PEG. Surface charge densities of conventional and stealth CLs were originally of 61.3 ± 2.7 mV and 62 ± 1 mM, respectively. With the inclusion of 5% DSPE-PEG(2000) conjugates, surface charge density decreased to 51.4 ± 4.4 mV. This result shows that increasing the amount of DSPE-PEG(2000) in stealth CL production resulted in a more successful incorporation of these molecules on the outer surface (Supplementary material 4.4).

When hypothesizing about the mechanism of liposome formation in the CA-MD, it is important to note that chaotic advection in three dimensions should promote a micro-ambient where the ethanol/water mixing is improved and faster than that in the D-MD. In this case, chaotic advection may influence phospholipid aggregation and consequently liposome formation. Its influence on the ethanol/water mixture in terms of mass transfer and flow rate was previously observed in our research group when we investigated the use of

single or double flow-focusing in a microfluidic device (Balbino et al., 2013). In the present study, we observed that the use of double flow-focusing required operation at higher flow velocities. It is also known that increasing the flow velocity causes the transverse diffusion to be depleted and this depends strongly on the Peclet number (Ismagilov 2000). Regarding double flow-focusing, the use of multi parallel flows is a strategy for improving mixture (Suh & Kang, 2010), since it increases molar flux. This result is an indirect evidence of the importance of mass transfer flux in the lipid aggregation process. Now considering the CA-MD system, the effect of overlapping the streamlines allows fast mixing. In this case, it is coherent to increase the amount of ethanol and the mixing time, allowing proper lipid aggregation into liposomes. Further studies on numerical simulations can be performed in order to understand the influence of fluid dynamics in the process of liposome synthesis.

3.3. Ethanol removal

As we previously discussed, the final ethanol concentration present in the CL formulation was 50% v/v on the CA-MD (three inlets, FRR = 1) and the CA-MD (two inlets), which is considered a significant limitation for further pharmaceutical and biomedical applications. Usually, ethanol removal from the final lipid solution is performed by dialysis. However, it is a time-consuming and labor-intensive process (depending on the final solution volume, it can take days). Therefore, the search for other processes can be an alternative for industrial productions. We investigated the use of CVCs to efficiently remove ethanol from the final liposomal dispersion. To this purpose, we explored CVC at low pressure and room temperature for an alternative distillation process. Briefly, CVCs use a combination of centrifugal force, vacuum and heat to speed up the evaporation rate of multiple small samples, but can significantly alter the structure and morphology of supramolecular aggregates. Therefore, all the physicochemical, structural and morphological analyses should be performed to verify if there was an alteration in these given properties. For this reason, we produced conventional and stealth CLs using the CA-MD (FRR = 1) and employed CVC to remove ethanol and replace it with water. After that, physicochemical characterization was performed, as presented in Table 4.1.

Table 4. 1. Physicochemical properties of conventional and stealth CLs produced on a CA-MD with two inlets and TFR of 500 μL/min and processed with centrifugal vacuum

concentrators (CVC) for ethanol removal. T-test was used between the before and after CVC processing groups and reliability limit was set to 95% (*p*-value < 0.05).

	Physicochemical properties	CA-MD synthesis (Ethanol 50% v/v)[i]	CVC processing (ethanol removal)
Conventional CL	[Ω]Size (nm) ± SD[ii]	187±28.3	185±17.4
	[Ω]PdI ± SD[ii]	0.12±0.03	0.14±0.04
	[Δ]Zeta Potential (mV) ± SD[ii]	59.8±0.7	50.4±5.4
Stealth CL	[Ω]Size (nm) ± SD[ii]	187±25	183±22
	[Δ]PdI ± SD[ii]	0.09±0.04	0.24±0.01
	[Δ]Zeta Potential (mV) ± SD[ii]	58.4±3.4	48.8±2.8

[i]*Microfluidics-generated liposome dispersions contained 50% (v/v) ethanol. The physicochemical characterization was performed after dilution with water, thus decreasing the ethanol content.*

[ii]*All of the obtained data were expressed as the mean of triplicates with standard deviation (SD) and significant difference was confirmed at p-value<0.05.*

[Ω]*p-value was bigger than 0.05, confirming no significant difference between groups.*

[Δ]*p-value was smaller than 0.05, confirming significant difference between groups.*

In Table 4.1, it can be observed that the average size of both conventional and stealth CLs was similar right after production on the CA-MD with two inlets. The difference in average size before and after CVC processing was not statistically significant (***p-value > 0.05***). The most significant changes after the ethanol removal process were observed in ζ-potential of both conventional and stealth CLs (decrease of ~10 mV). PdI of conventional CLs did not present significant alteration after ethanol removal, while the PdI of stealth CLs changed significantly (an increase from 0.09 to 0.24). Although this increase was statistically significant for stealth CLs, it is still acceptable depending on the biomedical application (Kim and Park, 1987). ζ-potential of conventional CLs produced on this micromixer is around 60 mV. Insertion of DSPE-PEG(2000) involves surface modification and therefore decreases the ζ-potential of colloidal systems. Even so, we observed an additional decrease in CL surface charge after employing CVC. This situation could be advantageous since a very high ζ-potential can have a toxic effect on animal cells (Fröhlich, 2012).

Time and drying rate are essential factors that affect ethanol evaporation speed. As previously stated, ethanol evaporates quicker than water due to differences in vapor pressure. Since conventional and stealth liposomes synthesized in the CA-MD present 50% v/v ethanol, this solvent is removed shortly after CVC processing begins. Thereafter, although almost all ethanol is removed from the CL dispersion, ethanol molecules can still be trapped in the dispersion or in liposome bilayers since ethanol and water molecules form an azeotrope. In our previous investigation (Balbino et al. 2013), ethanol residue in the final CL solution produced in the D-MD was around 8%, with no influence on *in vitro* biological studies. Moreover, this CL formulation did not show significant cytotoxicity to the cells. As we continue processing liposomes with CVCs, the CL dispersion begins losing a significant amount of water and becomes more concentrated. If the liposomes are continuously submitted to vacuum, they start to present some property alterations due to over-drying and lamellar phase can be achieved. Hence, it is essential to stop the CVC process on time to minimize the effect of ethanol removal on CLs. For this reason, 1 mL of 100% ethanol was added to a microtube containing half of the total volume of the CL samples (2 mL = 1 mL water + 1 mL ethanol) and was placed in CVC. When this 1 mL of ethanol was completely evaporated, the CVC process was stopped and the samples were taken for further analyses. This simple optimization was found to be sufficient for obtaining CLs with minimum alterations on their properties. In this situation, the total lipid concentration after processing was maintained.

3.4. Synchrotron small-angle X-ray scattering analysis of microfluidic produced liposomes

Liposome lamellarity (uni- or multi-) carries a great importance regarding biomedical applications and gene delivery efficiency. This is an important parameter to be considered in the validation of new liposome production processes. In this context, we used small angle X-ray (SAXS) analysis to access the structural characteristics of conventional and stealth liposomes synthesized via CA-MD and CVC. We first analyzed the effect of the chaotic advection microfluidic micromixer on cationic liposome structure with/without DSPE-PEG(2000). According to our knowledge, no studies have performed a structural analysis of liposomes produced by a microdevice operated with chaotic mixing. Figure 4.5A shows SAXS

curves for CLs with and without PEGylated lipids produced on microdevices “CA-MD with two or three inlets”. Curve fitting (not shown) using a model described elsewhere (Balbino et al. 2013; Balbino et al. 2012) allowed us to infer that these systems are unilamellar (>99%) and that there is a minor difference among their electronic density profiles. The presence of multilamellar vesicles can be tracked in the SAXS profile since it creates oscillations on the scattering pattern that can only be simulated considering a multilamellar structure factor in Equation 1. In this study, we also evaluated the effect of CVCs, which were used to replace ethanol with water in the final liposome formulation. Figure 4.5B shows SAXS curves for the same systems after CVC processing. From Figure 4.5A and B, it is possible to see a reasonable difference in the curve profiles when compared to the ones presented before ethanol removal. These differences are related to the removal of ethanol from the bilayer, changing its electronic density (bilayer form factor), as could be inferred from curve fittings (not shown). Also from fitting, it was also possible to see that the lamellarity did not significantly change (systems kept multilamellarity below 1%), showing that the systems are stable concerning this property even after CVC. Considering the SAXS analysis, the CA-MD coupled to CVC processing allows the synthesis of conventional and stealth CLs in unilamellar structures.

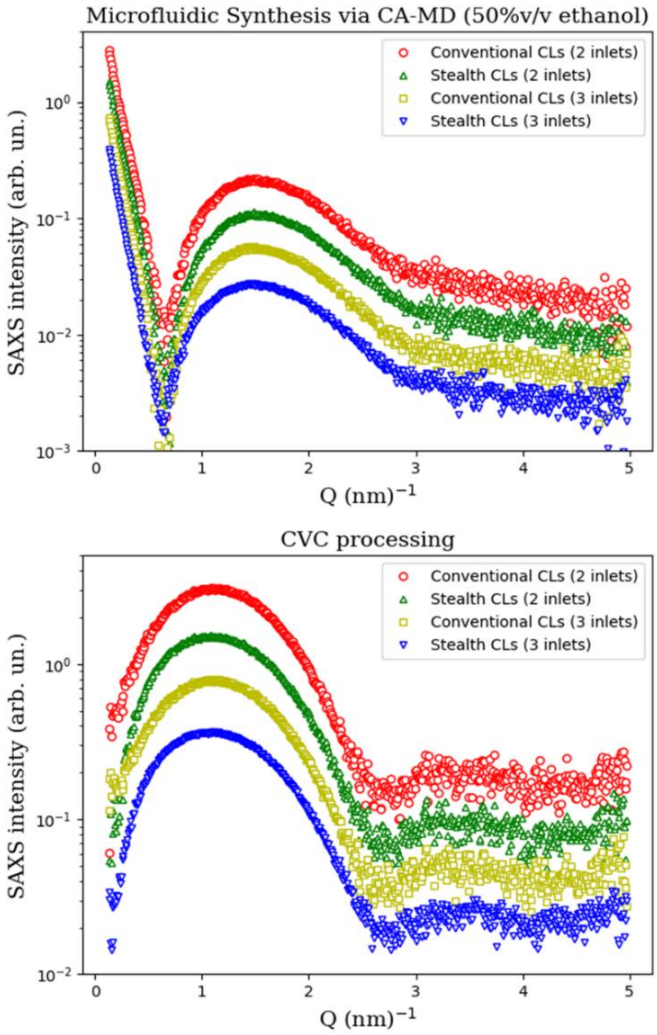

Figure 4. 5. Small-angle X-ray scattering intensity of conventional and stealth cationic liposomes produced by the CA-MD with two and three inlets at a total flow rate of 500 µL/min and submitted to CVC processing to replace excess ethanol. Measurement after CA-MD processing ***(A)***; B: After CVC processing ***(B)***.

3.5. Morphological characterization of cationic liposomes

Liposome lamellarity (uni- or multi-) carries a great importance regarding gene delivery efficiency. In most applications, unilamellar CLs are highly recommended and were shown to be more efficient in the delivery of genetic material (Kim and Park, 1987). Analyses such as DLS and SAXS can give crucial information on this property of CLs. However, morphological analysis can provide additional information whether the produced CL is unilamellar or not. For this reason, we used the Cryo-TEM technique to observe the conventional and stealth CLs produced via CA-MD and CVC.

According to the images shown in Figure 4.6, all the CL samples produced on the CA-MD (two inlets) were spherical. It is also possible to observe that the vesicles are unilamellar (arrows in Figure 4.6), supporting the results obtained by SAXS. We also observed that both conventional and stealth CLs had sizes between 150–200 nm, similar to previous DLS analyses (Table 4.1). Due to the small size of the PEG and its minor influence on liposomes' physicochemical properties, no morphological difference was observed between conventional and stealth CLs. Similar morphological structures of liposomes after PEG insertion were observed by Campos-Martorell et al. 2016 (Campos-Martorell et al. 2016). However, the lipid composition used in this study for producing stealth CLs was DLPC/CHOL/CHOL–PEG. Compared to conventional CLs, Cryo-TEM images did not show significant difference on liposome structure. Additionally, we analyzed a large amount of data on Cryo-TEM and we did not observe micelle-like structures in any of the images. Another indirect way to demonstrate that DSPE-PEG(2000) was inserted in the liposomes was by observing the decrease in transfection efficiency and the alteration in the physicochemical properties of liposomes when compared to the conventional CLs.

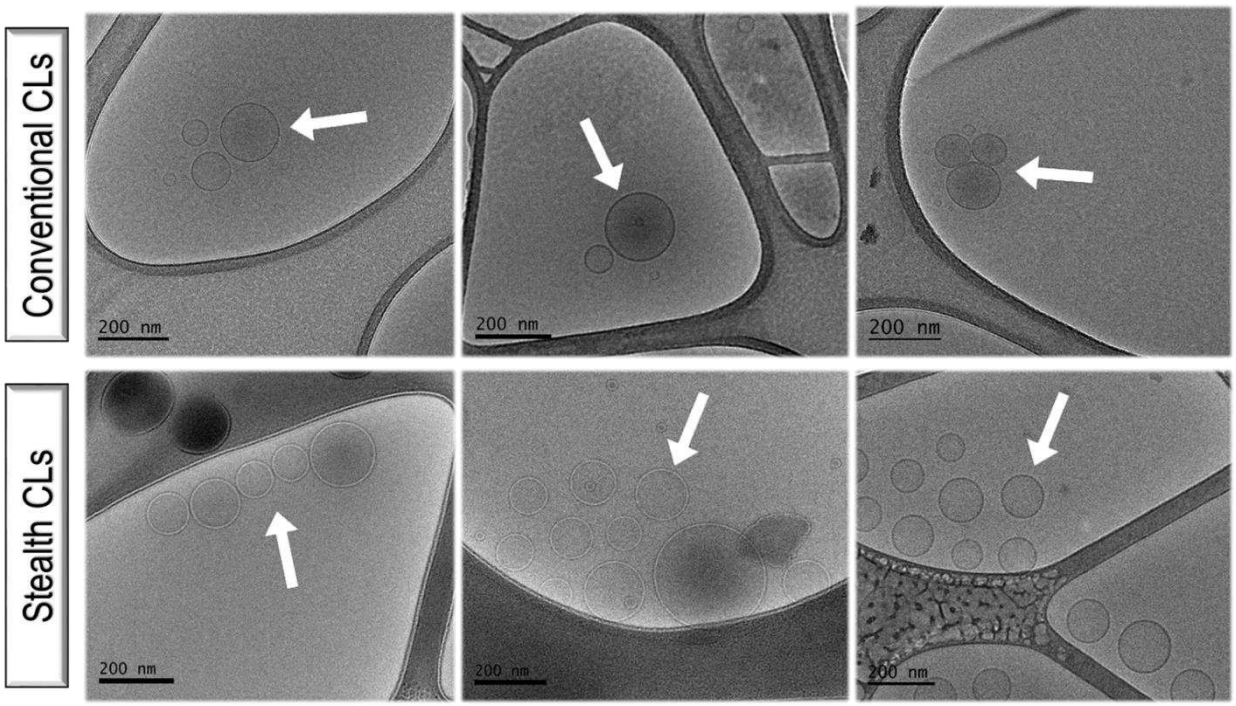

Figure 4. 6. Cryo-TEM images of conventional (EPC/DOTAP/DOPE) and stealth CLs (EPC/DOTAP/DOPE-%1 DSPE-PEG(2000)) obtained with the CA-MD (two inlets and TFR = 500 μL/min) and CVC. Scale bars indicate 200 nm. Arrows indicate liposomes.

3.6. *In vitro* evaluation of the transfection efficiency of lipoplexes

The biological activity of both conventional and stealth CLs was investigated regarding their ability to deliver plasmid DNA (EGFPpDNA) to cancer cell line PC-3 in *in vitro* transfection experiments. Conventional and stealth CLs were synthesized via CA-MD (three inlets, FRR = 1, TFR = 500 μL/min) followed by CVC processing and then complexed with EGFPpDNA at a molar charge rate (positive/negative) of 3 (Balbino et al. 2013) to generate lipoplexes. The transfection results are presented in Figure 4.7.

Conventional CLs showed a transfection level of approximately 20%, while stealth CLs presented a significantly lower transfection efficiency (~5%). The same pattern was observed for GFP fluorescence intensity. The decrease in transfection levels of PEGylated CLs could be explained by the stealth effect of DSPE-PEG(2000) on liposome surface, precluding their interaction with PC-3 cells. These results were in accordance with previous studies. Gjetting et al. 2010 (Gjetting et al. 2010) incorporated PEG polymer into DOTAP/Chol-based liposomes to produce stealth CLs and *in vitro* studies showed a significant reduction in

luciferase activity in adherent lung cancer H1299 and NCI-H69 cells (up to 10-fold, or three orders of magnitude). A similar decrease was observed when testing EGFP-expressing cells (one to two orders of magnitude, to a level just above the detection limit).

We also compared the cationic liposomes produced via D-MD and CA-MD techniques. We observed that the transfection efficiency of CA-MD liposomes was 3.18 times higher than the D-MD liposomes. This variation could be a result of process differences, since D-MD technique uses ethanol at a maximum concentration of 10% v/v which is not removed prior to transfection. On the contrary, the CA-MD technique produces liposomes with 50% v/v of ethanol, and it is removed via centrifugal vacuum concentrator. Further studies could be carried out in order to better elucidate these differences (Supplementary material, Transfection studies).

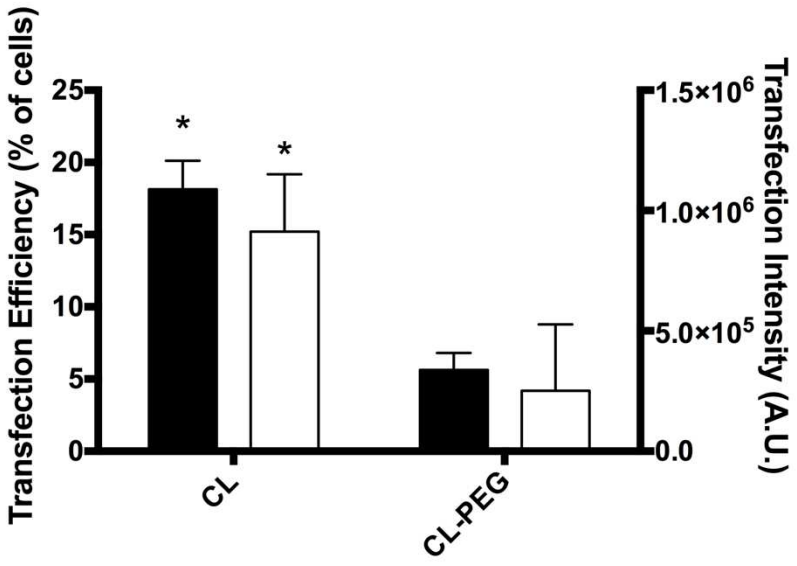

Figure 4. 7. Transfection Efficiency of conventional (CL) and stealth-CLs (CL-PEG) on PC-3 cells. EGFPpDNA containing lipoplex transfection efficiency (CL and CL-PEG) was measured through the percentage of transfected cells (left panel) and GFP fluorescence intensity (right panel). The graphs show mean ± SD means; n = 9. (***A***) represents the statistical difference ($p < 0.05$) between sample average and control (CTRL) corrected by the Dunnett test; (***B***) represents the statistical difference ($p < 0.05$) between sample average and vehicle average (Vehicle) corrected by the Dunnett test; (***C***) represents the statistical difference ($p < 0.05$) between sample average and PEG-containing cationic liposome average (CL-PEG) corrected by the Dunnett test.

The *in vitro* results validate the CA-MD synthesis and CVC processing as an efficient method to produce conventional and stealth CLs with expectable biological activities.

However, biological activity is strongly associated with phospholipid composition and the PEG polymer properties (molecular weight, chain length, concentration, etc.). Hence, future studies should focus on more efficient lipid formulations for the synthesis of stealth liposomes with more biological activities. Furthermore, of the lower efficiency of PEG-coated liposomes in transfection studies may be correlated to the size and growth properties of the tested cells since a longer pre-incubation time may be required for the uptake of lipoplexes (Bareford and Swaan, 2007; Cornelis et al. 2002).

4. Conclusion

Process productivity is an important issue in industrial production. This issue becomes more critical in pharmaceutical industries due to the complexity of the production system as well as the high cost of its materials, which brings serious economic concerns. In this study, we showed high-throughput microfluidic production of conventional and stealth cationic liposomes based on chaotic advection mixing without micelle formation, increasing the productivity by 70 times when compared to the microfluidics hydrodynamic flow-focusing process. However, a proper chaotic advection microfluidic process is only viable at a flow rate ratio of 1. In this case, the 50% v/v ethanol was removed and replaced with water using centrifugal vacuum concentrators at low pressure and room temperature as an alternative distillation process. DLS analysis demonstrated that both liposomes presented average diameters of approximately 200 nm and low polydispersity. According to Cryo-TEM and SAXS analyses, both conventional and stealth CLs showed unilamellar structures and significant transfection efficiencies into PC-3 human prostate cancer cell line. With a single microfluidic device (~4 cm × 7 cm), it could be possible to produce around 100 mL of CLs in an hour. Considering a 12 h continuous production, with sufficient microfluidic devices placed in parallel to occupy a 1 m^2 area, it could be possible to produce 400 L of CLs, which is highly acceptable for production in an industrial scale. Due to the simplicity of the ethanol removal process, the same amount of CLs could be processed using centrifugal vacuum concentrators adapted for industrial scale without altering the structural, morphological, and biological properties of CLs. This technique adjusts lipid concentration in pharmaceutical formulations, allowing operation in the maximum lipid concentration that guarantees aggregation into liposomes. The process proposed in this study is promising for industrial CL

production and with further post-production optimization, it could provide safe, efficient, and solvent-free non-viral vectors for gene delivery.

Acknowledgements

The authors thank the financial support from Fundação de Amparo à pesquisa do Estado de São Paulo (São Paulo Research Foundation FAPESP – process number 2015/26701-0) and Coordenação de Aperfeiçoamento de Pessoal de Nível Superior (CAPES) finance code 001 (Coordination for the Improvement of Higher Education Personnel). The authors kindly thank Sávio Souza Venâncio Vianna and Arthur Lopes Valente for preparing Figure 4.1 using ANSYS software. Authors also thank the Microfabrication Laboratory of Brazilian Center for Research in Energy and Materials (CNPEM) for the infrastructure to perform microfabrication as well as the Brazilian National Laboratory of Nanotechnology of CNPEM for the assistance in acquiring Cryo-TEM images of liposomes. The authors also want to thank the Brazilian Synchrotron Light Laboratory for beam times at SAXS1 beamline under research proposal (No. 20170804). Ismail Eş gratefully acknowledges the financial support of the São Paulo Research Foundation (FAPESP) (Grant # 2015/14468-0). Lucimara Gaziola de la Torre thanks Conselho Nacional de Desenvolvimento Científico e Tecnológico (CNPq – National Council for Scientific and Technological Development) for the productivity grant (310735/2016-5).

Author Contributions

I. E. and L. G. T. conceived the project and the main conceptual ideas. I. E. and L. J. M. performed the microfluidic experiments and processed the experimental data. I. E. and A. A. M. G. performed the SAXS experiment and analysis. A. R. and M. F. P. F. performed the transfection studies and analysis. M. B. J. contributed to the design of the transfection studies. L. G. T. supervised the project. All authors discussed the results and commented on the manuscript.

Conflict of Interest

Authors declare that they have no conflict of interest.

References

1. Aref, H., 2002. The development of chaotic advection. Physics of Fluids, 14(4), pp.1315-1325.
2. Balbino, T.A., Aoki, N.T., Gasperini, A.A., Oliveira, C.L., Azzoni, A.R., Cavalcanti, L.P. and Lucimara, G., 2013. Continuous flow production of cationic liposomes at high lipid concentration in microfluidic devices for gene delivery applications. Chemical engineering journal, 226, pp.423-433.
3. Balbino, T.A., Gasperini, A.A., Oliveira, C.L., Azzoni, A.R., Cavalcanti, L.P. and de La Torre, L.G., 2012. Correlation of the physicochemical and structural properties of pDNA/cationic liposome complexes with their *in vitro* transfection. Langmuir, 28(31), pp.11535-11545.
4. Balbino, T.A., Serafin, J.M., Malfatti-Gasperini, A.A., de Oliveira, C.L., Cavalcanti, L.P., de Jesus, M.B. and de La Torre, L.G., 2016. Microfluidic assembly of pDNA/Cationic liposome lipoplexes with high pDNA loading for gene delivery. Langmuir, 32(7), pp.1799-1807.
5. Balbino, T.A., Serafin, J.M., Radaic, A., de Jesus, M.B. and Lucimara, G., 2017. Integrated microfluidic devices for the synthesis of nanoscale liposomes and lipoplexes. Colloids and surfaces B: biointerfaces, 152, pp.406-413.
6. Bally, F., Garg, D.K., Serra, C.A., Hoarau, Y., Anton, N., Brochon, C., Parida, D., Vandamme, T. and Hadziioannou, G., 2012. Improved size-tunable preparation of polymeric nanoparticles by microfluidic nanoprecipitation. Polymer, 53(22), pp.5045-5051.
7. Bangham, A.D., Standish, M.M. and Watkins, J.C., 1965. The accumulation of steroids and streptolysin S on the permeability of phospholipid structures to cations. J Mol Biol, 13, pp.238-53.
8. Bedu-Addo, F.K. and Huang, L., 1995. Interaction of PEG-phospholipid conjugates with phospholipid: implications in liposomal drug delivery. Advanced drug delivery reviews, 16(2-3), pp.235-247.
9. Belliveau, N.M., Huft, J., Lin, P.J., Chen, S., Leung, A.K., Leaver, T.J., Wild, A.W., Lee, J.B., Taylor, R.J., Tam, Y.K. and Hansen, C.L., 2012. Microfluidic synthesis of highly potent

limit-size lipid nanoparticles for *in vivo* delivery of siRNA. Molecular Therapy-Nucleic Acids, 1, p.e37.

10. Broomhead, D.S. and Ryrie, S.C., 1988. Particle paths in wavy vortices. Nonlinearity, 1(3), p.409.
11. Campos-Martorell, M., Cano-Sarabia, M., Simats, A., Hernández-Guillamon, M., Rosell, A., Maspoch, D. and Montaner, J., 2016. Charge effect of a liposomal delivery system encapsulating simvastatin to treat experimental ischemic stroke in rats. International journal of nanomedicine, 11, p.3035.
12. Carugo, D., Bottaro, E., Owen, J., Stride, E. and Nastruzzi, C., 2016. Liposome production by microfluidics: potential and limiting factors. Scientific reports, 6, p.25876.
13. Collier, M.A., Bachelder, E.M. and Ainslie, K.M., 2017. Electrosprayed myocet-like liposomes: an alternative to traditional liposome production. Pharmaceutical research, 34(2), pp.419-426.
14. Cornelis, S., Vandenbranden, M., Ruysschaert, J.M. and Elouahabi, A., 2002. Role of intracellular cationic liposome–DNA complex dissociation in transfection mediated by cationic lipids. DNA and cell biology, 21(2), pp.91-97.
15. Danafar, H., Rostamizadeh, K., Davaran, S. and Hamidi, M., 2017. Drug-conjugated PLA–PEG–PLA copolymers: a novel approach for controlled delivery of hydrophilic drugs by micelle formation. Pharmaceutical development and technology, 22(8), pp.947-957.
16. Dertinger, S.K., Chiu, D.T., Jeon, N.L. and Whitesides, G.M., 2001. Generation of gradients having complex shapes using microfluidic networks. Analytical Chemistry, 73(6), pp.1240-1246.
17. Dowaidar, M., Abdelhamid, H.N., Hällbrink, M., Freimann, K., Kurrikoff, K., Zou, X. and Langel, Ü., 2017. Magnetic nanoparticle assisted self-assembly of cell penetrating peptides-oligonucleotides complexes for gene delivery. Scientific reports, 7(1), pp.1-11.
18. Egelhaaf, S.U., Wehrli, E., Müller, M., Adrian, M. and Schurtenberger, P., 1996. Determination of the size distribution of lecithin liposomes: a comparative study

using freeze fracture, cryoelectron microscopy and dynamic light scattering. Journal of microscopy, 184(3), pp.214-228.

19. Eş, I., Ok, M.T., Puentes-Martinez, X.E., de Toledo, M.A.S., de Pinho Favaro, M.T., Cavalcanti, L.P., Cassago, A., Portugal, R.V., Azzoni, A.R. and de la Torre, L.G., 2018. Evaluation of siRNA and cationic liposomes complexes as a model for *in vitro* siRNA delivery to cancer cells. Colloids and Surfaces A: Physicochemical and Engineering Aspects, 555, pp.280-289.
20. Evans, D.F. and Wennerstrom, H., 1999. Colloidal domain. Wiley-Vch.
21. Foster, R.T., Caillé, G., Ngoc, A.H., Lemko, C.H., Kherani, R. and Pasutto, F.M., 1994. Pharmacokinetics of zopiclone enantiomers in humans following oral dose administration of racemate. Pharm Res, 11, p.402.
22. Fröhlich, E., 2012. The role of surface charge in cellular uptake and cytotoxicity of medical nanoparticles. International journal of nanomedicine, 7, p.5577.
23. Gjetting, T., Arildsen, N.S., Christensen, C.L., Poulsen, T.T., Roth, J.A., Handlos, V.N. and Poulsen, H.S., 2010. *In vitro* and *in vivo* effects of polyethylene glycol (PEG)-modified lipid in DOTAP/cholesterol-mediated gene transfection. International journal of nanomedicine, 5, p.371.
24. Heuts, J., Varypataki, E.M., van der Maaden, K., Romeijn, S., Drijfhout, J.W., van Scheltinga, A.T., Ossendorp, F. and Jiskoot, W., 2018. Cationic liposomes: A flexible vaccine delivery system for physicochemically diverse antigenic peptides. Pharmaceutical research, 35(11), p.207.
25. Hood, R.R. and DeVoe, D.L., 2015. High-Throughput Continuous Flow Production of Nanoscale Liposomes by Microfluidic Vertical Flow Focusing. small, 11(43), pp.5790-5799.
26. Hood, R.R., Shao, C., Omiatek, D.M., Vreeland, W.N. and DeVoe, D.L., 2013. Microfluidic synthesis of PEG-and folate-conjugated liposomes for one-step formation of targeted stealth nanocarriers. Pharmaceutical research, 30(6), pp.1597-1607.
27. Hristova, K. and Needham, D., 1995. Phase behavior of a lipid/polymer-lipid mixture in aqueous medium. Macromolecules, 28(4), pp.991-1002.

28. Hristova, K., Kenworthy, A. and McIntosh, T.J., 1995. Effect of bilayer composition on the phase behavior of liposomal suspensions containing poly (ethylene glycol)-lipids. Macromolecules, 28(23), pp.7693-7699.

29. Hu, F.Q., Zhang, Y.Y., You, J., Yuan, H. and Du, Y.Z., 2012. pH triggered doxorubicin delivery of PEGylated glycolipid conjugate micelles for tumor targeting therapy. Molecular pharmaceutics, 9(9), pp.2469-2478.

30. Ismagilov, R.F., Stroock, A.D., Kenis, P.J., Whitesides, G. and Stone, H.A., 2000. Experimental and theoretical scaling laws for transverse diffusive broadening in two-phase laminar flows in microchannels. Applied Physics Letters, 76(17), pp.2376-2378.

31. Jahn, A., Vreeland, W.N., DeVoe, D.L., Locascio, L.E. and Gaitan, M., 2007. Microfluidic directed formation of liposomes of controlled size. Langmuir, 23(11), pp.6289-6293.

32. Johnson, B.K. and Prud'homme, R.K., 2003. Mechanism for rapid self-assembly of block copolymer nanoparticles. Physical review letters, 91(11), p.118302.

33. Karnik, R., Gu, F., Basto, P., Cannizzaro, C., Dean, L., Kyei-Manu, W., Langer, R. and Farokhzad, O.C., 2008. Microfluidic platform for controlled synthesis of polymeric nanoparticles. Nano letters, 8(9), pp.2906-2912.

34. Kastner, E., Kaur, R., Lowry, D., Moghaddam, B., Wilkinson, A. and Perrie, Y., 2014. High-throughput manufacturing of size-tuned liposomes by a new microfluidics method using enhanced statistical tools for characterization. International journal of pharmaceutics, 477(1-2), pp.361-368.

35. Kesharwani, P., Gajbhiye, V. and Jain, N.K., 2012. A review of nanocarriers for the delivery of small interfering RNA. Biomaterials, 33(29), pp.7138-7150.

36. Kim, C.K. and Park, D.K., 1987. Stability and drug release properties of liposomes containing cytarabine as a drug carrier. Archives of Pharmacal Research, 10(2), pp.75-79.

37. Koltover, I., Rädler, J.O., Salditt, T. and Safinya, C.R., 1998. The inverted hexagonal phase of DNA-cationic liposome complexes: Structure to gene release mechanism correlations. Science, 281, p.78.

38. Majzoub, R.N., Ewert, K.K. and Safinya, C.R., 2016. Cationic liposome–nucleic acid nanoparticle assemblies with applications in gene delivery and gene silencing.

Philosophical Transactions of the Royal Society A: Mathematical, Physical and Engineering Sciences, 374(2072), p.20150129.

39. McDonald, J.C., Duffy, D.C., Anderson, J.R., Chiu, D.T., Wu, H., Schueller, O.J. and Whitesides, G.M., 2000. Fabrication of microfluidic systems in poly (dimethylsiloxane). ELECTROPHORESIS: An International Journal, 21(1), pp.27-40.
40. Milla, P., Dosio, F. and Cattel, L., 2012. PEGylation of proteins and liposomes: a powerful and flexible strategy to improve the drug delivery. Current drug metabolism, 13(1), pp.105-119.
41. Mineart, K.P., Venkataraman, S., Yang, Y.Y., Hedrick, J.L. and Prabhu, V.M., 2018. Fabrication and characterization of hybrid stealth liposomes. Macromolecules, 51(8), pp.3184-3192.
42. Mui, B.L., Tam, Y.K., Jayaraman, M., Ansell, S.M., Du, X., Tam, Y.Y.C., Lin, P.J., Chen, S., Narayanannair, J.K., Rajeev, K.G. and Manoharan, M., 2013. Influence of polyethylene glycol lipid desorption rates on pharmacokinetics and pharmacodynamics of siRNA lipid nanoparticles. Molecular Therapy-Nucleic Acids, 2, p.e139.
43. Nag, O.K. and Awasthi, V., 2013. Surface engineering of liposomes for stealth behavior. Pharmaceutics, 5(4), pp.542-569.
44. Naldini, L., Trono, D. and Verma, I.M., 2016. Lentiviral vectors, two decades later. Science, 353(6304), pp.1101-1102.
45. Patil, Y.P. and Jadhav, S., 2014. Novel methods for liposome preparation. Chemistry and physics of lipids, 177, pp.8-18.
46. Pluvinage, J.V. and Wyss-Coray, T., 2017. Microglial Barriers to Viral Gene Delivery. Neuron, 93(3), pp.468-470.
47. Sala, M., Miladi, K., Agusti, G., Elaissari, A. and Fessi, H., 2017. Preparation of liposomes: A comparative study between the double solvent displacement and the conventional ethanol injection—From laboratory scale to large scale. Colloids and Surfaces A: Physicochemical and Engineering Aspects, 524, pp.71-78.
48. Sternberg, B., Sorgi, F.L. and Huang, L., 1994. New structures in complex formation between DNA and cationic liposomes visualized by freeze—fracture electron microscopy. FEBS letters, 356(2-3), pp.361-366.

49. Stroock, A.D., Dertinger, S.K., Ajdari, A., Mezić, I., Stone, H.A. and Whitesides, G.M., 2002. Chaotic mixer for microchannels. Science, 295(5555), pp.647-651.

50. Suh, Y.K. and Kang, S., 2010. A review on mixing in microfluidics. Micromachines, 1(3), pp.82-111.

51. Swaan, L.M.B. and Swaan, P.W., 2007. Endocytic Mechanisms for Targeted Drug Delivery Lisa. Adv. Drug Deliv. Rev., 59, pp.748-758.

52. Tóth, E.L., Holczer, E.G., Iván, K. and Fürjes, P., 2015. Optimized simulation and validation of particle advection in asymmetric staggered herringbone type micromixers. Micromachines, 6(1), pp.136-150.

53. Trevisan, J.E., Cavalcanti, L.P., Oliveira, C.L., De La Torre, L.G. and Santana, M.H.A., 2011. Technological aspects of scalable processes for the production of functional liposomes for gene therapy. Non-viral gene therapy. Intech, pp.267-292.

54. Tsai, W.C. and Rizvi, S.S., 2016. Liposomal microencapsulation using the conventional methods and novel supercritical fluid processes. Trends in Food Science & Technology, 55, pp.61-71.

55. Vijayendran, R.A., Motsegood, K.M., Beebe, D.J. and Leckband, D.E., 2003. Evaluation of a three-dimensional micromixer in a surface-based biosensor. Langmuir, 19(5), pp.1824-1828.

56. Villate-Beitia, I., Puras, G., Soto-Sánchez, C., Agirre, M., Ojeda, E., Zarate, J., Fernández, E. and Pedraz, J.L., 2017. Non-viral vectors based on magnetoplexes, lipoplexes and polyplexes for VEGF gene delivery into central nervous system cells. International journal of pharmaceutics, 521(1-2), pp.130-140.

57. Wang, G., Zhu, Y., Chen, L. and Zhang, X., 2015. Photoinduced electron transfer (PET) based label-free aptasensor for platelet-derived growth factor-BB and its logic gate application. Biosensors and Bioelectronics, 63, pp.552-557.

58. Woodle, M.C., 1995. Sterically stabilized liposome therapeutics. Advanced drug delivery reviews, 16(2-3), pp.249-265.

59. Zhigaltsev, I.V., Belliveau, N., Hafez, I., Leung, A.K., Huft, J., Hansen, C. and Cullis, P.R., 2012. Bottom-up design and synthesis of limit size lipid nanoparticle systems with aqueous and triglyceride cores using millisecond microfluidic mixing. Langmuir, 28(7), pp.3633-3640.

CHAPTER 5. DIFFUSION-BASED MICROFLUIDIC DEVICE TO MANUFACTURE LIPID-BASED VECTOR SYSTEM WITH STEALTH PROPERTIES TO IMPROVE THERAPEUTIC EFFECT OF SIRNA ON CANCER CELLS

ABSTRACT

The mixing process is crucial to the effective functioning of microfluidic devices for the synthesis of lipid-based nanotherapeutics for siRNA delivery. In such systems, efficient mixing can be achieved by molecular diffusion between two fluids, where takes place in the cross-section of the channel. This generates an intense contact interface between the two fluids, while particles undergo varying velocities, resulting in a concentration gradient that improves mass transfer. In our study, we investigated the impact of diffusion in a microfluidic device to complex lipid-based nanotherapeutics with siRNA by employing different mixing strategies. We compared one-step and two-step mixing strategies for the production of lipid nanoparticles (LNP) and lipoplexes (LPX), respectively. The synthesized nanoparticles presented notable physicochemical, structural, and morphological differences. According to Cryo-TEM analysis, LNPs exhibited a multi-lamellar structure while LPXs were multivesicular systems. Dynamic light scattering data showed that lipid nanoparticles had a bigger particle diameter compared to lipoplexes. Moreover, the insertion of DSPE-PEG(2000) was also investigated in the formation of lipid-based nanotherapeutics containing siRNA. PEG insertion resulted in a decrease in the surface charge of LNPs. This may explain that PEG insertion was effective in LNP synthesis with stealth properties.

Diffusion-based microfluidic device to manufacture lipid-based nanotherapeutics with stealth properties to improve therapeutic efficiency of siRNA on cancer cells

Ismail Eş[1,2], Antonio A.Malfatti-Gasperini[3], Nicolas Szita[2], Lucimara Gaziola de la Torre[1]

[1]Department of Biochemical Engineering, University College London, Bernard Katz Building, Gower Street, London WC1E 6BT, UK.

[2]Department of Material and Bioprocess Engineering, School of Chemical Engineering, University of Campinas (UNICAMP), Campinas, São Paulo, Brazil.

[3]Brazilian Synchrotron Light Laboratory (LNLS), Brazilian Center for Research in Energy and Materials (CNPEM), Zip Code 13083-970, Campinas, São Paulo, Brazil

**Corresponding author:*

Lucimara Gaziola de la Torre

E-mail address: latorre@feq.unicamp.br

Telephone: + 55 19 35210397

1. Introduction

Gene therapy initially arose as a new approach of medicine in the 1970s after the first studies carried out with the transformation of cell nuclei by polyoma virus or simian vacuolating virus 40 (SV40) containing viral DNA (*Sambrook et al. 1968*). The original idea of gene therapy was to replace the malfunctioning genes with corrected copies of DNA to treat genetic disorders. However, nowadays, the gene therapy approach has been diversified with new applications such as introducing recombinant proteins or immunostimulatory and anti-cancer genes in either naked form or using viral and non-viral vector systems (*Lundstrom, 2015*). One of the most notable examples for anti-cancer gene machinery is small interfering RNA (siRNA) that plays a key role in RNA interference (RNAi), which is one of the most significant advances in medicine (*Fire et al. 1998*). Recent advancements in RNAi has paved the way to numerous applications in gene therapy, which, inevitably, make the siRNA-based drugs an attractive alternative in nanomedicine. Therefore, the delivery of siRNA should be well-investigated to develop next-generation drugs for gene therapy.

Although new advancements in genetic engineering have significantly contributed to the design of novel genetic machinery such as hydrophobically-modified small interfering RNAs (hsiRNAs) (Didiot *et al*. 2016), splice switching oligonucleotides (SSOs) and antisense oligonucleotides (ASOs) (Scharner *et al*. 2019; Zhdanov *et al*. 2019) for specific cell targeting, delivery of such materials still represents a significant barrier to the clinical applications for the treatment of genetic disorders and potential of these systems is still overshadowed by the complexity of the delivery (Yin *et al*. 2014). The major challenge that prevents the success of this method is the degradation of the genetic material in the physiological fluids by the action of mononuclear phagocytes as a part of the immune system, glomerular filtration as well as endosomes inside the cells (Milla *et al*. 2012). Although viral vectors were shown to be effective to overcome the complexity of the gene delivery, limitations encountered during clinical trials, including the spread of the virus to other sites, neutralization by the host immune system, and other safety concerns such as toxicity and carcinogenesis, stimulated the studies to the design of non-viral vectors (Rodriguez *et al*. 2015).

Non-viral vectors drew significant attention for gene delivery systems due to their relatively safe (non-inflammatory, non-toxic, and non-infectious) characteristics, the

capacity to deliver larger amounts of genes, and high specificity (Ramamoorth and Narvekar, 2015). Among all, lipid-based vectors are highly attractive due to their capacity to form a varying type of nanostructures and the presence of positively charged, hydrophilic head groups to interact with negatively charged genetic materials, facilitating the uptake of gene delivery system by the cells (Fromen *et al*. 2016; Kesharwani *et al*. 2012). About 5% of all gene therapy clinical trials (~2600 trials) performed by the end of 2017 has involved the use of lipid-based vectors (Ginn *et al*. 2018). However, the transfection efficiency of these vector systems and the consequent success rate in clinical trials depends on several factors such as packing density of phospholipids, the number of charged groups per molecule, and the nature of phospholipids, hence, novel modifications should be made accordingly. Moreover, due to their surface properties, these vector systems possess reduced circulation time in the bloodstream since they usually suffer from opsonization, which is the molecular mechanism of the immune system to identify invading particles to the phagocytes (Blanco *et al*. 2015). Neutral polymer like polyethylene glycol (PEG) can be incorporated into a bilayer of vectors via specific lipids (i.e. DSPE as a spacer) to shield their surface and prolong the half-life to promote the accumulation of the vector system at tumor sites (Pasut *et al*. 2015).

Different types of lipid-based vector systems have been used in gene and drug delivery. The commonly-studied lipid nanocarriers are liposomes (*Hattori et al. 2019*), solid lipid nanoparticles (*Song et al. 2017*), ethosomes (*Bagchi et al. 2017*), elastic membrane vesicles (*Sharma et al. 2016*), and micellar nanoparticles (*Li et al. 2015*). Among all, liposomes stand out as one of the most powerful non-viral vectors especially for gene delivery and can be manufactured using different approaches such as ethanol injection (*Vitor et al. 2016*), thin-film hydration (*Ghanbarzadeh et al. 2013*), water-in-oil emulsion-transfer systems (*Tsuji et al. 2018*), high shear processes (*Toniazzo et al. 2017*), and high-throughput microfluidic devices (*Eş et al. 2020*). Comparing to other techniques, microfluidics presents technical advantages in terms of reaction time, ease of fabrication, automation, and real-time data acquisition (*Halldorsson et al. 2015*).

The conventional microfluidic system consists of an engineered fluidic device where the flow is non-turbulent and highly ordered therefore provides a more efficient heat, mass, and momentum transfer properties (Cui *et al*. 2017). Moreover, due to one-step production,

microfluidic platforms have been a great tool for the formation of lipid-based nanocarriers. Hence, besides lipid-based vector design, recently, the microfluidic platform has been widely used for the complexation of genetic materials by employing effective mixing techniques (Jahn *et al*. 2010). The mixing process is a critical issue to be taken into consideration in order to produce gene delivery systems with expected properties. Since laminar flow (Reynolds number much less than 100, often close to 1) is predominant, mass transfer is significantly reduced due to the absence of turbulence and consequently, mixing process may present poor characteristics, hence, new mixing strategies by modifying channel geometry should be followed to promote a proper particle formation. In microfluidic systems, providing a cross-stream to provoke diffusion-based laminar flow, which presents a non-uniform velocity profile along the channel, was shown to be highly effective for lipid-based vector design and complexation with genetic materials (Balbino *et al*. 2013a, Balbino *et al*. 2013b).

There is an increasing trend in complexation studies in microfluidic systems. Complexation in microfluidic devices can be achieved by following two approaches. In the first approach, the one-step synthesis, the genetic material in the aqueous phase is introduced into one inlet, while phospholipids dispersed in anhydrous ethanol are introduced from other inlets, hence, provoking the formation of lipid nanocarriers. Using this approach, it is possible to prompt the simultaneous incorporation of genetic material into these nanocarriers to form lipid nanoparticles (LNPs) in a single step. The second approach involves the introduction of previously-produced liposomes into channel together with genetic material to produce lipoplexes (LPXs). Considering both lipid nanocarriers, we hypnotized that LNPs and LPXs could present different phospholipid packing density and conformation and possess a unique mechanism of transfection as well as recognizably different physicochemical, morphological, and structural properties. Additionally, the production of LPXs containing pDNA in a diffusion-based microfluidic device (D-MD) has been previously investigated by our research group (*Balbino et al.2013b*). However, to the best of our knowledge, the effect of diffusion in microfluidic systems has not been investigated for the synthesis of LPXs and LNPs containing siRNA. In this context, the aim of this study is to fill the gap that exists in the literature for the microfluidic synthesis of LNPs

and LPXs for the delivery of siRNA to be used in gene therapy as a comparative study with complete physicochemical, structural, morphological, and transfection characteristics.

2. Materials and Methods

2.1. Materials

The phospholipids 1,2-dioleoyl-sn-glycero-3-phosphoethanolamine (DOPE), 1,2-dioleoyl-3-trimethylammonium-propane (DOTAP) and egg phosphatidylcholine (EPC) were purchased from Lipoid (Ludwigshafen, Germany) to manufacture lipid-based vector systems. 1,2-distearoyl-sn-glycero-3-phosphoethanolamine-N-[amino(polyethylene glycol)-2000] [DSPE-PEG(2000)] was purchased from Avanti Polar Lipids, Inc. (Alabama, USA) and used to produce lipid nanocarriers with stealth properties to prevent opsonization and improve therapeutic efficiency of siRNA on cancer cells. Ethanol was obtained from Labsynth (São Paulo, Brazil) and used to disperse phospholipids and DSPE-PEG(2000) following the dehydration process with molecular sieves (3Å beads). The Sylgard® 184 Silicone Elastomer Kit for the fabrication of microfluidic devices was purchased from Dow Corning (Auburn, MI, United States). Deionized water was obtained from Samtec Biotechnology (São Paulo, Brazil). Ambion® Silencer® GFP (eGFP) siRNA was obtained from ThermoFisher Scientific to knock-down green fluorescent protein (GFP) gene in human embryonic kidney 293 (HEK 293) cells (Cell Biolabs, San Diego, United States) that stably express GFP. For initial optimization studies, the plasmid pEGFP-N1 (BD Biosciences Clontech, Palo Alto, USA) was amplified in Escherichia coli and purified using PureLink™ HiPure Plasmid pDNA Purification Kit (Invitrogen, Carlsband, USA).

2.2. Microfluidic device fabrication

In this study, two different microfluidic devices were used. Chaotic advection-based microfluidic device (CA-MD), based on a staggered herringbone micromixer, with 2 inlets was designed for conventional (CL) and stealth cationic liposomes (S-CL) production. CA-MD was microfabricated using photolithography technique according to the method previously described by McDonald *et al*. (2000) and Eş et al. (2020) using Sylgard® 184 Silicone Elastomer Kit as the material precursor of polydimethylsiloxane (PDMS). Briefly, the geometrical design of the main channel and herringbone-like units of microdevice were

projected in Autodesk® AutoCAD 2018. After photolithography, the mask layouts were exposed to photo-plotting. The positive molds of Y-channel and herringbone units were formed as two PDMS layers and then were irreversibly sealed by O_2 plasma surface activation sealing techniques.

A diffusion-based microfluidic device (D-MD) was microfabricated to carry out the complexation study between lipid nanocarriers and siRNA. The method used in the microfabrication of CA-MD was also employed for the manufacturing of D-MD (Balbino *et al*. 2013a, 2013b, Eş et al. 2018). Unlike the microfabrication of CA-MD, PDMS and glass layers were irreversibly sealed. All channels had a rectangular cross-section with a depth of 100 μm and a width of 140 μm. The central channel where three streams joint together had a length of 34 mm.

2.3. Microfluidic synthesis of CL and S-CL

CL and S-CL synthesis was carried out using CA-MD with two inlets according to the method previously reported by Eş *et al*. 2020. EPC, DOTAP, and DOPE at a molar ratio of 50:25:25 (%) were dispersed in anhydrous ethanol at a lipid concentration of 25 mM. For S-CL production, the molar ratio of EPC, DOTAP, DOPE, and DSPE-PEG(2000) was 50-25-24-1 (%). Prior to production, the phospholipid solution and DSPE-PEG(2000) polymer dispersed in ethanol were sonicated for 15 min at 35 ^{o}C (Ultrasonic Cleaner 8890, Cole-Parmer). The lipid dispersion and deionized water were loaded into glass syringes (Hamilton, NV, USA). Syringe pumps (PHD Ultra, Harvard Apparatus) were used to maintain constant infusion rates of each solution into CA-MD. The flow rate was set to 500 μL/min for both CL and S-CL synthesis. During each run, the samples were collected at three different times to prove that the process is continuous.

2.4. Microfluidic synthesis of siRNA complexes

Two different complexation strategies were evaluated in order to compare their transfection efficiency as well as to explore important characteristics such as their physicochemical, structural, and morphological properties. The first configuration involves two-step synthesis. In this configuration, CLs were first synthesized in CA-MD then were complexed with siRNA in D-MD, generating RNA-containing lipoplexes (LPX). siRNA-

containing LPX with stealth properties (S-LPX) were obtained when S-CLs were included into the formulation during the complexation with siRNA. The second system is a one-step protocol and involves the direct complexation of lipid dispersion with siRNA in D-MD, leading to siRNA containing lipid nanoparticles (LNP). Similar to S-LPX, LNP with stealth properties (S-LNP) were produced when DSPE-PEG(2000) was included in the formulation (Figure 5.1).

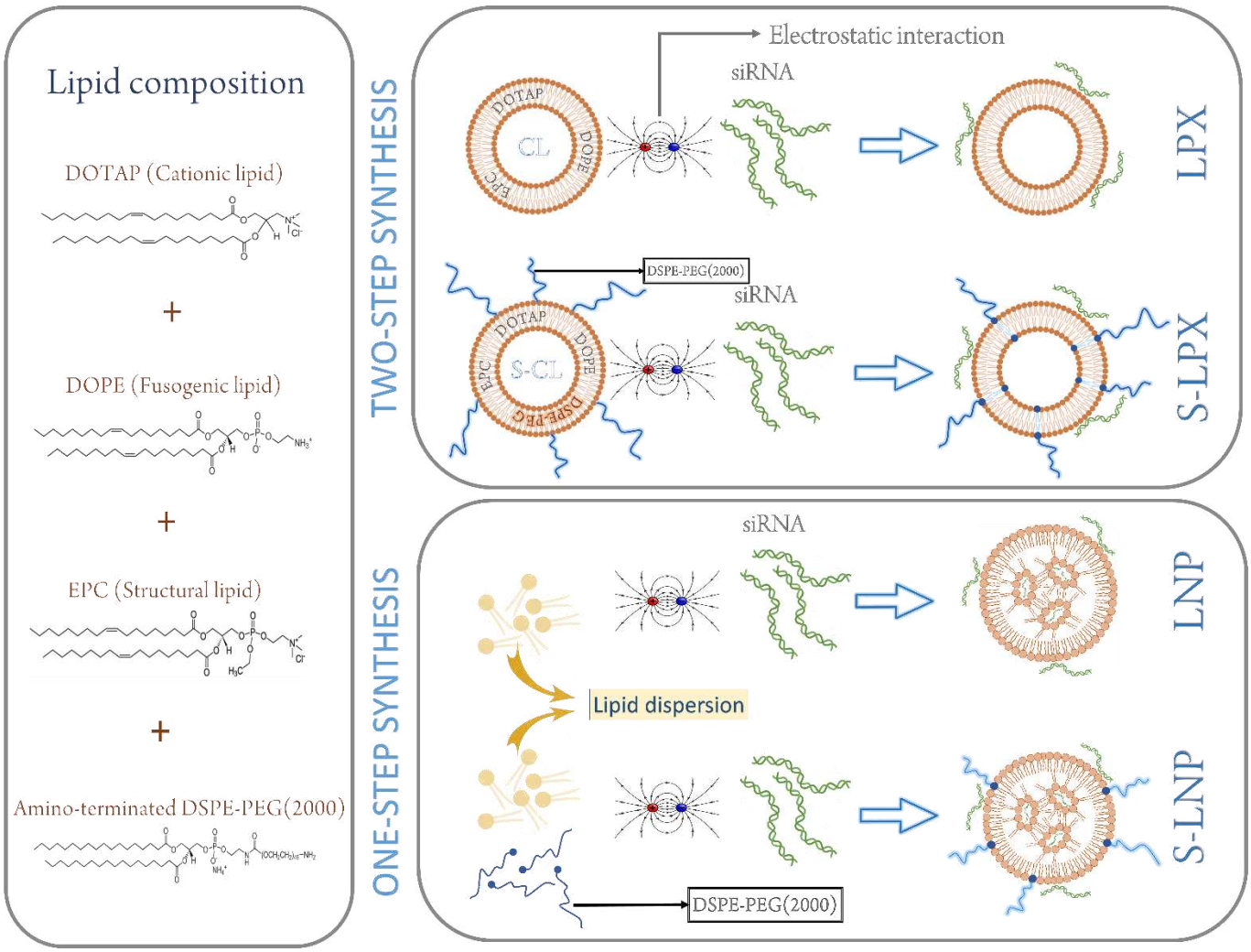

Figure 5. 1. Synthesis of LPX and LNP with and without stealth properties via diffusion-based microfluidic device. Schematic representation of LPX, S-LPX, LNP, and S-LNP synthesis.

For each system, important flow parameters such as the sequence of flow (either lipids or siRNA is introduced from the central channel), total flow rate (TFR, μL/min) and flow rate ratio (FRR), which is the ratio between lateral flow rate and central flow rate, were

investigated to obtain a desired size distribution using Dynamic Light Scattering (DLS) technique. Initially, we introduced siRNA from lateral channels, while the central flow was CLs produced in CA-MD or phospholipids dispersed in ethanol (Figure 5.2A). As the second flow configuration, we introduced an aqueous solution from the central channel to separate both lipids and siRNA, which were introduced from lateral channels (Figure 5.2B). Moreover, FRR between 1 and 15 were tested to evaluate the effect of FRR on the formation of LNPs or LPXs. The total flow rate was set to 300 μL/min for complexation study in D-MD.

Molar charge ratio (R±), which is the ratio between the number of positive charges present in cationic phospholipids (in this study DOTAP) and negative charges in the phosphate backbone of siRNA, was previously investigated and found to be 3.27 for an ideal electrostatic complexation (*Eş et al. 2018*). However, in the previous study, siRNA was designed to be 21-nucleotides long, while in this study, the nucleotide numbers in siRNA were 27. Therefore, we adjusted the concentration values of both siRNA and phospholipids to be complexed in D-MD, based on the new siRNA molecule.

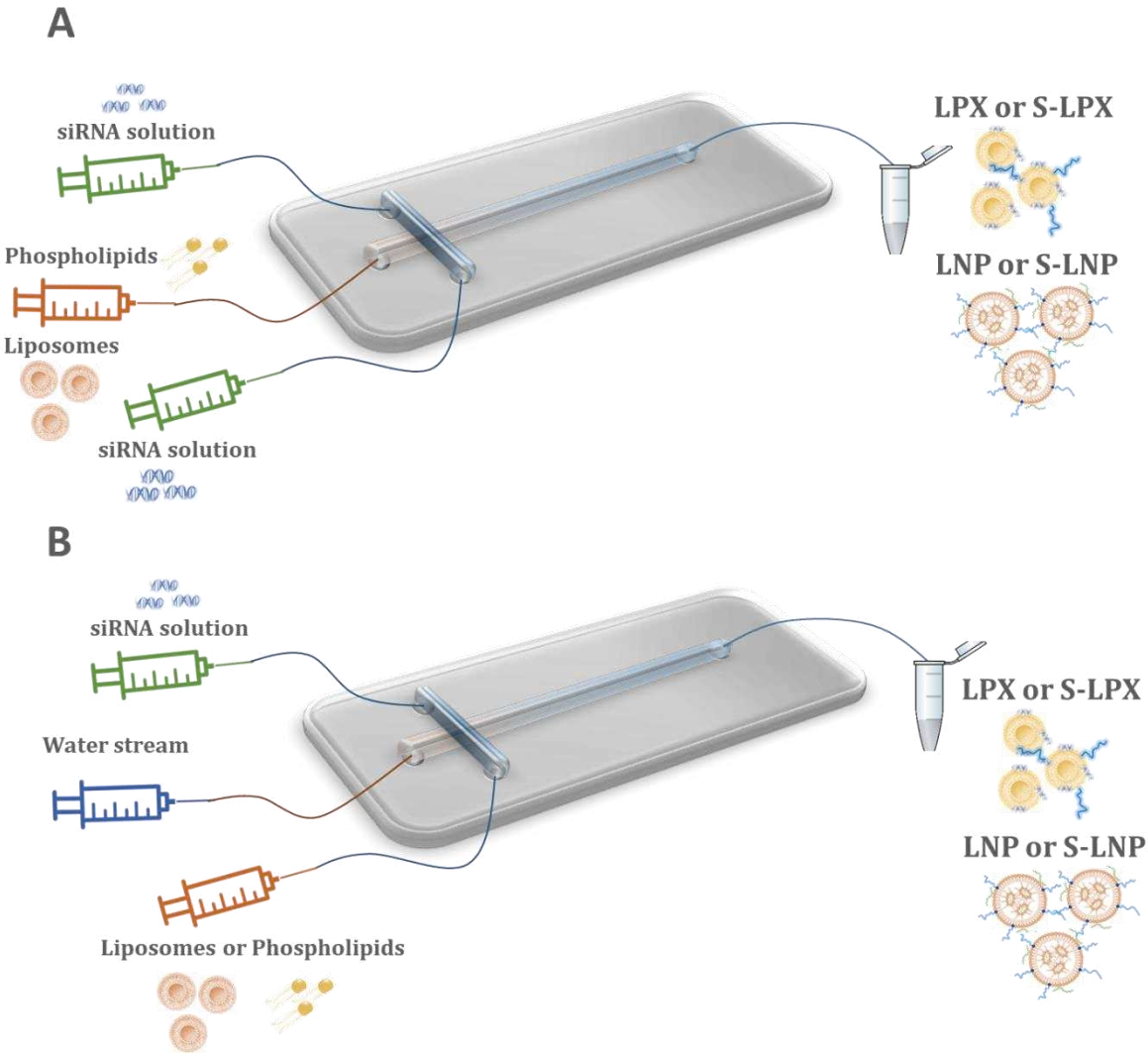

Figure 5. 2. The flow configurations performed in D-MD for the complexation study between CLs/phospholipids and siRNA to produce LPX or LNP, respectively. A) Cationic liposomes or lipid dispersion are hydro-dynamically focused by two lateral siRNA streams. B) A central water stream is used as a diffusion barrier and two different lateral streams are introduced with CLs/lipid dispersion and siRNA. Water stream served as a diffusion barrier, preventing two streams from immediate and intense contact at the entrance of the main channel.

2.5. Ethanol removal and sample concentration

Final ethanol concentrations in both CLs and S-LC (50%) and LNPs (25% at FRR 1 and over 25% at higher FRRs) were considerably higher comparing to LPX (close to zero when we use CL without any ethanol residue). To remove ethanol from CLs and LNPs, we employed centrifugal vacuum concentrator (CVC) (Savant DNA 110 SpeedVac Concentrator, Marshall Scientific, New Hampshire) using the same operation conditions (vacuum chamber

temperature of 43 °C and maximum vacuum pressure less than 10 Torr) set in the previous study (Eş *et al*. 2020). This system configuration didn't lead to any foam formation. The same equipment was also used for the concentration of samples (both LPX and LNP) by evaporation for further analyses in Cryo-Electron Microscopy (Cryo-EM) and Small Angle X-Ray Scattering (SAXS) techniques that require highly concentrated lipid content.

2.6. Physico-chemical analysis

Average size (Z-ave), intensity- and number-weighted size distribution and polydispersity index (PDI) of synthesized liposomes (CL and S-CL) as well as of LNPs and LPXs were measured using dynamic light scattering technique (Zetasizer NanoZS, Malvern). The backscattering configuration was set and detection was performed at a scattering angle of 173°. The He/Ne laser emission and power source to analyze lipid particles were 633 nm and 4.0 mW, respectively. All samples were diluted in ultrapure water before measurement. Zeta potential was determined using Laser Doppler Anemometry. The measurements were performed in triplicate in ultrapure water at 25 °C (Zetasizer NanoZS, Malvern).

2.7. Structural characterization using Synchrotron SAXS

The structural information of the LPX and LNPs to confirm phospholipid packing prior and after the complexation with siRNA was acquired through SAXS technique. The SAXS experiments were performed on the beamline SAXS1 at the Brazilian Synchrotron Light Laboratory (LNLS) using beam energy of 8 keV (λ = 1.55 Å) and a sample to detector distance of 561 mm. The measured intensity is displayed as a function of the reciprocal space momentum transfer modulus $q = 4\pi \sin(\theta)/\lambda$, where 2θ is the scattering angle and λ is the radiation wavelength. The typical range of q values was 0.017 $Å^{-1}$ to 0.45 $Å^{-1}$.

2.8. Morphological analysis

The morphology of LPX and LNPs either with DSPE-PEG(2000) incorporated or not was analyzed with Cryo-Transmission Electron Microscopy (Cryo-TEM). An automated vitrification system (Vitrobot Mark IV, FEI, The Netherlands) was used for grid preparation. Grids were exposed to glow discharge treatment (easiGlow discharge system, Pelco) with 15 mA current during 25 s to increase hydrophilicity. Samples were prepared in a controlled temperature (22 °C) and humidity (100%). 3 µL of the sample was dropped on a carbon-

coated copper grid of 300 mesh (Ted Pella) with a blot time of 3 s. Later on, samples were evaluated with Jeol JEM-2100 operating at 200 kV with a defocus range of -2 to -4 μm. Due to the maintaining of Jeol JEM-2100, the images of LNPs and LPXs with DSPE-PEG(2000) were taken using Talos™ transmission electron microscope (Thermo Scientific) Images were obtained using an F-416 CMOS camera (TVIPS, Germany). Data acquisition was performed in the Electron Microscopy Laboratory of the Brazilian National Laboratory of Nanotechnology.

2.9. Statistical analysis

All of the data obtained were expressed as the mean of triplicates with standard deviation (SD). Tukey's test was used to make a single-step multiple comparison of values obtained for each physico-chemical property between the following groups: LPX, S-LPX, LNP, and S-LNP. t-test was also applied to compare the physico-chemical properties with the same confidence level (α) of 0.05.

3. Results and Discussion

Lipid nanocarriers, especially cationic ones, are promising vector systems to deliver genetic materials. Due to their cationic characteristics, they electrostatically interact with poly-anionic genetic material such as siRNA as they spontaneously self-assembly into vesicles. Different investigations have been previously reported the synthesis of LNPs in microfluidic systems by direct complexation of phospholipids with siRNA in CA-MD (*Belliveau et al. 2012; Chen et al. 2012; Yang et al. 2014*). However, due to the possible difference in controlled release mechanism of LNPs and LPXs, we noticed a gap between two different lipid-based vector system produced in microfluidic, hence, we performed a comparative study involving physicochemical, structural and morphological analyses between LNP and LPX (with and without stealth characteristics) for the delivery of siRNA in a diffusion-based microfluidic device (D-MD).

3.1. Microfluidic synthesis of lipid nanocarriers for siRNA delivery

3.1.1. Microfluidic synthesis of lipid nanoparticles (LNPs and S-LNPs)

In this study, LNPs are synthesized in D-MD by direct complexation (one-step synthesis, Figure 5.1) of phospholipids (EPC/DOTAP/DOPE) (dispersed in ethanol – organic

phase) with siRNA (aqueous phase). Microfluidic production of LNPs with stealth properties (S-LNP) was also carried out by including DSPE-PEG(2000) together with phospholipids. The complexation process along the microchannel is driven by diffusion between phospholipids dispersed in anhydrous ethanol solution and genetic material in aqueous solution (Figure 5.2). The self-assembly of phospholipids takes place along the channel due to hydrophobic-hydrophilic interactions, while electrostatic interaction simultaneously induces the complexation between negatively-charged siRNA and positively-charged phospholipid "DOTAP". Recently, strategies on gene silencing by the intracellular delivery of small interfering RNA (siRNA) take benefit from existing expertise in pDNA delivery, which has been investigated intensely. Despite distinct differences between pDNA and siRNA, they still possess certain similarities in terms of complexation mechanism when complexed with lipid-based vesicles. Moreover, the cost of the chemical synthesis of siRNA is considerably higher than of pDNA design. Therefore, prior to the complexation studies with siRNA, we employed first tests with pDNA to evaluate the effect of different flow configurations on particle agglomeration along with the channel.

We used two different flow configurations (Figure 5.2) in D-MD while varying flow rate ratio (FRR) between 1 and 15 to evaluate the effect of FRR on the formation of LNPs. Initially, we introduced phospholipids dispersed in anhydrous ethanol from central inlet while separately introducing pDNA from lateral inlet channels, setting the total flow rate (TFR) at 300 μL/min and final phospholipid concentration at 1.2 mM (Figure 5.2A). We used the molar charge ratio ($R_{\pm}$) of ~3 between cationic lipid and negatively-charged DNA since previous studies have reported this $R_{\pm}$ is a more precise point to complex pDNA with DOTAP lipid (*Yan et al. 2012*). In this composition, the final pDNA concentration was 10μg/mL. At FRR 15, the distance between lateral flows and central flow along the main channel is extremely close, and after 2 minutes of continuous processing, we observed moderate formation of macroaggregates inside the microchannel, beginning to form at the cross-sectional area of the device. After ~6 minutes of run, the intensity of the macroaggregates robustly increased and it was not possible to continue the production (Figure 5.3). Similarly, the macroaggregates were observable at the end of the channel (data not shown). Probably these macroaggregates were the result of immediate interaction between phospholipids and

genetic material right after the streams junctions. Then, we gradually decreased FRR from 15 to 1 (step of 2.5), which, consequently, increases the distance between central and lateral flows. We hypothesized that the decrease in FRR could prevent particle agglomeration. Unfortunately, we continued observing the aggregation of precipitated particles along the microchannel. As a result, we concluded that this configuration leads to intense macroaggregation along the main channel at any tested FRR. Since precipitation could significantly influence the final lipid and pDNA concentration in the outlet, we did not perform any further DLS analysis to evaluate the physico-chemical properties of the produced LNPs. This type of precipitation was also observed during the complexation study between pDNA and previously-produced CLs using the same flow configuration (Balbino *et al*. 2017) but that experiment was limited to FRR values higher than 7.

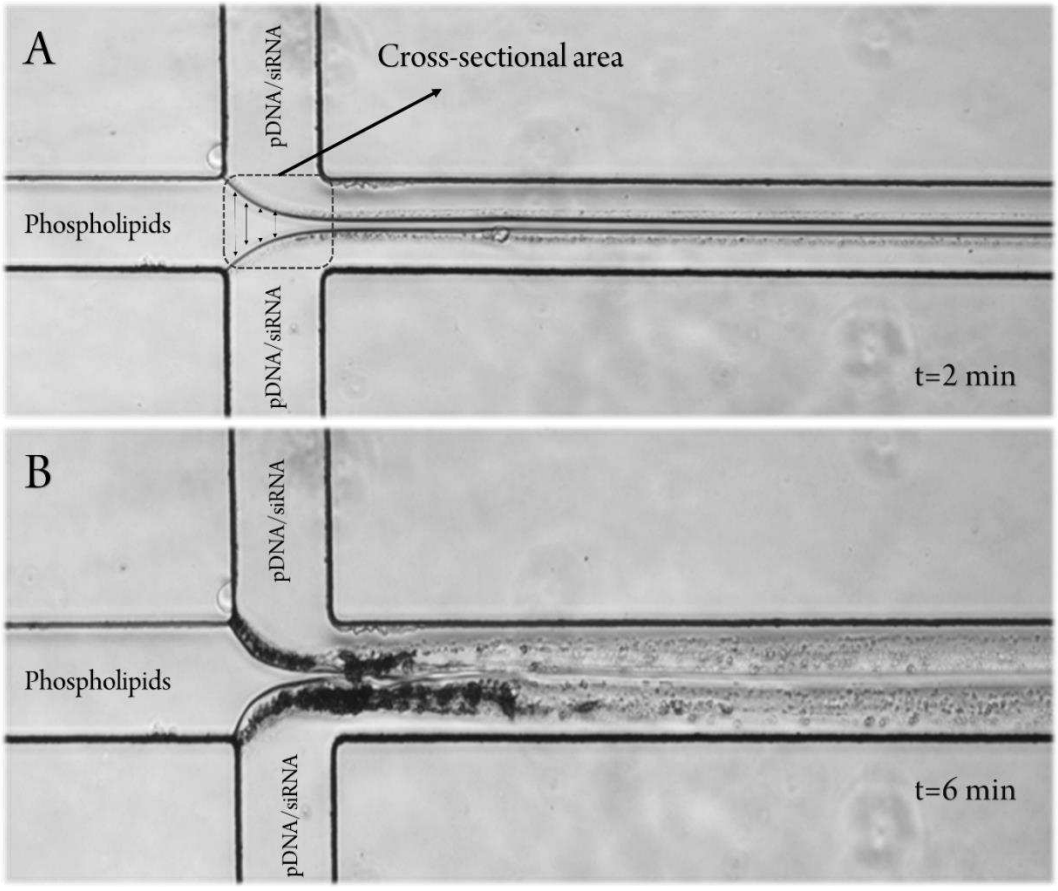

Figure 5. 3. Direct complexation between pDNA and phospholipids for LNP synthesis in D-MD at FRR 15 using the first flow configuration (phospholipids from central, pDNA from lateral inlets). The same flow configuration was employed for siRNA as well and resulted in a similar particle agglomeration.

Similar micro aggregate formation inside the microchannel was previously observed in the microfluidic assembly of chitosan/ATP nanoparticles (Pessoa *et al*. 2017). This unfavorable situation was eliminated by introducing an aqueous phase from the central channel, serving as a diffusive barrier to separate phospholipids in the ethanol solution and genetic material in the aqueous solution. Therefore, we used a similar flow configuration strategy to evaluate whether the precipitation could be avoided. In this system, we introduced phospholipids and pDNA from lateral inlets, while introducing aqueous phase from the central inlet of the D-MD (Figure 5.2B). We maintained final phospholipid concentration ($C_{phospholipid}$ = 1.2 mM) and R± 3 at the process exit by altering the amount of material introduced into the channel. At FRR 15, we could still observe macroaggregate formation but, as we gradually decrease FRR to 5 (step of 2.5), unlike the previous configuration, the precipitation started to disappear but was still observable. Under FRR 5, the precipitation was completely eliminated, leading to a continuous production without particle loss in the final solution (Figure 5.4). So, we defined our acceptable FRR region for LNP formation to be under 5 and performed a physico-chemical analysis of LNPs using this region (Figure 5.5). To ensure that the similar precipitation occurs for complexation with siRNA, we run a quick complexation test at different FRRs and we obtained a similar behavior as previously found for DNA (data not shown).

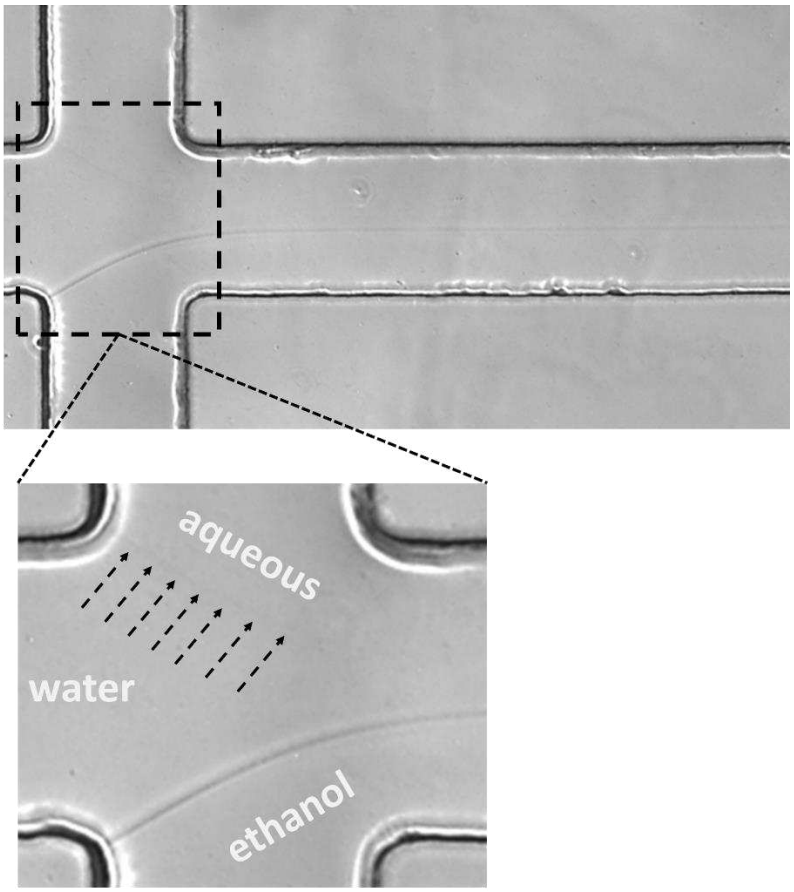

Figure 5. 4. The synthesis of LNP on D-MD using a flow rate ratio of 2.5. The total flow rate of 300 µL/min and molar charge ratio of 3 were used in this production. The ethanol and aqueous streams are phospholipids and siRNA, respectively. The arrows in the second image show the separation of aqueous stream from water stream. Total flow rate

After defining the desired flow configuration as well as FRR, at which no agglomeration occurs along the channel, we adapted these findings with the complexation studies with siRNA for further characterization. In this study, we employed the second flow configuration since this configuration during the complexation study with pDNA could allow the formation of LNPs with favorable properties and without any agglomeration as a continuous process. Moreover, we maintained TFR at 300 µL/min and we could conclude that lower FRRs could result in production without precipitation, hence, we varied FRRs between 1 and 5.

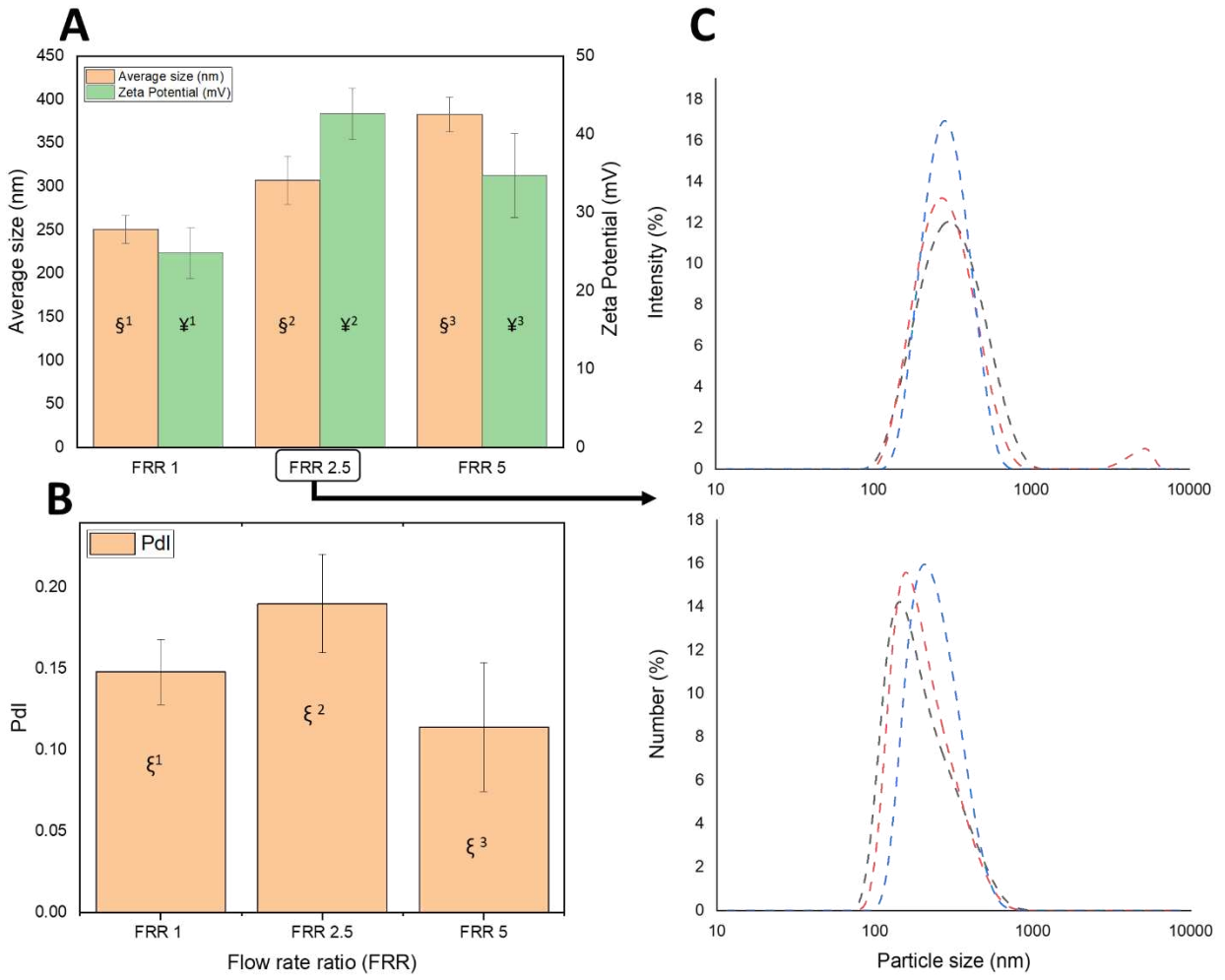

P>0.05, confirming no significant difference between the following groups: ξ^1 and ξ^2; ξ^2 and ξ^3. P<0.05, confirming significant difference between the following groups: §[1], §[2], and §[3]; ¥[1], ¥[2], and ¥[3]; ξ^1 and ξ^3.

Figure 5. 5. Physico-chemical properties of LNP synthesized with phospholipid dispersion (EPC/DOTAP/DOPE) and siRNA using D-MD at FRR varying between 1 and 5 **(A and B)**. PdI of the tested samples were found to be in the range of 0.1-0.20. Intensity and number-weighted size distribution of the analyzed particles **(C)**. Intensity and number-weighted size distribution of LNPs containing siRNA produced using D-MD at FRR 2.5. Initial lipid concentration in ethanolic dispersion was set to 25 mM, whereas final lipid concentration was found to be 0.2 mM. Total flow rate was set to 300 µL/min and molar charge ratio ($R_{+/}$) was 3. In this measurement, Z-ave was used. Average size indicates average hydrodynamic diameter of the particles. The lines in each size distribution represent the profile of three independent replicates.

According to the data obtained by DLS (Figure 5.5), particle size showed a decreasing trend as we decrease FRR for LNPs. At FRR 5, particle size was 383.1±20 nm and as we decrease FRR to 2.5 and then 1, the particle size reduced to 342.8±8.6 nm and at

250.6±16 nm, respectively. Each value was found to be statistically different. PdI values were statistically insignificant between FRR 1 and 2.5 and FRR 2.5 and 5. However, we observed significant difference between the samples obtained at FRR 1 and FRR 5. In terms of surface charge, zeta potential was significantly different for each FRR values. Zeta potential first showed an increasing trend from FRR 5 (~35 mV) to FRR 2.5 (~40 mV) then decreased to ~26 mV from FRR 2.5 to FRR 1.

Although we achieved a continuous complexation process in the channel without any precipitation below FRR 5, we observed significant differences in physico-chemical properties of the samples synthesized using FRR 1, 2.5 and 5 (Figure 5.5). As we decrease the FRR, the distance between lateral flows in the central channel where mixing occurs increases (Supplementary material 5.1A). We can assume that this increased distance may serve as a more efficient diffusion barrier between two lateral streams to prevent rapid mixing between genetic material and lipid molecules. The particle diameter was found to be smaller at smaller FRR values. This can be attributed to the slower diffusion process which gradually allows interaction between each molecules in the stream and their self-assemble into LNPs.

We also evaluated intensity and number-weighted particle size distribution using the DLS technique in order to confirm the presence of different populations with varying sizes. In this analysis, we selected the samples synthesized at FRR 2.5 which is a point where the mixing occurs without precipitation and the physico-chemical properties of the particles were favorable. According to the DLS results (Figure 5.5C), we observed a uniform particle distribution.

After selecting a prcise FRR for the particle synthesis, we investigated the effect of PEG insertion into the lipid formulation. We complexed EPC/DOTAP/DOPE/DSPE/PEG(2000) conjugates with siRNA in D-MD using FRR 2.5. The insertion of PEG decreased the particle diameter and zeta potential to 263±43.7 nm and 30.3±9.3 mV, respectively (Table 4.1). The difference between average size and zeta potential of LNP and S-LNPs was significantly different; however, no statistical difference was found for PdI values, which means that insertion of PEG didn't affect the polydispersity. The results obtained with LNP showed that the mixing in D-MD allowed continuous and one-step synthesis of nanoparticles without any agglomeration. Selected process conditions led to the particle formation with favorable

physico-chemical properties, hence, we employed similar mixing strategies and process conditions for the production of LPX and S-LPX as a two-step approach.

3.1.2. Microfluidic synthesis of Lipoplexes (LPX and S-LPX)

After concluding experiments with LNPs for siRNA delivery, we investigated the formation of LPXs as a two-step approach. Instead of direct complexation between phospholipids and siRNA, first, we produced CLs using CA-MD as we showed in our previous studies (Eş *et al*. 2020) and then complexed these CLs with siRNA in D-MD (Figure 5.1). In terms of flow configuration and FRR (1 to 15), we followed a similar strategy to observe whether the agglomeration along the channel occurs similar to what was observed during LNP synthesis. The precipitation was seen along the channel for FRR values over 5 and disappeared below FRR 5. Therefore, we maintained the desired conditions studied for LNP synthesis that lead to a continuous synthesis of LPX without any agglomeration, which is the TFR of 300 µL/min, FRR of 2.5, and R± of 3. We employed the flow configuration shown in Figure 5.2B.

Intensity and number-weighted size distribution showed that all the particles were in the range of 150-250 nm (Figure 5.6). The insertion of DSPE-PEG(2000) had a different impact on the formation of LPX as expected. We observed that the distribution of the particle size slightly shifted to the left with the formation of smaller particles. This shift was more visible in case of S-LPX. In two-step synthesis, the particle diameter, PdI, and zeta potential of CLs and S-CLS were [160 nm, 0.18, 60 mV] and [180 nm, 0.2, and 50 mV], respectively. After the complexation of CLs with siRNA, LPX had the diameter, PdI, and zeta potential of 212.4±34 nm, 0.18±0.08, and 33.7±4.4 mV, respectively. Electrostatic association between siRNA and CLs resulted in an increase in particle diameter and decrease in surface charge. However, complexing siRNA with S-CL no change in particle size was observed and zeta potential decreased to 204±4.3 nm and 52.1±1.1 mV, respectively while PdI significantly increased to 0.4±0.02.

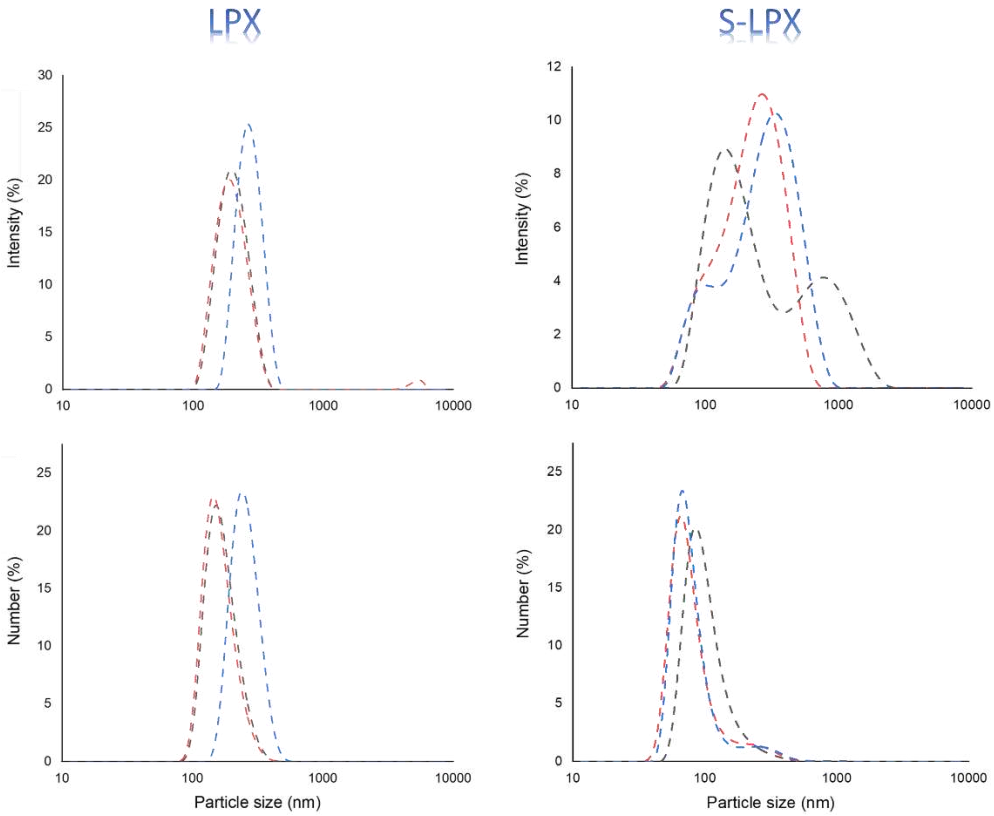

Figure 5. 6. Intensity and number-weighted particle size distribution of LPX and S-LPX produced in D-MD at FRR 2.5 with TFR of 300 µL/min and molar charge ratio of 3. The lines in each size distribution represent the profile of three independent replicates.

After obtaining DLS results for both LNP and LPX, we performed a comparative study in terms of physicochemical properties (Table 5.1). It can be concluded that LPXs are smaller in size comparing to LNPs. In terms of polydispersity, no significant difference was found between LNP, S-LNP, and LPX. However, S-LPX had higher PdI value compared to other samples.

Table 5. 1. Comparative demonstration of LNP and LPX containing siRNA with and without insertion of DSPE/PEG(2000).

Nanostructures		Average diameter (nm)	PdI	Zeta potential (mV)
Phospholipids (in ethanol) + siRNA	LNP	¥1312.4±38	¥20.15.4±0.05	¥339.1±5
	S-LNP	¥1263.5±43	¥20.17±0.03	¥330.3±9
Liposomes + siRNA	LPX	§1212.4±34	§20.18±0.08	§333.7±4.4
	S-LPX	§1208.5±8	§20.31±0.05	§354.3±1.6

The average diameter, PdI, and zeta potential of the CL was approximately 160 nm, 0.18, and 59 mV, whereas S-CLs had the size, PdI, and zeta potential of approx. 180 nm, 0.2, and 50 mV, respectively. P-value was higher than 0.05, confirming no significant difference between groups: **¥2** and **§1;** P-value was smaller than 0.05, confirming significant difference between groups: **¥1, ¥3, §2,** and **§3**.

Different investigations have reported that the insertion of PEG decreases the zeta potential value since it shows a stealth effect by sterically shielding nanoparticle surface (Cieślak *et al*. 2017). By analyzing the zeta potential values, we can have an idea of the efficiency of the PEG insertion process in D-MD. In our study, PEG insertion in LNP and LPX decreased the average diameter of particles. Belletti *et al*. (2016) employed a post PEGylation approach using a thin-film hydration method to the siRNA-containing LPXs. The average size was reported to decrease after PEG insertion but the decrease was not statistically significant. They also reported that size, PdI, and zeta potential behave differently depending on the method of PEG insertion, which was different than microfluidic synthesis. The polymer chain length and concentration of DSPE-PEG in phospholipid formulation were also found to be important determinants on physico-chemical properties of the lipid-based nanoparticles (Cheng *et al*. 2015). Using PEG polymer with higher molar concentration may decrease the average distance between neighboring PEG chains attached on the surface of nanoparticles, hence, it will change the shielding effect (Suk *et al*. 2016). In our study, we used 1% DSPE-PEG polymer with 1% of the molar concentration in total phospholipid formulation. The results were further supported by investigating the morphology of the synthesized particles.

3.2. Structural analysis of LNP and LPX

To investigate the nanostructure of LNP and LPX containing siRNA, synchrotron SAXS was used. Figure 5.7 shows that the X-ray intensity scattered from siRNA-containing LNP and LPX is well fitted by the usual form factor of the lipid bilayer based on the Gaussian description of the electron density profile (aqui cabe a referência do capítulo de livro da Lucimara com o Cristiano Oliveira). The model is based on the deconvolution of the scattered intensity in two contributions, one coming from the electronic density profile (EDP) across the bilayer, and one related to the stacking of these bilayers. To properly fit the experimental data, we have considered that LNP with and without PEGylated lipids should have the same EDP, although it can be different from LPX samples, which also share the same EDP between them. The presence of PEGylated lipids do not alter the EDP since (1) the lipids have almost the same electronic density and (2) PEG has electronic density similar to the water. However, its presence can change the distance between stacked bilayers since it works as a physical steric layer between two consecutive lipid bilayers. The fit was achieved considering two different structure factors for LNP samples (the bilayers stack in two different ways), but for LPX samples only one structure factor was present. According to our model for LNP and S-LNP, 16 parameters were used to adjust the curves: form factor (4), intensity (2; one for each curve), fractions of phases the lipids are in (4; 2 for each phase, for each curve), interlamellar distance (2), Caillé parameter (2 for with/without PEG), and number of stacking bilayers (2; one for each curve). Other parameters were kept constant or equal to another parameter.

The created model fit well with the experimental data. The model showed that the system self-organized into bilayer and didn't show presence of any micelle-like structures. The electron density of siRNA was observed between the bilayer. According to the model, the presence of siRNA destabilized the liposomal structure and eventually destroying them then the system self-assembled itself into multilamellar structures. For LNPs, the fraction of 0.40±0.01 of phospholipids self-assembled into multilamellar structure, containing the average of 7.1±0.5 lamella, whereas the fraction of 0.15±0.01 of the phospholipids had a double-bilayer structure (2 lamella). However, 45% of the lipids self-organize into unilamellar structure.

S-LNPs had a multilamellar fraction of 0.29±0.01 with an average lamella number of 4.0±0.5, proving the stacking effect of PEG on bilayers. The average distance between bilayer was found to be 6.64±0.05 nm, which was similar to the value obtained for LNP. 47% of the system was unilamellar. The fraction value of the system without the presence of siRNA in bilayer was 0.24±0.01. The average distance of the bilayer (without siRNA) is 7.58±0.05 nm, which is significantly bigger than of the average distance (6.64 nm) of bilayer in the population with siRNA. This can be an evidence to the fact that PEG acts as a steric barrier even inside of each particle.

In case of LPX and S-LPX, we used 12 parameters to adjust the curve: form factors (4), intensity (2; one for each curve), Caillé factor (1; the same for both curves), average distance between bilayers (1; the same for both curves), multilamellar fraction (2), and average number of stacking bilayer (2). We didn't find any evidence of a possible micelle-like structure. The fraction of lipids organized as multilamellar particles for LPX was found to be 0.41±0.01, indicating that 59% of the system was found to be unilamellar. For S-LPX, fraction of multilamellar particles was 0.28±0.01, indicating that 72% of the system was unilamellar.

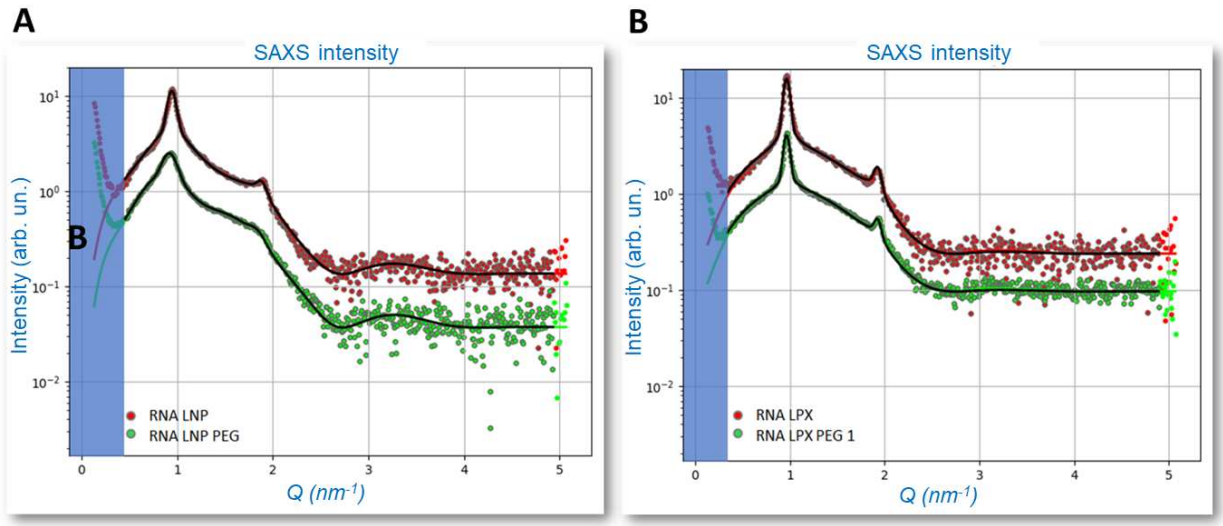

Figure 5. 7. Synchrotron SAXS patterns of LNP and S-LNP **(A)** and LPX and S-LPX **(B)** containing siRNA. Calculated small-angle X-ray scattering (SAXS) curves in a broad q-vector range, which provides information about the size, the shape and the surface roughness of the scattering nano-objects present in the bi-colloidal dispersion (black curves).

3.3. Morphological analysis

3.3.1. Lipid nanoparticles

The morphological analysis of LNP and LPX was performed using Cryo-TEM. The images showed that LNPs and S-LNPS showed different morphological structures (Figure 5.8). The scientific literature reports LNP structures with different models: (a) unilamellar, (b) bi-/oligo-lamellar, (c) multilamellar (onion-like), (d) multivesicular, and (e) homogeneous core-shell with smaller nanoparticles inside the core (Viger-Gravel *et al*. 2018). According to this classification, the analysis of CRYO-TEM images obtained for LNP (Figure 5.7) reveals that a major part of the total population of LNP was multilamellar. In some samples, up to 20 lamellae were observable (images not shown). Multi-lamellar LNPs showed particle size up to ~350 nm, which was also confirmed by the DLS technique. Furthermore, we confirmed the presence of particles with smaller diameter, which were detected with Cryo-TEM. The microfluidic synthesis of such small particles for siRNA delivery were also reported previously (Belliveau *et al*. 2012), in which the effect of chaotic advection was evaluated while we investigated the effect of diffusion on LNP synthesis.

We also investigated the effect of PEG insertion into the particles. As it can be shown in DLS data and morphological analysis, compared to LNP, the size and lamellarity of the particles decreased while PdI increased. A similar finding was also reported by Belliveau *et al*. 2012. Insertion of 1% PEG-c-DMA significantly decreased the particle diameter. Kulkarni *et al*. (2017) also reported the microfluidic synthesis of S-LNP with KC2/DSPC/cholesterol/PEG-DMG (50/10/38.5/ 1.5 mol %) in a chaotic advection device. Depending on the molar ratio of phospholipids, S-LNPs had either multilamellar or bi-/oligo-lamellar structures9.

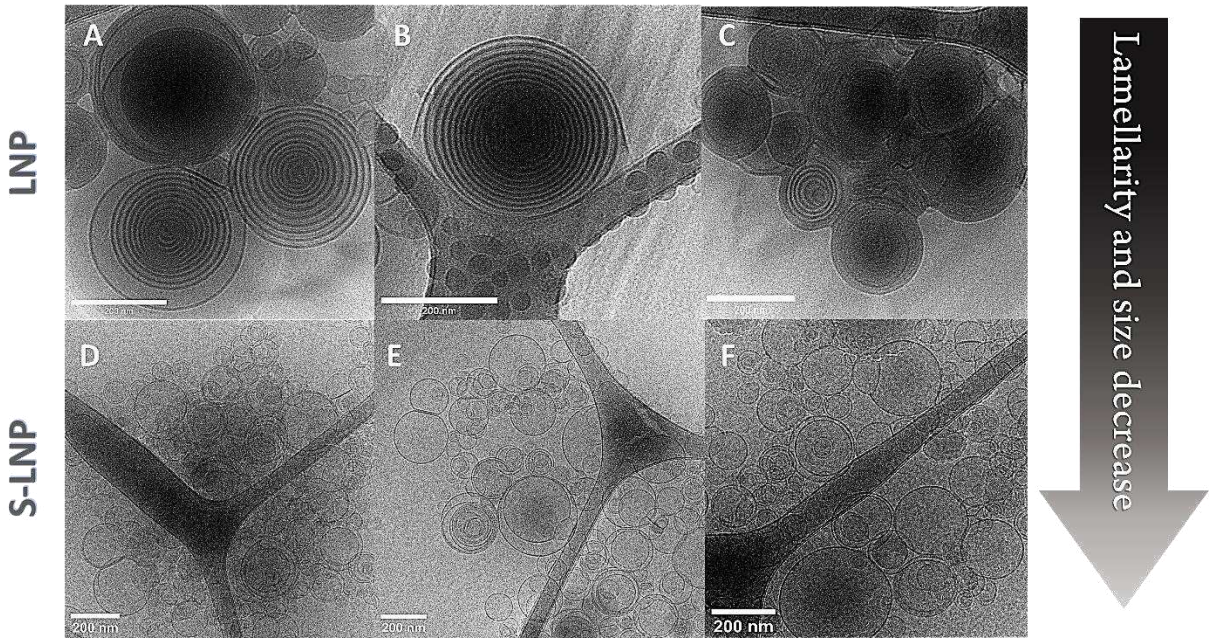

Figure 5. 8. Cryo-TEM images for identification of morphological structures of LNP and S-LNP. Darker sides on the images are carbon layer of the grids. LNPs presented multilamellarity while S-LNPs had more unilamellar particles. The images were sharpened by 50% using software to easily visualize the lamella. Scale bars indicate 200 nm.

4. Conclusion

Recently, the microfluidic synthesis of lipid-based nanotherapeutics in single-step (LNP) has been a rapid and attractive solution. Such microfluidic production may lead to a distinct therapeutic outcome compared to the two-step production (LPX). In our study, we investigated the impact of diffusion in microfluidic systems to manufacture LNPs and LPXs to establish the major differences between each formulation. We confirmed that each system possesses a different phospholipid packing density and conformation as well as diverse morphological and physicochemical characteristics. These variations are significantly important as they have been reported to influence their therapeutic effect on cancer cells. Further studies to explore *in vitro* transfection efficiency of these promising gene delivery systems are essential to confirm the fact that each system has a unique mechanism of action on cancer cells. As a future perspective, we will complete the SAXS analysis and Cryo-TEM characterization of LPX and S-LPX. And as the final step we will test their transfection efficiency on cancer cells as a possible biological application.

Acknowledgements

I. Eş gratefully acknowledges the financial support of the São Paulo Research Foundation (FAPESP) (Grant # 2015/14468-0). Authors also thank to Microfabrication Laboratory of Brazilian Center for Research in Energy and Materials (CNPEM) to provide infrastructure to perform microfabrication as well as to Brazilian National Laboratory of Nanotechnology of CNPEM to provide assistance for acquiring Cryo-EM images of liposomes. We also thank Coordination for the Improvement of Higher Education Personnel (CAPES) finance code 001. LGT thanks National Council for Scientific and Technological Development (CNPq) (productivity grant 310735/2016-5 and 302212/2019-1).

Conflict of Interest

Authors declare that they have no conflict of interest.

References

1. Bagchi, D., Dutta, S., Singh, P., Chaudhuri, S. and Pal, S.K., 2017. Essential dynamics of an effective phototherapeutic drug in a nanoscopic delivery vehicle: psoralen in Ethosomes for biofilm treatment. ACS omega, 2(5), pp.1850-1857.
2. Balbino, T.A., Aoki, N.T., Gasperini, A.A., Oliveira, C.L., Azzoni, A.R., Cavalcanti, L.P. and Lucimara, G., 2013a. Continuous flow production of cationic liposomes at high lipid concentration in microfluidic devices for gene delivery applications. Chemical engineering journal, 226, pp.423-433.
3. Balbino, T.A., Azzoni, A.R. and de La Torre, L.G., 2013b. Microfluidic devices for continuous production of pDNA/cationic liposome complexes for gene delivery and vaccine therapy. Colloids and Surfaces B: Biointerfaces, 111, pp.203-210.
4. Belletti, D., Tosi, G., Forni, F., Lagreca, I., Barozzi, P., Pederzoli, F., Vandelli, M.A., Riva, G., Luppi, M. and Ruozi, B., 2016. PEGylated siRNA lipoplexes for silencing of BLIMP-1 in primary effusion lymphoma: *in vitro* evidences of antitumoral activity. European Journal of Pharmaceutics and Biopharmaceutics, 99, pp.7-17.
5. Belliveau, N.M., Huft, J., Lin, P.J., Chen, S., Leung, A.K., Leaver, T.J., Wild, A.W., Lee, J.B., Taylor, R.J., Tam, Y.K. and Hansen, C.L., 2012. Microfluidic synthesis of highly potent

limit-size lipid nanoparticles for *in vivo* delivery of siRNA. Molecular Therapy-Nucleic Acids, 1, p.e37.

6. Blanco, E., Shen, H. and Ferrari, M., 2015. Principles of nanoparticle design for overcoming biological barriers to drug delivery. Nature biotechnology, 33(9), p.941.
7. Chen, G., Li, D., Jin, Y., Zhang, W., Teng, L., Bunt, C. and Wen, J., 2014. Deformable liposomes by reverse-phase evaporation method for an enhanced skin delivery of (+)-catechin. Drug development and industrial pharmacy, 40(2), pp.260-265.
8. Cheng, Y., Liu, M., Hu, H., Liu, D. and Zhou, S., 2016. Development, optimization, and characterization of PEGylated nanoemulsion of prostaglandin E1 for long circulation. AAPS PharmSciTech, 17(2), pp.409-417.
9. Cieślak, A., Wauthoz, N., Orellana, A.N., Lautram, N., Béjaud, J., Hureaux, J., Lafleur, M., Benoit, J.P., Salomon, C.J. and Bastiat, G., 2017. Stealth nanocarriers based sterosomes using PEG post-insertion process. European journal of pharmaceutics and biopharmaceutics, 115, pp.31-38.
10. Cui, X., Hartanto, Y. and Zhang, H., 2017. Advances in multicellular spheroids formation. Journal of The Royal Society Interface, 14(127), p.20160877.
11. Didiot, M.C., Hall, L.M., Coles, A.H., Haraszti, R.A., Godinho, B.M., Chase, K., Sapp, E., Ly, S., Alterman, J.F., Hassler, M.R. and Echeverria, D., 2016. Exosome-mediated delivery of hydrophobically modified siRNA for huntingtin mRNA silencing. Molecular Therapy, 24(10), pp.1836-1847.
12. Eş, I., Ok, M.T., Puentes-Martinez, X.E., de Toledo, M.A.S., de Pinho Favaro, M.T., Cavalcanti, L.P., Cassago, A., Portugal, R.V., Azzoni, A.R. and de la Torre, L.G., 2018. Evaluation of siRNA and cationic liposomes complexes as a model for *in vitro* siRNA delivery to cancer cells. Colloids and Surfaces A: Physicochemical and Engineering Aspects, 555, pp.280-289.
13. Eş, I., Ok, M.T., Puentes-Martinez, X.E., de Toledo, M.A.S., de Pinho Favaro, M.T., Cavalcanti, L.P., Cassago, A., Portugal, R.V., Azzoni, A.R. and de la Torre, L.G., 2018. Evaluation of siRNA and cationic liposomes complexes as a model for *in vitro* siRNA delivery to cancer cells. Colloids and Surfaces A: Physicochemical and Engineering Aspects, 555, pp.280-289.

14. Fire, A., Xu, S., Montgomery, M.K., Kostas, S.A., Driver, S.E. and Mello, C.C., 1998. Potent and specific genetic interference by double-stranded RNA in Caenorhabditis elegans. nature, 391(6669), pp.806-811.
15. Fromen, C.A., Rahhal, T.B., Robbins, G.R., Kai, M.P., Shen, T.W., Luft, J.C. and DeSimone, J.M., 2016. Nanoparticle surface charge impacts distribution, uptake and lymph node trafficking by pulmonary antigen-presenting cells. Nanomedicine: Nanotechnology, Biology and Medicine, 12(3), pp.677-687.
16. Ghanbarzadeh, S., Valizadeh, H. and Zakeri-Milani, P., 2013. Application of response surface methodology in development of sirolimus liposomes prepared by thin film hydration technique. BioImpacts: BI, 3(2), p.75.
17. Ginn, S.L., Alexander, I.E., Edelstein, M.L., Abedi, M.R. and Wixon, J., 2013. Gene therapy clinical trials worldwide to 2012–an update. The journal of gene medicine, 15(2), pp.65-77.
18. Halldorsson, S., Lucumi, E., Gómez-Sjöberg, R. and Fleming, R.M., 2015. Advantages and challenges of microfluidic cell culture in polydimethylsiloxane devices. Biosensors and Bioelectronics, 63, pp.218-231.
19. Hattori, Y., Nakamura, M., Takeuchi, N., Tamaki, K., Shimizu, S., Yoshiike, Y., Taguchi, M., Ohno, H., Ozaki, K.I. and Onishi, H., 2019. Effect of cationic lipid in cationic liposomes on siRNA delivery into the lung by intravenous injection of cationic lipoplex. Journal of drug targeting, 27(2), pp.217-227.
20. Jahn, A., Reiner, J.E., Vreeland, W.N., DeVoe, D.L., Locascio, L.E. and Gaitan, M., 2008. Preparation of nanoparticles by continuous-flow microfluidics. Journal of Nanoparticle Research, 10(6), pp.925-934.
21. Kesharwani, P., Gajbhiye, V. and Jain, N.K., 2012. A review of nanocarriers for the delivery of small interfering RNA. Biomaterials, 33(29), pp.7138-7150.
22. Li, J., Chen, Q., Zha, Z., Li, H., Toh, K., Dirisala, A., Matsumoto, Y., Osada, K., Kataoka, K. and Ge, Z., 2015. Ternary polyplex micelles with PEG shells and intermediate barrier to complexed DNA cores for efficient systemic gene delivery. Journal of Controlled Release, 209, pp.77-87.
23. Lundstrom, K., 2015. gene therapy with emphasis on RNA interference.

24. McDonald, J.C., Duffy, D.C., Anderson, J.R., Chiu, D.T., Wu, H., Schueller, O.J. and Whitesides, G.M., 2000. Fabrication of microfluidic systems in poly (dimethylsiloxane). ELECTROPHORESIS: An International Journal, 21(1), pp.27-40.

25. Milla, P., Dosio, F. and Cattel, L., 2012. PEGylation of proteins and liposomes: a powerful and flexible strategy to improve the drug delivery. Current drug metabolism, 13(1), pp.105-119.

26. Pasut, G., Paolino, D., Celia, C., Mero, A., Joseph, A.S., Wolfram, J., Cosco, D., Schiavon, O., Shen, H. and Fresta, M., 2015. Polyethylene glycol (PEG)-dendron phospholipids as innovative constructs for the preparation of super stealth liposomes for anticancer therapy. Journal of controlled release, 199, pp.106-113.

27. Pessoa, A.C., Sipoli, C.C. and Lucimara, G., 2017. Effects of diffusion and mixing pattern on microfluidic-assisted synthesis of chitosan/ATP nanoparticles. Lab on a Chip, 17(13), pp.2281-2293.

28. Pozzi, D., Colapicchioni, V., Caracciolo, G., Piovesana, S., Capriotti, A.L., Palchetti, S., De Grossi, S., Riccioli, A., Amenitsch, H. and Laganà, A., 2014. Effect of polyethyleneglycol (PEG) chain length on the bio–nano-interactions between PEGylated lipid nanoparticles and biological fluids: from nanostructure to uptake in cancer cells. Nanoscale, 6(5), pp.2782-2792.

29. Ramamoorth, M. and Narvekar, A., 2015. Non viral vectors in gene therapy-an overview. Journal of clinical and diagnostic research: JCDR, 9(1), p.GE01.

30. Rodriguez, A.L., Wang, T.Y., Bruggeman, K.F., Li, R., Williams, R.J., Parish, C.L. and Nisbet, D.R., 2016. Tailoring minimalist self-assembling peptides for localized viral vector gene delivery. Nano research, 9(3), pp.674-684.

31. Sambrook, J., Westphal, H., Srinivasan, P.R. and Dulbecco, R., 1968. The integrated state of viral DNA in SV40-transformed cells. Proceedings of the National Academy of Sciences of the United States of America, 60(4), p.1288.

32. Scharner, J., Qi, S., Rigo, F., Bennett, C.F. and Krainer, A.R., 2019. Delivery of GalNAc-conjugated splice-switching ASOs to non-hepatic cells through ectopic expression of asialoglycoprotein receptor. Molecular Therapy-Nucleic Acids, 16, pp.313-325.

33. Sharma, G., Goyal, H., Thakur, K., Raza, K. and Katare, O.P., 2016. Novel elastic membrane vesicles (EMVs) and ethosomes-mediated effective topical delivery of

aceclofenac: a new therapeutic approach for pain and inflammation. Drug delivery, 23(8), pp.3135-3145.

34. Song, C., Zhang, S., Zhou, Q., Shi, L., Du, L., Zhi, D., Zhao, Y., Zhen, Y. and Zhao, D., 2017. Bifunctional cationic solid lipid nanoparticles of β-NaYF 4: Yb, Er upconversion nanoparticles coated with a lipid for bioimaging and gene delivery. RSC advances, 7(43), pp.26633-26639.
35. Suk, J.S., Xu, Q., Kim, N., Hanes, J. and Ensign, L.M., 2016. PEGylation as a strategy for improving nanoparticle-based drug and gene delivery. Advanced drug delivery reviews, 99, pp.28-51.
36. Toniazzo, T., Galeskas, H., Dacanal, G.C. and Pinho, S.C., 2017. Production of cornstarch granules enriched with quercetin liposomes by aggregation of particulate binary mixtures using high shear process. Journal of food science, 82(11), pp.2626-2633.
37. Tsuji, G., Sunami, T. and Ichihashi, N., 2018. Production of giant unilamellar vesicles by the water-in-oil emulsion-transfer method without high internal concentrations of sugars. Journal of bioscience and bioengineering, 126(4), pp.540-545.
38. Viger-Gravel, J., Schantz, A., Pinon, A.C., Rossini, A.J., Schantz, S. and Emsley, L., 2018. Structure of lipid nanoparticles containing siRNA or mRNA by dynamic nuclear polarization-enhanced NMR spectroscopy. The Journal of Physical Chemistry B, 122(7), pp.2073-2081.
39. Vitor, M.T., Bergami-Santos, P.C., Zômpero, R.H.F., Cruz, K.S.P., Pinho, M.P., Barbuto, J.A.M. and de la Torre, L.G., 2017. Cationic liposomes produced via ethanol injection method for dendritic cell therapy. Journal of liposome research, 27(4), pp.249-263.
40. Yan, J., Berezhnoy, N.V., Korolev, N., Su, C.J. and Nordenskiöld, L., 2012. Structure and internal organization of overcharged cationic-lipid/peptide/DNA self-assembly complexes. Biochimica et Biophysica Acta (BBA)-Biomembranes, 1818(7), pp.1794-1800.
41. Yang, D.K. and Wu, S.T., 2014. Fundamentals of liquid crystal devices. John Wiley & Sons.
42. Yin, H. and Kanasty, R.L., 2014. A. a. Eltoukhy, AJ Vegas, JR Dorkin and DG Anderson. Nat. Rev. Genet, 15, pp.541-555.

43. Zhdanov, D.D., Plyasova, A.A., Gladilina, Y.A., Pokrovsky, V.S., Grishin, D.V., Grachev, V.A., Orlova, V.S., Pokrovskaya, M.V., Alexandrova, S.S., Lobaeva, T.A. and Sokolov, N.N., 2019. Inhibition of telomerase activity by splice-switching oligonucleotides targeting the mRNA of the telomerase catalytic subunit affects proliferation of human CD4+ T lymphocytes. Biochemical and biophysical research communications, 509(3), pp.790-796.

CHAPTER 6. MICROFLUIDIC PLATFORMS FOR THE FORMATION OF SPHEROIDS AS A RAPID DRUG SCREENING MODEL

ABSTRACT

In vivo studies are highly challenging due to several biological obstacles and in vitro 2D cell culture systems do not accurately represent dynamic *in vivo* models. In this context, 3D cell culture models, which mimic dynamic microenvironments of living organs, appear as a promising technique to study cell differentiation as well as cell response against controlled release systems. Moreover, when comparing with conventional 3D cell culture systems, microfluidic approaches are more advantageous since they allow high-throughput analysis with advanced real-time monitoring using microscopy techniques. Considering all these concepts, this part of the dissertation aims to develop a microfluidic tumor-on-a-chip platform that allows the formation of spheroids and their on-chip transfection using small interfering RNA (siRNA) incorporated into lipid-based vector system. The spheroids were formed on both static and dynamic microfluidic platforms and were morphologically characterized using confocal and multi-photon microscopy. Following characterization, the spheroids were transfected using lipid-based siRNA nanotherapeutics and transfection efficiency was determined with NucleoCounter® NC-200™ Automated Cell Counter. Our findings showed that both static and dynamic microdevices allowed the formation of spheroids, however, it was not possible to achieve an expected transfection efficiency when siRNA was delivered to spheroids in static culture. This project was developed in collaboration with the Department of Biochemical Engineering of University College London in the United Kingdom. The Microfluidic Research Group is led by Professor Nicolas Szita, who has broad expertise in advanced microfabrication techniques, Lab-on-a-chip systems, and system-wide integration of analytics. In this project, we expected to give a significant contribution to the field of tumor-on-a-chip concept for dynamic cell study in the 3D microenvironment.

Keywords: Microfluidics, tumor-on-a-chip, siRNA, spheroids, 3D cell culture

1. Introduction

There is a growing trend in the discovery of new drugs and their delivery methods for the treatment of genetic diseases such as cancer, which is responsible for approximately 9.6 million deaths in 2018 (WHO, 2018). However, the success rate of new drug approval is reasonably low due to the lack of the presence of an efficient biological system that accurately mimics *in vivo* systems (Wong et al. 2019). Hence, preclinical tests should be proceeded employing more efficient systems to increase the precision of drug tests and their consequent approval. For decades, preliminary drug tests have been performed using conventional 2D cell cultures represented in monolayer (Kelm et al. 2003). 2D cell culture is relatively cost-effective and due to the number of studies conducted since the early 1900s, there is a large amount of available data that can be systematically compared (Duval et al. 2017). Unfortunately, the behavior of cells in 2D culture can be predicted only partially as a consequence of the fact that cells do not completely interact with each other. Furthermore, in the case of drug testing, all the cells are exposed to the same amount of drug, resulting in a non-realistic interaction system that fails to simulate the complex behavior of cell-to-cell communication networks which is characterized by the heterogeneous distribution of oxygen, nutrients, metabolites as well as molecules that play a critical role in intercellular signaling (Kinney et al. 2014; Kijanska and Kelm, 2016). Hence, the use of more efficient systems that mimic *in vivo* is tremendously important. In this context, 3D cell cultures ultimately emerged as a new alternative for testing drug absorption and metabolic efficiency with highly accurate results.

The basic concept of 3D cell culture is of great importance for tissue engineering. 3D cell culture systems consist of two different approaches: (1) top-down and (2) bottom-up (Sultan et al. 2017). The “top-down” approach is employed by seeding cells together with 3D porous scaffolds as a support material, which is eventually degraded as the cells divide and a tissue analogs can be crafted. Despite the important benefits of this approach, the porous scaffold is most likely to fail to promote homogeneous cell distributions and mimic *in vivo* (Raphael et al. 2017). To overcome these challenges, “bottom-up” approach emerged as a new technique with an increasing number of publications since 2000 (Simian and Bissell, 2017). The bottom-up approach in tissue engineering comprises the formation of spheroids,

which are building blocks for the engineering of artificial organs (Laschke and Menger, 2017). The formation of these micro-tissues is governed by a series of complex cell-to-cell signaling processes such as activation of transmembrane receptors “integrins” that facilitate cell-ECM binding and expression of type-1 transmembrane protein “cadherin” (Klymenko et al. 2017). Expression of these proteins leads to a more realistic interaction between the cells and, consequently, enhances the response of the cells to the different stimuli, which makes the spheroids excellent candidates to be employed in medicine.

Spheroids are intensively used in regenerative medicine for crafting 3D tissues (Freedman et al. 2017), in drug metabolism to understand drug’s mechanism of action and body's response to the drug (Bell et al. 2016), and most importantly, in cancer research as a highly dynamic micro-tumor model to test new drugs (Mittler et al. 2017). Currently, chemotherapeutics are the most commonly-used drug formulations to treat cancer (Hu et al. 2016). However, chemotherapy drugs possess major safety concerns due to the side effects on healthy cells; hence, safer and more efficient drug formulations should be developed to specifically target cancer cells without harming healthy ones. Among a number of formulations, genetic materials come forward for their high effectiveness in cancer treatment as a gene therapy approach. Different types of genetic material such as microRNA (Lam et al. 2016), short hairpin RNA (shRNA) (Harata et al. 2018), CRISPR/Cas9 genome editing machinery (Li et al. 2019), and small interfering RNA (siRNA) (Cai et al. 2017) have been investigated for their efficiency in tumor spheroid models. Although each genetic material, especially CRISPR/Cas9 system, was found to be immensely potent, siRNA is still one of the most powerful tools to treat tumor spheroids. siRNA is the key molecule that plays role in RNA interference (RNAi), which is a post-transcriptional gene silencing process, and is capable of knocking-down specific genes to block the expression of proteins (Fire et al. 1998; Eş et al. 2018). To precisely evaluate the potential of siRNA-based drug formulations, spheroid models should be carefully developed with desired properties.

In the presence of convenient conditions, an autonomous organization of cells into spheroids, so-called self-assembly, occurs *in vitro* without any external intervention (Whitesides and Grzybowski, 2002). Therefore, new technological platforms to efficiently induce self-organization should be developed in a way that the cells show low or no affinity

to the surface of the material, hence, they are forced to interact with each other (Laschke and Menger, 2017). The rapid progress in science and technology allowed the design of different platforms for spheroid formation such as magnetic levitation (Souza et al. 2010), hanging-drop (Lin et al. 2016), suspension culture (Hookway et al. 2016), and micro-carrier beads (Wang et al. 2015). Even though these platforms have been well-established and widely used, they possess several disadvantages like tedious handling and media exchange as well as a low throughput rate. Moreover, spheroids formed with these methods vary in size, which reduces the precision of drug testing (Benien and Swami 2014). Hence, platforms such as microwell arrays as a static system (Lee et al. 2016) and microfluidics as a dynamic environment combined with microwell arrays (Chan et al. 2016) are shown to overcome the mentioned disadvantages in spheroid formation. Although microfluidic platforms provide a real-time screening of the effect of drugs on spheroid formation due to the continuous and automated flow, it is essential to optimize the culture conditions primarily in static systems before adapting to microfluidic systems.

Recent advancements in 3D printing technology combined with polymer chemistry and material science paved the way to fabricate high-quality architectures resistant to extreme conditions such as elevated temperatures. Resin-based materials are widely used in 3D printing and currently-available technologies allow rapid fabrication of structures with desired geometry and high-resolution thickness of layer (less than 50 μm). On the other hand, due to its potentially toxic nature, the resin is not suitable for cell culture, however, it is a good candidate to be used as a template in soft lithography technique to create micromolds using polydimethylsiloxane (PDMS), which is a promising silicon-based organic polymer (Marques and Szita 2016). The properties of PDMS such as hydrophobicity, high translucence, and good oxygen transfer rate make it an excellent material to fabricate static and dynamic microdevices for a high-throughput formation of spheroids with uniform size and high repeatability for the rapid screening of different drug formulations. Nevertheless, critical design parameters such as geometrical structure, microwell size, cell type, initial cell seeding concentration, and culture time should be carefully optimized for an efficient and economically-viable spheroid formation process (Fennema et al. 2013).

Tumor spheroid models have gained great popularity due to the characteristics of spheroids that efficiently mimic *in vivo* models and allow a more precise drug testing. Herein, human embryonic kidney 293 (HEK293) cells were used to form multicellular tumor spheroid models in microwells and were treated with siRNA for drug screening. PDMS-based micromolds at varying sizes and shapes were fabricated via soft lithography using 3D-printed molds as templates. Spheroid formation was systematically investigated throughout 7 days in terms of circularity, size, geometrical shape, and cell viability. The mold that leads to the formation of spheroids with desired properties was selected for further siRNA treatment. The selected spheroids were exposed to siRNA and the correlation between siRNA penetration behavior and spheroid size was evaluated to find the exact siRNA concentration to knockdown gene expression. Non-treated and treated spheroid models were analyzed using fluorescent, confocal, and multi-photon electron microscopy techniques. The present study is of great importance to contribute to the development of technologies for rapid spheroid growth and to understand how siRNA penetrates into these potential tumour models.

2. Materials and Methods

2.1. Materials

Human embryonic cells (HEK 293), human cervical cancer cells (HeLa), human colon adenocarcinoma cells (HT-29), and GFP-expressing human breast cancer cells (MCF-7) were kindly provided from Biochemical Engineering Department of University College London (London, United Kingdom). GFP expressing HEK 293 cell line was purchased from Cell Biolabs, Inc (San Diego, USA). Trypsin enzyme solution from bovine pancreas was used for detaching the cells from the surface of the T-flasks and was purchased from Sigma-Aldrich (St. Louis, MO). FluoroBrite™ Dulbecco's Modified Eagle Medium (DMEM), which is a formulation with background fluorescence that is 90% lower than that emitted by standard phenol red–free, was purchased from Gibco. GlutaMAX™ supplement and Fetal Bovine Serum (FBS) were purchased from Gibco and Thermo Fisher Scientific, respectively and were used as a supplement for media. Phosphate-buffered saline (PBS) was purchased from Gibco. Propidium iodide and Hoechst staining solutions were purchased from Chemometec (Denmark) and used to stain dead and live cells. The Sylgard™ 184 Silicone Elastomer Kit

was purchase from Dow Corning (Auburn, MI, United States) and was used to produce positive molds. NC-Slide A8™ was purchased from Chemometec and used to analyze the transfection efficiency.

2.2. Fabrication of static and dynamic microsystems for spheroid formation and siRNA transfection

Negative molds for both static and dynamic microfluidic systems were drawn in Autodesk Inventor 2019 (Figure 6.1A-C). The molds were then printed in desktop 3D printer "Form 2" (FormLabs) using the stereolithography technique. The molds were printed with white resin (FormLabs), which resists higher temperatures at which PDMS curing process occurs and printing resolution was set to 50 μm (Figure 6.1D). Non-processed resin residue after the STL process was first immersed in isopropyl solution for 15 min as a solvent treatment followed by simultaneous heat and UV-light treatments at 60 ^{o}C for 60 min. After the post-curing process, the negative molds were covered with high temperature-resistant tape (Figure 6.1D) then PDMS with curing agent at a ratio of 10:1 was prepared and poured over the 3D-printed negative molds for soft lithography processing. Afterward, the molds were left in the oven at 100 ^{o}C for 2 hours to cure PDMS (Figure 6.2A). A similar technique was used to fabricate continuous microfluidic device (Figure 6.2B-E). The negative molds to produce the lid to seal the channels of the dynamic microfluidic system were fabricated using Laser engraver (Epilog Legend Laser Series). Similarly, the support was covered with tape and cured in the oven. Prior to sealing process, both PDMS-based positive molds (channels and cover) were treated with BD-20A high-frequency generator as oxygen plasma cleaning. As the static micromold is designed to be an open system, no lid was fabricated for static micromold. The negative micromold for spheroid formation in the static system was designed to be 20 mm (arrow shown in Figure 6.1A) so each mold would perfectly fit in 12 well-plate. In the case of the continuous microfluidic system, the diameter of mold was set to 35 mm so each micromold would fit in a 6 well-plate. Moreover, in the static system, the diameter of the sphere-like structure varied between 400 and 800 μm (r_2 value shown in Figure 6.1C). After microfabrication, each device was cleaned and autoclaved prior to spheroid formation. No further sealing process was applied as this mold is used as an open system that allows cell seeding. The microwells were designed to be dome and sphere-like

structures to confirm whether each geometry affects the formation or not (Supplementary material 6.1).

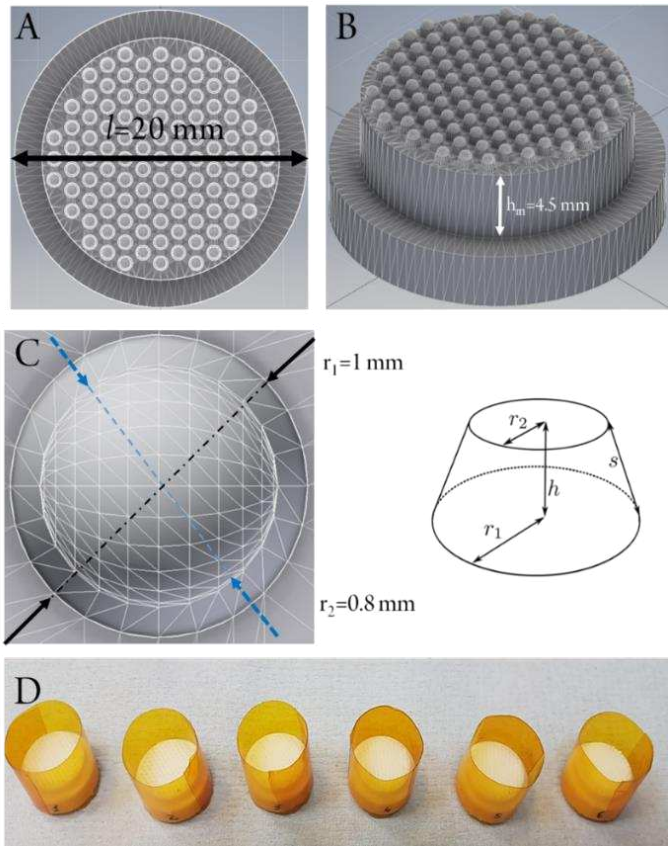

Figure 6. 1. The fabrication steps of the static microdevice for spheroids growth. The illustration of the entire CAD design of the 3D-printed negative mold (A) and (B); the illustration of one well with sphere-like structure (C); 3D-printed negative molds using white resin covered with high temperature-resistant tape (D).

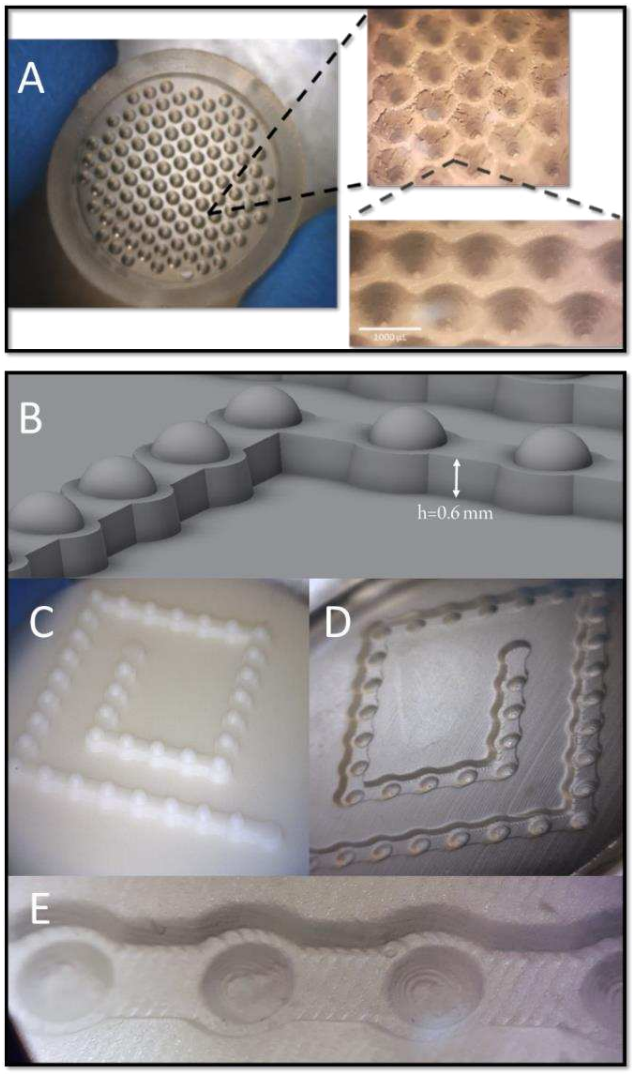

Figure 6. 2. Static and dynamic microdevices used for spheroid formation. Static microdevice: Image of PDMS-based negative molds with 109 microwells and their structural properties under the light microscope. The structure seen in the figure is sphere-like microwell with 0.4 mm of diameter (Bar represents 1000 μm) (A). Dynamic microdevice: CAD representation of dynamic microdevice to form spheroids (B). Negative mold 3D printed using white resin (C); PDMS-based positive mold (D); PDMS channels of dynamic microdevice (E). The channel height of dynamic microdevice is 0.6 mm. The diameter of the dynamic microdevice was set to 35 mm so each mold would fit in a well of 6-well plate. The number of microwell is determined to be 35. The diameter of each microwell was set to 1.25 mm, which is 0.45 mm bigger than the microwell of static microdevice.

2.3. Animal cell culture and spheroid formation

HEK 293, HeLa, HT-29, and MCF-7 cells lines were cultured in DMEM containing 10% FBS and 4 mM GlutaMAX™ supplement. Cells were passaged every 2 or 3 days in T25 cell

culture flask with the Thermo Scientific™ Nunclon™ Delta cell culture surface (Thermo Fisher) and maintained in incubator with 5% CO_2 at 37 ^oC.

2.3.1. Spheroid formation in round bottom microplate

Before starting the experiment using PDMS micromolds, mentioned cell lines were tested for their ability to form spheroids in commercial Corning® 96-well clear round bottom TC-treated microplate. Once 90% of cell confluency was achieved in T25 flask, the cells were dissociated from the surface of culture flask and counted using NucleoCounter® NC-3000™ (Chemometec) using Via1-Cassette™ that contains two immobilized fluorophores, acridine orange (AO) and DAPI. In this experiment, a highly-viscous culture media solution was prepared using 10% METHOCEL ® cellulose ethers with 90% of FluoroBrite DMEM with 10% FBS and Glutamax. After pouring 100 µL of methocel-containing culture media, the cell seeding concentration of 1.000, 2.000, and 3.000 was seeded in each well of the microplate. After two days of incubation, the microplate was analyzed under the fluorescent microscope to evaluate the spheroid formation of each cell.

2.3.2. Spheroid formation in static and dynamic PDMS-based microdevices

After selecting the cell line from the previous experiment, the spheroid formation was carried out in PDMS micromold. Prior to cell seeding, PDMS micromolds were placed in 12 well-plate under sterile conditions, and then the microwells were treated with AggreWell™ Rinsing Solution (500 µL) that prevents cell adhesion and promotes efficient spheroid formation. The 12 well plate containing microwells were centrifuged at 1.000 x g for 5 min to assure that the rinsing solution was distributed in each microwell. After centrifuge, PDMS mold was washed with culture medium to wash out non-coated rinsing solution. Afterward, the cells were seeded into microwells shown in Figure 6.2 with the varied initial cell seeding concentration (500, 1.000, and 1.500 cells per microwell). After seeding the cells, the 12 well-plate containing PDMS molds was centrifuged at 100 x g for 3 min to assure that the cells fall inside the microwells equally. The micromolds were analyzed under the microscope and placed in the incubator for spheroid formation. A similar spheroid formation protocol was employed for the dynamic microfluidic system. The initial cell concentration was set to 5.000 cells per microwell. The cell seeding was performed by pipetting.

2.4. Microscopy analysis

The spheroid formation was visualized using EVOS™ Digital Color Fluorescence Microscope (Invitrogen) and the images were taken daily for 7 days to analyze morphological properties of the spheroids. For a more advanced visualization, Leica SP8 confocal microscopy system in the London Centre for Nanotechnology (LCN) and Multiphoton Microscope Leica TCS SP8 MP in the Rockefeller Building of UCL Division of Medicine were used.

2.5. Spheroid analysis

2.5.1. Morphological properties

Characteristic properties of spheroids such as diameter, solidity, and the circularity were determined using ImageJ using the bright-field and fluorescent images. The images taken with multi photon microscopy were evaluated with Leica software and Microscopy Image Analysis Software Imaris.

2.5.2. Spheroid density and viability

The density of spheroids was calculated using TrypLE™ Select Enzyme (10X) solution without phenol red (Thermo Fisher). Approximately 50 spheroids were dissociated from microwells by gentle pipetting and were placed in a suspension culture plate. After counting the number of spheroids under the microscope or naked eye, they were put inside an Eppendorf tube (1.5 mL) with 500 μL of enzyme solution. The spheroids were gently mixed and kept in an incubator for ~3 min then the same solution was mixed vigorously to dissociate the spheroids. Afterward, FBS-containing DMEM media was added immediately to deactivate the enzyme solution to remove the negative effect on cell viability. The cell-containing solution was centrifuged at 1.000 rpm for 3 min to remove the excess media and replaced with fresh media followed by cell counting.

2.6. siRNA-mediated knockdown

2D cell culture of GFP expressing HEK 293 cell line was transfected using Lipofectamine 3000 and DharmaFECT transfection reagents. The transfection was carried out in 6-well plates with the Nunclon™ Delta surface treatment. Prior to transfection, each

well of the 6 well plate was coated with a collagen solution to increase the adherence characteristics of the cells. The collagen solution was prepared by mixing 150 µL of collagen, 14 µL of acetic acid and 10 mL of PBS. 1 mL of working solution was added into each well and the plate was left in the hood for 2 h and washed three times with PBS 1x. The plates were used immediately or stored in the fridge for further use. Approximately 200.000 cells were seeded in each well and left overnight in the incubator. The transfection was carried out once the cells reach ~70% of confluency. 3 µL of siRNA (50 µM) was separately complexed with 7.5 µL of Lipofectamine® 3000 and DharmaFECT 1 and left for 20 min in room temperature for complexation occurs between negatively-charged siRNA and positively-charged lipid-based vectors. The transfection solution was added into each well that contains cells and 1 mL of serum-free culture media. The cells were left in the incubator for 6 hours so the transfection could occur and after 6 hours, an additional 1 mL of serum-containing culture media was added with the total volume of 2 mL in each well. After 72 h, the plates were analyzed using Nucleocounter NC-8 slides to siRNA knock-down efficiency.

For spheroid transfection, only Lipofectamine® 3000 reagent was used. Spheroids were grown in static PDMS micromold and transfection reagent complexed with siRNA was added in the well. The concentration of siRNA and Lipofectamine® 3000 was estimated based on the values used in the transfection of 2D cell culture. After 72 h of transfection, the spheroids were dissociated using TrypLE™ Select Enzyme (10X) solution and knock-down efficiency was determined in Nucleocounter.

2.7. Statistical analysis

Quantitative experiments were conducted at least in biological triplicates and statistical significance was calculated using the Student's T-test or one way ANOVA. P-values are indicated. The number of replicates is always indicated in the Figure legends.

3. Results and Discussion

3.1. Design and microfabrication of static and dynamic microfluidic platforms

Similar strategies were employed for the fabrication (stereolithography) of both static and dynamic microfluidic platforms. Certain parameters were taken into considerations for an efficient spheroid formation in the fabricated systems. Before

proceeding with a dynamic microfluidic device, initial tests were carried out for static micromold. The geometrical structure is known to be an important parameter to induce the formation of spheroids. In our study, two different structures (dome-like and sphere-like) were tested (Supplementary material 6.1). According to the analysis of surface properties of both dome and sphere-like structures, no significant effect could be observed for spheroid formation. Hence, the final geometry was defined as sphere-like and was also applied for a dynamic system.

One of the most important criteria in the stereolithography technique is the proper selection of resin material, which will be used for the negative mold production. Several resin materials such as standard, engineering, dental, and ceramic resins are commercially-available for high-resolution rapid prototyping. Each resin has a different level of rigidity, light transmission, biocompatibility, and temperature resistance. High temperatures are highly required for the rapid curing of PDMS in soft lithography techniques. Hence, the resin should resist to high temperatures without losing its physical and chemical properties. Three different resin materials (temperature-resistant, clear, and white resins) were used to produce our micromold. The micromolds were firstly fabricated using temperature-resistant and clear resins. Both molds were left in the oven at temperature values varying from 50 to 100 ^{o}C for 2 h and at the end of PDMS curing process, certain physical changes (color and odor) were observed in both resins. After the curing process, peeling off the PDMS layers from the negative molds without breaking it down was challenging. This was probably due to the high porous characteristics of the resin material and extreme temperature probably resulted in a structural breakdown of the polymer chains inside the resin. However, when we tested white resin as a negative mold to produce PDMS-molds, the resin could resist temperatures as high as 120^{o}C and PDMS could be easily peeled off from the resin. Hence, the white resin was used for further fabrication.

3.1.1. Microfabrication of static platform

After defining the resin type and sphere-like structure, different diameter values were tested for spheroid formation in static micromold (Supplementary material 6.1). The diameter of sphere-like structures varied between 0.4 and 0.8 mm. r_1 and volume of conical frustum for each structure were fixed to 1 mm and 1.468 µL, respectively, whereas r_2 and h

values were changed to maintain the volume to 1.468 µL (Supplementary material 6.1). After PDMS curing, spheroids were formed in each PDMS micromolds and the mold with higher r_2 value resulted in the formation of bigger spheroids. Hence, r_2 value was fixed to 800 µm since more time was required to form a spheroid with the desired size using micromolds with smaller diameters.

The static micromold shown previously (Figure 6.2A) was designed for high-throughput spheroid formation. Such systems are excellent platforms to test novel drugs and acquire more precise results about their efficiency. Testing certain drug formulations in high-throughput systems can bring financial drawbacks to the experiments. As stated previously, the cost of chemical synthesis of siRNA is considerably high, hence the tests with siRNA should be performed in platforms that don't require excessive use of the genetic material. Our static design contains 109 microwells, which requires the use of siRNA at high amounts, therefore, a new static micromold was designed with a decreased number of microwells for performing drug tests using a reasonable number of siRNA. The micromold to be used in siRNA transfection had the same diameter (800 µm) and geometry (sphere-like). To decrease the number of microwells, the space between each microwell in static mold had to be increased. One should keep in mind that spheroid formation in static device requires a centrifugal step to induce the cells to fall into each microwell (Supplementary material 6.2). But, the distance between each microwell should be carefully calculated. In static micromold, for high-throughput spheroid formation, the distance between each micromold was determined to be 400 µm. However, different distances were also tested (0.8 – 1.2 mm) for spheroid formation (Supplementary material 6.3).

The number of microwell decreased as we increased the distance between each microwell so a certain number of microwell that will allow spheroid formation as well as siRNA transfection with less material cost could be achieved. Our test with GFP-expressing HEK 293 cell line showed that the cells could easily fall in each microwell after centrifuge step using microwells with 0.8 mm of distance. After 0.8 mm of distance, the cells didn't fall into microwells even ta higher centrifugal forces. Hence, the micromold with 0.8 mm of the distance between each microwell was defined as the desired geometry for siRNA transfection.

3.1.2. Microfabrication of dynamic platform

After defining micromold design for the high-throughput spheroid formation and siRNA transfection in a static system, where drug formulation is introduced into the system once and expect for the drugs to be delivered into the cells in spheroids without continuous flow. We hypothesized that the continuous introduction of drugs into spheroids would significantly increase the penetration of siRNA. Hence, a novel microfluidic platform that allows continuous seeding of drugs was fabricated. In such a device, the number of microwells was kept at acceptable levels for siRNA transfection. Similar to static micromold, the microfluidic device was designed so the cells would be equally contributed in each microwell using centrifugal force. In the first design, it was observed that the channel height was too high so once the drug is introduced into the system, a great number of siRNA would be required so each spheroid is treated with a sufficient number of genetic material. However, prior to the continuous transfection of spheroids in microchannels, the cells should have enough medium to maintain high viability to form spheroids. For this, different channel heights were tested to confirm high cell viability (data not shown). Our result showed that the micromold with 0.6 mm of channel height provided enough volume (~100 μL) so the cells have high viability for spheroid formation (Supplementary material 6.4). In such a system, the medium exchange has to be carried out every day to avoid cell death.

3.2. Spheroid formation analysis

We tested two different microfluidic platforms to form and transfect spheroids. The static microfluidic platform is an open platform where there is no continuous flow and the cells are seeded into the system at time t_0 and every day the culture media is changed so cells maintained their viability for spheroid formation, in a conventional manner. From a bioprocess point of view, this system can be compared to the batch process. Unlike a static system, a dynamic microfluidic platform is a closed channel system with inlet and outlet, where there is a continuous flow of culture media and drug/gene formulation and can be compared to the perfusion system. Before spheroids were formed in microfluidic platforms, the initial tests were conducted using commercial kits for spheroids formation.

3.2.1. Spheroid formation in commercial kits

Before proceeding with the experiments using PDMS micromolds, initially, different cell lines (HEK 293, HeLa, HT-29, and MCF-7) were tested in Corning® 96-well clear round bottom TC-treated microplate as a commercial kit to evaluate their ability to form spheroids, as a control. Among 4 cell lines, only HEK 293 was not a cancer cell line but, due to its immortal characteristics, it is widely used in cancer studies as an efficient model. Highly-viscous culture media solution was prepared using 10% METHOCEL ® cellulose ethers for spheroid formation in microplate. METHOCEL ® is a water-soluble methylcellulose and hydroxypropyl methylcellulose polymers and is used to increase the viscosity of tissue-culture fluids for spheroid formation. The advantage of this gel is that the spheroids can be easily separated by cooling the culture in a refrigerator for a short time, during which the gel liquefies, enabling it to be removed by pipetting. According to the images acquired under the microscope, it was confirmed that both HeLa and MCF-7 cell lines couldn't form spheroids (Figure 6.3).

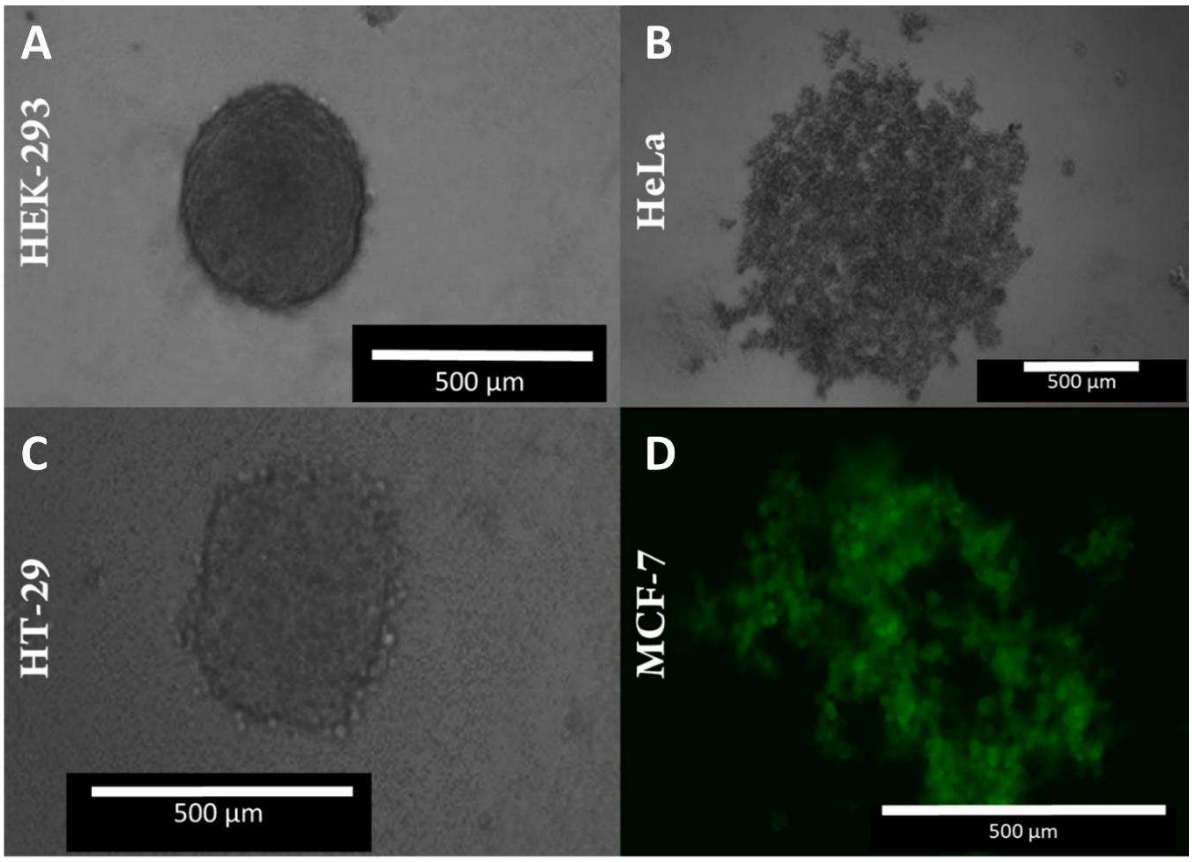

Figure 6. 3. Ability of forming spheroids of different cell lines tested in Corning® 96-well clear round bottom TC-treated microplate. HEK-293 (A), HeLa (B), HT-29 (C), and eGFP-expressing MCF-7 cell lines (D). The images are taken at the end of 2nd day. The initial cell seeding concentration was 1000 cells per well.

3.2.2. Spheroid formation in static micromold

As it is shown in Figure 6.3, HEK 293 and HT-29 cells could efficiently form spheroids and further experiments were performed using non-fluorescent and eGFP-HEK 293 cell lines. No significant difference in the ability of spheroid formation for non-fluorescent and eGFP-HEK 293 cell lines was observed. The spheroids formed in static micromold with different size and cell seeding concentration using non-fluorescent HEK 293 cell line at the end of 7th day is shown in Supplementary material 6.5. The total working volume of the micromold was 800 µL and before seeding the cells into the micromolds, the surface of the PDMS-based molds was treated with anti-adherence rinsing solution as a surfactant to reduce the surface tension in microwells and prevent cell adhesion. The use of a surfactant before seeding the

cells into the system is extremely crucial. Our results showed that the cells don't form spheroids with desired characteristics if the surface is not treated with surfactant.

As it can be seen in Figure 6.4, the spheroid size in each seeding condition increased significantly throughout 7 days. In our investigation, it was found that higher cell seeding concentration and bigger microwell size led to the formation of spheroids with the desired size more rapidly. The selection of these criteria is important as the main goal of this study is to investigate drug efficiency as a part of gene therapy. In drug testing, the time and precision are extremely essential and the use of such a platform that allows the formation of spheroids as fast as possible with proper size and geometry is highly required so the drugs can be immediately tested. Hence, we selected microwell size of 800 µm and cell seeding concentration of 1500 cells/microwell for our further drug testing with spheroids formed using eGFP-HEK 293 cell line.

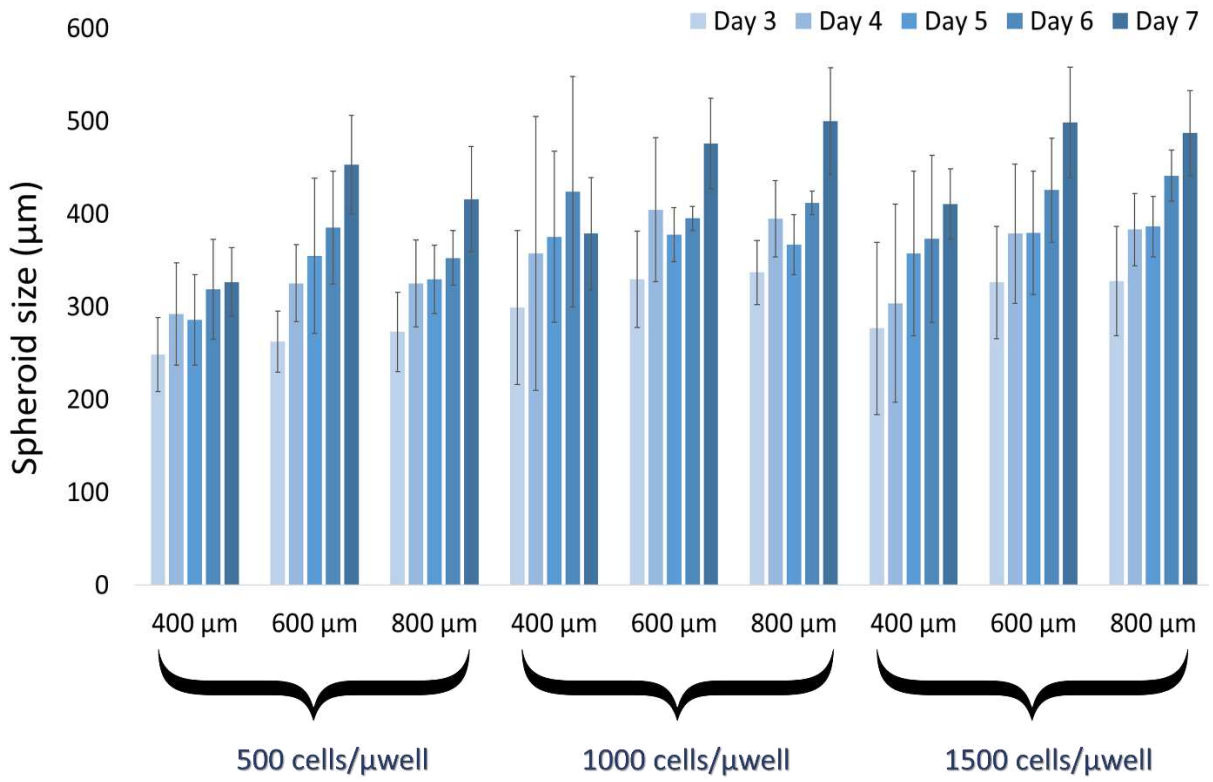

Figure 6. 4. Spheroid growth analysis during 7 days. The first 2 days are not shown in the Figure as it takes 2 days to start spheroid formation. The static microdevices with microwell size varying from 400 to 800 µm were used. Initial cell seeding concentration varied from

500 to 1500 cells per μwell. The spheroids were formed using non-fluorescent HEK 293 cell line.

After confirming the ability of spheroid formation of HEK 293 cell lines, the replicates for spheroid formation were completed using the eGFP-HEK 293 cell line. Compared to non-fluorescent HEK 293 cell line, there was no significant difference in size values. The change in spheroid size during 5 days of culture is shown in Supplementary Material 6.6. It must be noted that day 0 is the time when cells are seeded into the system for the first time. In day 1, the cells start to form spheroids with weak interaction between cells and in day 2, the spheroids become more solid as more extracellular matrix compounds are involved in the process.

The transfection efficiency depends on the number of cells treated with siRNA. Therefore, it is important to optimize both drug concentration as well as the number of cells that will receive the drug. In a monolayer (2D) cell culture, determining the number and viability of cells is easy, however, in 3D cell culture, it is hard to determine these parameters. Prior to this, spheroids should be dissociated with physical or enzymatic methods. The chosen method should not interfere with the viability of the cells and dissociate the entire spheroid without leaving any cell aggregates. Dissociation of spheroids using only physical methods is challenging and most likely to damage the cells and decrease their viability. On the other hand, enzymatic methods can be more effective for such dissociation. When trypsin was used followed by vigorous pipetting and trypsin deactivation with serum, the viability of the cells was found to be below 50% with several cell populations in aggregate form. Once TrypLE Select Enzyme (10X) solution was used, the viability of the cells was found to be over 90% with an insignificant number of cell aggregates. The number of cells per each spheroid is shown in Table 4.1. Using the average numbers given in Supplementary Material 6.7, one can estimate how many cells each spheroid with a certain size has and the amount of drug to be delivered into a tumor microtissue can be calculated.

3.2.3. Spheroid formation in dynamic microfluidic system

A similar strategy was followed to seed the cells inside the dynamic microfluidic system followed by centrifuge step. The microwells placed inside the microfluidic device

were designed to be 1.25 mm of diameter. It must be noted that the previous static device had the microwells with a diameter of 0.8 mm. Hence, a new estimation had to be done to determine cell seeding concentration by considering the volume of the microwells. The volume of each microwell in static device was ~0.7 µL while this value was~0.25 µL in dynamic system. According to these values, the cell seeding concentration was set to 5000 cells per microwell, which is around 3 times higher than the cell concentration of the static device. The cells were seeded into the channels as shown in Supplementary material 6.8 and after centrifuge step, the cells could successfully fall in each microwell with an equal contribution (Supplementary material 6.8), then left for spheroid formation. After our microscope imaging, the spheroids could achieve considerably bigger sizes (over 500 µm) in less than 3 days. This is a great advantage for drug testing since the spheroids reach a desired size rapidly so the siRNA can be tested.

3.3. siRNA-mediated knockdown

After completing the microfluidic platform design and assure that spheroids can form with desired properties in both static and dynamic platforms, we conducted transfection studies with siRNA to evaluate the penetration rate of siRNA into spheroids. Before the transfection of spheroids, initial tests were performed using 2D monolayer cell culture. The transfection efficiency highly depends on the concentration of genetic material complexed with non-viral vector systems as well as the number of cells in the cell culture. Hence, as the first step, these parameters were optimized so new concentration values could be estimated to use for spheroid transfection. Our tests with different siRNA and Lipofectamine® 3000 showed that complexing 3 µL of siRNA (50 µM) with 7.5 µL of Lipofectamine® 3000 was sufficient to knockdown GFP expression of ~300.000 cells. The transfection efficiency and fluorescent images of the transfection experiment in monolayer culture are shown in Figure 6.5. It can be seen that siRNA complexed with Lipofectamine didn't show a significant effect on the viability of the cells as the cell viability was over 90% after 72 h. According to the GFP mean intensity values, the GFP expression was below 50% after silencing with eGFP-siRNA.

CONTROL

Estimated viability	90 to 100 %
Transfection ratio - viable cells [%]	94
Transfection ratio - nonviable cells [%]	11
Transfection ratio - all cells [%]	89
GFP mean intensity	1.02E6
GFP standard deviation	8.37E5
GFP main number	3.42E4

ONLY LIPOFECTAMINE

Estimated viability	90 to 100 %
Transfection ratio - viable cells [%]	94
Transfection ratio - nonviable cells [%]	9
Transfection ratio - all cells [%]	88
GFP mean intensity	9.78E5
GFP standard deviation	8.31E5
GFP main number	4.30E4

CONTROL siRNA

Estimated viability	90 to 100 %
Transfection ratio - viable cells [%]	93
Transfection ratio - nonviable cells [%]	8
Transfection ratio - all cells [%]	86
GFP mean intensity	1.13E6
GFP standard deviation	9.30E5
GFP main number	3.37E4

eGFP siRNA

Estimated viability	90 to 100 %
Transfection ratio - viable cells [%]	87
Transfection ratio - nonviable cells [%]	5
Transfection ratio - all cells [%]	80
GFP mean intensity	4.44E5
GFP standard deviation	5.28E5
GFP main number	3.13E4

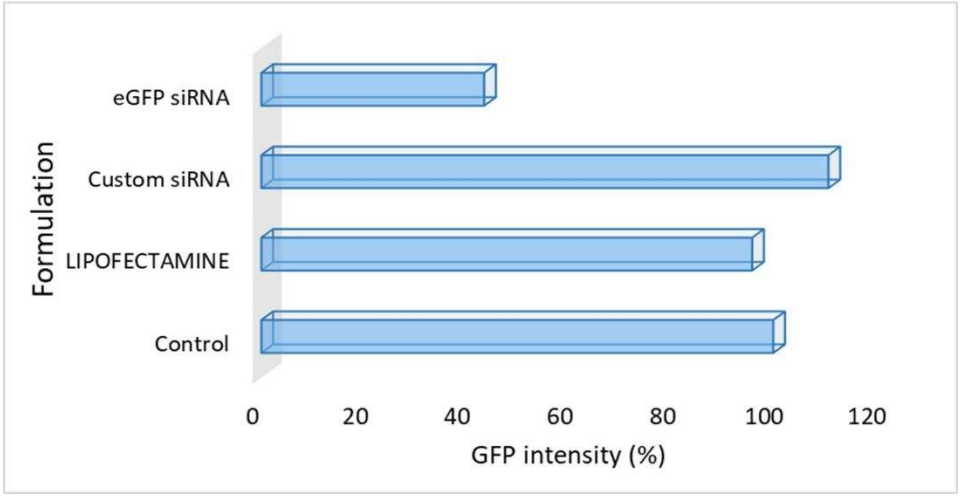

Figure 6. 5. Transfection results obtained from Nucleocounter after 72 hours of incubation time in 2D culture. The study was carried out using control (non-treated), only Lipofectamine, control siRNA (non-eGFP targeting siRNA), and eGFP-targeting siRNA. The transfection was carried out in conventional 6-well plates.

3.3.1. siRNA delivery in static micromold

After assuring that GFP genes expressed in HEK 293 cell line could be knocked-down by siRNA-containing Lipofectamine as a gene delivery approach, we proceeded with our investigations with the transfection of spheroids with the same formulation. Spheroids are solid micro-tissues containing complex intercellular communication, where several extracellular molecules are involved. Therefore, the penetration of drugs inside such cellular organization is a highly challenging process. In reality, the reason behind the failure of different drugs tested in solid tissues such as cancer tissues is the fact that drugs cannot effectively be delivered into the target site. Therefore, new strategies should be followed to enhance the penetration of molecules such as siRNA for efficient targeting.

In order to transfect spheroids, the first thing was to define at which stage the spheroids should be selected for transfection studies. As we previously showed, spheroids constantly grow in size and cell intensity inside the cell also increases with time. Using the information shown in Supplementary material 6.7, we could culture the spheroids and once they achieve the desired size, we could isolate them for transfection analysis.

We estimated the concentration of siRNA-Lipofectamine formulation based on this equation and also the values that we used for siRNA transfection on monolayer culture. We also started the transfection studies in our static microfluidic platform after the 3rd day of spheroid growth. After the 3rd day of spheroid growth, the estimated size of the spheroid was found to be around 300 μm and cell intensity is ~8000 cells/spheroid. Considering that we had 37 microwells to produce 37 individual spheroids which give us around 300.000 cells to transfect. This value is very similar to the number of cells we transfected in monolayer culture. Hence, we used similar siRNA and Lipofectamine concentration values to transfect the spheroids. After preparing our siRNA-Lipofectamine solution, we introduced them into the micromold with 37 microwells (with spheroids at the end of 3rd day) and mixed gently to be sure that drug formulation was homogeneously distributed in the mold. We waited 72 hours to analyze the transfection efficiency of spheroids. The results of the spheroid transfection are shown in Figure 6.6. GFP intensity values showed that we could achieve only 3% of transfection. This result is in accordance with previous investigations, which have also

reported that the transfection efficiency of spheroids is extremely low and challenging (Morgan et al. 2018).

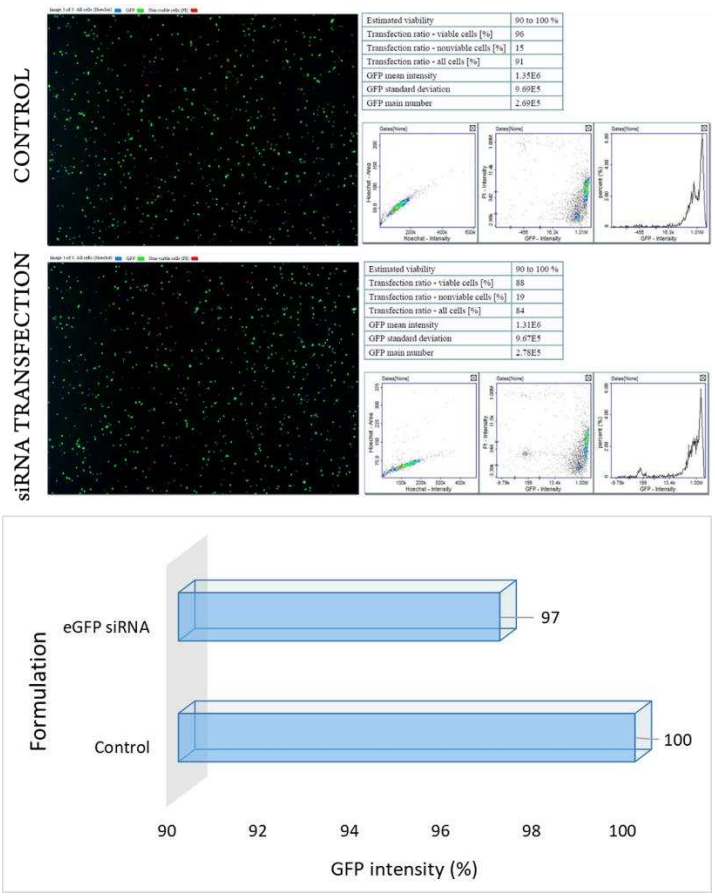

Figure 6. 6. Spheroid transfection using siRNA-Lipofectamine combination compared to control. The transfection was carried out using static microfluidic device. The spheroids were transfected at the end of 3rd day of cultivation. The initial cell seeding concentration was 8000 cells/microwell. The transfection was analyzed 72 h after initial transfection.

3.3.2. siRNA delivery in dynamic microfluidic system

The main goal of this study was to develop a microfluidic platform with the dynamic flow by continuously feeding the siRNA as a drug formulation to evaluate its penetration rate into the tumor microtissue models. The spheroids were successfully formed in this system and siRNA and Lipofectamine was previously mixed and the final transfection solution with the desired concentration (siRNA/cell) was continuously pumped into the channel. However, the first transfection studies were not successful and we noticed that the penetration rate of siRNA could be enhanced by filling the microchannels with a commercially-available

collagen-based extracellular matrix, this way, it will be possible to mimic *in vivo* conditions more precisely, and bearing in mind that manufacturing mimicry system that completely represents *in vivo* condition is currently not possible.

3.4. Advanced microscopy analysis

Spheroid visualization is a difficult process and their visualization is quite impossible with conventional fluorescent microscopy techniques since there must be a certain photon penetration to visualize the inner part of the 3D microtissues. Conventional confocal microscopes are also not very effective in penetrating into the deep layers of spheroids. Thus, the use of advanced microscopy techniques is especially essential to observe cells inside the spheroid. Advanced microscopy analysis can give critical information about the proliferation, hypoxic, and necrotic zone of spheroids. Moreover, it is also possible to obtain viable data about transfection efficiency by employing different filters to acquire different fluorescent signals from each zone.

In this study, the confocal microscope Leica SP8 was initially used to visualize the spheroids that were formed with non-GFP expressing HEK 293 cell lines. Prior to visualization, the cells were stained with Hoechst dye. As can be seen in the image taken with a confocal microscope shown in Figure 6.7, the edge and the shape of the spheroid can be visualized, however, we couldn't penetrate inside the spheroid. Moreover, the spheroid shape is observed as oval, which was a result of the sedimentation of spheroids on the surface of the microscope slide. Considering that each spheroid used in this experiment had a size of ~400 μm and at least half of the spheroid (~200 μm) had to be visualized so the entire geometry of the spheroid could be estimated.

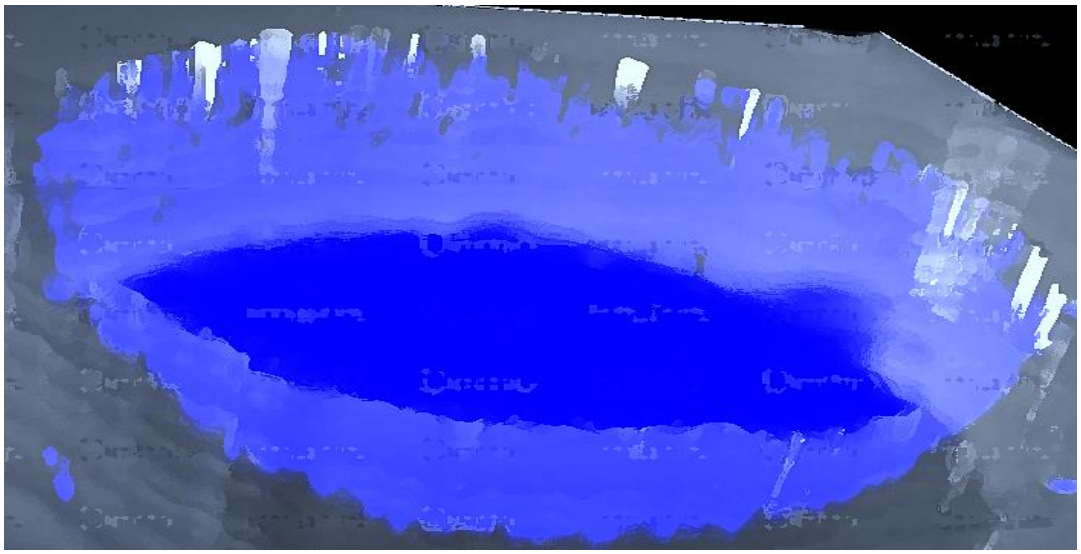

Figure 6. 7. Confocal image of a spheroid visualized under Leica SP8 confocal system. The spheroid was left for growth for 4 days.

Due to the penetration limitation of this confocal imaging system, a more effective imaging system was required. Hence, two-photon microscopy was employed to penetrate more into the spheroids. The spheroid was stained with PI to observe the position of the dead cells. After the 7th day of spheroid growth, no necrotic zone was observed and the dead cells can be seen in Figure 6.8. The viability of the spheroid was calculated to be over 80% (data not shown). The high viability was because of the continuous feeding of the spheroid culture with culture medium. According to the images, the spheroid was not completely observable due to the certain limitations of two-photon penetration. One of the reasons for not being able to observe the entire spheroid was its size. The spheroid size at the end of the 7th day was over 600 µm, but around 200 µm was still observable.

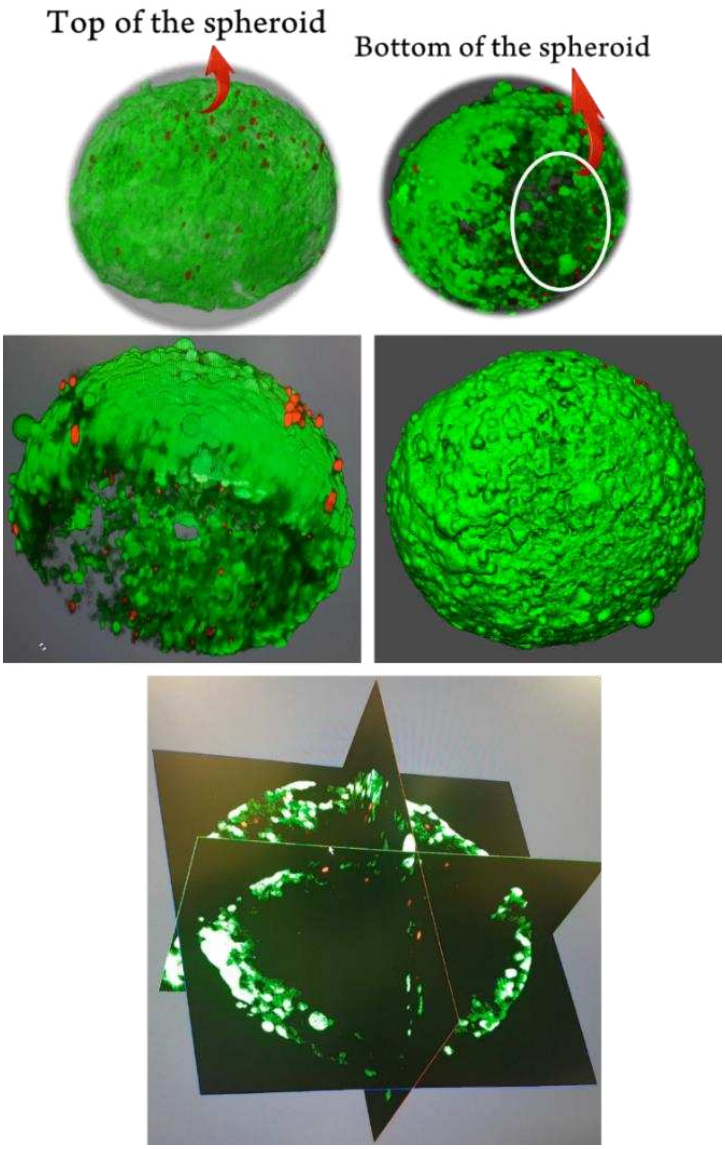

Figure 6. 8. Fluorescent imaging of spheroids at the end of day 7 visualized by two-photon microscopy system. The red dots represent the dead cells which were stained with PI dye.

4. Conclusion

In the present study, we developed microfluidic platforms that allow the formation of spheroids with controllable size. The first microfluidic device was designed for the formation of spheroids in large quantities with the static flow. The second device was manufactured to provide a continuous flow to generate dynamic conditions that better mimic *in vivo* fluid flows. Using this in vitro tumor model, we expected to observe more significant therapeutic responses to the delivery of siRNA as a potential gene therapy application

compared to other in vitro models. After our transfection studies in a static system, the penetration rate of siRNA into spheroids was very low. This may be due to the lack of continuous flow that would enhance the penetration of the genetic drug into the microtissues. Along with the scientific progress of the current project, we noticed that new paths can be followed to overcome this limitation observed in the static flow system. In the microfluidic system with the dynamic flow, the spheroids were continuously fed with culture media to induce their growth for several days. However, to enhance siRNA delivery into the spheroids, new strategies should be adapted. Currently, we are investigating the formation of spheroids in a collagen-based extracellular matrix (ECM) to surround the spheroids for a better cell to cell communication followed by the continuous introduction of lipid-based nanotherapeutics containing siRNA to evaluate the drug penetration.

References

1. Bell, C.C., Hendriks, D.F., Moro, S.M., Ellis, E., Walsh, J., Renblom, A., Puigvert, L.F., Dankers, A.C., Jacobs, F., Snoeys, J. and Sison-Young, R.L., 2016. Characterization of primary human hepatocyte spheroids as a model system for drug-induced liver injury, liver function and disease. *Scientific reports*, *6*, p.25187.
2. Bray, F., Ferlay, J., Soerjomataram, I., Siegel, R.L., Torre, L.A. and Jemal, A., 2018. Global cancer statistics 2018: GLOBOCAN estimates of incidence and mortality worldwide for 36 cancers in 185 countries. CA: a cancer journal for clinicians, 68(6), pp.394-424.
3. Cai, R.Q., Liu, D.Z., Cui, H., Cheng, Y., Liu, M., Zhang, B.L., Mei, Q.B. and Zhou, S.Y., 2017. Charge reversible calcium phosphate lipid hybrid nanoparticle for siRNA delivery. Oncotarget, 8(26), p.42772.
4. Duval, K., Grover, H., Han, L.H., Mou, Y., Pegoraro, A.F., Fredberg, J. and Chen, Z., 2017. Modeling physiological events in 2D vs. 3D cell culture. Physiology, 32(4), pp.266-277.
5. Eş, I., Ok, M.T., Puentes-Martinez, X.E., de Toledo, M.A.S., de Pinho Favaro, M.T., Cavalcanti, L.P., Cassago, A., Portugal, R.V., Azzoni, A.R. and de la Torre, L.G., 2018. Evaluation of siRNA and cationic liposomes complexes as a model for *in vitro* siRNA

delivery to cancer cells. Colloids and Surfaces A: Physicochemical and Engineering Aspects, 555, pp.280-289.

6. Fire, A., Xu, S., Montgomery, M.K., Kostas, S.A., Driver, S.E. and Mello, C.C., 1998. Potent and specific genetic interference by double-stranded RNA in Caenorhabditis elegans. nature, 391(6669), pp.806-811.
7. Freedman, B.S., Brooks, C.R., Lam, A.Q., Fu, H., Morizane, R., Agrawal, V., Saad, A.F., Li, M.K., Hughes, M.R., Vander Werff, R. and Peters, D.T., 2015. Modelling kidney disease with CRISPR-mutant kidney organoids derived from human pluripotent epiblast spheroids. Nature communications, 6, p.8715.
8. Hookway, T.A., Butts, J.C., Lee, E., Tang, H. and McDevitt, T.C., 2016. Aggregate formation and suspension culture of human pluripotent stem cells and differentiated progeny. Methods, 101, pp.11-20.
9. Hu, Q., Sun, W., Wang, C. and Gu, Z., 2016. Recent advances of cocktail chemotherapy by combination drug delivery systems. Advanced drug delivery reviews, 98, pp.19-34.
10. Jiang, W., Kim, B.Y., Rutka, J.T. and Chan, W.C., 2008. Nanoparticle-mediated cellular response is size-dependent. Nature nanotechnology, 3(3), pp.145-150.
11. Kelm, J.M., Timmins, N.E., Brown, C.J., Fussenegger, M. and Nielsen, L.K., 2003. Method for generation of homogeneous multicellular tumor spheroids applicable to a wide variety of cell types. Biotechnology and bioengineering, 83(2), pp.173-180.
12. Kijanska, M. and Kelm, J., 2016. *In vitro* 3D spheroids and microtissues: ATP-based cell viability and toxicity assays. In Assay Guidance Manual [Internet]. Eli Lilly & Company and the National Center for Advancing Translational Sciences.
13. Kinney, M.A., Hookway, T.A., Wang, Y. and McDevitt, T.C., 2014. Engineering three-dimensional stem cell morphogenesis for the development of tissue models and scalable regenerative therapeutics. Annals of biomedical engineering, 42(2), pp.352-367.
14. Klymenko, Y., Kim, O., Loughran, E., Yang, J., Lombard, R., Alber, M. and Stack, M.S., 2017. Cadherin composition and multicellular aggregate invasion in organotypic models of epithelial ovarian cancer intraperitoneal metastasis. Oncogene, 36(42), pp.5840-5851.

15. Lam, S.S.N., Ip, C.K.M., Mak, A.S.C. and Wong, A.S.T., 2016. A novel p70 S6 kinase-microRNA biogenesis axis mediates multicellular spheroid formation in ovarian cancer progression. Oncotarget, 7(25), p.38064.
16. Laschke, M.W. and Menger, M.D., 2017. Life is 3D: boosting spheroid function for tissue engineering. Trends in biotechnology, 35(2), pp.133-144.
17. Lee, G., Lee, J., Oh, H. and Lee, S., 2016. Reproducible construction of surface tension-mediated honeycomb concave microwell arrays for engineering of 3D microtissues with minimal cell loss. PloS one, 11(8).
18. Li, M., Xie, H., Liu, Y., Xia, C., Cun, X., Long, Y., Chen, X., Deng, M., Guo, R., Zhang, Z. and He, Q., 2019. Knockdown of hypoxia-inducible factor-1 alpha by tumor targeted delivery of CRISPR/Cas9 system suppressed the metastasis of pancreatic cancer. Journal of Controlled Release, 304, pp.204-215.
19. Lin, B., Miao, Y., Wang, J., Fan, Z., Du, L., Su, Y., Liu, B., Hu, Z. and Xing, M., 2016. Surface tension guided hanging-drop: producing controllable 3D spheroid of high-passaged human dermal papilla cells and forming inductive microtissues for hair-follicle regeneration. ACS applied materials & interfaces, 8(9), pp.5906-5916.
20. Raphael, B., Khalil, T., Workman, V.L., Smith, A., Brown, C.P., Streuli, C., Saiani, A. and Domingos, M., 2017. 3D cell bioprinting of self-assembling peptide-based hydrogels. Materials Letters, 190, pp.103-106.
21. Simian, M. and Bissell, M.J., 2017. Organoids: a historical perspective of thinking in three dimensions. Journal of Cell Biology, 216(1), pp.31-40.
22. Sultan, S., Siqueira, G., Zimmermann, T. and Mathew, A.P., 2017. 3D printing of nano-cellulosic biomaterials for medical applications. Current Opinion in Biomedical Engineering, 2, pp.29-34.
23. Wang, J., Cheng, Y., Yu, Y., Fu, F., Chen, Z., Zhao, Y. and Gu, Z., 2015. Microfluidic generation of porous microcarriers for three-dimensional cell culture. ACS applied materials & interfaces, 7(49), pp.27035-27039.
24. Wong, C.H., Siah, K.W. and Lo, A.W., Estimation of clinical trial success rates and related parameters [published online January 31, 2018]. Biostatistics.

CHAPTER 7. CONCLUSION AND FUTURE PERSPECTIVE

1. Conclusion

The synthesis of novel nanotherapeutics for the delivery of powerful genetic machinery to treat genetic diseases such as cancer is notably necessary. Among all genetic materials, siRNA has been investigated for over a decade to discover practical treatment methods for genetic diseases. The delivery of siRNA can be drastically improved by including it into lipid-based carriers like liposomes. Though, the complexation between siRNA and liposomes should be investigated thoroughly to determine the optimum amount of siRNA and liposomes for more effective transfection. In this context, as the first part of our study, we electrostatically complexed siRNA and liposomes at varying molar charge ratios (Chapter 3). After our investigations utilizing dynamic light scattering and siRNA accessibility assays, we confirmed that optimum molar charge ratio between positively-charged phospholipids present in the liposome formulation and negatively-charged phosphate backbone in the structure of siRNA was 3.27. This finding was supported by morphological analysis and transfection studies on cancer cells. This investigation was essential to promote further studies in microfluidic devices to complex siRNA with different lipid-based vector systems. More importantly, when nanotherapeutics is delivered to cancer cells for *in vitro* and *in vivo* applications, as most of the genetic material is incorporated into the lipid carrier system, the cytotoxic effect of both siRNA and carrier system can be avoided.

New technological tools should be exploited to increase the productivity and efficiency of the production of novel nanotherapeutics. Microfluidics offers several advantages over other techniques as we previously mentioned. In the next part of the study, two separate microfluidic platforms were employed to assess the synthesis of conventional and stealth cationic liposomes, which were used for further complexation with genetic material (Chapter 4). In the device, where the diffusion process was dominant, the production of conventional liposomes has been previously explored by different research groups; however, the device was not effective in manufacturing stealth liposomes as we observed severe particle agglomeration in the channels. As a solution, we tested the effect of chaotic advection mixing for the production of stealth liposomes. In a chaotic advection-

based device, we eliminated the particle agglomeration in the channel and successfully synthesized stealth liposomes. Besides, the production in this device was high-throughput and the productivity was ~70 times higher compared to the production in the diffusion-based device, which is highly suitable in the industry for the synthesis of such colloidal systems to be used in pharmaceutical, food, or cosmetic industry. Additionally, the final ethanol content in the final liposomal solution was 50%, which is considered cytotoxic to the cells and may lead to safety concerns in their pharmaceutical applications. Hence, we employed a centrifugal vacuum concentrator (CVC) system to completely remove ethanol to reduce the safety issues in their application. Compared to the dialysis that is extensively used for solvent extraction in such processes, CVC can remove solvent from liposomal solution on a big scale as the extraction with dialysis is not a feasible option. This solvent removal system can be readily integrated into large scale systems to simultaneously manufacture liposomes and extract the solvent.

The aforementioned devices are competent in the practical complexation of siRNA and lipid-based vectors. Complexation in microfluidic devices can be accomplished by two mixing strategies (Chapter 5). In the first strategy, siRNA and phospholipids can be introduced and mixed in the channel as a single-step approach. In the second strategy, siRNA can be complexed with pre-formed liposomes, which requires an additional step to synthesize liposomes. Both nanotherapeutics formulations may have distinctive phospholipid packing density and conformation and possess a unique mechanism of transfection as well as recognizably distinct characteristics. The effect of diffusion in microfluidic systems has not been investigated for the mentioned complexation strategies with siRNA. In this context, this study aimed to fill the gap that exists in the literature for the microfluidic synthesis of these nanotherapeutics to be used in gene therapy as a comparative study. After the analyses using powerful analytical tools, we confirmed the critical distinctions between two nanotherapeutics formulations. Parameters such as the surface charge density, size distribution, lamellarity, and/or PEGylation efficiency were found to be significantly different. Due to these differences, a different strategy should be followed for *in vivo* delivery as these parameters significantly affect the therapeutic outcome of these nanotherapeutics formulations. The microfluidic synthesis of both formulations was

optimized in terms of flow rate, flow configuration, and final phospholipid and siRNA concentration for a continuous synthesis. We showed that optimized parameters can be adapted for the microfluidic synthesis of other nanotherapeutics formulations composed of diverse genetic materials and vector systems.

After developing the nanotherapeutics, their analysis is vital to define their effectiveness. *In vivo* studies are highly challenging due to several biological restrictions and *in vitro* 2D cell culture systems do not accurately represent dynamic *in vivo* models. In this context, 3D cell culture models, which mimic dynamic microenvironments of living organs, emerge as a promising technique to study cell differentiation as well as cell response against nanotherapeutics. As the last part of this study, we manufactured d a new microfluidic 3D cell culture platform (static and dynamic system) for the formation of spheroids as a biomimetic model to precisely test diverse nanotherapeutics (Chapter 6). The spheroid formation was optimized in both devices and the siRNA delivery to the spheroids was tested in a static device and the transfection efficiency was found to be very low.

In conclusion, this project is expected to contribute to the understanding of the association between cationic liposomes and siRNA for further gene therapy applications. Using new strategies in microfluidic mixing, the productivity of stealth liposome synthesis was improved and the micelle formation in the microchannel was eliminated for continuous production. After the characterization studies, the synthesized nanotherapeutics have shown good efficacy for siRNA transfection into cancer cells. Furthermore, the development of innovative microchips enables the investigation of the in vitro transfection of tumor spheroids in dynamic conditions. This way, we expect this microfluidic 3D cell culture system to better mimic the *in vivo* tumor microenvironment to improve the precision of drug testing and consequently eliminating animal tests.

2. Future perspective

Nanotechnology drew substantial attentions in treatment of genetic diseases such as cancer. Despite intense studies in the nanotechnology to explore gene delivery systems, there are still various critical issues to be addressed to improve the efficiency of these promising

nanotherapeutics. Considering all the limitations encountered during this project, the following suggestions as future perspectives can be proposed:

- Conventional liposomes suffer from non-specific interaction with cell/tissues or proteins in the bloodstream, which leads to a random uptake of these vector systems by non-target cells. To eliminate this random uptake, PEG polymer is a widely used polymer to be included in the lipid formulation to increase the circulation time in bloodstream. Several investigations have shown that the circulation half-life of vector system strongly depends on the quantity of PEG molecules on the surface, and, most importantly, its molecular weight (MW). In our study, we used 1% of PEG polymer with chain length of 2000 Da. However, different MW range should be investigated to enhance the stealth properties of the liposomes synthesized in microfluidic system.

- Although PEG has promising applications in gene delivery, surprisingly, several studies reported the existence of antibodies (anti-PEG) that could recognize PEGylated liposomes and repeated *in vivo* administration of PEGylated nanoparticles results in both immunogenic and antigenic reactions in the body. Due to the rising concerns associated with PEG, new alternatives should be considered to replace with PEG to be employed in gene delivery. As a future work, zwitterions (e.g. poly(carboxybetaine)), which are polyelectrolytes that contain both positively and negatively-charged groups, can be included in liposomal formulation to produce in microfluidic systems.

- Liposomes are widely used vesicular vector systems and have a wide range of application in gene therapy. Despite their advantages, they may have certain limitations in specific applications. As a future study, microfluidic technology can be employed to synthesize more effective vesicular vectors such as exosomes and lipidoid nanoparticles. Additionally, these vesicular vectors can be further functionalized with antibodies, aptamers, or peptides to improve their gene delivery efficiency.

- The microfluidic technology is mostly limited by its low productivity due to the existing challenges in scale-up process. This drawback can be eliminated by improving mixing patterns in microfluidic channel that leads to an increased productivity and efficient synthesis of the mentioned lipid-based nanotherapeutics.

- In terms of drug/gene delivery to the spheroids in microfluidic cell cultures, we noticed that new paths can be followed to enhance the penetration rate of nanotherapeutics into the spheroids. The results of spheroid transfection showed that static microfluidic platforms are not satisfactory to test drug/gene formulations. Furthermore, the continuous flow of siRNA into the system in the presence of culture media would not entirely mimic *in vivo* systems. Inside the body, there is an extracellular matrix (ECM) that fills the space between cells to serve as a three-dimensional network of extracellular macromolecules that provide structural and biochemical support to surrounding cells. As a future perspective of this part of the project, microfluidic platforms can be filled with commercially-available ECM matrix then siRNA can be introduced into the system for more efficient penetration of siRNA into spheroids as micro-tissue models. Such technological platforms may speed up drug tests, increase the precision of the tests before clinical trials, and eliminate undesirable animal tests. More importantly, such microfluidic technology can be utilized as a rapid and effective micro-tissue formation platform to test new drug formulation on different types of tumour cells with high-throughput.

General References

1. Abina, S.H.B., Gaspar, H.B., Blondeau, J., Caccavelli, L., Charrier, S., Buckland, K., Picard, C., Six, E., Himoudi, N., Gilmour, K. and McNicol, A.M., 2015. Outcomes following gene therapy in patients with severe Wiskott-Aldrich syndrome. Jama, 313(15), pp.1550-1563.
2. Abuchowski, A., McCoy, J.R., Palczuk, N.C., van Es, T. and Davis, F.F., 1977. Effect of covalent attachment of polyethylene glycol on immunogenicity and circulating life of bovine liver catalase. Journal of Biological Chemistry, 252(11), pp.3582-3586.
3. Angelov, B., Angelova, A., Filippov, S.K., Karlsson, G., Terrill, N., Lesieur, S. and Štěpánek, P., 2011. Topology and internal structure of PEGylated lipid nanocarriers for neuronal transfection: synchrotron radiation SAXS and cryo-TEM studies. Soft Matter, 7(20), pp.9714-9720.
4. Aref, H., 2002. The development of chaotic advection. Physics of Fluids, 14(4), pp.1315-1325.
5. Ásgeirsdóttir, S.A., Talman, E.G., de Graaf, I.A., Kamps, J.A., Satchell, S.C., Mathieson, P.W., Ruiters, M.H. and Molema, G., 2010. Targeted transfection increases siRNA uptake and gene silencing of primary endothelial cells *in vitro*—a quantitative study. Journal of controlled release, 141(2), pp.241-251.
6. Baek, J., Allen, P.M., Bawendi, M.G. and Jensen, K.F., 2011. Investigation of indium phosphide nanocrystal synthesis using a high-temperature and high-pressure continuous flow microreactor. Angewandte Chemie International Edition, 50(3), pp.627-630.
7. Bagchi, D., Dutta, S., Singh, P., Chaudhuri, S. and Pal, S.K., 2017. Essential dynamics of an effective phototherapeutic drug in a nanoscopic delivery vehicle: psoralen in Ethosomes for biofilm treatment. ACS omega, 2(5), pp.1850-1857.
8. Balbino, T.A., Aoki, N.T., Gasperini, A.A., Oliveira, C.L., Azzoni, A.R., Cavalcanti, L.P. and Lucimara, G., 2013. Continuous flow production of cationic liposomes at high lipid concentration in microfluidic devices for gene delivery applications. Chemical engineering journal, 226, pp.423-433.

9. Balbino, T.A., Azzoni, A.R. and de La Torre, L.G., 2013. Microfluidic devices for continuous production of pDNA/cationic liposome complexes for gene delivery and vaccine therapy. Colloids and Surfaces B: Biointerfaces, 111, pp.203-210.
10. and vaccine therapy. Colloids and Surfaces B: Biointerfaces, 111, pp.203-210.
11. Balbino, T.A., Gasperini, A.A., Oliveira, C.L., Azzoni, A.R., Cavalcanti, L.P. and de La Torre, L.G., 2012. Correlation of the physicochemical and structural properties of pDNA/cationic liposome complexes with their *in vitro* transfection. Langmuir, 28(31), pp.11535-11545.
12. Balbino, T.A., Serafin, J.M., Malfatti-Gasperini, A.A., de Oliveira, C.L., Cavalcanti, L.P., de Jesus, M.B. and de La Torre, L.G., 2016. Microfluidic assembly of pDNA/Cationic liposome lipoplexes with high pDNA loading for gene delivery. Langmuir, 32(7), pp.1799-1807.
13. Balbino, T.A., Serafin, J.M., Radaic, A., de Jesus, M.B. and Lucimara, G., 2017. Integrated microfluidic devices for the synthesis of nanoscale liposomes and lipoplexes. Colloids and surfaces B: biointerfaces, 152, pp.406-413.
14. Bally, F., Garg, D.K., Serra, C.A., Hoarau, Y., Anton, N., Brochon, C., Parida, D., Vandamme, T. and Hadziioannou, G., 2012. Improved size-tunable preparation of polymeric nanoparticles by microfluidic nanoprecipitation. Polymer, 53(22), pp.5045-5051.
15. Bangham, A.D., Standish, M.M. and Watkins, J.C., 1965. The accumulation of steroids and streptolysin S on the permeability of phospholipid structures to cations. J Mol Biol, 13, pp.238-53.
16. Barisam, M., Saidi, M.S., Kashaninejad, N. and Nguyen, N.T., 2018. Prediction of necrotic core and hypoxic zone of multicellular spheroids in a microbioreactor with a u-shaped barrier. Micromachines, 9(3), p.94.
17. Bedi, D., Musacchio, T., Fagbohun, O.A., Gillespie, J.W., Deinnocentes, P., Bird, R.C., Bookbinder, L., Torchilin, V.P. and Petrenko, V.A., 2011. Delivery of siRNA into breast cancer cells via phage fusion protein-targeted liposomes. Nanomedicine: Nanotechnology, Biology and Medicine, 7(3), pp.315-323.

18. Bedu-Addo, F.K. and Huang, L., 1995. Interaction of PEG-phospholipid conjugates with phospholipid: implications in liposomal drug delivery. Advanced drug delivery reviews, 16(2-3), pp.235-247.
19. Beebe, D.J., Mensing, G.A. and Walker, G.M., 2002. Physics and applications of microfluidics in biology. Annual review of biomedical engineering, 4(1), pp.261-286.
20. Bell, C.C., Hendriks, D.F., Moro, S.M., Ellis, E., Walsh, J., Renblom, A., Puigvert, L.F., Dankers, A.C., Jacobs, F., Snoeys, J. and Sison-Young, R.L., 2016. Characterization of primary human hepatocyte spheroids as a model system for drug-induced liver injury, liver function and disease. *Scientific reports*, *6*, p.25187.
21. Belletti, D., Tosi, G., Forni, F., Lagreca, I., Barozzi, P., Pederzoli, F., Vandelli, M.A., Riva, G., Luppi, M. and Ruozi, B., 2016. PEGylated siRNA lipoplexes for silencing of BLIMP-1 in primary effusion lymphoma: *in vitro* evidences of antitumoral activity. European Journal of Pharmaceutics and Biopharmaceutics, 99, pp.7-17.
22. Belliveau, N.M., Huft, J., Lin, P.J., Chen, S., Leung, A.K., Leaver, T.J., Wild, A.W., Lee, J.B., Taylor, R.J., Tam, Y.K. and Hansen, C.L., 2012. Microfluidic synthesis of highly potent limit-size lipid nanoparticles for *in vivo* delivery of siRNA. Molecular Therapy-Nucleic Acids, 1, p.e37.
23. Bergstrom, S., 1992. The HBV model-its structure and applications.
24. Bersini, S., Jeon, J.S., Dubini, G., Arrigoni, C., Chung, S., Charest, J.L., Moretti, M. and Kamm, R.D., 2014. A microfluidic 3D *in vitro* model for specificity of breast cancer metastasis to bone. Biomaterials, 35(8), pp.2454-2461.
25. Bertrand, N., Wu, J., Xu, X., Kamaly, N. and Farokhzad, O.C., 2014. Cancer nanotechnology: the impact of passive and active targeting in the era of modern cancer biology. Advanced drug delivery reviews, 66, pp.2-25.
26. Blaese, R.M., Culver, K.W., Miller, A.D., Carter, C.S., Fleisher, T., Clerici, M., Shearer, G., Chang, L., Chiang, Y., Tolstoshev, P. and Greenblatt, J.J., 1995. T lymphocyte-directed gene therapy for ADA− SCID: initial trial results after 4 years. Science, 270(5235), pp.475-480.
27. Blanco, E., Shen, H. and Ferrari, M., 2015. Principles of nanoparticle design for overcoming biological barriers to drug delivery. Nature biotechnology, 33(9), p.941.

28. Bordet, T. and Behar-Cohen, F., 2019. Ocular gene therapies in clinical practice: Viral vectors and nonviral alternatives. Drug discovery today.
29. Bozzuto, G. and Molinari, A., 2015. Liposomes as nanomedical devices. International journal of nanomedicine, 10, p.975.
30. Braxton, S.M., Incyte Corp, 1998. Cysteine-pegylated proteins. U.S. Patent 5,766,897.
31. Bray, F., Ferlay, J., Soerjomataram, I., Siegel, R.L., Torre, L.A. and Jemal, A., 2018. Global cancer statistics 2018: GLOBOCAN estimates of incidence and mortality worldwide for 36 cancers in 185 countries. CA: a cancer journal for clinicians, 68(6), pp.394-424.
32. Broomhead, D.S. and Ryrie, S.C., 1988. Particle paths in wavy vortices. Nonlinearity, 1(3), p.409.
33. Buñuales, M., Düzgüneş, N., Zalba, S., Garrido, M.J. and Tros de ILarduya, C., 2011. Efficient gene delivery by EGF-lipoplexes *in vitro* and *in vivo*. Nanomedicine, 6(1), pp.89-98.
34. Cai, R.Q., Liu, D.Z., Cui, H., Cheng, Y., Liu, M., Zhang, B.L., Mei, Q.B. and Zhou, S.Y., 2017. Charge reversible calcium phosphate lipid hybrid nanoparticle for siRNA delivery. Oncotarget, 8(26), p.42772.
35. Campos-Martorell, M., Cano-Sarabia, M., Simats, A., Hernández-Guillamon, M., Rosell, A., Maspoch, D. and Montaner, J., 2016. Charge effect of a liposomal delivery system encapsulating simvastatin to treat experimental ischemic stroke in rats. International journal of nanomedicine, 11, p.3035.
36. Cao, F., Ju, X., Chen, D., Jiang, L., Zhu, X., Qing, S., Fang, F., Shen, Y., Jia, Z. and Zhang, H., 2017. Phosphorothioate-modified antisense oligonucleotides against human telomerase reverse transcriptase sensitize cancer cells to radiotherapy. Molecular medicine reports, 16(2), pp.2089-2094.
37. Cao, Z., Zhang, L. and Jiang, S., 2012. Superhydrophilic zwitterionic polymers stabilize liposomes. Langmuir, 28(31), pp.11625-11632.
38. Carugo, D., Bottaro, E., Owen, J., Stride, E. and Nastruzzi, C., 2016. Liposome production by microfluidics: potential and limiting factors. Scientific reports, 6, p.25876.
39. Cavalli, G. and Heard, E., 2019. Advances in epigenetics link genetics to the environment and disease. Nature, 571(7766), pp.489-499.

40. Chang, R.S., Suh, M.S., Kim, S., Shim, G., Lee, S., Han, S.S., Lee, K.E., Jeon, H., Choi, H.G., Choi, Y. and Kim, C.W., 2011. Cationic drug-derived nanoparticles for multifunctional delivery of anticancer siRNA. Biomaterials, 32(36), pp.9785-9795.
41. Chen, G., Li, D., Jin, Y., Zhang, W., Teng, L., Bunt, C. and Wen, J., 2014. Deformable liposomes by reverse-phase evaporation method for an enhanced skin delivery of (+)-catechin. Drug development and industrial pharmacy, 40(2), pp.260-265.
42. Cheng, Y., Liu, M., Hu, H., Liu, D. and Zhou, S., 2016. Development, optimization, and characterization of PEGylated nanoemulsion of prostaglandin E1 for long circulation. AAPS PharmSciTech, 17(2), pp.409-417.
43. Cieślak, A., Wauthoz, N., Orellana, A.N., Lautram, N., Béjaud, J., Hureaux, J., Lafleur, M., Benoit, J.P., Salomon, C.J. and Bastiat, G., 2017. Stealth nanocarriers based sterosomes using PEG post-insertion process. European journal of pharmaceutics and biopharmaceutics, 115, pp.31-38.
44. Collier, M.A., Bachelder, E.M. and Ainslie, K.M., 2017. Electrosprayed myocet-like liposomes: an alternative to traditional liposome production. Pharmaceutical research, 34(2), pp.419-426.
45. Colombo, S., Beck-Broichsitter, M., Bøtker, J.P., Malmsten, M., Rantanen, J. and Bohr, A., 2018. Transforming nanomedicine manufacturing toward Quality by Design and microfluidics. Advanced drug delivery reviews, 128, pp.115-131.
46. Cornelis, S., Vandenbranden, M., Ruysschaert, J.M. and Elouahabi, A., 2002. Role of intracellular cationic liposome–DNA complex dissociation in transfection mediated by cationic lipids. DNA and cell biology, 21(2), pp.91-97.
47. Cui, P. and Wang, S., 2019. Application of microfluidic chip technology in pharmaceutical analysis: A review. Journal of Pharmaceutical Analysis, 9(4), pp.238-247.
48. Cui, X., Hartanto, Y. and Zhang, H., 2017. Advances in multicellular spheroids formation. Journal of The Royal Society Interface, 14(127), p.20160877.
49. Cuomo, F., Ceglie, A. and Lopez, F., 2012. Specific interactions between nucleolipid doped liposomes and DNA allow a more efficient polynucleotide condensation. Journal of colloid and interface science, 365(1), pp.184-190.

50. Dai, W.J., Zhu, L.Y., Yan, Z.Y., Xu, Y., Wang, Q.L. and Lu, X.J., 2016. CRISPR-Cas9 for *in vivo* gene therapy: promise and hurdles. Molecular Therapy-Nucleic Acids, 5, p.e349.

51. Danafar, H., Rostamizadeh, K., Davaran, S. and Hamidi, M., 2017. Drug-conjugated PLA–PEG–PLA copolymers: a novel approach for controlled delivery of hydrophilic drugs by micelle formation. Pharmaceutical development and technology, 22(8), pp.947-957.

52. Day, D.A. and Tuite, M.F., 1998. Post-transcriptional gene regulatory mechanisms in eukaryotes: an overview. The Journal of endocrinology, 157(3), pp.361-371.

53. de la Torre, L.G., Rosada, R.S., Trombone, A.P.F., Frantz, F.G., Coelho-Castelo, A.A., Silva, C.L. and Santana, M.H.A., 2009. The synergy between structural stability and DNA-binding controls the antibody production in EPC/DOTAP/DOPE liposomes and DOTAP/DOPE lipoplexes. Colloids and surfaces B: Biointerfaces, 73(2), pp.175-184.

54. Decuzzi, P. and Ferrari, M., 2008. Design maps for nanoparticles targeting the diseased microvasculature. Biomaterials, 29(3), pp.377-384.

55. Degors, I.M., Wang, C., Rehman, Z.U. and Zuhorn, I.S., 2019. Carriers break barriers in drug delivery: endocytosis and endosomal escape of gene delivery vectors. Accounts of chemical research, 52(7), pp.1750-1760.

56. Dertinger, S.K., Chiu, D.T., Jeon, N.L. and Whitesides, G.M., 2001. Generation of gradients having complex shapes using microfluidic networks. Analytical Chemistry, 73(6), pp.1240-1246.

57. Desigaux, L., Sainlos, M., Lambert, O., Chevre, R., Letrou-Bonneval, E., Vigneron, J.P., Lehn, P., Lehn, J.M. and Pitard, B., 2007. Self-assembled lamellar complexes of siRNA with lipidic aminoglycoside derivatives promote efficient siRNA delivery and interference. Proceedings of the National Academy of Sciences, 104(42), pp.16534-16539.

58. Didiot, M.C., Hall, L.M., Coles, A.H., Haraszti, R.A., Godinho, B.M., Chase, K., Sapp, E., Ly, S., Alterman, J.F., Hassler, M.R. and Echeverria, D., 2016. Exosome-mediated delivery of hydrophobically modified siRNA for huntingtin mRNA silencing. Molecular Therapy, 24(10), pp.1836-1847.

59. Dimov, N., Kastner, E., Hussain, M., Perrie, Y. and Szita, N., 2017. Formation and purification of tailored liposomes for drug delivery using a module-based micro continuous-flow system. Scientific reports, 7(1), pp.1-13.

60. Ditto, A.J., Shah, P.N. and Yun, Y.H., 2009. Non-viral gene delivery using nanoparticles. Expert opinion on drug delivery, 6(11), pp.1149-1160.

61. Dowaidar, M., Abdelhamid, H.N., Hällbrink, M., Freimann, K., Kurrikoff, K., Zou, X. and Langel, Ü., 2017. Magnetic nanoparticle assisted self-assembly of cell penetrating peptides-oligonucleotides complexes for gene delivery. Scientific reports, 7(1), pp.1-11.

62. Duval, K., Grover, H., Han, L.H., Mou, Y., Pegoraro, A.F., Fredberg, J. and Chen, Z., 2017. Modeling physiological events in 2D vs. 3D cell culture. Physiology, 32(4), pp.266-277.

63. Egelhaaf, S.U., Wehrli, E., Müller, M., Adrian, M. and Schurtenberger, P., 1996. Determination of the size distribution of lecithin liposomes: a comparative study using freeze fracture, cryoelectron microscopy and dynamic light scattering. Journal of microscopy, 184(3), pp.214-228.

64. Elbashir, S.M., Harborth, J., Lendeckel, W., Yalcin, A., Weber, K. and Tuschl, T., 2001. Duplexes of 21-nucleotide RNAs mediate RNA interference in cultured mammalian cells. nature, 411(6836), pp.494-498.

65. Eş, I., Ok, M.T., Puentes-Martinez, X.E., de Toledo, M.A.S., de Pinho Favaro, M.T., Cavalcanti, L.P., Cassago, A., Portugal, R.V., Azzoni, A.R. and de la Torre, L.G., 2018. Evaluation of siRNA and cationic liposomes complexes as a model for *in vitro* siRNA delivery to cancer cells. Colloids and Surfaces A: Physicochemical and Engineering Aspects, 555, pp.280-289.

66. Evans, D.F. and Wennerstrom, H., 1999. Colloidal domain. Wiley-Vch.

67. Farokhzad, O.C., Khademhosseini, A., Jon, S., Hermmann, A., Cheng, J., Chin, C., Kiselyuk, A., Teply, B., Eng, G. and Langer, R., 2005. Microfluidic system for studying the interaction of nanoparticles and microparticles with cells. Analytical chemistry, 77(17), pp.5453-5459.

68. Fennema, E., Rivron, N., Rouwkema, J., van Blitterswijk, C. and de Boer, J., 2013. Spheroid culture as a tool for creating 3D complex tissues. Trends in biotechnology, 31(2), pp.108-115.

69. Fernández, M., Javaid, F. and Chudasama, V., 2018. Advances in targeting the folate receptor in the treatment/imaging of cancers. Chemical science, 9(4), pp.790-810.

70. Ferrari, M.E., Rusalov, D., Enas, J. and Wheeler, C.J., 2001. Trends in lipoplex physical properties dependent on cationic lipid structure, vehicle and complexation procedure do not correlate with biological activity. Nucleic acids research, 29(7), pp.1539-1548.

71. Fire, A., Xu, S., Montgomery, M.K., Kostas, S.A., Driver, S.E. and Mello, C.C., 1998. Potent and specific genetic interference by double-stranded RNA in Caenorhabditis elegans. Nature, 391(6669), pp.806-811.

72. Foged, C., Nielsen, H.M. and Frokjaer, S., 2007. Liposomes for phospholipase A2 triggered siRNA release: preparation and *in vitro* test. International journal of pharmaceutics, 331(2), pp.160-166.

73. Foster, R.T., Caillé, G., Ngoc, A.H., Lemko, C.H., Kherani, R. and Pasutto, F.M., 1994. Pharmacokinetics of zopiclone enantiomers in humans following oral dose administration of racemate. Pharm Res, 11, p.402.

74. Freedman, B.S., Brooks, C.R., Lam, A.Q., Fu, H., Morizane, R., Agrawal, V., Saad, A.F., Li, M.K., Hughes, M.R., Vander Werff, R. and Peters, D.T., 2015. Modelling kidney disease with CRISPR-mutant kidney organoids derived from human pluripotent epiblast spheroids. Nature communications, 6, p.8715.

75. Friedmann, T. and Roblin, R., 1972. Gene therapy for human genetic disease?. Science, 175(4025), pp.949-955.

76. Fröhlich, E., 2012. The role of surface charge in cellular uptake and cytotoxicity of medical nanoparticles. International journal of nanomedicine, 7, p.5577.

77. Fromen, C.A., Rahhal, T.B., Robbins, G.R., Kai, M.P., Shen, T.W., Luft, J.C. and DeSimone, J.M., 2016. Nanoparticle surface charge impacts distribution, uptake and lymph node trafficking by pulmonary antigen-presenting cells. Nanomedicine: Nanotechnology, Biology and Medicine, 12(3), pp.677-687.

78. Gary, D.J., Puri, N. and Won, Y.Y., 2007. Polymer-based siRNA delivery: perspectives on the fundamental and phenomenological distinctions from polymer-based DNA delivery. Journal of Controlled Release, 121(1-2), pp.64-73.

79. Gasperini, A.A., Puentes-Martinez, X.E., Balbino, T.A., de Paula Rigoletto, T., de Sá Cavalcanti Corrêa, G., Cassago, A., Portugal, R.V., de La Torre, L.G. and Cavalcanti, L.P.,

2015. Association between cationic liposomes and low molecular weight hyaluronic acid. Langmuir, 31(11), pp.3308-3317.

80. Geusens, B., Lambert, J., De Smedt, S.C., Buyens, K., Sanders, N.N. and Van Gele, M., 2009. Ultradeformable cationic liposomes for delivery of small interfering RNA (siRNA) into human primary melanocytes. Journal of controlled release, 133(3), pp.214-220.
81. Ghanbarzadeh, S., Valizadeh, H. and Zakeri-Milani, P., 2013. Application of response surface methodology in development of sirolimus liposomes prepared by thin film hydration technique. BioImpacts: BI, 3(2), p.75.
82. Ginn, S.L., Alexander, I.E., Edelstein, M.L., Abedi, M.R. and Wixon, J., 2013. Gene therapy clinical trials worldwide to 2012–an update. The journal of gene medicine, 15(2), pp.65-77.
83. Gjetting, T., Arildsen, N.S., Christensen, C.L., Poulsen, T.T., Roth, J.A., Handlos, V.N. and Poulsen, H.S., 2010. *In vitro* and *in vivo* effects of polyethylene glycol (PEG)-modified lipid in DOTAP/cholesterol-mediated gene transfection. International journal of nanomedicine, 5, p.371.
84. Gomez, F.A. ed., 2008. Biological applications of microfluidics. John Wiley & Sons.
85. Gregoriadis, G. and Perrie, Y., 2010. Liposomes in Nanomedicine. Wiley.
86. Grimaldi, N., Andrade, F., Segovia, N., Ferrer-Tasies, L., Sala, S., Veciana, J. and Ventosa, N., 2016. Lipid-based nanovesicles for nanomedicine. Chemical Society Reviews, 45(23), pp.6520-6545.
87. Guckenberger, D.J., de Groot, T.E., Wan, A.M., Beebe, D.J. and Young, E.W., 2015. Micromilling: a method for ultra-rapid prototyping of plastic microfluidic devices. Lab on a Chip, 15(11), pp.2364-2378.
88. Guidolin, K. and Zheng, G., 2019. Nanomedicines Lost in Translation. ACS nano.
89. Gupta, P., Pérez-Mancera, P.A., Kocher, H., Nisbet, A., Schettino, G. and Velliou, E.G., 2020. A Novel Scaffold-Based Hybrid Multicellular Model for Pancreatic Ductal Adenocarcinoma—Toward a Better Mimicry of the *in vivo* Tumor Microenvironment. Frontiers in Bioengineering and Biotechnology, 8, p.290.

90. Halldorsson, S., Lucumi, E., Gómez-Sjöberg, R. and Fleming, R.M., 2015. Advantages and challenges of microfluidic cell culture in polydimethylsiloxane devices. Biosensors and Bioelectronics, 63, pp.218-231.
91. Hannon, G.J., 2002. RNA interference. Nature, 418(6894), pp.244-251.
92. Hansen, C. and Quake, S.R., 2003. Microfluidics in structural biology: smaller, faster… better. Current opinion in structural biology, 13(5), pp.538-544.
93. Harris, S.S. and Giorgio, T.D., 2005. Convective flow increases lipoplex delivery rate to *in vitro* cellular monolayers. Gene therapy, 12(6), pp.512-520.
94. Hatakeyama, H., Akita, H. and Harashima, H., 2011. A multifunctional envelope type nano device (MEND) for gene delivery to tumours based on the EPR effect: a strategy for overcoming the PEG dilemma. Advanced drug delivery reviews, 63(3), pp.152-160.
95. Hattori, Y., Nakamura, M., Takeuchi, N., Tamaki, K., Shimizu, S., Yoshiike, Y., Taguchi, M., Ohno, H., Ozaki, K.I. and Onishi, H., 2019. Effect of cationic lipid in cationic liposomes on siRNA delivery into the lung by intravenous injection of cationic lipoplex. Journal of drug targeting, 27(2), pp.217-227.
96. He, Z.Y., Zheng, X., Wu, X.H., Song, X.R., He, G., Wu, W.F., Yu, S., Mao, S.J. and Wei, Y.Q., 2010. Development of glycyrrhetinic acid-modified stealth cationic liposomes for gene delivery. International journal of pharmaceutics, 397(1-2), pp.147-154.
97. Herweijer, H. and Wolff, J.A., 2003. Progress and prospects: naked DNA gene transfer and therapy. Gene therapy, 10(6), pp.453-458.
98. Heuts, J., Varypataki, E.M., van der Maaden, K., Romeijn, S., Drijfhout, J.W., van Scheltinga, A.T., Ossendorp, F. and Jiskoot, W., 2018. Cationic liposomes: A flexible vaccine delivery system for physicochemically diverse antigenic peptides. Pharmaceutical research, 35(11), p.207.
99. Hoffman, A. (2017). Acta Biomaterialia Gold Medal lecture: "PEG and PEGylation, Then and Now—A Historical Commentary and Review", Acta Biomaterialia Medal plenary session, Society For Biomaterials (SFB) Annual Meeting & Exposition, Minneapolis, USA.
100. Honigmann, A. and Pralle, A., 2016. Compartmentalization of the cell membrane. Journal of molecular biology, 428(24), pp.4739-4748.

101. Hood, R.R. and DeVoe, D.L., 2015. High-Throughput Continuous Flow Production of Nanoscale Liposomes by Microfluidic Vertical Flow Focusing. small, 11(43), pp.5790-5799.

102. Hood, R.R., Shao, C., Omiatek, D.M., Vreeland, W.N. and DeVoe, D.L., 2013. Microfluidic synthesis of PEG-and folate-conjugated liposomes for one-step formation of targeted stealth nanocarriers. Pharmaceutical research, 30(6), pp.1597-1607.

103. Hookway, T.A., Butts, J.C., Lee, E., Tang, H. and McDevitt, T.C., 2016. Aggregate formation and suspension culture of human pluripotent stem cells and differentiated progeny. Methods, 101, pp.11-20.

104. Hristova, K. and Needham, D., 1995. Phase behavior of a lipid/polymer-lipid mixture in aqueous medium. Macromolecules, 28(4), pp.991-1002.

105. Hristova, K., Kenworthy, A. and McIntosh, T.J., 1995. Effect of bilayer composition on the phase behavior of liposomal suspensions containing poly (ethylene glycol)-lipids. Macromolecules, 28(23), pp.7693-7699.

106. Hu, F.Q., Zhang, Y.Y., You, J., Yuan, H. and Du, Y.Z., 2012. pH triggered doxorubicin delivery of PEGylated glycolipid conjugate micelles for tumor targeting therapy. Molecular pharmaceutics, 9(9), pp.2469-2478.

107. Hu, Q., Sun, W., Wang, C. and Gu, Z., 2016. Recent advances of cocktail chemotherapy by combination drug delivery systems. Advanced drug delivery reviews, 98, pp.19-34.

108. Huang, C., Quinn, D., Sadovsky, Y., Suresh, S. and Hsia, K.J., 2017. Formation and size distribution of self-assembled vesicles. Proceedings of the National Academy of Sciences, 114(11), pp.2910-2915.

109. Immordino, M.L., Dosio, F. and Cattel, L., 2006. Stealth liposomes: review of the basic science, rationale, and clinical applications, existing and potential. International journal of nanomedicine, 1(3), p.297.

110. Ismagilov, R.F., Stroock, A.D., Kenis, P.J., Whitesides, G. and Stone, H.A., 2000. Experimental and theoretical scaling laws for transverse diffusive broadening in two-phase laminar flows in microchannels. Applied Physics Letters, 76(17), pp.2376-2378.

111. Jaafar-Maalej, C., Diab, R., Andrieu, V., Elaissari, A. and Fessi, H., 2010. Ethanol injection method for hydrophilic and lipophilic drug-loaded liposome preparation. Journal of liposome research, 20(3), pp.228-243.

112. Jahn, A., Reiner, J.E., Vreeland, W.N., DeVoe, D.L., Locascio, L.E. and Gaitan, M., 2008. Preparation of nanoparticles by continuous-flow microfluidics. Journal of Nanoparticle Research, 10(6), pp.925-934.

113. Jahn, A., Vreeland, W.N., DeVoe, D.L., Locascio, L.E. and Gaitan, M., 2007. Microfluidic directed formation of liposomes of controlled size. Langmuir, 23(11), pp.6289-6293.

114. Jeffs, L.B., Palmer, L.R., Ambegia, E.G., Giesbrecht, C., Ewanick, S. and MacLachlan, I., 2005. A scalable, extrusion-free method for efficient liposomal encapsulation of plasmid DNA. Pharmaceutical research, 22(3), pp.362-372.

115. Jiang, W., Kim, B.Y., Rutka, J.T. and Chan, W.C., 2008. Nanoparticle-mediated cellular response is size-dependent. Nature nanotechnology, 3(3), pp.145-150.

116. Joanicot, M. and Ajdari, A., 2005. Droplet control for microfluidics. *Science*, *309*(5736), pp.887-888.

117. Johnson, B.K. and Prud'homme, R.K., 2003. Mechanism for rapid self-assembly of block copolymer nanoparticles. Physical review letters, 91(11), p.118302.

118. Kamei, K.I., 2013. Cutting-edge microfabricated biomedical tools for human pluripotent stem cell research. Journal of laboratory automation, 18(6), pp.469-481.

119. Karnik, R., Gu, F., Basto, P., Cannizzaro, C., Dean, L., Kyei-Manu, W., Langer, R. and Farokhzad, O.C., 2008. Microfluidic platform for controlled synthesis of polymeric nanoparticles. Nano letters, 8(9), pp.2906-2912.

120. Kastner, E., Kaur, R., Lowry, D., Moghaddam, B., Wilkinson, A. and Perrie, Y., 2014. High-throughput manufacturing of size-tuned liposomes by a new microfluidics method using enhanced statistical tools for characterization. International journal of pharmaceutics, 477(1-2), pp.361-368.

121. Kelm, J.M., Timmins, N.E., Brown, C.J., Fussenegger, M. and Nielsen, L.K., 2003. Method for generation of homogeneous multicellular tumor spheroids applicable to a wide variety of cell types. Biotechnology and bioengineering, 83(2), pp.173-180.

122. Kesharwani, P., Gajbhiye, V. and Jain, N.K., 2012. A review of nanocarriers for the delivery of small interfering RNA. Biomaterials, 33(29), pp.7138-7150.

123. Khadke, S., Roces, C.B., Cameron, A., Devitt, A. and Perrie, Y., 2019. Formulation and manufacturing of lymphatic targeting liposomes using microfluidics. Journal of Controlled Release, 307, pp.211-220.

124. Kijanska, M. and Kelm, J., 2016. *In vitro* 3D spheroids and microtissues: ATP-based cell viability and toxicity assays. In Assay Guidance Manual [Internet]. Eli Lilly & Company and the National Center for Advancing Translational Sciences.

125. Kim, C.K. and Park, D.K., 1987. Stability and drug release properties of liposomes containing cytarabine as a drug carrier. Archives of Pharmacal Research, 10(2), pp.75-79.

126. Kinney, M.A., Hookway, T.A., Wang, Y. and McDevitt, T.C., 2014. Engineering three-dimensional stem cell morphogenesis for the development of tissue models and scalable regenerative therapeutics. Annals of biomedical engineering, 42(2), pp.352-367.

127. Klymenko, Y., Kim, O., Loughran, E., Yang, J., Lombard, R., Alber, M. and Stack, M.S., 2017. Cadherin composition and multicellular aggregate invasion in organotypic models of epithelial ovarian cancer intraperitoneal metastasis. Oncogene, 36(42), pp.5840-5851.

128. Koltover, I., Rädler, J.O., Salditt, T. and Safinya, C.R., 1998. The inverted hexagonal phase of DNA-cationic liposome complexes: Structure to gene release mechanism correlations. Science, 281, p.78.

129. Koltover, I., Salditt, T., Rädler, J.O. and Safinya, C.R., 1998. An inverted hexagonal phase of cationic liposome-DNA complexes related to DNA release and delivery. Science, 281(5373), pp.78-81.

130. Kuntsche, J., Horst, J.C. and Bunjes, H., 2011. Cryogenic transmission electron microscopy (cryo-TEM) for studying the morphology of colloidal drug delivery systems. International journal of pharmaceutics, 417(1-2), pp.120-137.

131. Lam, S.S.N., Ip, C.K.M., Mak, A.S.C. and Wong, A.S.T., 2016. A novel p70 S6 kinase-microRNA biogenesis axis mediates multicellular spheroid formation in ovarian cancer progression. Oncotarget, 7(25), p.38064.

132. Laschke, M.W. and Menger, M.D., 2017. Life is 3D: boosting spheroid function for tissue engineering. Trends in biotechnology, 35(2), pp.133-144.

133. Lee, G., Lee, J., Oh, H. and Lee, S., 2016. Reproducible construction of surface tension-mediated honeycomb concave microwell arrays for engineering of 3D microtissues with minimal cell loss. PloS one, 11(8).

134. Lee, J., Kim, J., Kim, H., Bae, Y.M., Lee, K.H. and Cho, H.J., 2013. Effect of thermal treatment on the chemical resistance of polydimethylsiloxane for microfluidic devices. Journal of Micromechanics and Microengineering, 23(3), p.035007.

135. Leung, A.K., Hafez, I.M., Baoukina, S., Belliveau, N.M., Zhigaltsev, I.V., Afshinmanesh, E., Tieleman, D.P., Hansen, C.L., Hope, M.J. and Cullis, P.R., 2012. Lipid nanoparticles containing siRNA synthesized by microfluidic mixing exhibit an electron-dense nanostructured core. The Journal of Physical Chemistry C, 116(34), pp.18440-18450.

136. Li, C. and Samulski, R.J., 2020. Engineering adeno-associated virus vectors for gene therapy. Nature Reviews Genetics, pp.1-18.

137. Li, J., Chen, Q., Zha, Z., Li, H., Toh, K., Dirisala, A., Matsumoto, Y., Osada, K., Kataoka, K. and Ge, Z., 2015. Ternary polyplex micelles with PEG shells and intermediate barrier to complexed DNA cores for efficient systemic gene delivery. Journal of Controlled Release, 209, pp.77-87.

138. Li, J., Chen, Y.C., Tseng, Y.C., Mozumdar, S. and Huang, L., 2010. Biodegradable calcium phosphate nanoparticle with lipid coating for systemic siRNA delivery. Journal of controlled release, 142(3), pp.416-421.

139. Li, M., Xie, H., Liu, Y., Xia, C., Cun, X., Long, Y., Chen, X., Deng, M., Guo, R., Zhang, Z. and He, Q., 2019. Knockdown of hypoxia-inducible factor-1 alpha by tumor targeted delivery of CRISPR/Cas9 system suppressed the metastasis of pancreatic cancer. Journal of Controlled Release, 304, pp.204-215.

140. Lin, B., Miao, Y., Wang, J., Fan, Z., Du, L., Su, Y., Liu, B., Hu, Z. and Xing, M., 2016. Surface tension guided hanging-drop: producing controllable 3D spheroid of high-passaged human dermal papilla cells and forming inductive microtissues for hair-follicle regeneration. ACS applied materials & interfaces, 8(9), pp.5906-5916.

141. Lodish, H., Baltimore, D., Berk, A., Zipursky, S.L., Matsudaira, P. and Darnell, J., 1995. Molecular cell biology (Vol. 3). New York: Scientific American Books.

142. Lovchik, R.D., Wolf, H. and Delamarche, E., 2011. High-grade optical polydimethylsiloxane for microfluidic applications. Biomedical microdevices, 13(6), pp.1027-1032.
143. Lu, P. Y., Woodle, M. C. In: Fire, A., Nirenberg, M., (Ed.), 2005. RNA interference technology: From basic science to drug development. Cambridge University Press, p. 303-305, 2005.
144. Lundstrom, K., 2015. gene therapy with emphasis on RNA interference.
145. Luo, D. and Saltzman, W.M., 2000. Synthetic DNA delivery systems. Nature biotechnology, 18(1), pp.33-37.
146. Ma, J., Jiang, L., Pan, X., Ma, H., Lin, B. and Qin, J., 2010. A simple photolithography method for microfluidic device fabrication using sunlight as UV source. Microfluidics and nanofluidics, 9(6), pp.1247-1252.
147. Majzoub, R.N., Ewert, K.K. and Safinya, C.R., 2016. Cationic liposome–nucleic acid nanoparticle assemblies with applications in gene delivery and gene silencing. Philosophical Transactions of the Royal Society A: Mathematical, Physical and Engineering Sciences, 374(2072), p.20150129.
148. Manikandan, C., Kaushik, A. and Sen, D., 2019. Viral vector: potential therapeutic for glioblastoma multiforme. Cancer Gene Therapy, pp.1-10.
149. Manz, A., Graber, N. and Widmer, H.Á., 1990. Miniaturized total chemical analysis systems: a novel concept for chemical sensing. Sensors and actuators B: Chemical, 1(1-6), pp.244-248.
150. Marwah, M., Perrie, Y., Badhan, R.K.S. and Lowry, D., 2019. Intracellular uptake of EGCG-loaded deformable controlled release liposomes for skin cancer. Journal of liposome research, pp.1-14.
151. McDonald, J.C., Duffy, D.C., Anderson, J.R., Chiu, D.T., Wu, H., Schueller, O.J. and Whitesides, G.M., 2000. Fabrication of microfluidic systems in poly (dimethylsiloxane). ELECTROPHORESIS: An International Journal, 21(1), pp.27-40.
152. McManus, M.T. and Sharp, P.A., 2002. Gene silencing in mammals by small interfering RNAs. Nature reviews genetics, 3(10), pp.737-747.
153. Mehling, M. and Tay, S., 2014. Microfluidic cell culture. Current opinion in Biotechnology, 25, pp.95-102.

154. Milla, P., Dosio, F. and Cattel, L., 2012. PEGylation of proteins and liposomes: a powerful and flexible strategy to improve the drug delivery. Current drug metabolism, 13(1), pp.105-119.

155. Mineart, K.P., Venkataraman, S., Yang, Y.Y., Hedrick, J.L. and Prabhu, V.M., 2018. Fabrication and characterization of hybrid stealth liposomes. Macromolecules, 51(8), pp.3184-3192.

156. Mingozzi, F. and High, K.A., 2011. Therapeutic *in vivo* gene transfer for genetic disease using AAV: progress and challenges. Nature reviews genetics, 12(5), pp.341-355.

157. Miri, A.K., Nieto, D., Iglesias, L., Goodarzi Hosseinabadi, H., Maharjan, S., Ruiz-Esparza, G.U., Khoshakhlagh, P., Manbachi, A., Dokmeci, M.R., Chen, S. and Shin, S.R., 2018. Microfluidics-enabled multimaterial maskless stereolithographic bioprinting. Advanced Materials, 30(27), p.1800242.

158. Mui, B.L., Tam, Y.K., Jayaraman, M., Ansell, S.M., Du, X., Tam, Y.Y.C., Lin, P.J., Chen, S., Narayanannair, J.K., Rajeev, K.G. and Manoharan, M., 2013. Influence of polyethylene glycol lipid desorption rates on pharmacokinetics and pharmacodynamics of siRNA lipid nanoparticles. Molecular Therapy-Nucleic Acids, 2, p.e139.

159. Nag, O.K. and Awasthi, V., 2013. Surface engineering of liposomes for stealth behavior. Pharmaceutics, 5(4), pp.542-569.

160. Naldini, L., Trono, D. and Verma, I.M., 2016. Lentiviral vectors, two decades later. Science, 353(6304), pp.1101-1102.

161. Nathwani, A.C., Reiss, U.M., Tuddenham, E.G., Rosales, C., Chowdary, P., McIntosh, J., Della Peruta, M., Lheriteau, E., Patel, N., Raj, D. and Riddell, A., 2014. Long-term safety and efficacy of factor IX gene therapy in hemophilia B. New England Journal of Medicine, 371(21), pp.1994-2004.

162. Nyamay'Antu, A., Dumont, M., Kedinger, V. and Erbacher, P., 2019. Non-viral vector mediated gene delivery: the outsider to watch out for in gene therapy. Cell Gene Ther Insights, 5, pp.51-57.

163. Park, J.S., Yi, S.W., Kim, H.J. and Park, K.H., 2016. Receptor-mediated gene delivery into human mesenchymal stem cells using hyaluronic acid-shielded polyethylenimine/pDNA nanogels. Carbohydrate polymers, 136, pp.791-802.

164. Pasut, G., Paolino, D., Celia, C., Mero, A., Joseph, A.S., Wolfram, J., Cosco, D., Schiavon, O., Shen, H. and Fresta, M., 2015. Polyethylene glycol (PEG)-dendron phospholipids as innovative constructs for the preparation of super stealth liposomes for anticancer therapy. Journal of controlled release, 199, pp.106-113.

165. Patil, Y.P. and Jadhav, S., 2014. Novel methods for liposome preparation. Chemistry and physics of lipids, 177, pp.8-18.

166. Pessoa, A.C., Sipoli, C.C. and Lucimara, G., 2017. Effects of diffusion and mixing pattern on microfluidic-assisted synthesis of chitosan/ATP nanoparticles. Lab on a Chip, 17(13), pp.2281-2293.

167. Pluvinage, J.V. and Wyss-Coray, T., 2017. Microglial Barriers to Viral Gene Delivery. Neuron, 93(3), pp.468-470.

168. Pozzi, D., Colapicchioni, V., Caracciolo, G., Piovesana, S., Capriotti, A.L., Palchetti, S., De Grossi, S., Riccioli, A., Amenitsch, H. and Laganà, A., 2014. Effect of polyethyleneglycol (PEG) chain length on the bio–nano-interactions between PEGylated lipid nanoparticles and biological fluids: from nanostructure to uptake in cancer cells. Nanoscale, 6(5), pp.2782-2792.

169. Ramamoorth, M. and Narvekar, A., 2015. Non viral vectors in gene therapy-an overview. Journal of clinical and diagnostic research: JCDR, 9(1), p.GE01.

170. Ramezani, M., Khoshhamdam, M., Dehshahri, A. and Malaekeh-Nikouei, B., 2009. The influence of size, lipid composition and bilayer fluidity of cationic liposomes on the transfection efficiency of nanolipoplexes. Colloids and Surfaces B: Biointerfaces, 72(1), pp.1-5.

171. Raphael, B., Khalil, T., Workman, V.L., Smith, A., Brown, C.P., Streuli, C., Saiani, A. and Domingos, M., 2017. 3D cell bioprinting of self-assembling peptide-based hydrogels. Materials Letters, 190, pp.103-106.

172. Rideau, E., Dimova, R., Schwille, P., Wurm, F.R. and Landfester, K., 2018. Liposomes and polymersomes: a comparative review towards cell mimicking. Chemical Society Reviews, 47(23), pp.8572-8610.

173. Rodriguez, A.L., Wang, T.Y., Bruggeman, K.F., Li, R., Williams, R.J., Parish, C.L. and Nisbet, D.R., 2016. Tailoring minimalist self-assembling peptides for localized viral vector gene delivery. Nano research, 9(3), pp.674-684.

174. Rodríguez-Pulido, A., Ortega, F., Llorca, O., Aicart, E. and Junquera, E., 2008. A physicochemical characterization of the interaction between DC-Chol/DOPE cationic liposomes and DNA. The Journal of Physical Chemistry B, 112(39), pp.12555-12565.

175. Sackmann, E.K., Fulton, A.L. and Beebe, D.J., 2014. The present and future role of microfluidics in biomedical research. Nature, 507(7491), pp.181-189.

176. Safinya, C.R., Ewert, K.K., Majzoub, R.N. and Leal, C., 2014. Cationic liposome–nucleic acid complexes for gene delivery and gene silencing. New Journal of Chemistry, 38(11), pp.5164-5172.

177. Sala, M., Miladi, K., Agusti, G., Elaissari, A. and Fessi, H., 2017. Preparation of liposomes: A comparative study between the double solvent displacement and the conventional ethanol injection—From laboratory scale to large scale. Colloids and Surfaces A: Physicochemical and Engineering Aspects, 524, pp.71-78.

178. Sambrook, J., Westphal, H., Srinivasan, P.R. and Dulbecco, R., 1968. The integrated state of viral DNA in SV40-transformed cells. Proceedings of the National Academy of Sciences of the United States of America, 60(4), p.1288.

179. Scharner, J., Qi, S., Rigo, F., Bennett, C.F. and Krainer, A.R., 2019. Delivery of GalNAc-conjugated splice-switching ASOs to non-hepatic cells through ectopic expression of asialoglycoprotein receptor. Molecular Therapy-Nucleic Acids, 16, pp.313-325.

180. Scholz, C. and Wagner, E., 2012. Therapeutic plasmid DNA versus siRNA delivery: common and different tasks for synthetic carriers. Journal of controlled release, 161(2), pp.554-565.

181. Schooley, R.T., Spritzler, J., Wang, H., Lederman, M.M., Havlir, D., Kuritzkes, D.R., Pollard, R., Battaglia, C., Robertson, M., Mehrotra, D. and Casimiro, D., 2010. AIDS clinical trials group 5197: a placebo-controlled trial of immunization of HIV-1-infected persons with a replication-deficient adenovirus type 5 vaccine expressing the HIV-1 core protein. The Journal of infectious diseases, 202(5), pp.705-716.

182. Semple, S.C., Chonn, A. and Cullis, P.R., 1998. Interactions of liposomes and lipid-based carrier systems with blood proteins: Relation to clearance behaviour *in vivo*. Advanced drug delivery reviews, 32(1-2), pp.3-17.

183. Shaegh, S.A.M., Pourmand, A., Nabavinia, M., Avci, H., Tamayol, A., Mostafalu, P., Ghavifekr, H.B., Aghdam, E.N., Dokmeci, M.R., Khademhosseini, A. and Zhang, Y.S.,

2018. Rapid prototyping of whole-thermoplastic microfluidics with built-in microvalves using laser ablation and thermal fusion bonding. Sensors and Actuators B: Chemical, 255, pp.100-109.

184. Sharma, G., Goyal, H., Thakur, K., Raza, K. and Katare, O.P., 2016. Novel elastic membrane vesicles (EMVs) and ethosomes-mediated effective topical delivery of aceclofenac: a new therapeutic approach for pain and inflammation. Drug delivery, 23(8), pp.3135-3145.
185. Shin, H.S., Kim, H.J., Sim, S.J. and Jeon, N.L., 2009. Shear stress effect on transfection of neurons cultured in microfluidic devices. Journal of nanoscience and nanotechnology, 9(12), pp.7330-7335.
186. Simian, M. and Bissell, M.J., 2017. Organoids: a historical perspective of thinking in three dimensions. Journal of Cell Biology, 216(1), pp.31-40.
187. Sioud, M. and Sørensen, D.R., 2003. Cationic liposome-mediated delivery of siRNAs in adult mice. Biochemical and biophysical research communications, 312(4), pp.1220-1225.
188. Sivasankar, B., 2008. Engineering chemistry (pp. 145-150). New Delhi: Tata McGraw-Hill.
189. Song, C., Zhang, S., Zhou, Q., Shi, L., Du, L., Zhi, D., Zhao, Y., Zhen, Y. and Zhao, D., 2017. Bifunctional cationic solid lipid nanoparticles of β-NaYF 4: Yb, Er upconversion nanoparticles coated with a lipid for bioimaging and gene delivery. RSC advances, 7(43), pp.26633-26639.
190. Spagnou, S., Miller, A.D. and Keller, M., 2004. Lipidic carriers of siRNA: differences in the formulation, cellular uptake, and delivery with plasmid DNA. Biochemistry, 43(42), pp.13348-13356.
191. Sternberg, B., Sorgi, F.L. and Huang, L., 1994. New structures in complex formation between DNA and cationic liposomes visualized by freeze—fracture electron microscopy. FEBS letters, 356(2-3), pp.361-366.
192. Stroock, A.D., Dertinger, S.K., Ajdari, A., Mezić, I., Stone, H.A. and Whitesides, G.M., 2002. Chaotic mixer for microchannels. Science, 295(5555), pp.647-651.
193. Suh, Y.K. and Kang, S., 2010. A review on mixing in microfluidics. Micromachines, 1(3), pp.82-111.

194. Suk, J.S., Xu, Q., Kim, N., Hanes, J. and Ensign, L.M., 2016. PEGylation as a strategy for improving nanoparticle-based drug and gene delivery. Advanced drug delivery reviews, 99, pp.28-51.

195. Sultan, S., Siqueira, G., Zimmermann, T. and Mathew, A.P., 2017. 3D printing of nano-cellulosic biomaterials for medical applications. Current Opinion in Biomedical Engineering, 2, pp.29-34.

196. Swaan, L.M.B. and Swaan, P.W., 2007. Endocytic Mechanisms for Targeted Drug Delivery Lisa. Adv. Drug Deliv. Rev., 59, pp.748-758.

197. Terova, O., Soltys, S., Hermans, P., De Rooij, J. and Detmers, F., 2018. Overcoming downstream purification challenges for viral vector manufacturing: enabling advancement of gene therapies in the clinic. Cell. Gen. Ther. Ins, 4(2), pp.101-111.

198. Toledo, M.A., Janissen, R., Favaro, M.T., Cotta, M.A., Monteiro, G.A., Prazeres, D.M.F., Souza, A.P. and Azzoni, A.R., 2012. Development of a recombinant fusion protein based on the dynein light chain LC8 for non-viral gene delivery. Journal of controlled release, 159(2), pp.222-231.

199. Toniazzo, T., Galeskas, H., Dacanal, G.C. and Pinho, S.C., 2017. Production of cornstarch granules enriched with quercetin liposomes by aggregation of particulate binary mixtures using high shear process. Journal of food science, 82(11), pp.2626-2633.

200. Tóth, E.L., Holczer, E.G., Iván, K. and Fürjes, P., 2015. Optimized simulation and validation of particle advection in asymmetric staggered herringbone type micromixers. Micromachines, 6(1), pp.136-150.

201. Touzot, F., Moshous, D., Creidy, R., Neven, B., Frange, P., Cros, G., Caccavelli, L., Blondeau, J., Magnani, A., Luby, J.M. and Ternaux, B., 2015. Faster T-cell development following gene therapy compared with haploidentical HSCT in the treatment of SCID-X1. Blood, The Journal of the American Society of Hematology, 125(23), pp.3563-3569.

202. Trevisan, J.E., Cavalcanti, L.P., Oliveira, C.L., De La Torre, L.G. and Santana, M.H.A., 2011. Technological aspects of scalable processes for the production of functional liposomes for gene therapy. Non-viral gene therapy. Intech, pp.267-292.

203. Tsai, W.C. and Rizvi, S.S., 2016. Liposomal microencapsulation using the conventional methods and novel supercritical fluid processes. Trends in Food Science & Technology, 55, pp.61-71.

204. Tsuji, G., Sunami, T. and Ichihashi, N., 2018. Production of giant unilamellar vesicles by the water-in-oil emulsion-transfer method without high internal concentrations of sugars. Journal of bioscience and bioengineering, 126(4), pp.540-545.

205. Turajlic, S., Sottoriva, A., Graham, T. and Swanton, C., 2019. Resolving genetic heterogeneity in cancer. Nature Reviews Genetics, 20(7), pp.404-416.

206. Tuschl, T., 2001. RNA interference and small interfering RNAs. Chembiochem, 2(4), pp.239-245.

207. Valencia, P.M., Pridgen, E.M., Rhee, M., Langer, R., Farokhzad, O.C. and Karnik, R., 2013. Microfluidic platform for combinatorial synthesis and optimization of targeted nanoparticles for cancer therapy. ACS nano, 7(12), pp.10671-10680.

208. Viger-Gravel, J., Schantz, A., Pinon, A.C., Rossini, A.J., Schantz, S. and Emsley, L., 2018. Structure of lipid nanoparticles containing siRNA or mRNA by dynamic nuclear polarization-enhanced NMR spectroscopy. The Journal of Physical Chemistry B, 122(7), pp.2073-2081.

209. Vijayendran, R.A., Motsegood, K.M., Beebe, D.J. and Leckband, D.E., 2003. Evaluation of a three-dimensional micromixer in a surface-based biosensor. Langmuir, 19(5), pp.1824-1828.

210. Villate-Beitia, I., Puras, G., Soto-Sánchez, C., Agirre, M., Ojeda, E., Zarate, J., Fernández, E. and Pedraz, J.L., 2017. Non-viral vectors based on magnetoplexes, lipoplexes and polyplexes for VEGF gene delivery into central nervous system cells. International journal of pharmaceutics, 521(1-2), pp.130-140.

211. Vitor, M.T., Bergami-Santos, P.C., Zômpero, R.H.F., Cruz, K.S.P., Pinho, M.P., Barbuto, J.A.M. and de la Torre, L.G., 2017. Cationic liposomes produced via ethanol injection method for dendritic cell therapy. Journal of liposome research, 27(4), pp.249-263.

212. Wang, G., Zhu, Y., Chen, L. and Zhang, X., 2015. Photoinduced electron transfer (PET) based label-free aptasensor for platelet-derived growth factor-BB and its logic gate application. Biosensors and Bioelectronics, 63, pp.552-557.

213. Wang, H., Jiang, Y., Peng, H., Chen, Y., Zhu, P. and Huang, Y., 2015. Recent progress in microRNA delivery for cancer therapy by non-viral synthetic vectors. Advanced drug delivery reviews, 81, pp.142-160.

214. Wang, J., Cheng, Y., Yu, Y., Fu, F., Chen, Z., Zhao, Y. and Gu, Z., 2015. Microfluidic generation of porous microcarriers for three-dimensional cell culture. ACS applied materials & interfaces, 7(49), pp.27035-27039.

215. Weibel, D.B., DiLuzio, W.R. and Whitesides, G.M., 2007. Microfabrication meets microbiology. Nature Reviews Microbiology, 5(3), pp.209-218.

216. Weisman, S., Hirsch-Lerner, D., Barenholz, Y. and Talmon, Y., 2004. Nanostructure of cationic lipid-oligonucleotide complexes. Biophysical journal, 87(1), pp.609-614.

217. Whitehead, K.A., Langer, R. and Anderson, D.G., 2009. Knocking down barriers: advances in siRNA delivery. Nature reviews Drug discovery, 8(2), pp.129-138.

218. Whitesides, G.M., 2006. The origins and the future of microfluidics. Nature, 442(7101), pp.368-373.

219. Wolff, J.A., Malone, R.W., Williams, P., Chong, W., Acsadi, G., Jani, A. and Felgner, P.L., 1990. Direct gene transfer into mouse muscle *in vivo*. Science, 247(4949), pp.1465-1468.

220. Wong, C.H., Siah, K.W. and Lo, A.W., Estimation of clinical trial success rates and related parameters [published online January 31, 2018]. Biostatistics.

221. Woodle, M.C., 1995. Sterically stabilized liposome therapeutics. Advanced drug delivery reviews, 16(2-3), pp.249-265.

222. Xie, T. and Xu, C., 2017. Numerical and experimental investigations of chaotic mixing behavior in an oscillating feedback micromixer. Chemical engineering science, 171, pp.303-317.

223. Yager, P., Edwards, T., Fu, E., Helton, K., Nelson, K., Tam, M.R. and Weigl, B.H., 2006. Microfluidic diagnostic technologies for global public health. Nature, 442(7101), pp.412-418.

224. Yan, J., Berezhnoy, N.V., Korolev, N., Su, C.J. and Nordenskiöld, L., 2012. Structure and internal organization of overcharged cationic-lipid/peptide/DNA self-assembly complexes. Biochimica et Biophysica Acta (BBA)-Biomembranes, 1818(7), pp.1794-1800.

225. Yang, D.K. and Wu, S.T., 2014. Fundamentals of liquid crystal devices. John Wiley & Sons.

226. Yin, H. and Kanasty, R.L., 2014. A. a. Eltoukhy, AJ Vegas, JR Dorkin and DG Anderson. Nat. Rev. Genet, 15, pp.541-555.

227. Yin, H., Kanasty, R.L., Eltoukhy, A.A., Vegas, A.J., Dorkin, J.R. and Anderson, D.G., 2014. Non-viral vectors for gene-based therapy. Nature Reviews Genetics, 15(8), pp.541-555.

228. Zanoni, M., Piccinini, F., Arienti, C., Zamagni, A., Santi, S., Polico, R., Bevilacqua, A. and Tesei, A., 2016. 3D tumor spheroid models for *in vitro* therapeutic screening: a systematic approach to enhance the biological relevance of data obtained. Scientific reports, 6(1), pp.1-11.

229. Zhang, C., Xing, D. and Li, Y., 2007. Micropumps, microvalves, and micromixers within PCR microfluidic chips: Advances and trends. Biotechnology advances, 25(5), pp.483-514.

230. Zhang, H., Zhu, Y. and Shen, Y., 2018. Microfluidics for cancer nanomedicine: from fabrication to evaluation. Small, 14(28), p.1800360.

231. Zhang, Y., Li, H., Sun, J., Gao, J., Liu, W., Li, B., Guo, Y. and Chen, J., 2010. DC-Chol/DOPE cationic liposomes: a comparative study of the influence factors on plasmid pDNA and siRNA gene delivery. International journal of pharmaceutics, 390(2), pp.198-207.

232. Zhang, Y., Satterlee, A. and Huang, L., 2012. *In vivo* gene delivery by nonviral vectors: overcoming hurdles?. Molecular therapy, 20(7), pp.1298-1304.

233. Zhao, Y., Wang, W., Guo, S., Wang, Y., Miao, L., Xiong, Y. and Huang, L., 2016. PolyMetformin combines carrier and anticancer activities for *in vivo* siRNA delivery. Nature communications, 7(1), pp.1-9.

234. Zhdanov, D.D., Plyasova, A.A., Gladilina, Y.A., Pokrovsky, V.S., Grishin, D.V., Grachev, V.A., Orlova, V.S., Pokrovskaya, M.V., Alexandrova, S.S., Lobaeva, T.A. and Sokolov, N.N., 2019. Inhibition of telomerase activity by splice-switching oligonucleotides targeting the mRNA of the telomerase catalytic subunit affects proliferation of human CD4+ T lymphocytes. Biochemical and biophysical research communications, 509(3), pp.790-796.

235. Zhigaltsev, I.V., Belliveau, N., Hafez, I., Leung, A.K., Huft, J., Hansen, C. and Cullis, P.R., 2012. Bottom-up design and synthesis of limit size lipid nanoparticle systems with aqueous and triglyceride cores using millisecond microfluidic mixing. Langmuir, 28(7), pp.3633-3640.

236. Zook, J.M. and Vreeland, W.N., 2010. Effects of temperature, acyl chain length, and flow-rate ratio on liposome formation and size in a microfluidic hydrodynamic focusing device. Soft Matter, 6(6), pp.1352-1360.

ANNEX I

Supplementary Materials for Chapter 4

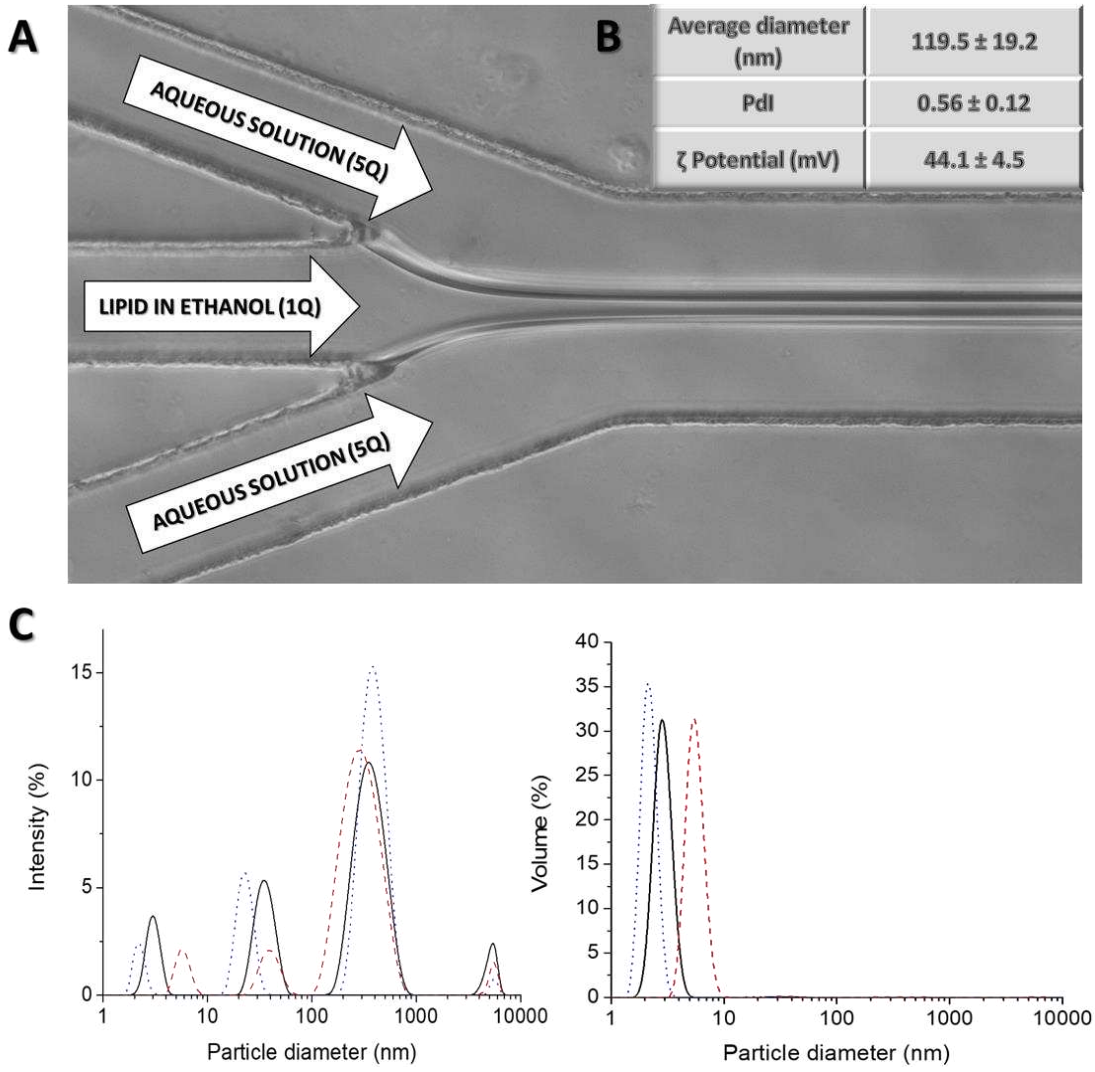

Supplementary material 4.1. Conventional CL production using the CA-MD with three inlets at FRR = 10 and TFR = 120 uL/min (A); Physico-chemical properties of conventional CL obtained at TFR 120.12 µL/min (B); Intensity and volume-weighted diameter distribution of CLs produced using the same TFR ***(C)***. "Q" represents the volumetric flow rate of the given inlet as shown in **A**. The lines in each size distribution represent the profile of three independent replicates.

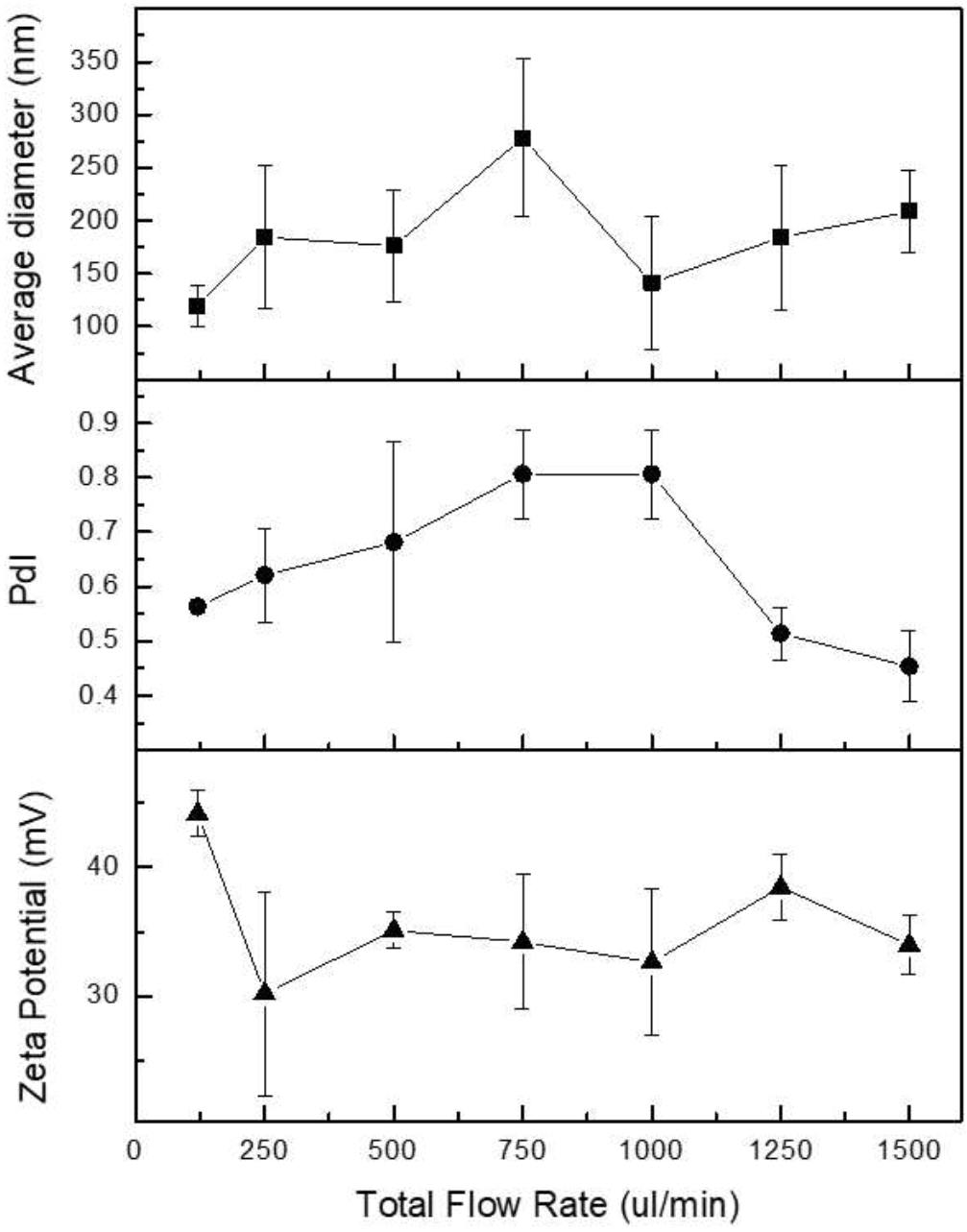

Supplementary material 4.2. Physico-chemical properties of conventional CLs produced on the CA-MD (three-inlets) at FRR = 10 TFR varying from 100 to 1500 µL/min.

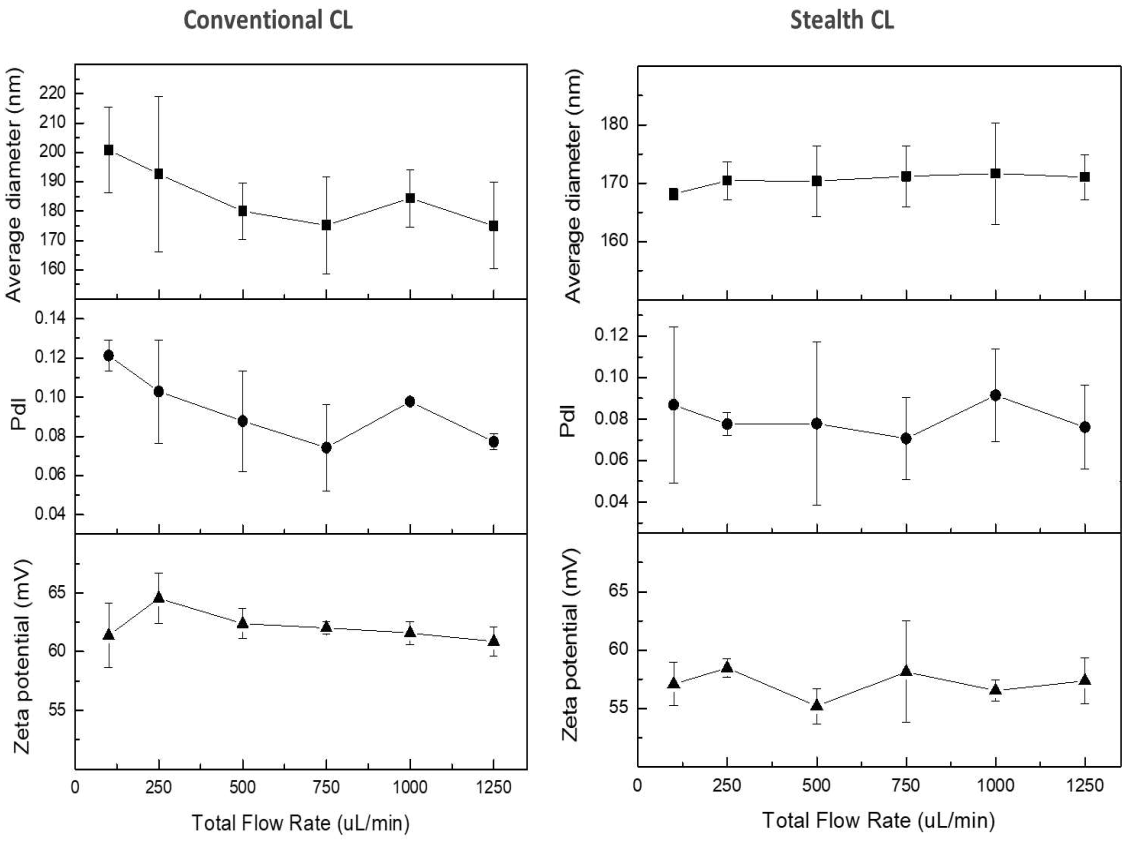

Supplementary material 4.3. Physico-chemical properties of conventional and stealth CLs produced on the CA-MD with three inlets at FRR = 1 using varied TFRs.

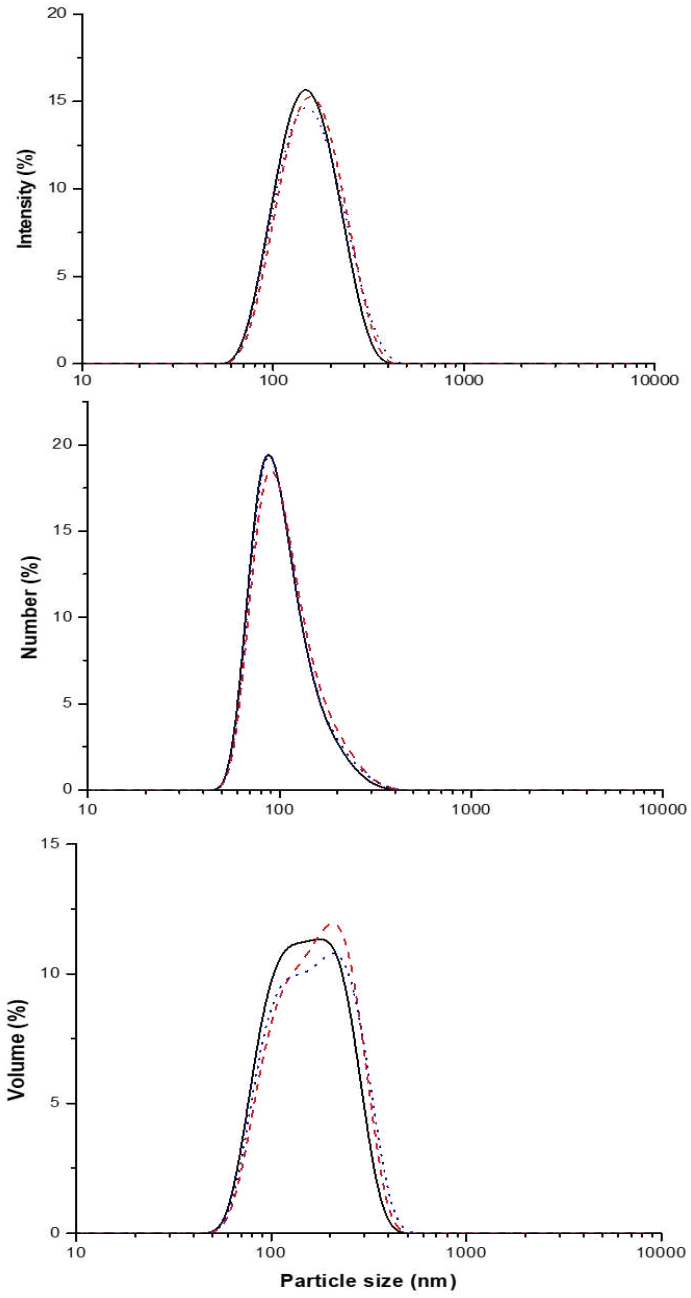

Supplementary material 4.4. Intensity, number and volume-weighted particle size of stealth CLs (5% DSPE-PEG(2000)) produced on CA-MD with two inlets at TFR = 500 µL/min. The lines in each size distribution represent the profile of three independent replicates.

Transfection studies

Transfection studies using cationic liposomes obtained via D-MD technique: The transfection efficiency of PC-3 cells using cationic liposomes obtained via D-MD technique was 5.6% (±1.8). It is important to note that the previous transfection studies involving cationic liposomes produced via D-MD technique (Balbino et al., 2016) used a different protocol than the one used in this work. Then it is not possible to simply compare the previous transfection results with the present one. In the previous study, it was used 1 ug of DNA per well, and in this current manuscript, 1.6 ug of DNA was used. Many factors influence transfection efficiency such as DNA:lipid ratio, DNA concentration, culture medium, presence of serum, and transfection time (Park et al. 2011).

References:

1. Balbino, T.A., Serafin, J.M., Malfatti-Gasperini, A.A., de Oliveira, C.L., Cavalcanti, L.P., de Jesus, M.B. and de La Torre, L.G., 2016. Microfluidic assembly of pDNA/Cationic liposome lipoplexes with high pDNA loading for gene delivery. Langmuir, 32(7), pp.1799-1807.

2. Park, J.S., Surendran, S., Kamendulis, L.M. and Morral, N., 2011. Comparative nucleic acid transfection efficacy in primary hepatocytes for gene silencing and functional studies. BMC research notes, 4(1), p.8.

ANNEX II

Supplementary Materials for Chapter 4

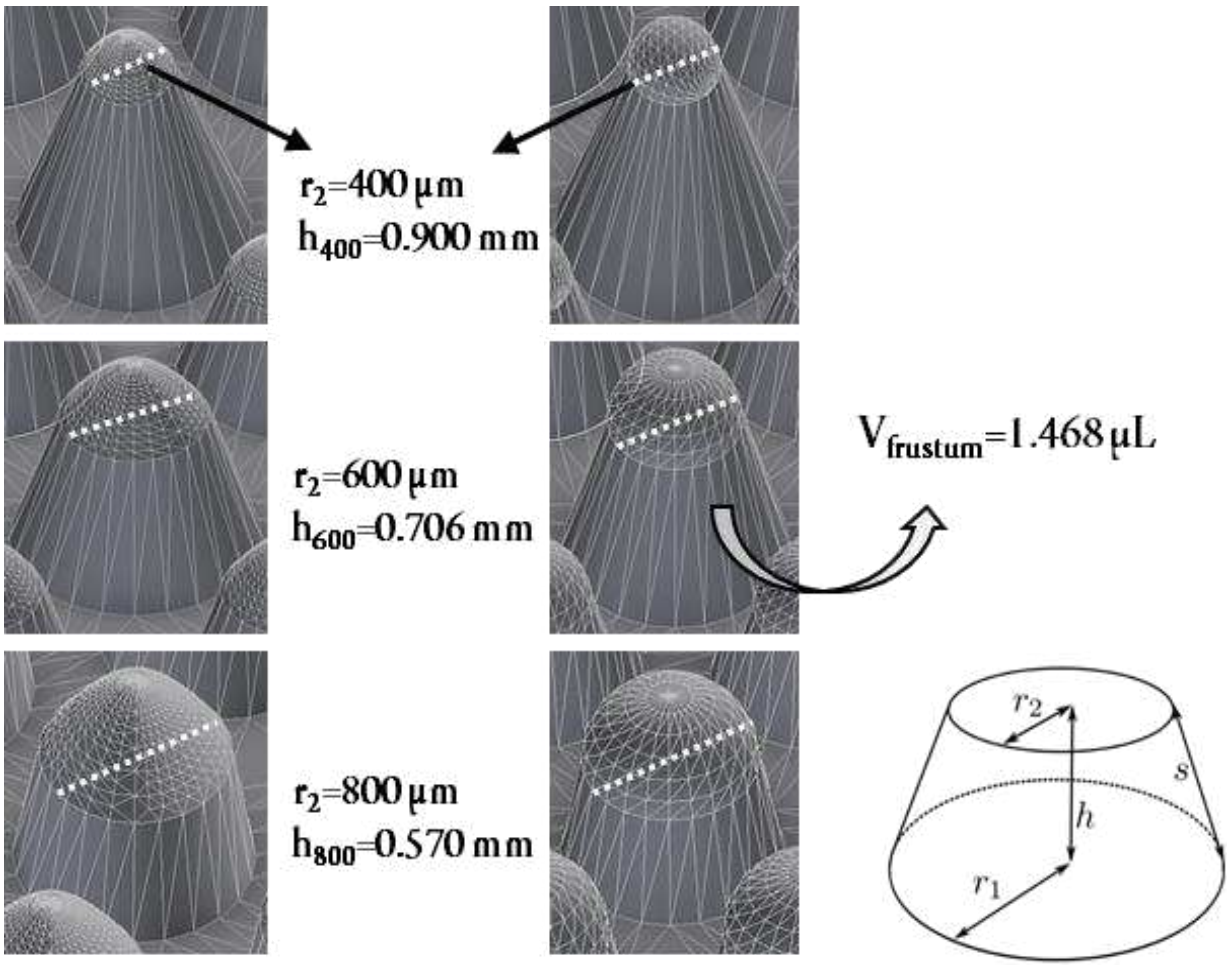

Supplementary material 6.1. Schematic representation of dome- and sphere-like micromolds with the r2 and h values. The volume of the conical frustum for each micromold design was fixed to 1.468 µL.

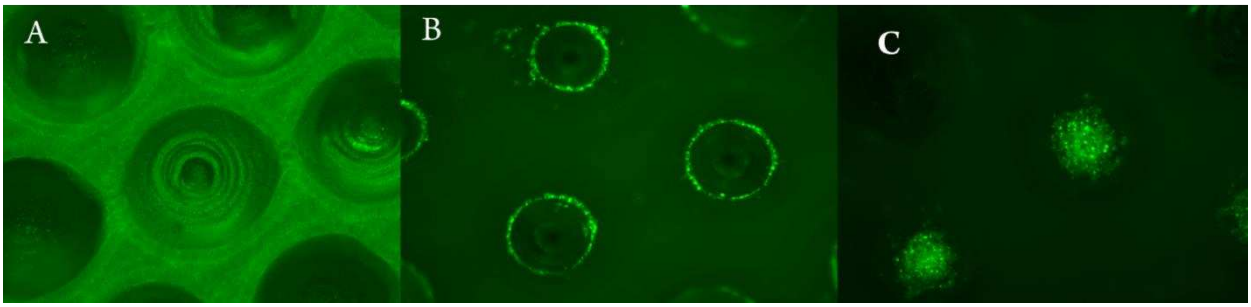

Supplementary material 6.2. (A) Empty microwell; (B) the cells at the edge of microwells before centrifugal step, (C) the cells inside of microwells after centrifugal step.

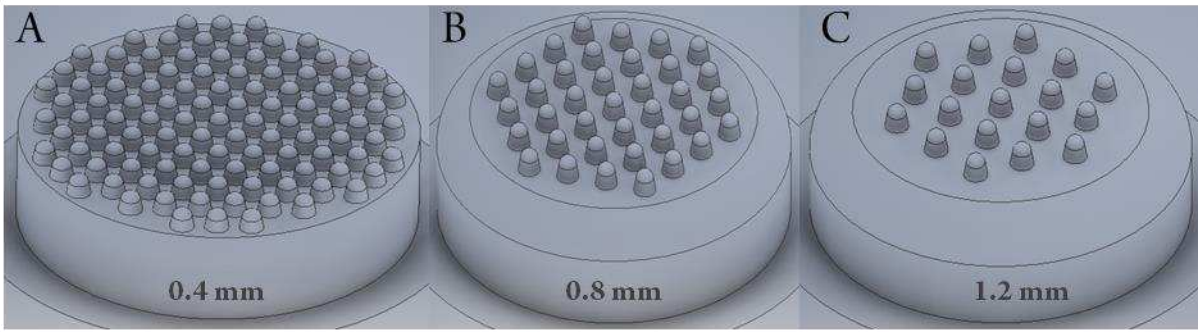

Supplementary material 6.3. New micromolds with different distance between each micromold for the transfection of spheroids. (A) Micromold with 109 microwells and 0.4 mm distance; (B) Micromold with 37 microwells with 0.8 mm distance, and (C) micromold with 19 microwells with 1.2 mm distance between each microwell.

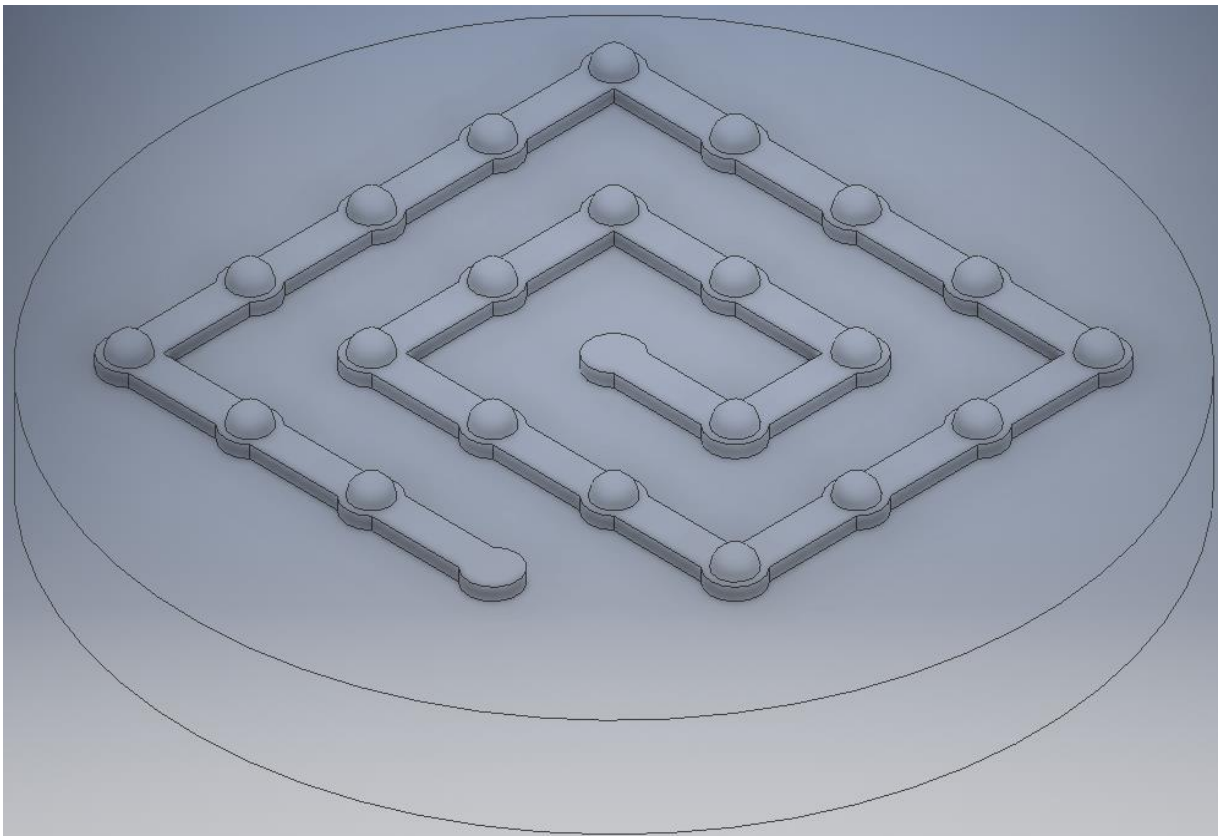

Supplementary material 6.4. CAD design of the perfusion microfluidic system to form spheroids. The channel height is 0.6 mm with 22 microwells. The design shown is used to fabricate negative molds. Each microwell has an approximate volume of 0.5 µL. Total volume of channels with

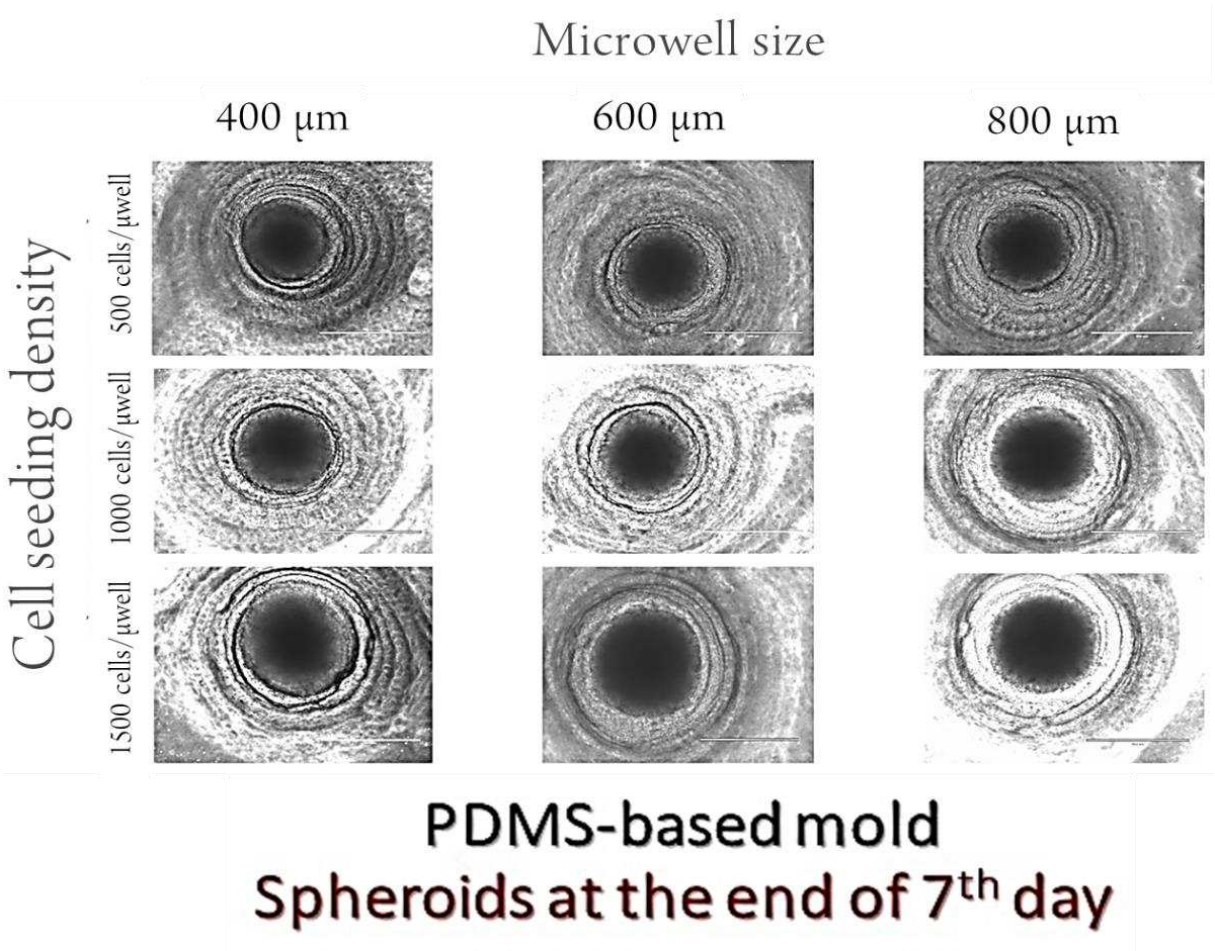

Supplementary material 6.5. The configuration of 12 well plate used in spheroid formation studies with non-fluorescent HEK 293 cell line. Each vertical column represents a micromold with microwell diameter (400, 600, and 800 μm). The horizontal columns represent the tested seeding cell concentration. Spheroids are formed in our PDMS-based micromolds with sphere-like structures.

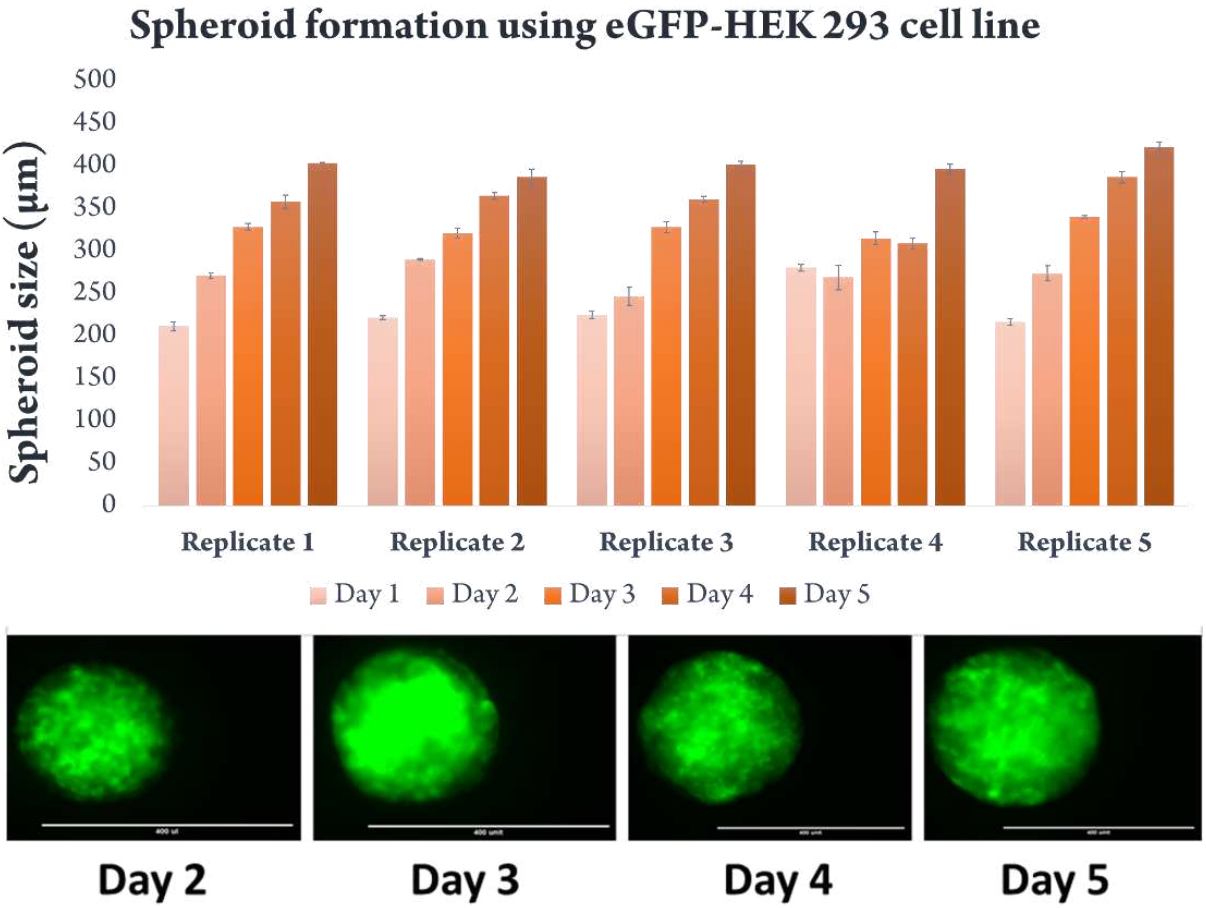

Supplementary material 6.6. Spheroid growth of eGFP-HEK 293 cells throughout 5 days. The fluorescent images of spheroids formed during 5 days are also shown. 10 different spheroid formed in PDMS-mold was analyzed for each replicate.

Days	Spheroid size (µm)	Average cell number
Day 2	~200	4835±863.3
Day 3	250-300	7857±2161.2
Day 4	300-350	8178±2648.9
Day 5	400-450	13975±1917.5

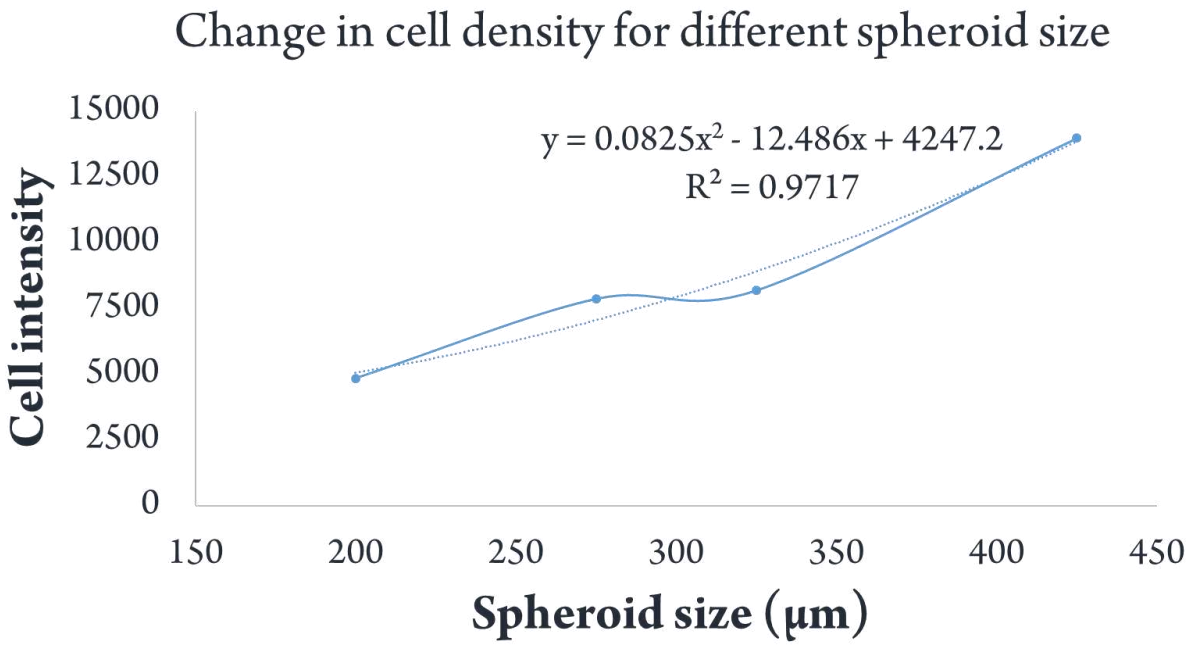

Supplementary material 6.7. Average cell number per spheroid during 5 days. In equation, polynomial approximation with the order of 2 was used.

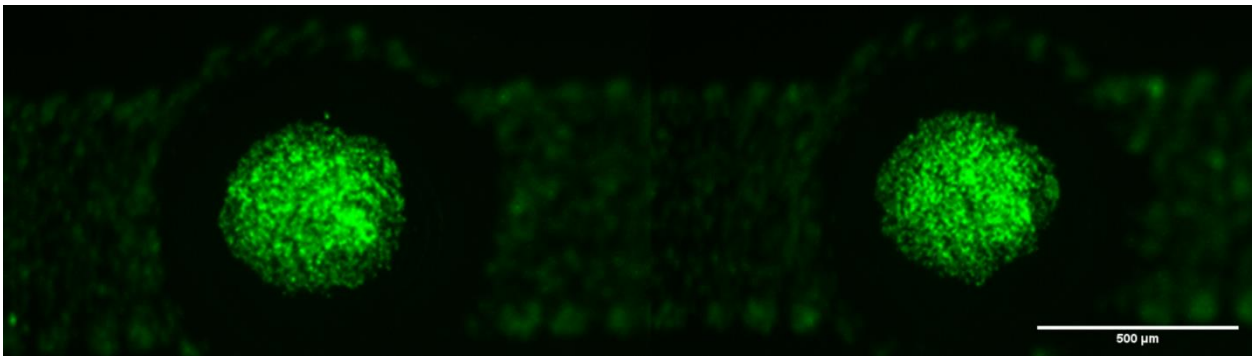

Supplementary material 6.8. Spheroid formation in the microwells of dynamic microfluidic device in day 1. The scale bar is 500 µm.

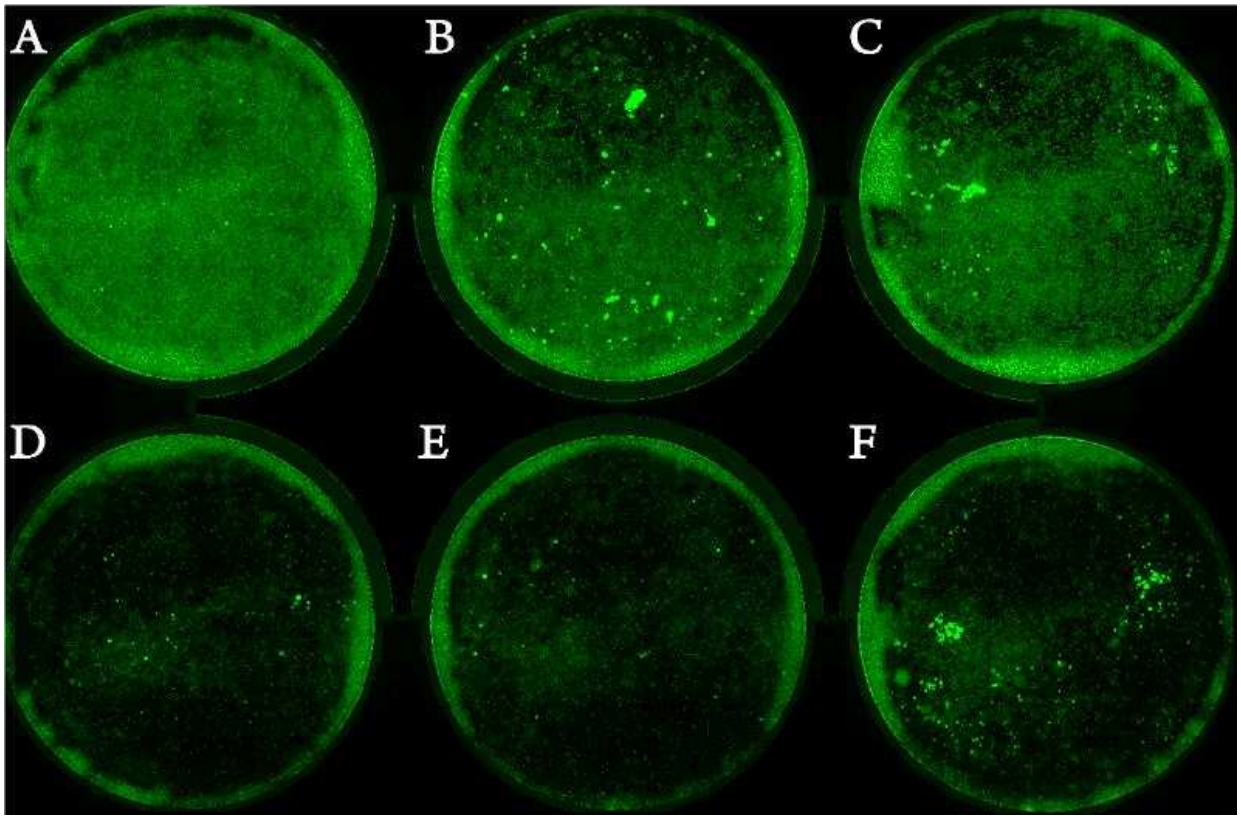

Supplementary material 6.9. The fluorescent images of conventional transfection. Control group (A); only Lipofectamine (B); Control siRNA (non-eGFP targeting siRNA) (C); eGFP siRNA (D, E, and F). The transfection was performed in 6-well plates.

Transfection studies in monolayer (2D) culture

After completing microfluidic platform design and make sure that we can form spheroids in both static and dynamic platforms, we conducted transfection studies with siRNA to achieve our goal which was set at the beginning of this project.

Before the transfection of spheroids, we had to test our cells if they could be transfected or not. For this, we tested two commercial lipid-based vector system: Lipofectamine® 3000 from ThermoFisher and DharmaFECT 1 Transfection Reagent from Horizon Discovery. The test was done in monolayer culture, which is a technique well-optimized and has been used for decades. However, such a technique doesn't give precise drug testing results hence, our objective is testing the efficiency of the drug in spheroids, which better mimics *in vivo* conditions. The first step was to optimize the concentration of vectors and siRNA as well as the number of cells to be treated with the drugs. After testing different drug concentration (10 nM, 25 nM, 50 nM, and 75 nM), the details of our protocol can be found as follows:

1. The transfection was carried out in 6-well plates with the Nunclon™ Delta surface treatment from Thermo Fisher.
2. Each well of the plate was additionally coated with collagen solution to increase the adherence characteristics of the cells.
3. The solution was prepared by mixing 150 µL of collagen, 14 µL of acetic acid and 10 mL of PBS. 1 mL of working solution was added into each well and the plate was left in the hood for 2 hours and washed 3 times with PBS 1x. The plates were used immediately or stored in the fridge.
4. ~200.000 cells were seeded in each well and left for 24 hours so the confluency of the cells could reach ~70%.
5. 3 µL of siRNA (50 µM) and 7.5 µL of Lipofectamine® 3000 and DharmaFECT 1 were prepared separately. Both vectors were separately mixed with siRNA and left for 20 min for complexation occurs between negatively-charged genetic material and positively-charged lipid-based vectors.
6. The transfection solution was added into each well that contains cells and 1 mL of serum-free culture media. We left 6 hours so the transfection could occur and after 6 hours we added additional 1 mL of serum-containing culture media.

7. Every 24 hours, we observed the plate under fluorescent microscope and at the end of 72 hours, we analyzed the well plate using Nucleocounter NC-8 slides.